Analysis and Ad-hoc Networking Solutions for Cooperative Relaying Systems

TECHNISCHE UNIVERSITÄT ILMENAU

Fakultät für Elektrotechnik und Informationstechnik

Bilal Zafar

Communications Research Laboratory

Ilmenau University of Technology

A thesis submitted for the degree of

Doktor-Ingenieur (Dr.-Ing.)

July 2013

urn:nbn:de:gbv:ilm1-2014000041

I would like to dedicate this thesis to my late grandmother.

Acknowledgements

This thesis would not have been possible without the support of many people. First and foremost, I would like to acknowledge the support and guidance of Prof. Martin Haardt, who is my main supervisor. He took a lot of time out of his busy schedule to constantly guide me throughout this work. His comments and questions were also very helpful in ensuring the quality of this thesis. I would also like to acknowledge the guidance and supervision of Prof. Andreas Mitschele-Thiel, who was my secondary advisor.

Deepest gratitude is also due to Dipl.-Ing. Soheyl Gherekhloo, Dipl.-Ing. Florian Roemer, Dipl.-Ing. Jens Steinwandt, and Mehdi Tavakoli Garrossi who offered me invaluable assistance and support during my research. Without their knowledge and assistance, this study would not have been successful.

This work was carried as part of the project "Self-organized Mobile Communication Systems for Disaster Scenarios", which is the focus of research for the International Graduate School on Mobile Communications (GS-Mobicom), Ilmenau University of Technology. The graduate school supported and encouraged me every step of the way during my time as a member of the graduate school, for which I am very grateful.

Abstract

Users of mobile networks are increasingly demanding higher data rates from their service providers. To cater to this demand, various signal processing and networking algorithms have been proposed. Amongst them the multiple input multiple output (MIMO) scheme of wireless communications is one of the most promising options. However, due to certain physical restrictions, e.g., size, it is not possible for many devices to have multiple antennas on them. Also, most of the devices currently in use are single-antenna devices. Such devices can make use of the MIMO scheme by employing cooperative MIMO methods. This involves nearby nodes utilizing the antennas of each other to form virtual antenna arrays (VAAs). Nodes with limited communication ranges can further employ multi-hopping to be able to communicate with far away nodes. However, an ad-hoc communications scheme with cooperative MIMO multi-hopping can be challenging to implement because of its de-centralized nature and lack of a centralized controling entity such as a base-station. This thesis looks at methods to alleviate the problems faced by such networks.

In the first part of this thesis, we look, analytically, at the relaying scheme under consideration and derive closed form expressions for certain performance measures (signal to noise ratio (SNR), symbol error rate (SER), bit error rate (BER), and capacity) for the co-located and cooperative multiple antenna schemes in different relaying configurations (amplify-and-forward and decode-and-forward) and different antenna configurations (single input single output (SISO), single input multiple output (SIMO) and MIMO). These expressions show the importance of reducing the number of hops in multi-hop communications to achieve a better performance. We can also see the impact

of different antenna configurations and different transmit powers on the number of hops through these simplified expressions.

We also look at the impact of synchronization errors on the cooperative MIMO communications scheme and derive a lower bound of the SINR and an expression for the BER in the high SNR regime. These expressions can help the network designers to ensure that the quality of service (QoS) is satisfied even in the worst-case scenarios.

In the second part of the thesis we present some algorithms developed by us to help the set-up and functioning of cluster-based ad-hoc networks that employ cooperative relaying. We present a clustering algorithm that takes into account the battery status of nodes in order to ensure a longer network life-time. We also present a routing mechanism that is tailored for use in cooperative MIMO multi-hop relaying. The benefits of both schemes are shown through simulations.

A method to handle data in ad-hoc networks using distributed hash tables (DHTs) is also presented. Moreover, we also present a physical layer security mechanism for multi-hop relaying. We also analyze the physical layer security mechanism for the cooperative MIMO scheme. This analysis shows that the cooperative MIMO scheme is more beneficial than co-located MIMO in terms of the information theoretic limits of the physical layer security.

Contents

List of Figures

Chapter 1

Introduction and the scope of the thesis

During the last few years users have been increasingly demanding higher data rates and more robust connections from their mobile service providers. In order to take care of these requirements it is possible to use devices with more than one antenna, by employing Multiple Input Multiple Output (MIMO) communications, to take advantage of the diversity as well as the spatial multiplexing techniques. Though in practice, the physical size, limited battery power and the available bandwidth are the limiting factors for the use of MIMO techniques. Therefore, sometimes it is not possible to employ the conventional MIMO techniques which calls for the use of novel signal processing methods, such as cooperative communication, to achieve higher date rates. These methods basically make use of the cooperation between distributed users. Multiuser cooperation diversity has been used in [SEA03], where the distributed nature of the mobile users in a wireless network is used in order to introduce a new form of diversity. We analyzed and described some solutions for cooperative MIMO networks in [ZSGH11].

In cooperative communications, physically separate devices share their antennas and resources in order to create a virtual antenna array (VAA) to ensure more reliable communications. Some nodes play the role of relays in order to forward the message to the destination, thus generating multiple paths. This way, the benefits of spatial diversity can be exploited using single antenna devices. Employing such techniques has some design challenges as a result of the physical separation of devices and the absence of a fixed infrastructure. Also, there are some other serious problems, e.g., possible synchronization errors, and inaccurate channel state information (CSI) at the destination side.

In this thesis, we will focus on cooperative multi-hop relaying networks. The thesis is divided into two parts. The first part (Chapters 2-4) focuses on an analytical and mathematical analysis of multi-hop relaying with different antenna configurations such as single input single output (SISO), multiple input multiple output (MIMO) and single input multiple output (SIMO), and different relaying techniques such as amplify-and-forward (AF) and decode-and-forward (DF). We will also take into account the impact of imperfect CSI and lack of perfect synchronisation on cooperative communications. The objective is to study the restrictions on the distributed communication in order to develop robust algorithms.

In the second part of the thesis (Chapters 5-7), we present some solutions and algorithms developed by us for improving the performance of ad-hoc networks that employ cooperative relaying. These include new clustering and routing algorithms (Chapter 5), a distributed data management algorithm (Chapter 6), and a new physical layer security mechanism for multi-hop relaying (Chapter 7).

1.1 Cluster based multi-hop relaying

The vision for future communication systems stems from the need to render networks more robust in the wake of unforeseen situations. Therefore the need to reduce the dependence on fixed infrastructure is paramount. We envision future communication networks to be self-organizing and cognitive. To this end, it is possible to view mobile handsets as radio resources in a network and to utilize them as 'intelligent' relays to form communication links in the absence of base stations. Figure 1.1 illustrates the communication between two nodes in a cluster-based multi-hop network.

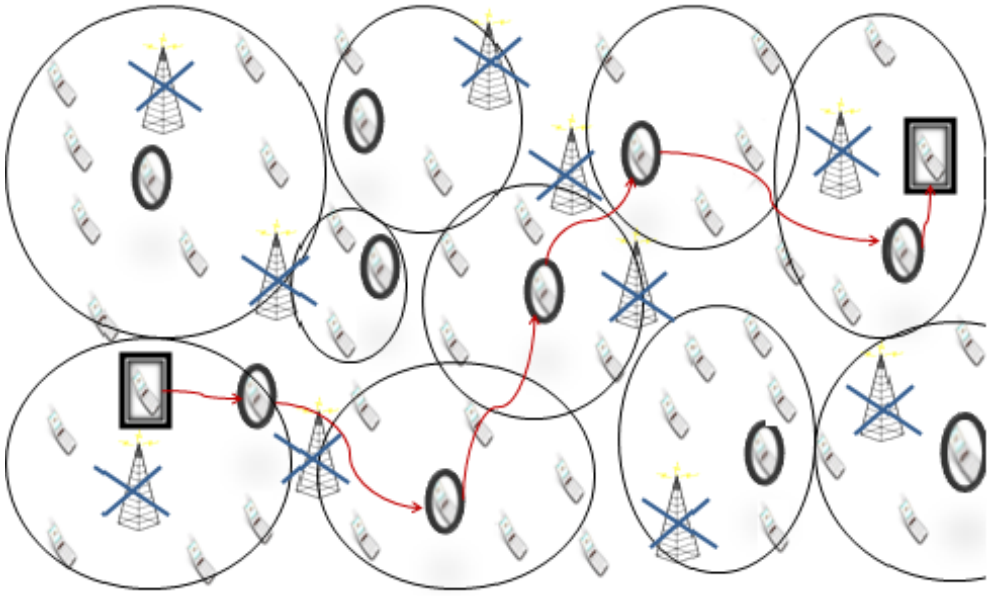

Figure 1.1: Cluster-based multi-hop system

For such a system to become operational to the stage described in Figure

1.1, we need to go through various steps. The fact that the network has no centralized control means that we have to deal with complex issues of scheduling, synchronization and interference cancellation in an ad-hoc manner which is not easy. Since the exact number of nodes in a particular area is not known and neither are their clocks synchronized, it is difficult to apply channel access schemes like Time Division Multiple Access (TDMA). One option is to perform extensive piloting and gossiping in the network to synchronize the clocks of all the nodes present. Applying multiple access schemes becomes easier once the network is clustered [HCB00]. However in an unclustered network, it is very hard to avoid collisions. The clustering process is performed by extensive piloting between the nodes to determine the cluster-heads and the cluster members. It involves several piloting phases, in which each node transmits one short pilot. After each phase the information in the pilot reflects the status of the node. It is reasonable to assume that the collisions (packets arriving at the same time) are less likely if the piloting messages are short and intermittent and that the time for each clustering phase is quite long in comparison. In ad-hoc networks pilots can be used to gauge the quality of the wireless communications link as well as to exchange networking information, e.g., location and cluster-head association, between nodes [HCB00].

We can further decrease the probability of interference by employing Frequency Division Multiple Access (FDMA) as well. The entire bandwidth is divided into a certain number of bands, and every node can transmit in one of these frequency ranges. The frequency bands in which the signal can be transmitted are known to the receiver. The received signal will be shifted in the base band by every frequency and then passed through a low pass filter. If the power of the output signal of the filter exceeds a threshold, the frequency recovery is accomplished and demodulation can be performed but if it is not the case, it can be concluded that either no signal is sent in this time slot, or the transmitter node is so far away that the sent signal is completely attenuated and the received SNR is so low that the decoding of the received packet is very defective. In this way the packets can be decoded by nearby nodes based on the RSSI (Received Signal Strength Indicator) [17006].

Even though ad-hoc mobile networks that support multi-hopping have been around for a while, we are still some way off the practical deployment of a com-

pletely self-organized version of a cluster-based multi-hop network that can deal with the various issues for network management, routing, localization, interference, suitable physical layer strategies, etc. These issues are not trivial and have been, mostly individually, the subject of a lot of interest over the years. Schemes like [WS10], [YC05], [AKK04] try to solve the various issues for a self organized network with multi-hop capabilities. However there is a lack of an architecture that brings together the various methods developed over the years in order to implement, view, and possibly optimize a complete system based on them. For this purpose, we have built a software SONIR [ZGA+10] (Self-Organizing Network with Intelligent Relaying), in MATLAB, which implements an end-to-end multi-hop, virtual MIMO system, capable of dealing with the mobility of nodes in a Rayleigh fading environment. Methods for clustering, mobility management, routing, virtual MIMO, etc. have been implemented. These methods work on different OSI layers. The system shown in Figure 1 is the result of several steps. First, clustering is performed, then the nodes do extensive piloting to gather as much local information as needed, which helps them in identifying optimal gateways to the neighboring clusters which is essential for routing. Finally we are able to establish a route from the source to the destination. These steps are illustrated in Figure 1.2.

1.2 Multi-hop relaying networks

As it was mentioned before, in cooperative communication, some nodes serve as relays. A communication including a relay, consists of two phases; in the first phase the source/transmitter sends the message to the relay, and in the second phase the relay processes the message and forwards it to the destination/receiver. It is also possible to extend this communication to a multi-hop scenario.

In large networks, where the source and the destination are located far away from each other, a multi-hop scenario can be very helpful. Selecting the relay nodes in the appropriate positions in order to reduce the transmission distance, will lead to low energy consumption and increase the reliability.

In this work, we will frequently use ergodic capacity [PNG08] as the parameter for evaluating the performance of the wireless communication scenario. In

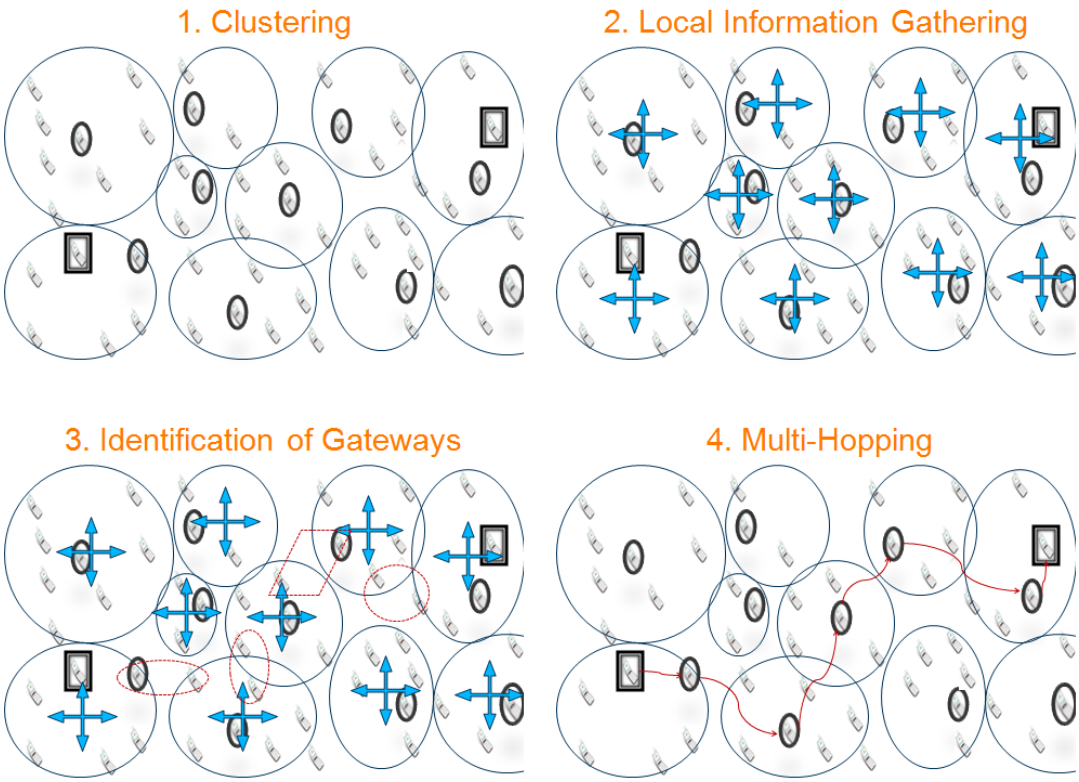

Figure 1.2: Steps for multi-hop routing in ad-hoc networks

case of the AWGN (Additive Wide Gaussian Noise) channel, Shannon capacity [SW48] describes the maximum data rate that can be sent over the channel with asymptotically small error probability. Considering a random MIMO channel and assuming that the channel matrix $\boldsymbol{H}$ is generated by an ergodic process, the capacity is a random variable and the ergodic capacity is the expected value of that random variable [PNG08].

Several different relaying schemes can be employed in multi-hop networks, e.g., amplify-and-forward (AF) relaying [LTW04], decode-and-forward (DF) relaying [JHHN04], and compress-and-forward relaying [KGG05]. This thesis studies the capacity and performance for the AF and DF relaying schemes in the multi-hop scenario. The performance of wireless relaying has been extensively studied in terms of outage probability and error rate in [HA03], [KTM06], and [FB08], but

very few studies have taken a look at the ergodic capacity for the case of fading relay channels. In [HMZ05], the authors have studied the upper and lower bounds of the ergodic capacity for a single relay channel. Therefore we study the ergodic capacity for the multi-hop case with Rayleigh fading in this thesis.

In the second chapter of this thesis, AF and DF relaying are studied from the efficiency point of view. No interference issues or synchronization errors are considered for simplicity. This makes the model analytically solvable and closed-form solutions can be produced. These issues are assumed to be tackled already by other mechanisms in the network such as interference suppression and mitigation mechanisms, proper scheduling, multiple access schemes, various synchronisation mechanisms from literature, etc. It is assumed that the presented model can achieve the maximum capacity for a given relaying scheme considering all the nodes have identical characteristics. Also, it is assumed that accurate channel state information (CSI) is always available. In this part, the objective is to theoretically analyze the best possible performance improvements in multi-hop networks in case of AF and DF relaying schemes without considering the problematic factors e.g., the synchronization errors, channel estimation errors, and interferences.

In the third chapter, the impact of the number of the hops on the multi-hop network's performance is studied considering the AF and DF the relaying schemes. Also, the effect of changing the spatial diversity order on the transmission gain and on the number of the hops is studied, by altering the number of transmit and receive antennas at the relay nodes.

1.3 Cooperative communication and synchronization error

A simple multi-hop network with two hops consists of one source, one destination, and a group of relay nodes, without any direct link between the source/transmitter and the destination/receiver. In such a network, the benefits of having multiple antennas at the transmitter can be exploited. This can be done employing diversity coding, spatial multiplexing or precoding.

Recently the idea of co-operative/virtual MIMO has been integrated into such networks as well, for the case of nodes with single antennas. Co-operative or virtual MIMO is a good concept for mobile nodes with a single antenna to be able to achieve the benefits of MIMO communications. It is ideally suited for the distributed clustered system under investigation, where we can employ nearby nodes to co-operate and form a virtual antenna array. It is also imperative to modify the routing scheme to incorporate the need for multiple paths between clusters.

Employing diversity coding, the transmission robustness increases in terms of the BER (bit error rate). This happens because in this method several physically separated antennas are used and as a result there is a lower probability that all the paths between the transmit and the receive antennas experience fading simultaneously. Also, no channel knowledge is required at the transmitter when the signal is coded based on the space time coding technique [PNG08]. Space-time coding and beamforming are the most successful techniques for increasing the diversity of multiple-antenna systems [Jaf05], [HTR03].

Orthogonal space time block codes (STBC) have been introduced in [TJC99] and [TSC98]. If channel knowledge is not available at the transmitter but the perfect CSI is available at the destination, STBC is the most suitable and accepted technique in order to increase the diversity.

In [LW03], [CH03] and [CGB04], research has been performed in order to increase the network's reliability when employing space-time codes between the relay nodes. Knowing that perfect synchronization is the most important requirement of STBCs and considering that the synchronization algorithms presented, e.g., in [SV03], increase the network's time and energy consumption, it is essential to study the robustness of the STBCs.

Chapter 4 of this thesis looks at the impact of synchronization error on cooperative MIMO communication. Although synchronization errors and their impact on the performance of cooperative MIMO systems have been studied in [NBS08a] among others, these analytical studies become more reliable and practical if the transmission quality is studied in the worst case, as is done in Chapter 4. The signal to interference and noise ratio (SINR) is a key parameter in order to evaluate the network performance, because synchronization errors yield an inter symbol

interference (ISI) at the destination. Synchronization errors in cooperative MIMO can be counted as an inaccuracy in the available CSI at the destination. Also, the generated additive inaccuracy matrix of the CSI is considered to be norm bounded because the synchronization between the relay nodes is not perfect and has some errors.

When considering cooperative MIMO it is crucial to also look at the impairments. As mentioned before, one of these impairments is the synchronization problem. Since nodes suffer from unequal hardware, self heating, and environmental changes (e.g., temperature change), the clocks will not run perfectly synchronized. Most of this problem is solved via suitable synchronization protocols on higher layers and on the physical layer. On the physical layer one can make use of multiple synchronization techniques to achieve a certain level of phase synchronization. These techniques include, e.g., reference tone synchronization where (as proposed in [MHMB05]) the receiver emits a signal and all relay nodes change their phase until their respective SNRs are maximized. Another well known technique is the firefly synchronization shown in [TAB06] which basically makes use of coupled oscillator theory. There are also blind techniques which estimate the phase information from the signal subspace (e.g., [TT08]).

While in a simulator environment we are able to simulate under ideal conditions, for the real world implementation we have to consider practical issues as shown in [NBS08b] and [JH06]. As mentioned above, these effects can be mitigated via suitable protocols or even via suitable channel estimation [SV03]. However, some delays are randomly distributed so that their effect is not reflected by the measured channel. These kind of synchronization problems are assumed to cause positive and negative delays within one symbol pulse. This problem has been investigated in [PAR06] for the case of space-time coding. The third chapter of this thesis focuses on deriving the lower bound of the SINR for the cooperative MIMO systems.

1.4 Clustering mechanisms in ad-hoc networks

The most promising option to deal with such cluster-based ad-hoc networks is clustering. It involves grouping together of neighboring nodes to form groups

or 'clusters' with one node, designated to act as the local coordinator, known as the 'cluster-head'. Common clustering schemes include LEACH (Low-Energy Adaptive Clustering Hierarchy) [HCB00], a RSSI (Received Signal Strength Indicator) based method [FPL09], and a GPS based scheme to tackle mobility similar to [AP01]. Reference [FPL09] is one of the newest proposed clustering schemes and a good option to simplify the process of clustering through piloting and local information gathering but cannot deal well with the mobility of the nodes. A very good scheme to maintain clustering in the face of the mobility of the nodes in the system is presented in [AP01]. To provide an increased network life-time, we propose a new clustering scheme, Enhanced Received Signal Strength Indicator based clustering (E-RSSI), in Chapter 5.

1.5 Routing in ad-hoc networks

Localization and routing for self-organized networks is a non-trivial task and has many implementational issues. Having GPS (Global Positioning System) equipped nodes helps with the localization but it is still quite difficult for nodes to get accurate information about their surroundings and their neighboring nodes. In our system [ZGA+10], the cluster-heads deal with most of the routing functions. They maintain tables of the IDs of nodes in their cluster and use the nodes to gather information about the presence of neighboring clusters. Moreover they have tables indicating the most suitable node (or nodes, in case of cooperative MIMO) to use in order to communicate with a particular neighboring cluster. AODV (Ad-hoc On-demand Distance Vector routing) [PR99] is a promising option to deal with the routing issue. In our system, we have improved upon AODV in that we update the route when we perform re-clustering even during the same session of communication between two nodes to cater for the movement of nodes in the network. AODV, on the other hand, maintains the same route during one session of communication. The cluster maintenance tables and the routing tables are also updated periodically, and the optimal update interval can be determined as described in Chapter 5. An interesting and significant future work would be to establish a routing scheme that performs routing based on the (co-operative) MIMO channel between clusters from the start, rather than extending AODV for

this purpose. Our new routing scheme AOCMR (Ad-hoc On-demand Cooperative MIMO Routing), which is specially tailored for use in networks employing cooperative MIMO, is presented in Chapter 5.

1.6 Data management in ad-hoc networks

There has been a rapid growth of distributed data management systems for large amounts of data. These are either unstructured, and therefore built directly on the existing underlay network, or structured such that participating nodes are abstracted from their underlay network. While unstructured systems benefit from routing and searching using underlay logic, structured overlays have the decisive advantage of providing guarantees on data availability.

Some existing proximity aware distributed hash table (DHT) approaches, such as DHash++ [KAKH09] (which is an extension of Chord [SMLN$^+$03]), and RBFM (resource based finger management, an extension of DHash++) [RB11], indirectly address the underlay overhead by reducing the total average physical distance that messages travel by choosing nearby links. However, to the best of our knowledge, no current DHT scheme takes into account the inherent ad-hoc properties and utilizes them effectively to directly reduce the underlay load and lookup latency.

In Chapter 6, we consider the compatibility of structured overlays, or distributed hash tables (DHTs), and decentralized wireless ad-hoc networks. In doing so, we must consider the complex and unpredictable nature of wireless ad-hoc networks - for example, the lack of Quality-of-Service (QoS) or high performance guarantees in mobile ad-hoc networks (MANETs) - and the restricted resources of wireless nodes - such as battery power, bandwidth, or computing power.

1.7 Security mechanisms in ad-hoc networks

One of the biggest challenges facing the wide-spread adoption of ad-hoc networks is the threat that the data is easily vulnerable to any eavesdroppers. The decentralized and ad-hoc nature of the connections render the usual data security mechanisms unsuitable for use in the networks under consideration. Physical

layer security mechanisms [BBRM08] are an interesting and viable option for such networks. The ubiquitous and on-the-fly nature of such mechanisms are highly suited for providing security in self-organizing cooperative relaying networks.

The specific form of physical layer security that we will focus on is called reciprocal channel key generation (RCKG). It was proposed in [HHY95] and has recently been discussed extensively in [WS10] for co-located MIMO systems. RCKG can be used in conditions when the wireless channel between two communicating nodes is nearly reciprocal. Reciprocity is not an impractical assumption as it is practically achieved in a variety of wireless systems employing time-division duplex (TDD), such as IEEE 802.11 [IEE97], IEEE 802.16 (WiMAX) [IEE97], and 3rd Generation Partnership Project (3GPP) Long Term Evolution (LTE) [DPS11].

In Chapter 7, we will extend the analysis from [WS10] to the case of cooperative MIMO systems, and also propose a new incremental method for providing physical layer security to multi-hop networks.

1.8 Simulation tool

We have created a Matlab-based simulation tool SONIR (Self-Organized Network with Intelligent Relaying) [ZGA+10] that allows for the evaluation of ad-hoc and cooperative MIMO-based multi-hop relaying networks on the system level. SONIR can be used to analyze and visualize signal processing algorithms for heterogeneous distributed MIMO systems. Since it is MATLAB-based and tailored for ad-hoc, mobile, and cooperative communication scenarios with a handy GUI (Graphical User Interface) and a visualization tool to boot, we have a greater flexibility for simulating new techniques as opposed to other network simulators. The simulator provides an ideal platform for the implementation and testing of various techniques for ad-hoc and cooperative MIMO based multi-hop relaying networks, and to see the benefits of these techniques on a system level. We have tested algorithms for a new clustering scheme, new routing scheme, physical layer security, robust beamforming, as well as a DHT implementation in ad-hoc settings.

A user's guide for the SONIR tool is provided in Appendix A.

1.9 Overview and contributions

In the first part of the thesis we analyze cooperative multi-hop relaying networks and derive some closed form expressions for different parameters of such networks. Based on these analyses we present some algorithms as solutions for some common problems faced by the ad-hoc networks under consideration. The results presented in this thesis are of importance to network designers as we move towards the standardization of cooperative multi-hop networks. The closed form expressions derived in this thesis can help network designers to ensure that the quality of service is ensured even in worst-case scenarios.

1.9.1 Part 1: An Analytical look at Relaying

- **Chapter 2** of this thesis analyses the most popular relaying schemes, amplify-and-forward (AF) and decode-and-forward (DF) in terms of capacity for single antenna devices. The received signal-to-noise ratio (SNR) and the ergodic capacity of these relaying schemes are studied considering a multi-hop wireless transmission in the presence of Rayleigh fading. To maximize the ergodic capacity, we consider the relays to be optimally located (equidistant) and also assume that the channel statistics remain the same for all hops and the noise power is equal at all relays and terminals. Considering these assumptions, the ergodic capacity of the two aforementioned relaying schemes is analyzed and compared. Closed form expressions for the capacity have been derived and they show that decreasing the number of hops in multi-hop can give an improvement in the performance in terms of the capacity. The analytical results can help to determine the thresholds at which nodes can switch between different modes of transmission, such as the relaying scheme and the appropriate number of hops, in multi-hop networks, to ensure the QoS.

- **Chapter 3** of this thesis studies the case of multiple co-located antennas at the relay nodes (without considering antenna selection) in multi-hop networks. The goal of this chapter is to study the performance of the transmission over an optimum multi-hop route (using equidistant relays,

as discussed in the last chapter) which is found based on MIMO, single input multiple output (SIMO) and SISO links. Closed form expressions for the upper bound of the symbol error rate (SER) have been derived for these multiple antenna configurations and the effect of increasing the number of antennas, the number of hops, and the transmit power has also been studied. The analysis shows that the gain obtained by employing SIMO multi-hop networks is larger than that for MIMO (Alamouti) multi-hop networks when assuming the same total number of antennas. In other words, assuming a network with single antenna devices cooperating with each other, increasing the transmit diversity should be given lower priority over increasing the receive diversity.

- **Chapter 4** of this thesis focuses on the cooperative MIMO scheme in wireless communications. In this chapter, the users are considered to be equipped with single antennas only and generating indigenous SIMO and MIMO channels will thus be impossible. Therefore, a combination of the single-antenna users is employed to constitute a virtual antenna array in order to generate a cooperative MIMO channel. First, we describe a method devised by us to employ SISO piloting in order to gauge the quality of prospective cooperative MIMO links. Then, the performance of the cooperative MIMO in the presence of synchronization errors is studied. The synchronization error, caused by the distributed nature of the scheme, is considered as inaccurate channel state information, which is modeled as an additive norm-bounded inaccuracy matrix. A closed-form expression is derived for the lower bound of the SINR. Using this, a closed-form expression of the Bit Error Rate (BER) in the high SNR regime for the worst case error vector is also derived. These expressions are, to the best of our knowledge, not present in the literature before and we feel that these worst case performance expressions are of interest to system designers as it helps them to design the system with specific guarantees about the outage behavior.

1.9.2 Part 2: Ad-hoc Networking Solutions

- **Chapter 5** of this thesis presents some proposed improvements for cluster-based ad-hoc networks on the data link layer and the network layer will be discussed. Specifically, we will look at clustering and routing for such a communication scheme involving cooperative relaying. The first part of this chapter presents a new clustering scheme developed by us that forms clusters in such a way that it enables low energy transmissions and distributes the transmission energy consumption over all the nodes in a more even way which leads to a significantly longer network life-time. A new routing method tailored for use in cooperative MIMO networks is also presented in this chapter. Using cooperative MIMO for range extension of individual hops in a multi-hop network can provide a much improved link throughput capacity. Using our proposed scheme can make it simpler for cluster-heads to employ cooperative MIMO techniques in an ad-hoc manner since we use simple piloting and employ that to form tables at the cluster-heads which will be used for routing between clusters using heterogeneous cooperative MIMO links.

- **Chapter 6** of this thesis presents an analysis on data management in multi-hop ad-hoc networks through the use of distributed hash tables. There is a current interest in the creation of new methods to handle data in decentralized wireless networks, and this chapter provides a solution to that effect. Novel DHT protocols which incorporate knowledge about the underlay network clustering configuration are presented in this chapter and are designed to perform well on heterogeneous dynamic ad-hoc networks. We show a ten to fifteen percent decrease in the network load for our scenario compared to schemes which do not take clustering information into account. Simulations also show that some claimed overlay benefits from earlier schemes are less pronounced when coupled with a real wireless underlay network. This highlights the importance of simulating both overlay and underlay networks together.

- **Chapter 7** of this thesis looks at methods for providing physical layer secu-

rity to cooperative multi-hop networks. Security is a critical issue faced by ad-hoc networks, where the distributed nature and the lack of infrastructure may lead to a network that is vulnerable to eavesdropping. The focus of this chapter is on exploiting the benefits of cooperative communications to improve the information theoretic limit of reciprocal channel key generation (RCKG). The information theoretical limit of RCKG for co-located multiple input multiple output (MIMO) scheme is compared with the cooperative MIMO scheme using numerical simulations. We also propose a new method for providing incremental physical layer security to multi-hop networks. This two-step encryption drastically reduced the vulnerability of RCKG and is very suitable when high levels of security are required. It is also especially suitable for providing security in cooperative MIMO communication as it performs well even for the specific scenario when the eavesdropper is close to the cluster-head. This chapter highlights the benefit of cooperative communications over co-located communications in terms of physical layer security.

1.10 List of publications

Here is the list of publications during my tenure as a doctoral researcher:

1.10.1 Journal:

- B. Zafar, D. Schulz, S. Gherekhloo, and M. Haardt, "Ad-Hoc Networking Solutions for Cooperative MIMO Multi-hop Networks", *IEEE Vehicular Technology Magazine*, volume 6, number 1, pages 31-36, March 2011.

- B. Zafar, S. Gherekhloo, and M. Haardt, "Analysis of Cooperative Multi-hop Relaying Networks: Communication Between Range-Limited and Cooperative Nodes", *IEEE Vehicular Technology Magazine*, volume 7, number 3, pages 40-47, September 2012.

1.10.2 Conference:

- B. Zafar, R. Alieiev, L. Ribe-Baumann, and M. Haardt, "DHTs for cluster-based ad-hoc networks employing multi-hop relaying", *in Proc. 17th International Workshop on Wireless Mesh and Ad Hoc Networks (WiMAN 2013), at the 22nd International Conference on Computer Communications and Networks (ICCCN)*, Nassau, Bahamas, July 2013.

- B. Zafar, S. Gherekhloo, and M. Haardt: "Analysis of Cooperative Multi-hop Relaying Networks" , *in Proc. 28-th Meeting of the Wireless World Research Forum (WWRF 28)*, Athens, Greece, April 2012.

- M. T. Garrosi , B. Zafar, and M. Haardt, "Prolonged Ad-hoc Network Lifetime using a Distributed Clustering Scheme Based on RF Signal Strength" , *in Proc. IEEE International Conference on Communications (ICC 2012), 4th Workshop on Cooperative and Cognitive Communications (CoCoNet 4)*, Ottawa, Canada, June 2012.

- B. Zafar, S. Gherekhloo, and M. Haardt, "Impact of Synchronization Errors on Alamouti-STBC-based Cooperative MIMO Schemes", *in Proc. 7th IEEE Sensor Array and Multi-channel Signal Processing Workshop (SAM 2012)*, (New Jersey, USA), June. 2012.

- B. Zafar, S. Gherekhloo, and M. Haardt, "A joint clustering and routing algorithm to maximize link performance in cooperative MIMO ad-hoc networks", *in Proc. 22nd IEEE Symposium on Personal, Indoor, Mobile and Radio Communications (PIMRC 2011)*, (Toronto, Canada), September 2011.

- B. Zafar, S. Gherekhloo, D. Schulz, M. Haardt, and J. Seitz, "A novel multi-hop routing scheme for Ad-hoc Cooperative MIMO systems", *Proc. 26-th Meeting of the Wireless World Research Forum (WWRF 26)*, (Doha, Qatar), April 2011

- B. Zafar, D. Schulz, S. Gherekhloo, and M. Haardt, "Ad-Hoc Networking Solutions for Cooperative MIMO Multi-hop Networks", *Proc. 25-th Meet-*

ing of the Wireless World Research Forum (WWRF 25), (London, UK), November 2010

- B. Zafar, S. Gherekhloo, A. Asgharzadeh, M. T. Garrosi, and M. Haardt, "Self-Organizing Network with Intelligent Relaying (SONIR)", *Proc. 7th IEEE International Conference on Mobile Ad-hoc and Sensor Systems (IEEE MASS 2010)*, (San Francisco, USA), November 2010

Part I

An Analytical look at Relaying

Chapter 2

Multi-hop Relaying schemes involving single-antennas

2.1 Introduction

Employing relays in wireless communication networks can result in many adavantages [PWS+04], [LTW04], [HA03]. Relays can be used to extend the coverage as well as provide a greater capacity. Relays can also be used for the purpose of load balancing in areas where the network traffic is high. Wireless relaying can also reduce the transmission power consumption at the terminals and thus prolong battery life.

Different relaying strategies have been developed in the literature depending on the processing at the relays, e.g., amplify-and-forward (AF) relaying [LTW04], decode-and-forward (DF) relaying [JHHN04], and compress-and-forward relaying [KGG05]. Their capacity and performance has been studied in the literature for the multi-hop scenario using different channel models. The capacity of a Gaussian degraded relay channel (where only additive white Gaussian noise is taken into account) has been obtained in [CE79] and [EZ05]. Studying the capacity of multi-hop network in the fading environment is, however, a more interesting task. The performance of wireless relaying has been extensively studied in terms of outage probability and error rate in [HA03] [KTM06] [FB08], but very few studies have taken a look at the ergodic capacity for the case of fading relay channels. In [HMZ05], the authors have studied the upper and lower bounds of the ergodic capacity for a single relay channel. Therefore we study the ergodic capacity for the multi-hop case with Rayleigh fading in this chapter.

In this chapter, the received signal-to-noise ratio (SNR) and the ergodic capacity of relaying systems are studied considering a multi-hop wireless transmission in the presence of Rayleigh fading. To do so, distributed relays are considered between the source and the destination with Single Input Single Output (SISO) links between the relay nodes employing Amplify-and-Forward (AF) or Decode-and-Forward (DF) relaying, which are the two most popular relaying schemes. To maximize the ergodic capacity, we consider the relays to be optimally located (equidistant) and also assume that the channel statistics remain the same for all hops and the noise power is equal at all relays and terminals. Considering these assumptions, the ergodic capacity of the two aforementioned relaying schemes is analyzed and compared. This work was published by us

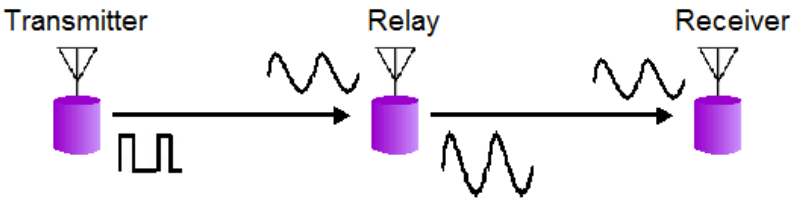

(a) AF scheme

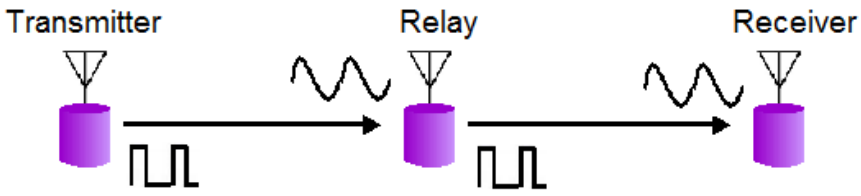

(b) DF scheme

Figure 2.1: AF and DF relaying schemes.

in [ZGS+11], [ZGH11b], [ZGH12a], [ZGH12b] and [Ghe12]. Note that in this chapter we only consider single-antenna devices. Multiple-antenna devices are considered in Chapter 3.

Considering nodes with limited transmission ranges, multi-hop relaying is a promising communication technique between a source and a destination via some relay nodes in between. In the case of a channel subject to a deep fade and limited power resources at the source, multi-hop relaying is even more interesting. In multi-hop relaying each relay processes the received signal depending on the relaying schemes in use, e.g., amplify-and-forward relaying (AF), decode-and-forward relaying (DF), or compress-and-forward relaying and then retransmits it. Because of the simplicity of the AF and DF schemes, these are of particular interest. In the AF scheme, each relay simply amplifies the received noisy signal and retransmits it to the next relay, while in the DF scheme each relay decodes the received signal and then forwards it. Figure 2.1 illustrates the AF and DF scheme.

This chapter starts by analyzing the ergodic capacity of the AF and DF relaying schemes in case of a SISO link, assuming that the channel state information of each hop is available at the corresponding terminal and the transmit power

of each relay is limited to a threshold. A closed form solution is achieved as a function of the number of the hops for the DF scheme, but in case of the AF scheme only a closed form solution in the high SNR regime is achieved. Furthermore, the performances of AF and DF schemes are compared from the ergodic capacity view-point. These analyses show this important fact that the ergodic capacity of the multi-hop transmission can be increased in the high SNR regime by decreasing the number of hops (as long as the quality-of-service requirements are fulfilled).

In multi-hop networks, the direct transmission between the source (TX) and the destination (RX) is so weak that some relays have to be employed on the path between the source and the destination to aid in the communication. Figure 3.1 illustrates the model of the multi-hop relaying between the transmitter and the receiver over M hops using SISO links between the relays.

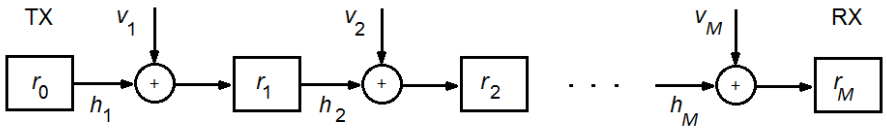

Figure 2.2: The relaying model in multi-hop scenarios.

The received signal at the ith relay is given by

$$y_i = \sqrt{P_s} \cdot h_i \cdot x_{i-1} + \nu_i, \quad i = 1, 2, \cdots, M \tag{2.1}$$

where

P_s	is the transmit power of the nodes
x_{i-1}	is the signal transmitted by the $(i-1)$th relay
h_i	is the coefficient of the SISO quasi static frequency flat block fading channel between the $(i-1)$th and ith relay nodes
ν_i	is the Additive white Gaussian noise (AWGN) for the ith relay

Channel Model:

We consider the communication to be affected by AWGN and Rayleigh fading. The channel h_i is modeled by independent identically distributed zero mean circularly symmetric complex Gaussian (ZMCSCG) random variables with variance σ_i^2. The noise ν_i is also modeled as ZMCSCG. Note that the transmit power of the relays is assumed constant and does not change by changing the number of hops. We do not consider the effect of shadowing in our analysis to simplify the problem at hand. So our channel is affected only by fast fading and the path gain. The variance of h_i denotes the power of the channel which depends on the path gain as the variance of the fast fading is 1. The variance of the noise (σ_ν^2) is assumed to be the same for all of the relay nodes. It is assumed that all the relay nodes are located equidistant to each other and on a straight line between the transmitter and the receiver. Therefore the channel variance (average path gain) of all the hops is the same. From Friis transmission equation:

$$\xi = G_r G_t \left(\frac{\lambda}{4\pi R}\right)^{\alpha}, \tag{2.2}$$

where

ξ	is the path gain
G_r	is the antenna gain of the receiver
G_t	is the antenna gain of the transmitter
λ	is the wavelength
R	is the distance between the transmitter and the receiver
α	is the path loss exponent

If d is the distance between the transmitter and the receiver in Figure 3.1, and there is a total of M hops, then the distance between any two relays is d/M. If h_D denotes the direct channel between source and destination, then the path gain corresponding to it (ξ_D) is given by

$$\xi_D = G_r G_t \left(\frac{\lambda}{4\pi d}\right)^{\alpha}, \tag{2.3}$$

and the path gain on each of the M hops (ξ_M) is given by

$$\xi_M = \mathbb{E}_h\{|h_i|^2\} = G_r G_t \left(\frac{M\lambda}{4\pi d}\right)^{\alpha}, \quad i = 1, 2, \cdots, M \tag{2.4}$$

where

$\mathbb{E}\{\cdot\}$:	is the statistical expectation
$\lvert\cdot\rvert$	is the magnitude of a complex number

Also, because the statistics of the channels for all the hops are the same, the subscript of h, which refers to the hop-number, can be dropped, i.e.,

$$\mathbb{E}_h\{|h_i|^2\} = \mathbb{E}_h\{|h|^2\} = \xi_M = \xi_D \cdot M^{\alpha}, \quad i = 1, 2, \cdots, M \tag{2.5}$$

As equation (2.5) implies, increasing the number of hops decreases the distance between the relay nodes which increases the path gain. The maximum number of the hops can be defined considering a reference distance in order to express the path loss of a channel. In other words, the length of all the hops is the same as the reference distance and the channel variance of each hop is 1, using the maximum number of the hops. By considering a reference distance to describe the path loss of the channel, we can define the maximum number of hops. If the maximum number of hops which can be used in the transmission is denoted by $\hat{M}$, then using (2.5), we can write

$$\frac{\xi_M}{\xi_{\hat{M}}} = \frac{M^{\alpha} \cdot \xi_D}{\hat{M}^{\alpha} \cdot \xi_D} = \left(\frac{M}{\hat{M}}\right)^{\alpha}.$$

Using the maximum number of hops, the path gain will be 1 ($\xi_{\hat{M}} = 1$) i.e. so many relay nodes are employed that the channels do not deteriorate the signal power. Therefore, ξ_M can be written as

$$\xi_M = \left(\frac{M}{\hat{M}}\right)^{\alpha} \tag{2.6}$$

Because the channels are all modeled as ZMCSCG, it can be concluded that the channel's magnitude distribution is Chi-squared with 2 degrees of freedom. If q denotes $|h|^2$, the Probability Density Function (PDF) and Cumulative Dis-

tribution Function (CDF) of $q \sim \chi_2^2$ for $q \in [0, \infty)$ can be written as

$$f_Q(q) = \frac{1}{\xi_M} \cdot \exp\left(-\frac{q}{\xi_M}\right)$$
$$F_Q(q) = 1 - \exp\left(-\frac{q}{\xi_M}\right). \tag{2.7}$$

The instantaneous channel state information (CSI) of h_i is known at the next relay node r_i. With the aid of the known CSI at the relay, the channel phase is compensated at the relay nodes. Depending on the relaying scheme, the relay nodes do some processing on the received signal before forwarding the signal to the next relay node and this chapter focuses on the AF and DF relaying scheme.

The channel capacity defines the maximum amount of information that can be reliably transmitted over a communication channel. Therefore it is possible to compare the designed systems with this theoretical upper bound. The ergodic capacity is considered as a parameter to study the multi-hop network as it gives a very good indication of the performance of wireless systems [SW48].

2.2 Analysis of capacity for Amplify and forward relaying (AF)

In the AF (Amplify and Forward) transmission technique, the receiver node amplifies the signal after compensating the channel phase and sends it on to the next node, without any other processing. In AF relaying, at the ith relay node, the signal is amplified by an amplification factor of A_i before transmission to the next relay. The amplification gain is a function of the channel corresponding to the ith hop and can be written as

$$A_i = \sqrt{\frac{P_s}{P_s |h_i|^2 + \sigma_\nu^2}}. \tag{2.8}$$

where P_s is the average transmit power of the node, which is assumed to be the same for all of the relays. It should be considered that the relay nodes amplify the

noisy received signal and as a result the noise component is also amplified. The received signal at the destination after forwarding over M hops can be written as

$$y_{\text{rx}} = \underbrace{\sqrt{P_s} \cdot x \prod_{i=1}^{M} A_i \cdot |h_i|}_{\text{signal component}} + \underbrace{\sum_{i=1}^{M-1} A_i \cdot \nu_i \prod_{k=i+1}^{M} A_k \cdot |h_k| + A_M \cdot \nu_M}_{\text{total noise}}, \tag{2.9}$$

where x is the unit-power signal transmitted by the source.

Based on (2.9), the power of the signal component can be written as

$$P_{\text{sig}} = P_s \cdot \mathbb{E}\left\{ \prod_{i=1}^{M} A_i^2 \cdot |h_i|^2 \right\}. \tag{2.10}$$

and assuming that the relay noise $\{\nu_i\}_{i=1}^{M}$, and the channel coefficients $\{h_i\}_{i=1}^{M}$ are independent from each other, $A_i = A$, and

$$\mathbb{E}\left\{A_i^2 |h_i|^2\right\} = \mathbb{E}\left\{A^2 |h|^2\right\}, \quad i = 1, 2, \cdots, M.$$

The power of the signal component can be obtained as

$$P_{\text{sig}} = P_s \, \mathbb{E}\{A^2 |h|^2\}^M. \tag{2.11}$$

The noise power can be written as,

$$P_n = \mathbb{E}\left\{ \left| \sum_{i=1}^{M-1} A_i \nu_i \prod_{k=i+1}^{M} A_k h_k + A_M \nu_M \right|^2 \right\}$$

$$P_n = \sigma_\nu^2 \left[\mathbb{E}\{A_M^2\} + \sum_{i=1}^{M-1} \mathbb{E}\{A_i^2\} \mathbb{E}\{A_i^2 |h|^2\}^{M-i} \right]$$

Using the change of variable: $\mathbb{E}\{A_i^2\} = G_M$, for $i = 1, 2, \cdots, M$, we get

$$P_n = \sigma_\nu^2 \, G_M \left[1 + \sum_{i=1}^{M-1} \mathbb{E}\{A^2|h|^2\}^{M-i} \right]$$

By using the geometric series we can simplify the equation of the noise power as

$$P_n = \sigma_\nu^2 G_M \frac{1 - \mathbb{E}\{A^2|h|^2\}^M}{1 - \mathbb{E}\{A^2|h|^2\}} \tag{2.12}$$

If β denotes $E\{A^2|h|^2\}$, the received SNR after multi-hopping ($\text{SNR}|_{\text{mh,rx}}$) can be writen as

$$\text{SNR}|_{\text{mh,rx}} = \frac{P \, \beta^M (1-\beta)}{\sigma_\nu^2 \, G_M (1-\beta^M)}. \tag{2.13}$$

The SNR after the single-hop direct channel communication ($\text{SNR}|_{\text{sh,rx}}$) is given by P/σ_ν^2, so we can write

$$\frac{\text{SNR}|_{\text{mh,rx}}}{\text{SNR}|_{\text{sh,rx}}} = \frac{\beta^M (1-\beta)}{G_M (1-\beta^M)}. \tag{2.14}$$

For the special case of no fading and high SNR ($P \gg \sigma_\nu^2$), β goes to one, because β denotes $E\{A^2|h|^2\}$ and for $P \gg \sigma_\nu^2$ equation (2.8) becomes

$$A_i = \frac{1}{|h_i|}. \tag{2.15}$$

and using equation (2.5), we can write

$$G_M = \mathbb{E}\{A_i^2\} = \frac{1}{\mathbb{E}\{|h|^2\}} = M^{-\alpha}, \quad i = 1, 2, \cdots, M. \tag{2.16}$$

Note that the number of the hops in the multi-hop network is considered as M. If β approaches one, $\frac{1-\beta^M}{(1-\beta)\beta^M}$ approaches M. This is obtained using the de l'Hopital's rule as follows

$$\frac{\partial \left(\frac{1-\beta^M}{\beta^M - \beta^{M+1}} \right)}{\partial \beta} = \frac{-M\beta^{M-1}}{M\beta^{M-1} - (M+1)\beta^M} = M, \quad \beta = 1. \tag{2.17}$$

So for the special case of $\beta = 1$, equation (2.14) becomes

$$\frac{\text{SNR}|_{\text{mh,rx}}}{\text{SNR}|_{\text{sh,rx}}} = \frac{1}{MG_M}. \tag{2.18}$$

Using equation (2.16), the ratio of the SNR in the multi-hop relaying with M hops (the distance between the relays is d/M) to the SNR in the single-hop transmission in the high SNR regime can be written as

$$\frac{\text{SNR}|_M^{\text{AF}}}{\text{SNR}|_1^{\text{AF}}} = M^{\alpha-1}. \tag{2.19}$$

Equation (2.19) shows that for $\beta = 1$ and $\alpha = 2$, increasing the number of hops gives us a gain equal to M. This enhancement can be decreased if β is different from one. In the worst case multi hoping can even decay the performance. Figure 2.3 illustrates the received SNR as a function of the number of hops for the fading channels and different ratios of (P/σ_ν^2).

Based on the calculated SNR the ergodic capacity of the multi-hop AF transmission based on the equidistant model is

$$C_{AF} = \frac{1}{M}\log_2\left(1 + \underbrace{\frac{P\,\beta^M(1-\beta)}{\sigma_\nu^2\,G_M(1-\beta^M)}}_{\text{SNR at the Rx}}\right) \tag{2.20}$$

As it was shown, in the ideal case, the SNR will increase linearly with the increasing number of hops. The ergodic capacity, however, increases logarithmically with the SNR but decreases linearly with the number of hops. Figure 2.4 shows the ergodic capacity of the channel, expressed in equation (2.20) as a function of the number of hops.

On the other hand, the ergodic capacity decreases linearly with the number of the hops because of the increased number of retransmissions. Therefore, it can be concluded that an increase in the number of the hops yields a decrease in the ergodic capacity of the transmission in the high SNR regime. In order to analyze the capacity in the low SNR regime, a simulation has been done for different values of the path loss exponent α because a change in the environmental

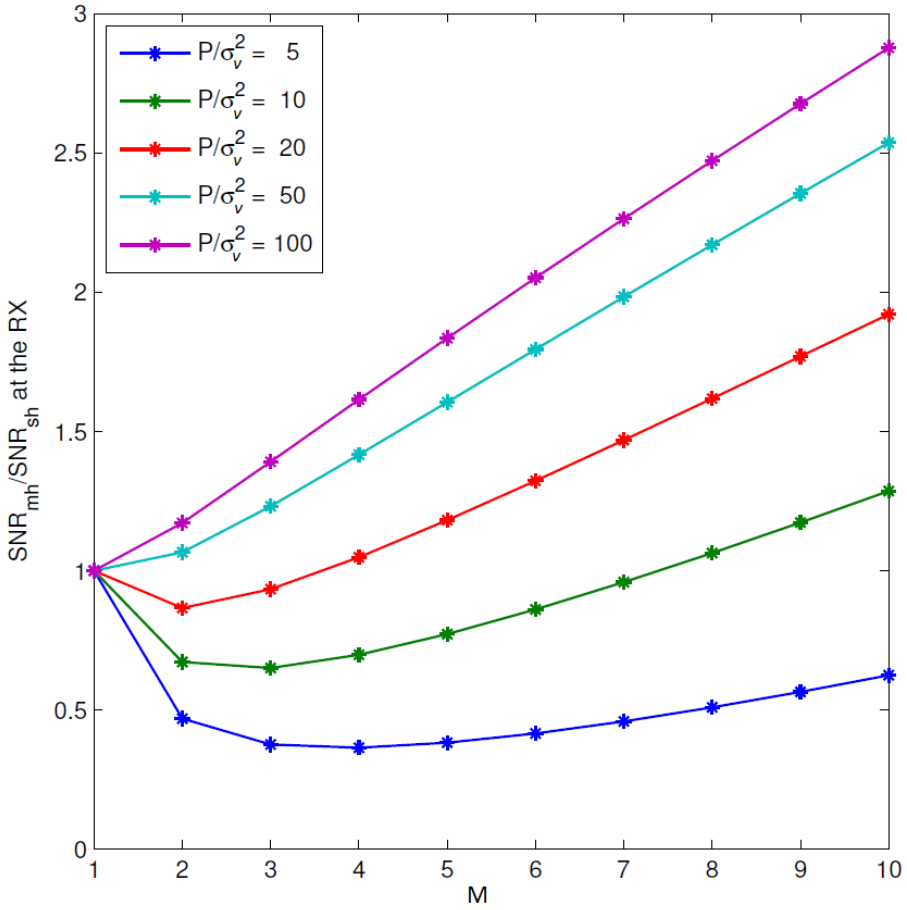

Figure 2.3: Received SNR as a function of the number of hops (BPSK modulation and $\alpha = 2$).

conditions, e.g., the path loss exponent, can influence the results. The ergodic capacity of the channel as a function of the transmission power in case of different numbers of hops is shown Figure 2.5.

The analysis points to a common misconception that shorter hops, by employing more relay nodes, result in an increased performance. While it is true that the received SNR for each hop is better in that case, the increased number of re-transmissions due to multi-hopping translates into a linear decrease in the throughput capacity of the multi-hop link which overtakes the logarithmic increase in capacity due to the increased SNR, and in the end we are left with a reduced overall performance. Note that in this analysis we have not considered

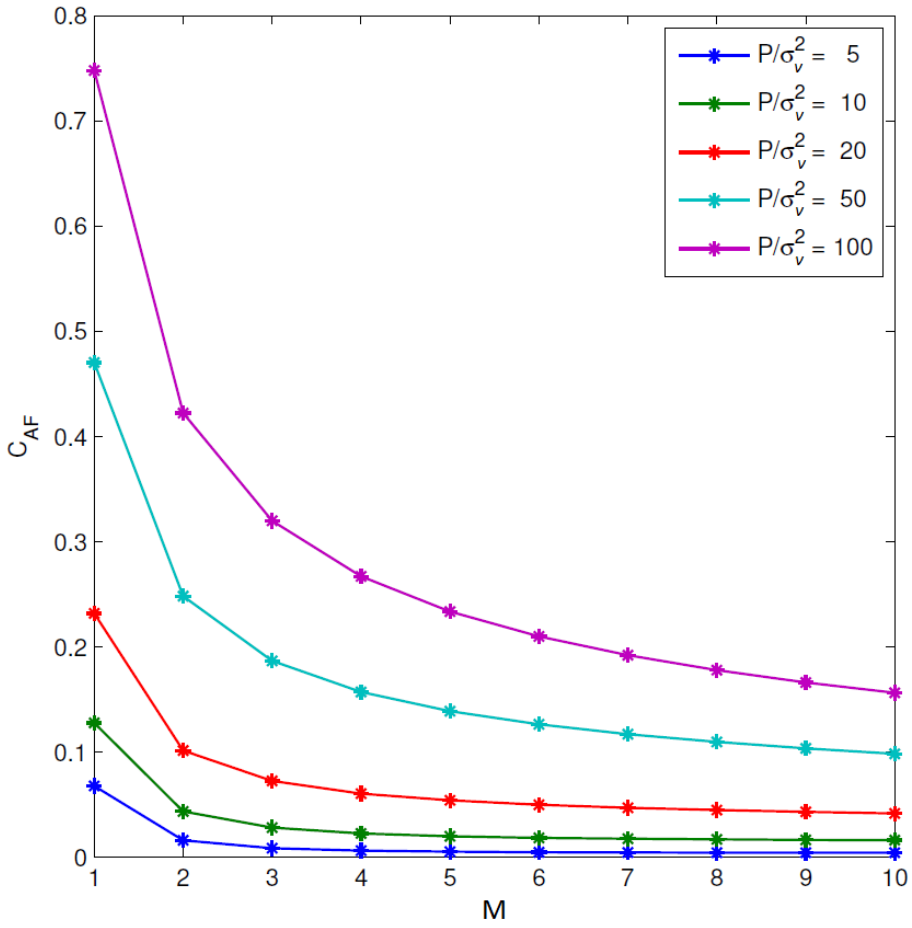

Figure 2.4: Ergodic capacity (bits/sec/Hz) of the channel as a function of the number of hops (BPSK modulation and $\alpha = 2$).

the re-use of resources. Re-using the resources, such as frequency bands used for transmission, for simultaneous interference-free transmissions will reduce this linear decrease due to re-transmsissions. On the other hand, increasing the number of the hops can increase the capacity in the low SNR regime, as depicted in Figure 2.5(b). If the path loss exponent is high, e.g., in an indoor environment, this phenomenon becomes more noticeable.

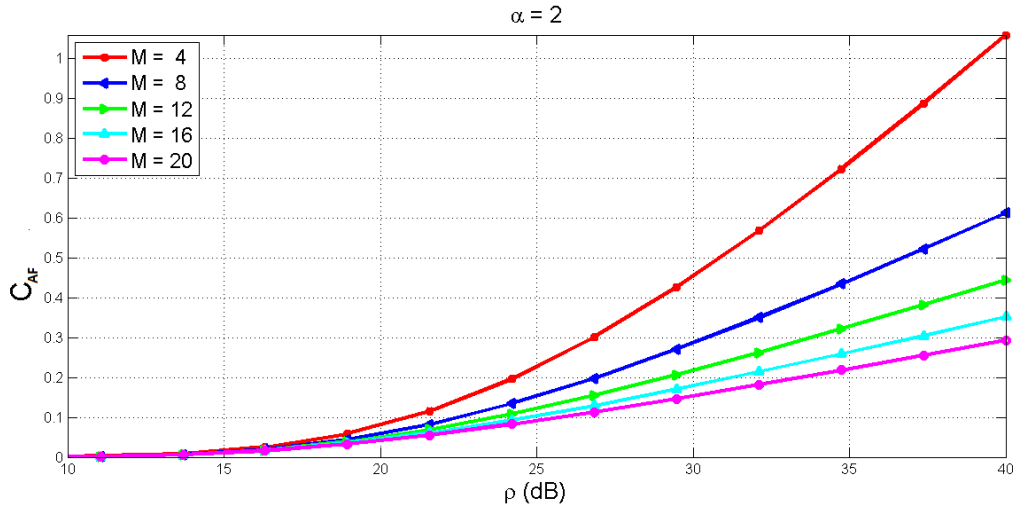

(a)

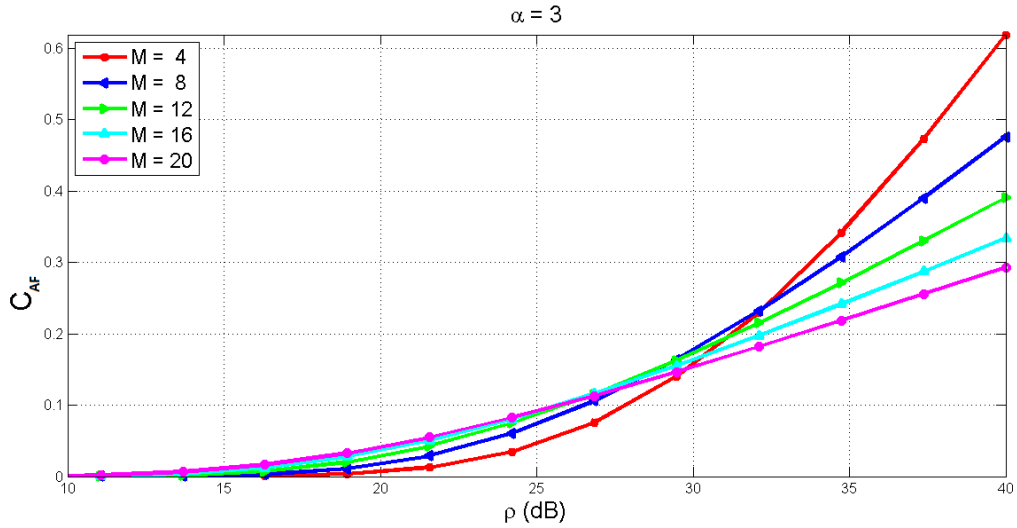

(b)

Figure 2.5: Ergodic capacity (bits/sec/Hz) of the channel in case of different numbers of hops (M) in the AF relaying scenario considering that the maximum number of hops ($\hat{M}$) is 20, where $\rho = P_s/\sigma_\nu^2$ and BPSK modulation is used. (α is the path loss exponent)

2.3 Analysis of capacity for Decode and forward relaying (DF)

In case of DF transmission, the relay nodes fully decode the received signal, and re-encode it before the transmission. Using the result in [CE79], the overall system capacity cannot be larger than the capacity of each hop. Therefore, the ergodic capacity of the DF relay network with M hops is written as

$$C_{\mathrm{DF}} = \frac{1}{M} \cdot \mathbb{E}\left\{\min\{c_1, c_2, \ldots, c_M\}\right\}, \tag{2.21}$$

where c_i is the channel capacity of the ith hop. The instantaneous capacity of ith hop is expressed as

$$c_i = \log_2\left(1 + \frac{P_s}{\sigma_\nu^2}|h_i|^2\right). \tag{2.22}$$

Considering equidistant relays and the same distribution for all channels h_i ($i = 1, 2, \cdots, M$), the distribution of the instantaneous channel capacity of all hops will be the same. For simplicity in writing the equations, we use c' to denote the instantaneous channel capacity. Using this notation, we derive the distribution of c', which is the same for all hops. If q denotes $|h_i|^2$, the CDF of $c' = \log_2(1+\rho\cdot q)$, where $\rho = P_s/\sigma_\nu^2$, can be written as

$$\begin{aligned} F_{C'}(c') &= P\left(\log_2\left(1+\rho\cdot q\right) \le c'\right) \\ &= P\left(q \le \frac{2^{c'}-1}{\rho}\right) \\ &= F_Q\left(\frac{2^{c'}-1}{\rho}\right). \end{aligned}$$

Using equation (2.7), we can rewrite the CDF of c' as

$$F_{C'}(c') = \begin{cases} 1 - \exp\left(-\frac{2^{c'}-1}{\rho\cdot V}\right) & \text{if } c' \ge 0 \\ 0 & \text{if } c' < 0 \end{cases} \tag{2.23}$$

It is clear that $c' \in [0, \infty)$, and $F_{C'}(0) = 0$, and $F_{C'}(\infty) = 1$. By forming the derivative of the CDF with respect to c', we can get the PDF as

$$f_{C'}(c') = \exp\left(-\frac{2^{c'}-1}{\rho \cdot V}\right) \frac{2^{c'} \cdot \ln(2)}{\rho \cdot V}. \tag{2.24}$$

where $\rho = P_s/\sigma_\nu^2$. Next, we find the distribution of $C_{\mathrm{DF}} = \frac{1}{M}\min\{c_1, c_2, \ldots, c_M\}$. It is obvious that $M \cdot C_{\mathrm{DF}} = c_i$, if $c_i \leq c_k$, where $k = \{1, 2, \ldots, i-1, i+1, \ldots, M\}$. This can be expressed as

$$P(M \cdot C_{\mathrm{DF}} = c_i) = P(c_i) \cdot \prod_{\substack{k=1 \\ i \neq k}}^{M} P(c_i \geq c_k),$$

and the PDF of $c'' = M \cdot C_{\mathrm{DF}}$ can be expressed as

$$\begin{aligned} f_{C''}(c'') &= P(c'') \cdot \prod_{\substack{k=1 \\ i \neq k}}^{M} P(c'' \leq c') \\ &== P(c'') \cdot \prod_{\substack{k=1 \\ i \neq k}}^{M} (1 - P(c' \leq c'')) \\ &= \sum_{i=1}^{M} f_{C'}(c'') \prod_{\substack{l=1 \\ l \neq i}}^{M} (1 - F_{C'}(c'')) \\ &= \frac{2^{c''} \cdot \ln(2) \cdot M}{\rho \cdot V} \exp\left(-M \frac{2^{c''}-1}{\rho \cdot V}\right). \end{aligned} \tag{2.25}$$

Using the PDF of c'', the average of C_{DF} is obtained as

$$\begin{aligned} \mathbb{E}\{C_{\mathrm{DF}}\} &= \frac{1}{M} \int_0^\infty c'' \cdot f_{C''}(c'') dc'' \\ &= -\frac{\mathrm{Ei}\left(\frac{-M}{\rho \cdot V}\right) \cdot \exp\left(\frac{M}{\rho \cdot V}\right)}{M \cdot \ln(2)}, \end{aligned} \tag{2.26}$$

where $\mathrm{Ei}(x)$ denotes the exponential integral given by

$$\mathrm{Ei}(x) = \int_{-\infty}^{x} \frac{\exp(-t)}{t}\, dt$$

and

$$\frac{\partial \mathrm{Ei}(x)}{\partial x} = \frac{\exp(x)}{x} \tag{2.27}$$

It is interesting to understand analytically, how the ergodic capacity changes with respect to the number of hops. It is true that number of hops is a natural number, but for simplicity, we assume that M is a real positive number. Therefore, remembering that $V = \left(\frac{M}{\hat{M}}\right)^{\alpha}$, we calculate the derivative of $\mathbb{E}\{C_{\mathrm{DF}}\}$ with respect to M as

$$\frac{\partial \mathbb{E}\{C_{\mathrm{DF}}\}}{\partial M} = \frac{\exp\left(\frac{\hat{M}^{\alpha}}{\rho \cdot M^{(\alpha-1)}}\right) \cdot \mathrm{Ei}\left(-\frac{\hat{M}^{\alpha}}{\rho \cdot M^{(\alpha-1)}}\right) \cdot \left[\frac{\hat{M}^{\alpha}}{\rho \cdot M^{(\alpha-1)}} \cdot (\alpha-1) + 1\right] + (\alpha-1)}{(M^2 \cdot \ln(2))}. \tag{2.28}$$

By studying the sign of (2.28), we figure out that the equation (2.28) is negative in the high SNR regime, and it is independent of the choice of α. However in the low SNR regime, the choice of α plays a decisive role in determining the sign of the equation (2.28). This phenomenon is shown is Figure 2.6, where $x = \frac{\hat{M}}{\sqrt[\alpha-1]{\rho} \cdot M}$.

Figure 2.6 shows that in the very low SNR regime, changing the number of hops cannot result in an improvement in the performance of the transmission, while in the high SNR regime, increasing the number of hops can increase the performance, if the environment imposes a high value of the path loss exponent. Figure 2.7 also confirms this conclusion. In this figure the analytical result of $\mathbb{E}\{C_{\mathrm{DF}}\}$ versus ρ is illustrated for different numbers of hops and for different values of α by using the equation (2.26).

The analysis of the ergodic capacity for the DF scheme has shown the fact that improving the performance of the transmission by changing the number of hops depends on different factors such as the SNR regime, the path loss exponent and the distance between the transmitter and the destination. In the non-line-

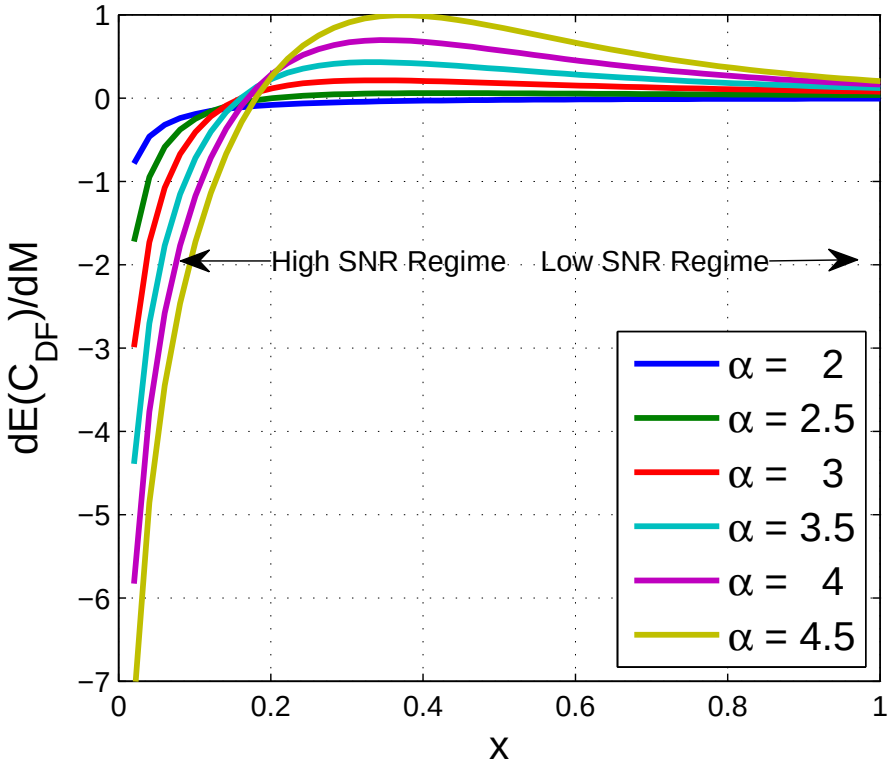

Figure 2.6: The differentiation of $\mathbb{E}\{C_{DF}\}$ with respect to M, where $x = \frac{\hat{M}}{\alpha - \sqrt[1]{\rho} \cdot M}$ and $\hat{M} = 10$.

of-sight case or relatively lossy environments (high value of α) the reliability of the transmission in the low SNR regime is improved by using more hops, while in the high SNR regime it is always more reliable to decrease the number of hops without the need for taking any environmental conditions into consideration.

2.4 Comparison of AF and DF relaying schemes

After analyzing the ergodic capacity of the AF and DF relaying schemes in the last two sections, it is possible to compare these two relaying schemes from the

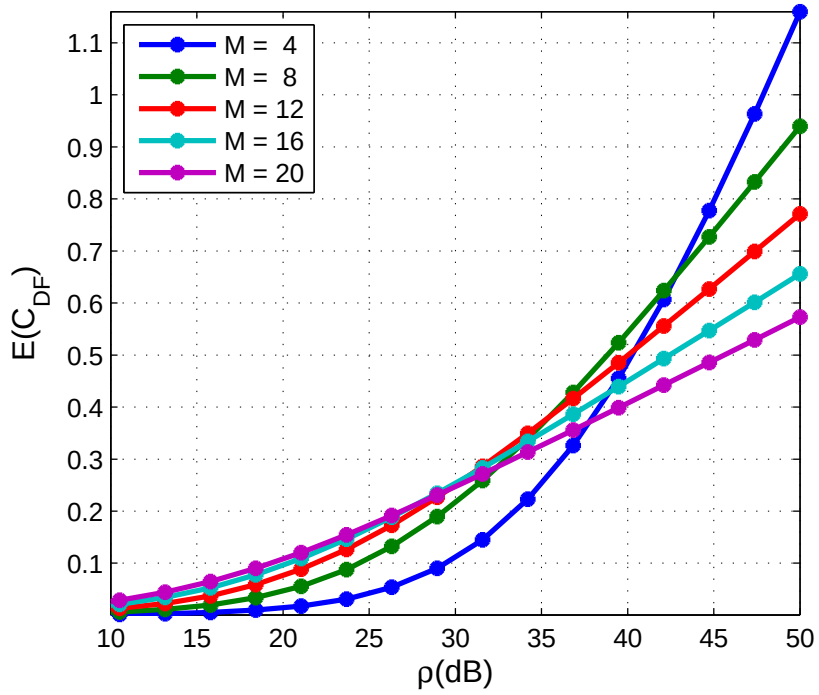

(a) $\alpha = 4$

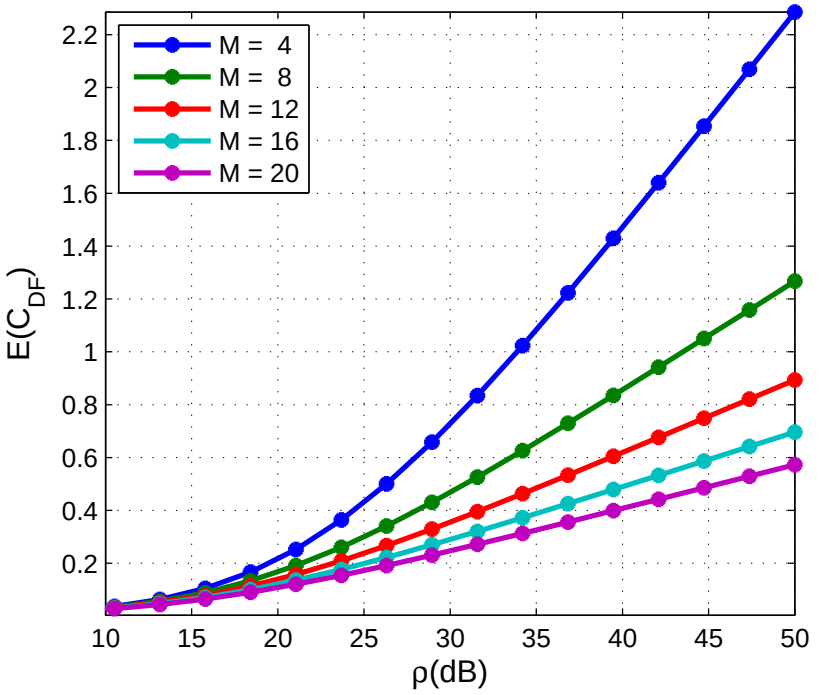

(b) $\alpha = 2$

Figure 2.7: Analytical result of $\mathbb{E}\{C_{\mathrm{DF}}\}$ versus $\rho = P_s/\sigma_\nu^2$ for different numbers of hops, different path loss exponents (α) and BPSK modulation.

capacity point of view. We know that the capacity for the DF scheme is given by

$$\begin{aligned} C_{\mathrm{DF}} &= \frac{1}{M} \min\{c_1, c_2, \ldots, c_M\} \\ &= \frac{1}{M} \log_2 \left(1 + \min\{\gamma_1, \gamma_2, \ldots, \gamma_M\}\right), \end{aligned}$$

where γ_i denotes the received SNR for the ith hop and c_i is the channel capacity of the ith hop. The ergodic capacity for the AF scheme is given by

$$C_{\mathrm{AF}} = \frac{1}{M} \log_2 \left(1 + \gamma_{\mathrm{total}}\right),$$

where γ_{total} stands for the received SNR at the destination. It is shown for the AF scheme that the relays amplify the received noisy signal. Therefore, the SNR is not changed after amplifying. On the other hand, the amplified signal is attenuated over the channel towards the next relay, and the antenna at the relay adds some noise to the received attenuated signal. Therefore, the received SNR decreases by forwarding over the hops. Let the kth hop be the weakest hop between the source and the destination for the DF scheme. Considering the aforementioned facts about the AF scheme, one can easily show that $\gamma_{\mathrm{total}} \leq \gamma_k$ and

$$\begin{aligned} C_{\mathrm{DF}} &= \frac{1}{M} \log_2 \left(1 + \min\{\gamma_k\}\right) \\ C_{\mathrm{DF}} &\geq C_{\mathrm{AF}}. \end{aligned} \tag{2.29}$$

This comparison is also shown through a simulation for different number of hops and a varying transmit power of the nodes. The result of the simulation is illustrated in Figure 2.8.

2.5 Conclusions

The results presented in this chapter are of importance to network designers as we move towards the standardization of cooperative multi-hop networks. The analytical results can help to determine the thresholds at which nodes can switch between different modes of transmission, such as the relaying scheme, and the

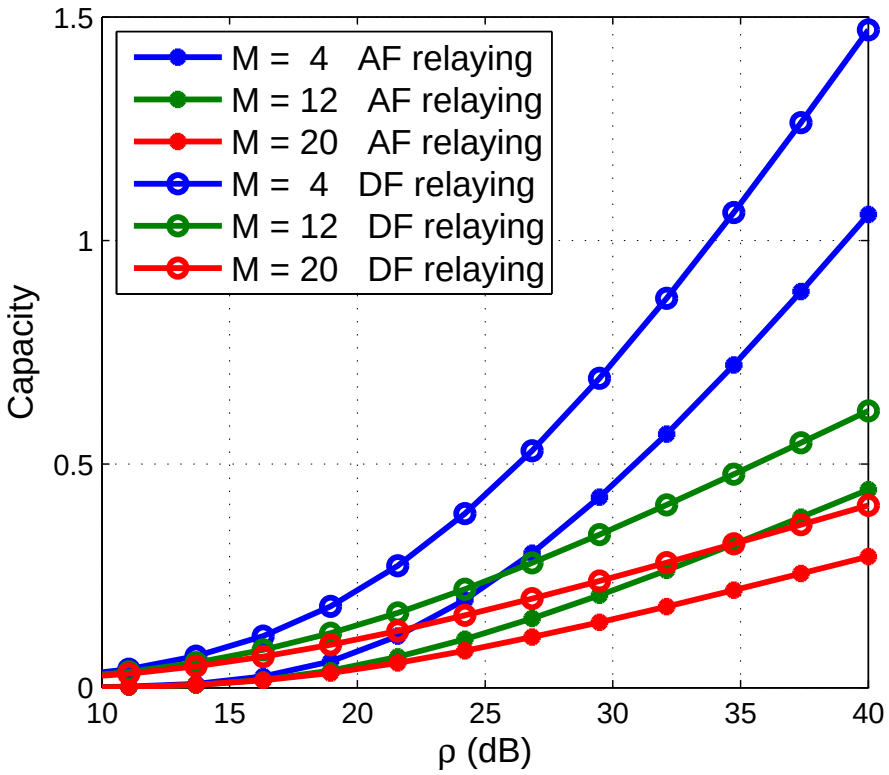

Figure 2.8: Comparison of AF and DF scheme from ergodic capacity (bits/sec/Hz) point of view considering different numbers of hops where $\rho = P_s/\sigma_\nu^2$ (using BPSK modulation and $\alpha = 2$).

appropriate number of hops to ensure the QoS.

The ergodic capacity has been studied in case of the most popular relaying schemes of the multi-hop network (AF and DF relaying schemes). An optimum multi-hop network (equidistant relays) was assumed, in which the variances of the channels of all the hops is the same and the antennas at the relays are identical. The analysis of the ergodic capacity for both relaying schemes has identified that in the high SNR regime, decreasing the number of the hops yields an increase in the performance of the transmission. But in case of the low SNR regime, the environmental factors, e.g., the path loss exponent and the distance between the source and the destination have to be considered before increasing or decreasing the number of the hops in order to improve the performance of the network. In case of an environment which has a large path loss exponent, decreasing the

number of the hops decays the performance in the low SNR regime. Using the AF relaying scheme, as a result of transmitting the signal over more hops in the low SNR regime, the received SNR is decreased, because of the fact that by amplifying the received signal the noise component is also amplified. But using more hops in the high SNR regime increases the received SNR. Comparing AF and DF relaying schemes, it has been observed that the DF relaying scheme provides higher ergodic capacity than the AF relaying scheme using the same number of hops.

For future work, it would be interesting to evaluate these relaying schemes in the presence of interference from external users and from those within the network. In the analysis presented in this chapter we have only considered single active multi-hop communication links at a time. Also, it would be essential to have a look at the overall network throughput instead of looking at only the link throughput and future work should take into account the effect of error propagation in the DF relaying scheme.

It is important to point out here that we are assuming that new resources such as frequency are considered to be used for each hop. A future analysis that takes into account frequency re-use will yield an even better spectral efficiency.

Chapter 3

Relaying schemes involving multiple co-located antennas

3.1 Introduction

We have shown in the last chapter that reducing the number of hops improves the performance of the transmission, especially in the high SNR regime, for SISO links between relays. However, reducing the number of hops also causes an increased BER and thereby a drop in the quality of service (QoS) at the destination. One attractive method for reducing the number of hops and ensuring the QoS is to employ additional antennas at the transmitter and/or at the receiver side and/or at the relays. By using more antennas we can extract the benefits of the MIMO channels, and increase the range of the transmission. Space-time coding and beamforming are among the most popular techniques for increasing the diversity of multiple-antenna systems [Jaf05], [HTR03]. Orthogonal space time block codes (STBC) have been introduced in [TJC99] and [TSC98]. If channel knowledge is not available at the transmitter but perfect CSI is available at the destination, STBC is the most suitable and accepted technique in order to increase the diversity. Further work has been done in [LW03], [CH03], and [CGB04] to increase the networks reliability when employing space-time codes between the relay nodes. In [WZHM05], the lower and upper bounds of the ergodic capacity have been derived considering multiple input multiple output (MIMO) single relay channels in Rayleigh fading. We felt that there was a lack of simplified expressions for the SER (symbol error rate) in the literature for the MIMO, the single input multiple output (SIMO), and the single input single output (SISO) cases, that can be conveniently used to compare the effects of different configurations, e.g., different numbers of hops, different transmit energies of nodes, different number of transmit antennas, and different number of receive antennas, on the performance of the multi-hop scheme. This chapter addresses this issue. This work was published by us in [ZGH12a], [ZGH12b] and [Ghe12].

The goal of this chapter is to study the performance of the transmission over an optimum multi-hop route (using equidistant relays, as discussed in the last chapter) which is found based on MIMO, single input multiple output (SIMO) and SISO links. We assume that the number of transmit and receive antennas is the same for all the hops. Moreover, antenna selection methods for the transmit antennas are not considered in this work. The decode-and-forward (DF)

relaying scheme is used and channel state information (CSI) is not needed at the transmitter. We evaluate the wireless communications scenarios in the presence of Rayleigh fading and assume non-correlated channels. For simplicity, we do not consider more than two antennas at the transmitter side, and we study only the Alamouti STBCs (Space-Time Block Codes)-based scheme for the MIMO multi-hop network. This chapter only looks at devices with co-located multiple antennas. Cooperative (virtual) multiple antenna schemes are considered in the next chapter.

3.2 Number of receive antennas and number of hops

3.2.1 Optimum multi-hop network

Assuming that we can put the relay nodes wherever required between the transmitter and the destination and that the number of antennas at the relay nodes is not limited, we can generate a multi-hop network for a varying number of transmit and receive antennas. This multi-hop network is optimum in terms of the number of hops because we use the smallest number of hops for a given threshold of the QoS (Quality of Service). The QoS in this chapter relates to ensuring that the bit error rate (BER) does not exceed a certain threshold.

Figure 3.1 illustrates the model of the multi-hop relaying between transmitter and receiver over M hops. It is similar to the model used in the last chapter except here the relays can be equipped with multiple antennas.

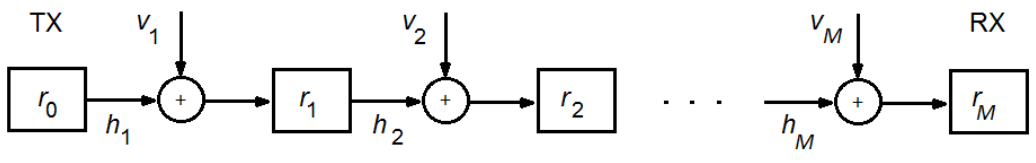

Figure 3.1: The model of relaying for multi-hop scenarios.

Assuming that the average of the loss of the channels of all hops and the noise at the relays are identical, the SER (Symbol Error Rate) is the same for all hops.

The SER at the destination is written as

$$\mathrm{SER}_{\mathrm{total}} = 1 - (1 - \mathrm{SER})^{M}\,, \tag{3.1}$$

where M and SER denote the number of required hops and the symbol error rate of one hop, respectively. Let $\mathrm{SER}_{\mathrm{th}}$ denotes the maximum allowable symbol error rate at the destination. In other words, $\mathrm{SER}_{\mathrm{th}}$ is the given threshold for the QoS. Now the goal is to find the minimum number of required hops under this SER constraint.

In general, for maximum-likelihood estimation, the probability of the SER in additive white Gaussian noise channel can be approximated as

$$\mathrm{SER} \approx \frac{\bar{N}_e}{2} \cdot \mathrm{erfc}\left(\frac{d_{\min}}{2 \cdot \sqrt{\sigma_\nu^2}}\right) = \bar{N}_e \cdot Q\left(\sqrt{\frac{d_{\min}^2}{2 \cdot \sigma_\nu^2}}\right), \tag{3.2}$$

where

Q	is the Q-function which is the tail probability of the standard normal distribution
$\bar{N}_e$	is the number of nearest neighbors
$d_{\min}$	is the minimum Euclidean distance of underlying constellation
$\sigma_\nu^2/2$	is the noise power spectral density

The Q-function is

$$\mathrm{Q}(x) = \frac{1}{2} \cdot \mathrm{erfc}\left(\frac{x}{\sqrt{2}}\right) \tag{3.3}$$

where

$$\mathrm{erfc}(x) = \frac{2}{\sqrt{\pi}} \cdot \int_x^\infty \exp(-a^2)\, da$$

We assume that P_s is the transmit power per symbol and $\tilde{d}_{\min} = \frac{d_{\min}}{\sqrt{P_s}}$. Then,

we can write equation (3.2) as

$$\begin{aligned} \mathrm{SER} &= \bar{N}_e \cdot Q\left(\sqrt{\frac{\tilde{d}^2_{\min} \cdot P_s}{2 \cdot \sigma^2_\nu}}\right) \\ &= \bar{N}_e \cdot Q\left(\sqrt{\frac{\tilde{d}^2_{\min} \cdot \rho}{2}}\right) \end{aligned} \tag{3.4}$$

where $\rho = \frac{P_s}{\sigma^2_\nu}$ is the average SNR at the receiver. Assuming a Rayleigh fading channel with D-fold diversity, where $D = M_t \cdot M_r$ (M_t and M_r are the number of transmit and receive antennas respectively), and maximum ratio combining (MRC) at the receiver, the SER can be written as [Gol05]

$$\mathrm{SER} = \bar{N}_e \cdot Q\left(\sqrt{\frac{\tilde{d}^2_{\min} \cdot \eta}{2}}\right) \tag{3.5}$$

where η stands for the average SNR at the receiver after receive combining and is related to ρ as

$$\eta = \frac{1}{D} \sum_{i=1}^{D} |h_i|^2 \cdot \rho \tag{3.6}$$

where h_i is the Rayleigh fading channel between the transmitter and the i^{th} receiver. Then, we can employ the Chernoff bound $Q(x) \leq 1/2 \cdot \exp(-x^2/2)$ [Gol05]. Using this it is possible to bound equation (3.5), which results in

$$\mathrm{SER} \leq \frac{1}{2} \cdot \bar{N}_e \cdot \exp\left(-\frac{\eta \cdot \tilde{d}^2_{\min}}{4}\right), \tag{3.7}$$

where η stands for the average SNR at the receiver after receive combining.

If $\boldsymbol{H} \in \mathbb{C}^{M_r \times M_t}$ denotes the channel matrix whose elements are zero mean and experience correlated Rayleigh fading, we can employ the property of the

Rayleigh fading channels $\boldsymbol{H} \in \mathbb{C}^{M_r \times M_t}$ [PNG08] that

$$\mathbb{E}\{\exp(-\boldsymbol{z}^H \boldsymbol{A} \boldsymbol{z})\} = \frac{\exp\{-\boldsymbol{\mu}^H \boldsymbol{A}(\boldsymbol{I}_n + \boldsymbol{\Sigma}\boldsymbol{A})^{-1}\boldsymbol{\mu}\}}{\det(\boldsymbol{I}_n + \boldsymbol{\Sigma}\boldsymbol{A})}, \tag{3.8}$$

where

$\boldsymbol{A}$	is a Hermitian matrix
$\boldsymbol{z}$	$\sim CN(\boldsymbol{\mu}, \boldsymbol{\Sigma})$.

Using $\boldsymbol{A} = a \cdot \boldsymbol{I}_{\boldsymbol{M_r} \cdot \boldsymbol{M_t} \times \boldsymbol{M_r} \cdot \boldsymbol{M_t}}$ and $\boldsymbol{z} = \mathrm{vec}(\boldsymbol{H})$, thus $\boldsymbol{z} \sim CN(\boldsymbol{0}, \boldsymbol{R})$, we can easily write that

$$\mathbb{E}\{\exp(-a \cdot \|\boldsymbol{H}\|_F^2)\} = \prod_{i=1}^{M_t \cdot M_r} \frac{1}{1 + a \cdot \lambda_i(\boldsymbol{R})}, \tag{3.9}$$

where

a	is a real number
$\boldsymbol{R}$	is $\mathbb{E}\{\mathrm{vec}(\boldsymbol{H}) \cdot \mathrm{vec}(\boldsymbol{H}^H)\}$
$\lambda_i(\boldsymbol{R})$	is the ith eigenvalue of $\boldsymbol{R}$
$\mathrm{vec}(\boldsymbol{H})$	stacks $\boldsymbol{H}$ into a vector columnwise
$\boldsymbol{A}^H$	is the Hermitian transpose of the matrix $\boldsymbol{A}$

3.2.1.1 SISO DF multi-hop network

It is assumed that for a given P_s and a given $\mathrm{SER}_{\mathrm{th}}$, $\hat{M}$ is the maximum number of required hops. Note that this is the threshold for the whole transmission. Employing SISO links over M hops, with equidistant relays, it can be written that

$$h = \breve{h} \sqrt{\left(\frac{M}{\hat{M}}\right)^{\alpha}}, \tag{3.10}$$

where h stands for the channel between any two relays, $\breve{h}$ stands for a normalized SISO channel with $\mathbb{E}\left\{|\breve{h}|^2\right\} = 1$. And $\hat{M}$ denotes the maximum number of

hops possible (same as the last chapter). If $|\breve{h}|$ is a Rayleigh distributed random variable with unit variance, then $|\breve{h}|^2$ would be a chi-squared random variable with two degrees of freedom. The received SNR (η) at each relay is written as

$$\eta = \left(\frac{M}{\hat{M}}\right)^{\alpha} \cdot \rho \cdot |\breve{h}|^2, \tag{3.11}$$

Employing (3.11) and (3.7), for the ith hop, the upper bound of the SER can be calculated as

$$\text{SER} \leq \frac{1}{2} \cdot \bar{N}_e \cdot \exp\left(-\left(\frac{M}{\hat{M}}\right)^{\alpha} \cdot \frac{\rho \cdot |\breve{h}|^2 \cdot \tilde{d}_{\min}^2}{4}\right).$$

Employing (3.9), for $a = \left(\frac{M}{\hat{M}}\right)^{\alpha} \cdot \frac{\rho \cdot \tilde{d}_{\min}^2}{4}$ and $\lambda_i(\boldsymbol{R}) = 1$, the upper bound of the average SER for a SISO link can be written as

$$\text{SER} \leq \frac{1}{2} \cdot \bar{N}_e \cdot \left(1 + \left(\frac{M}{\hat{M}}\right)^{\alpha} \cdot \frac{\rho \cdot \tilde{d}_{\min}^2}{4}\right)^{-1}. \tag{3.12}$$

Note that for the SISO case $\boldsymbol{H}$ is a scalar and $\boldsymbol{R} = \mathbb{E}\left\{|\breve{h}|^2\right\} = 1 = \lambda_i(\boldsymbol{R})$. Equation (3.12) can be rewritten in the high SNR regime ($\rho \gg 1$) as

$$\text{SER} \leq \frac{\bar{N}_e}{2} \cdot \left(\left(\frac{M}{\hat{M}}\right)^{\alpha} \cdot \frac{\rho \cdot \tilde{d}_{\min}^2}{4}\right)^{-1}. \tag{3.13}$$

Substituting (3.13) into (3.1) gives the SER at the destination for SISO multi-hop network over M hops in the high SNR regime as

$$\text{SER}_{\text{SISO}} \leq 1 - \left(1 - \frac{\bar{N}_e}{2} \cdot \left(\left(\frac{M}{\hat{M}}\right)^{\alpha} \cdot \frac{\rho \cdot \tilde{d}_{\min}^2}{4}\right)^{-1}\right)^{M} = \text{SER}_{\text{SISO}}^{\text{bound}}. \tag{3.14}$$

3.2.1.2 SIMO DF multi-hop network

A network with SIMO channels and flat fading is considered. As a result of the optimality condition in multi-hop networks, it is assumed that all the hops have the same path loss and the received noise variance is identical for all the relay nodes. Therefore, the SER is studied for one hop and then applied for all the other ones. In the aforementioned system, the channel vector $\boldsymbol{h}$ can be written as

$$\boldsymbol{h} = \begin{bmatrix} h_1 & h_2 & \dots & h_{M_r} \end{bmatrix}^T, \tag{3.15}$$

where

M_r	is the number of receive antennas
$(\boldsymbol{A})^T$	is the transpose of a matrix $\boldsymbol{A}$

The received signal can be written as

$$\boldsymbol{y} = \sqrt{P_s} \cdot \boldsymbol{h} \cdot x + \boldsymbol{\nu}, \tag{3.16}$$

$\boldsymbol{y}$	is the received signal vector with a size $M_r \times 1$
$\boldsymbol{\nu}$	is the ZMCSCG noise with $\mathbb{E}\left\{\boldsymbol{\nu} \cdot \boldsymbol{\nu}^H\right\} = \sigma_n^2 \cdot \boldsymbol{I}_{M_r}$

Assuming that perfect channel knowledge is available at the receiver in each hop and employing maximal ratio combining (MRC), the received SNR is maximized and the received signal after maximal ratio combining (y') can be written as

$$y' = \sqrt{P_s} \cdot \boldsymbol{h}^H \cdot \boldsymbol{h} \cdot x + \boldsymbol{h}^H \cdot \boldsymbol{\nu}. \tag{3.17}$$

Considering that the noise vector $\boldsymbol{\nu}$ is white and zero mean, the received SNR

can be given by

$$\eta = \|\boldsymbol{h}\|_2^2 \cdot \rho, \tag{3.18}$$

where $\|\boldsymbol{h}\|_2$ denotes the 2-norm of $\boldsymbol{h}$. At least M hops are needed in order to generate a reliable transmission between the source and the destination. Assuming that the distance between antennas is negligible compared to the length of the hops, the path loss for each pair of transmit and receive antennas would be the same and can be normalized, which is written as

$$\boldsymbol{h} = \breve{\boldsymbol{h}} \cdot \sqrt{\left(\frac{M}{\hat{M}}\right)^{\alpha}},$$

where $\mathbb{E}\left\{|\breve{h}_i|^2\right\} = 1$ for $i = 1, 2, \cdots, M_r$. Employing (3.9), for $a = \left(\frac{M}{\hat{M}}\right)^{\alpha} \cdot \frac{\rho \cdot \tilde{d}_{\min}^2}{4}$ and $\lambda_i(\boldsymbol{R}) = 1$, the upper bound of the average SER for a SIMO link can be written as

$$\mathrm{SER} \leq \frac{\bar{N}_e}{2}\left[1 + \left(\frac{M}{\hat{M}}\right)^{\alpha} \frac{\rho \cdot \tilde{d}_{\min}^2}{4}\right]^{-M_r}. \tag{3.19}$$

In the case of the high SNR regime, equation (3.19) can be simplified to

$$\mathrm{SER} \leq \frac{\bar{N}_e}{2}\left[\left(\frac{M}{\hat{M}}\right)^{\alpha} \frac{\rho \cdot \tilde{d}_{\min}^2}{4}\right]^{-M_r}. \tag{3.20}$$

Considering (3.20) and (3.1), in the case of the high SNR regime and for a SIMO multi-hop network over M hops, the SER at the destination can be written as

$$\mathrm{SER}_{\mathrm{SIMO}} \leq 1 - \left(1 - \frac{\bar{N}_e}{2}\left[\left(\frac{M}{\hat{M}}\right)^{\alpha} \frac{\rho \cdot \tilde{d}_{\min}^2}{4}\right]^{-M_r}\right)^{M} = \mathrm{SER}_{\mathrm{SIMO}}^{\mathrm{bound}}. \tag{3.21}$$

3.2.1.3 MIMO DF multi-hop network for the Alamouti STBCs-based scheme

In this section only the Alamouti code [Ala98] is considered for the MIMO scheme. Therefore, it is assumed that there are two transmit antennas and M_r receive antennas. An example of the Alamouti scheme with two receive antennas is shown in Figure 3.2.

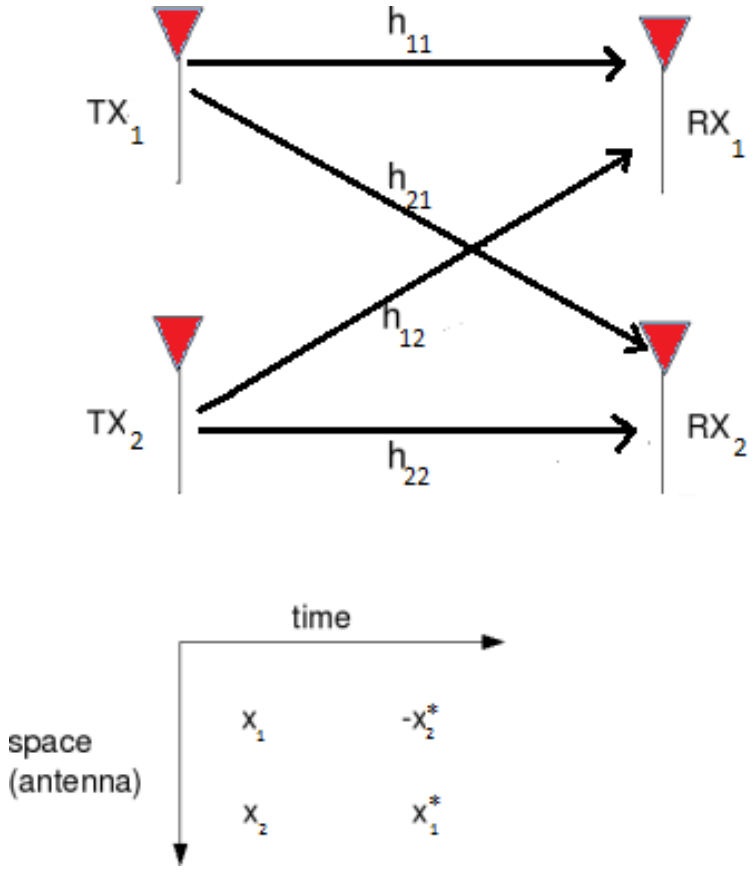

Figure 3.2: The model of relaying for multi-hop scenarios.

Similar to the analysis of the SIMO case, it is assumed that the path loss is the same for all the hops and that the noise variance (σ_ν^2) at all the antennas is the same. Therefore, the SER is studied for just one hop and the results are used for all the other ones. The channel matrix $\boldsymbol{H}$ is defined as

$$\boldsymbol{H} = \begin{bmatrix} \boldsymbol{h}_1 & \boldsymbol{h}_2 \end{bmatrix} \in \mathbb{C}^{M_r \times 2},$$

where $\boldsymbol{h}_i$ denotes the Rayleigh fading channel between the ith transmit antennas and all of the receive antennas. It is assumed that the channel is a quasi-static block fading channel. Therefore during the first and the second time interval, the received signals $\boldsymbol{y}_1$ and $\boldsymbol{y}_2$ can be written as

$$\begin{bmatrix} \boldsymbol{y}_1 & \boldsymbol{y}_2 \end{bmatrix} = \sqrt{\frac{P_s}{2}} \cdot \boldsymbol{H} \cdot \begin{bmatrix} x_1 & -x_2^* \\ x_2 & x_1^* \end{bmatrix} + \begin{bmatrix} \boldsymbol{\nu}_1 & \boldsymbol{\nu}_2 \end{bmatrix}, \tag{3.22}$$

x_i:	is the ith transmitted signal with $\mathbb{E}\{\lvert x_i\rvert^2\} = 1$
a^*:	is the complex conjugate of a
$\boldsymbol{\nu}_i$:	is the ZMCSCG noise for the ith time slot at the receiver.

Defining a new matrix $\boldsymbol{H}_{\text{eff}}$ as

$$\boldsymbol{H}_{\text{eff}} = \begin{bmatrix} \boldsymbol{h}_1 & \boldsymbol{h}_2 \\ \boldsymbol{h}_2^* & -\boldsymbol{h}_1^* \end{bmatrix} \in \mathbb{C}^{2 \cdot M_r \times 2}.$$

After combining $\boldsymbol{y}_1$ and $\boldsymbol{y}_2^*$ from equation (3.22), the received signal can be written as

$$\tilde{\boldsymbol{y}} = \sqrt{\frac{P_s}{2}} \cdot \boldsymbol{H}_{\text{eff}} \cdot \boldsymbol{x} + \tilde{\boldsymbol{\nu}}, \tag{3.23}$$

where the tilde operator is defined as $\tilde{\boldsymbol{a}} = \begin{bmatrix} \boldsymbol{a}_1^T & \boldsymbol{a}_2^H \end{bmatrix}^T$ and $\boldsymbol{x} = \begin{bmatrix} x_1 & x_2 \end{bmatrix}^T$. It is assumed that perfect channel state information is available at the receiver. Therefore the received signal after processing at the receiver side is written as

$$\boldsymbol{x}' = \sqrt{\frac{P_s}{2}} \boldsymbol{H}_{\text{eff}}^H \cdot \boldsymbol{H}_{\text{eff}} \cdot \boldsymbol{x} + \boldsymbol{H}_{\text{eff}}^H \cdot \tilde{\boldsymbol{\nu}}.$$

It is considered that M denotes the minimum number of required hops. Assuming that the distance between the antennas is negligible compared to the length of the hops, the path loss would be the same for every pair of transmit

and receive antennas. Therefore it is possible to normalize the path loss and write

$$\boldsymbol{H} = \sqrt{\left(\frac{M}{\hat{M}}\right)^{\alpha}} \cdot \breve{\boldsymbol{H}}, \tag{3.24}$$

where, if $h_{i,j}$ are the elements of $\boldsymbol{H}$, $\mathbb{E}\left\{|\breve{h}_{i,j}|^2\right\} = 1$ for $i = 1, 2$ and $j = 1, 2, \cdots, M_r$. Then, the received SNR can be calculated as

$$\eta = \frac{\rho}{2} \cdot \left(\frac{M}{\hat{M}}\right)^{\alpha} \cdot \|\breve{\boldsymbol{H}}\|_F^2. \tag{3.25}$$

Employing 3.9, for $a = \left(\frac{M}{\hat{M}}\right)^{\alpha} \cdot \frac{\rho \cdot \tilde{d}_{\min}^2}{8}$ and $\lambda_i(\boldsymbol{R}) = 1$, it is concluded that the average SER is upper bounded by

$$\text{SER} \leq \frac{\bar{N}_e}{2}\left[1 + \left(\frac{M}{\hat{M}}\right)^{\alpha} \cdot \frac{\rho \cdot \tilde{d}_{\min}^2}{8}\right]^{-2 \cdot M_r}. \tag{3.26}$$

Considering the SER in the high SNR regime, it can be simplified as

$$\text{SER} \leq \frac{\bar{N}_e}{2}\left[\left(\frac{M}{\hat{M}}\right)^{\alpha} \cdot \frac{\rho \cdot \tilde{d}_{\min}^2}{8}\right]^{-2 \cdot M_r}. \tag{3.27}$$

Considering (3.27) and (3.1), for a MIMO (Alamouti) multi-hop network and over M hops in the case of high SNR regime the SER at the destination can be written as

$$\text{SER}_{\text{Alamouti}} \leq 1 - \left(1 - \frac{\bar{N}_e}{2}\left[\left(\frac{M}{\hat{M}}\right)^{\alpha} \cdot \frac{\rho \cdot \tilde{d}_{\min}^2}{8}\right]^{-2 \cdot M_r}\right)^{M} = \text{SER}_{\text{MIMO}}^{\text{bound}}. \tag{3.28}$$

3.2.2 Comparison between MIMO (Alamouti STBCs-based), SIMO and SISO multi-hop networks

In the last section we have studied the SER of the multi-hop networks as a function of the number of hops, transmit energy per symbol, and the number of receive antennas for the SIMO and the Alamouti STBCs-based MIMO schemes. The purpose of using SIMO and MIMO links in the multi-hop networks is to increase the diversity and extend the transmission distance, which leads to a decrease in the number of hops. In that analysis, we have assumed that the devices are equipped with a large number of receive antennas. However, this assumption cannot be accomplished in a real scenario. Therefore, we need cooperation among users with a limited number of antennas, or just one antenna each. By using this cooperation, we can exploit the benefits of the spatial diversity but at the same time we make the users busier due to their participation in many transmissions and thus increase the interference in the network. Also, some synchronisation mechanism will become necessary at the transmitter side. Considering these facts, it becomes more important to figure out the conditions in which increasing the number of antennas is worthwhile.

In this section we compare SISO, SIMO and MIMO (Alamouti STBCs-based) multi-hop, with respect to the number of hops and the rate of the transmission.

3.2.2.1 Number of hops versus number of receive antennas

In this simulation, we assume that the achieved SER for a SISO multi-hop network for a given transmit energy per symbol and number of hops ($\hat{M}$) is the threshold of the SER. For a SIMO and MIMO (Alamouti STBCs-based) multi-hop network, the minimum number of hops for a reliable transmission is found for different number of receive antennas by using the same transmit energy per symbol as in the SISO case. In this work, we call a transmission a 'reliable transmission', if the total SER is lower than the threshold of the SER (SER_{th}) for a given QoS. This simulation is done for the binary phase-shift keying (BPSK) digital modulation scheme, in which the number of nearest neighbors is 1 and the minimum Euclidean distance of the underlying constellation ($d_{\min}$) is equal to $2\cdot\sqrt{E_s}$. Figure 3.3 shows the minimum number of hops versus number of receive antennas for SIMO and

MIMO (Alamouti STBCs-based) multi-hop networks.

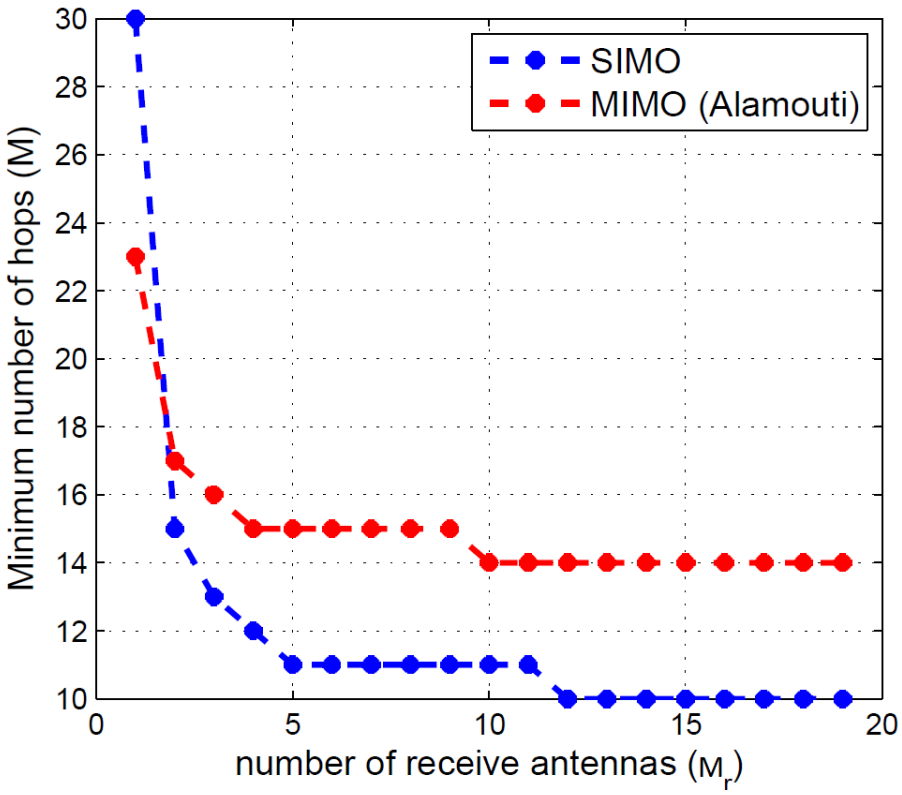

Figure 3.3: Comparison of MIMO (Alamouti) and SIMO multi-hop networks from the minimum number of hops point of view over different number of receive antennas considering $\text{SER}_{th} = 10^{-3}$, $\rho = \frac{E_s}{N_0} = 10$ dB, $\tilde{d}_{\min} = 2$, $\bar{N}_e = 1$, BPSK modulation and $\alpha = 2$.

Figure 3.3 shows that increasing the number of receive antennas can lead to a decrease in the number of hops, while increasing number of transmit antennas cannot always reduce the number of hops. This result can be explained better, by comparing the equations (3.21) with (3.28). These suggested SER upper bounds were calculated using the Chernoff bound. It is this approximation that yields the crossing over of the MMO and SIMO curves.

It is really important to find out how transmit antenna diversity can be exploited in the multi-hop networks in that way that the number of hops would be reduced. It is assumed that the same number of hops, M, is required for both SIMO and MIMO (Alamouti) multi-hop networks. Now the objective is to

find the transmit energy range for which the total SER of the MIMO (Alamouti) multi-hop scheme is lower than that of the SIMO multi-hop scheme. This can be written as

$$\mathrm{SER}_{\mathrm{Alamouti}}^{\mathrm{bound}} \leq \mathrm{SER}_{\mathrm{SIMO}}^{\mathrm{bound}}. \tag{3.29}$$

Using the upper bound of the equations (3.21) and (3.28), the inequality (3.29) can be easily solved which results in

$$\rho \geq \frac{16}{\tilde{d}_{\min}^2} \cdot \left(\frac{\hat{M}}{M}\right)^{\alpha}. \tag{3.30}$$

The inequality (3.30) determines a region of the transmit power, in which the number of hops can be reduced by using the Alamouti STBCs-based scheme. This inequality implies that if we use fewer hops for the transmission, we need more transmit energy to extract the benefits of transmit diversity.

3.2.2.2 Number of the hops versus transmit energy

In this simulation, we will figure out how much gain we will obtain in a multi-hop network by increasing the number of antennas. In this simulation we determine a fixed value of the SER as a threshold of the SER for the entire transmission. By implementing equations (3.14), (3.21) and (3.28), the minimum number of hops is computed for a given transmit energy per symbol. It is obvious that the SER of the entire transmission should not exceed the fixed threshold. The minimum number of hops versus the transmit energy per symbol for SISO, MISO, and MIMO (Alamouti STBCs-based) multi-hop networks for different numbers of receive antennas has been simulated. The result of this simulation is illustrated in Figure 3.4.

We can see that the obtained gain by adding just one receive antenna to the SISO case and thus creating a SIMO link is much higher than the gain by adding one receive antenna to SIMO ($N_r = 2$). Figure 3.4 shows that adding receive antennas is more effective at lower orders of SIMO. In other words the amount of

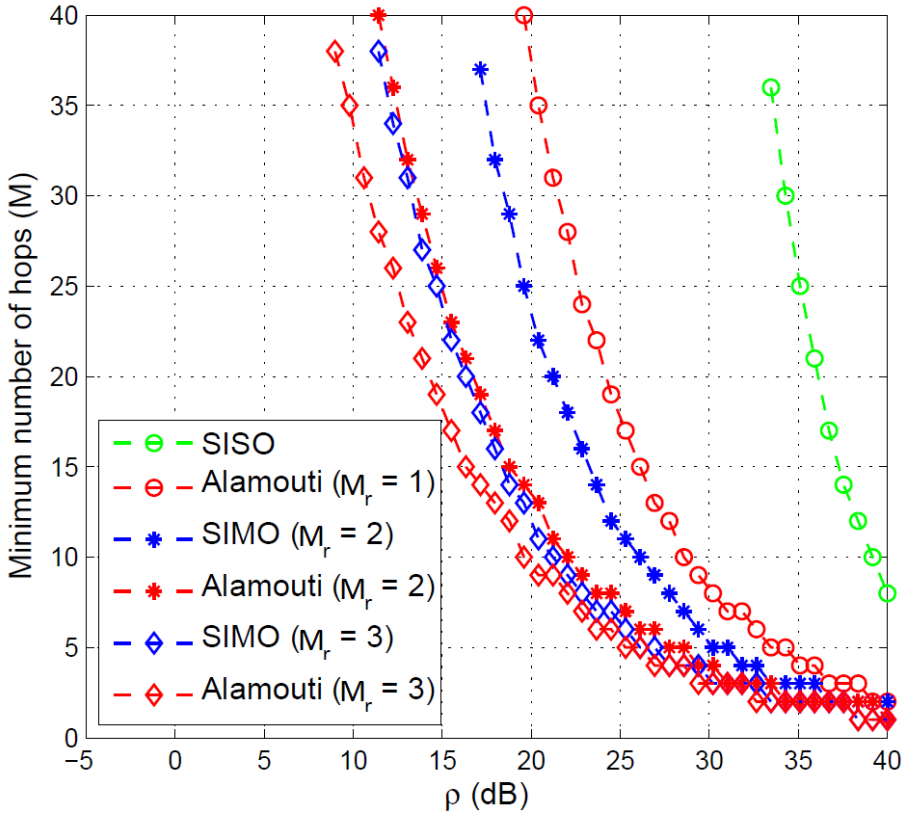

Figure 3.4: Minimum number of hops versus transmit SNR per symbol for SISO, MISO, and MIMO (Alamouti STBCs-based) multi-hop networks for different numbers of receive antennas, where $\hat{M} = 40$, $\text{SER}_{\text{th}} = 0.01$, and $\rho = P_s/\sigma_\nu^2$ (BPSK modulation and $\alpha = 2$).

gain decreases when a receive antenna is added if the order of the receive array was already high.

The effectiveness of increasing the number of transmit antennas can also be seen clearly, by comparing SIMO and Alamouti STBCs-based curves with the same number of receive antennas, in this figure. The comparison between SIMO and Alamouti STBCs-based MIMO is performed, from the total number of antennas point of view. Under the condition that the total number of antennas is the same for both the Alamouti STBCs-based MIMO network and the SIMO multi-hop network, we can see that the gain by SIMO will always be better than Alamouti STBCs-based MIMO. Thus for cooperative MIMO, when the antennas belong to different devices, if the position of a device is somewhere in the middle

of the transmitter and receiver, it gives us a greater gain if this device is used as an antenna element on the receiver side.

Another important comparison is the one concerning the rate of the transmission. Our system is based on DF relaying so the mutual information for the multi-hop case is given by

$$I_{DF} = \frac{1}{M} \cdot \min\left\{I_1, I_2, \cdots, I_M\right\}, \tag{3.31}$$

where I_i is the open loop capacity of the ith hop (no channel knowledge is available at the transmit relay) and given by

$$I_i = \log\left[\det\left(\boldsymbol{I}_{M_r} + \frac{\rho}{M_t} \cdot \left(\frac{M}{\hat{M}}\right)^{\alpha} \cdot \breve{\boldsymbol{H}} \cdot \breve{\boldsymbol{H}}^H\right)\right], \tag{3.32}$$

where the elements of $\breve{\boldsymbol{H}} \in \mathbb{C}^{N_r \times N_t}$ are modeled as independent identically distributed ZMCSCG random variables with unit variance, and N_t stands for number of transmit antennas. The result of this simulation is shown in Figure 3.5.

3.3 Conclusions

In this chapter, we have studied the case of increasing the number of the antennas at the relay nodes (without considering antenna selection) in multi-hop networks. The analysis has revealed that even though the obtained gain by employing MIMO (Alamouti) multi-hop networks is more than that when employing SIMO multi-hop networks assuming the same number of receive antennas, the gain obtained by employing SIMO multi-hop networks is more than that for MIMO (Alamouti) multi-hop networks when assuming the same total number of antennas. In other words, assuming a network with single antenna devices, increasing the transmit diversity should be given a lower priority over increasing the receive diversity.

The suggestions for future work are similar to those in the last chapter due to the similar model and assumption. So instead of just looking at the link throughput, it would be essential to have a look at the overall network throughput. Also, the presence of interference from other nodes can be considered and the

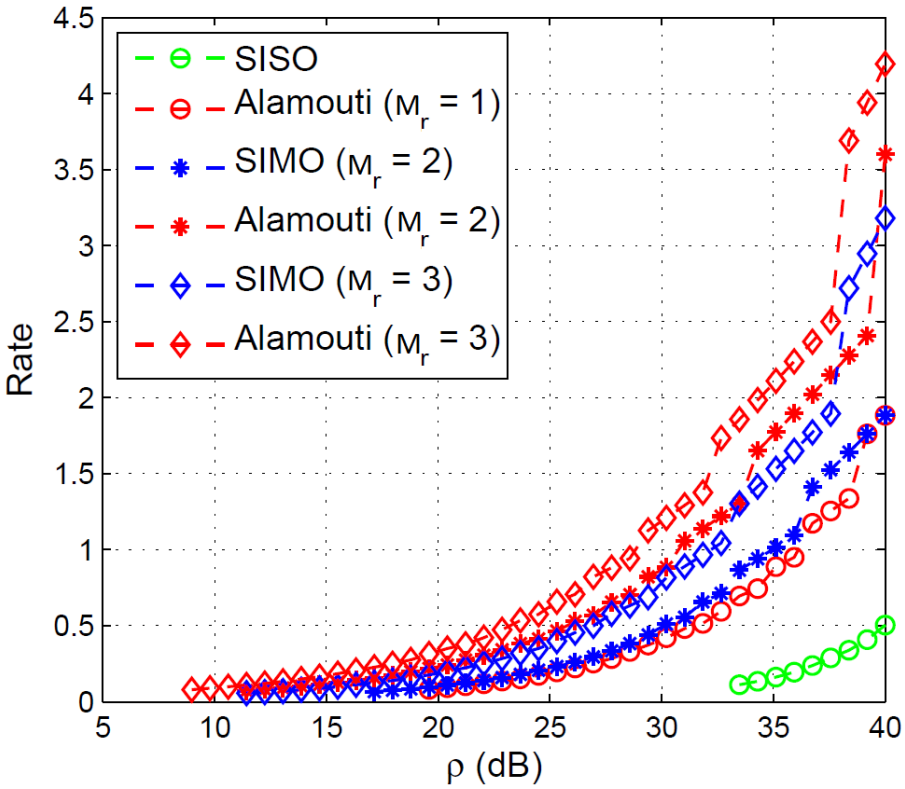

Figure 3.5: Rate of the transmission based on the computed minimum number of hops in Figure 3.4, where $\rho = P_s/\sigma_\nu^2$ (BPSK modulation and $\alpha = 2$).

evaluation can be performed for that case. As future work, the bounds for the SER can also be derived for the case of Rician fading. As mentioned at the end of the last chapter, the effects of frequency re-use and error propagation should also be studied in future work.

Chapter 4

Relaying schemes involving multiple cooperative antennas

4.1 Introduction

For single antenna devices, the benefits of spatial diversity can be exploited so that the separate devices share their antennas and resources to generate a virtual antenna array (VAA) and thereby improve the reliability of the communication. However, the lack of the fixed infrastructure and the physical separation of the devices create some challenges to the design of such cooperative techniques. In this chapter, the users are considered to be equipped with single antennas only and generating indigenous SIMO and MIMO channels will thus be impossible. Therefore, a combination of the single-antenna users is employed to constitute a virtual antenna array in order to generate a cooperative MIMO channel which results in a reduction in the number of hops. Cooperative MIMO techniques can be employed in order to improve the performance of the links and therefore to increase the range of each hop while providing the required QoS. However, implementing it in an ad-hoc network is difficult. Due to the lack of a centralized control of the network, e.g., a base station, the task of establishing a link is challenging. We will address two main issues that arise due to the distributed nature of cooperative MIMO communication.

The first part of the chapter will address the piloting issues in such networks. The issue arises because piloting is used extensively to gauge the quality of channels in order to determine if the quality of a certain transmission over them will be enough to fulfill the requirements. However, for single nodes, the piloting is done with only one antenna and it is a challenge to ascertain the quality of a cooperative MIMO transmission over a channel assessed through a SISO pilot. The first part of this chapter will take a look at the mechanism devised by us to utilize SISO piloting information to ensure the QoS in cooperative MIMO transmissions in clustered networks. This work was published by us in [ZGH11b] and in [Ghe12].

Cooperative MIMO schemes have some disadvantages as well. In a real scenario, each element of the VAA works separately with a different clock, a different distance to the destination node, i.e., the transmitter nodes do not work completely synchronized with each other. Most of this problem is solved via suitable synchronization protocols on higher layers and on the physical layer. On the phys-

ical layer one can make use of multiple synchronization techniques to achieve a certain level of phase synchronization. These techniques include, e.g., reference tone synchronization where (as proposed in [MHMB05]) the receiver emits a signal and all relay nodes change their phase until their respective SNRs are maximized. Another well known technique is the firefly synchronization shown in [SS+93] and [TAB06] which basically makes use of the coupled oscillator theory. There are also blind techniques which estimate the phase information from the signal subspace (e.g., [TT08]).

In [LW03], [CH03] and [CGB04], research has been performed in order to increase the network′s reliability when employing space-time codes between the relay nodes. Knowing that perfect synchronization is the most important requirement of STBCs and considering that the synchronization algorithms presented in [SV03] increase the network′s time and energy consumption, it is essential to study the robustness of the STBCs.

Although the synchronization error and its impact on the performance of cooperative MIMO systems has been studied in [NBS08a] among others, these analytical studies become more reliable and practical if the transmission quality is studied in the worst case, as we have done. The signal to interference and noise ratio (SINR) is a key parameter in order to evaluate the network′s performance, because the synchronization error yields an inter symbol interference (ISI) at the destination.

The effect of synchronization errors on the performance of a cooperative MIMO scheme that uses the Alamouti space-time block code is studied in the second part of the chapter. The focus is on finding a lower bound of the received Signal to Interference and Noise Ratio (SINR). The synchronization error, caused by the distributed nature of the scheme, is considered as inaccurate channel state information, which is modeled as an additive deterministic norm-bounded inaccuracy matrix. A closed-form expression is derived for the lower bound of the SINR. Using this, a closed-form expression of the Bit Error Rate (BER) in the high SNR regime for the worst case error vector is also derived. These expressions were, to the best of our knowledge, not present in the literature before and we feel that these worst case performance expressions are of interest to system designers as it helps them to design the system with specific guarantees about the

outage behavior. One interesting observation from the presented results is that the larger the synchronization error gets, the quicker we reach the interference limited high SNR region, in which the 'MIMO benefits' are absent. This work was published by us in [ZGRH12] and in [Ghe12].

4.2 BER bound estimation

It is proposed to employ the link information from the SISO piloting in order to come up with an idea on how to perform a cooperative/collocated MIMO link in the same place. A high power pilot is used in order to reach distant clusters, even the ones for which the SISO link is not usable due to high error rate. The following section shows how the performance of a virtual MIMO link can be derived based on the SISO links. The upper bound of the error probability estimates is considered to ensure that the Quality of Service (QoS) is met.

In this section we explain a novel procedure that we developed to find out how the quality of transmission for higher order MIMO can be extracted from the available SISO link information. In this section we focus on the symbol error rate as a parameter of the link quality. Let us assume that the system has a diversity order D. The received signal at the receiver can be written as

$$y_i = \sqrt{\frac{P_s}{D}} h_i \cdot x + \nu_i, \quad i = 1, 2, \ldots, D, \tag{4.1}$$

where x denotes the transmitted signal, P_s denotes the transmit power, h_i, y_i, and w_i represent the channel transfer function, the received signal, and the additive noise which is modeled as a ZMCSCG random variable with variance σ_n^2 corresponding to the ith diversity branch, respectively. The symbol error rate can be approximated as

$$P_e(\eta) \approx \bar{N}_e \cdot Q\left(\sqrt{\frac{\eta \cdot d_{\min}^2}{2}}\right). \tag{4.2}$$

where Q represents the Q-function, defined in (3.3), which is the tail probability of the standard normal distribution. Moreover, $\bar{N}_e$ and $d_{\min}$ denote the number of

nearest neighbors and the minimum Euclidean distance of the underlying scalar constellation. The variable η represents the received SNR over a fading channel h_i which, for maximum ratio combining, is given by

$$\eta = \frac{1}{D} \sum_{i=1}^{D} |h_i|^2 \cdot \rho, \tag{4.3}$$

where $\rho = P_s/\sigma_n^2$ is the received SNR of the equivalent SISO link. By using the Chernoff bound: $Q(x) \leq 1/2 \cdot \exp(-x^2/2)$, the equation (4.2) can be bounded, which yields

$$P_e(\eta) \leq \frac{1}{2} \bar{N}_e \cdot \exp\left(-\frac{\eta \cdot d_{\min}^2}{4}\right). \tag{4.4}$$

Assuming an uncorrelated Rayleigh fading channel with unit variance, it follows that the average probability of symbol error in the high SNR region is upper-bounded by

$$P_e = \mathbb{E}\{P_e(\eta)\} \leq \frac{1}{2} \bar{N}_e \left(\frac{\rho \cdot d_{\min}^2}{4 \cdot D}\right)^{-D}. \tag{4.5}$$

The diversity order D should be minimized in order to find an upper bound which is independent of the MIMO scheme. We assume maximum ratio combining at the receiver. Then depending on the correlation between the transmit antennas (we assume uncorrelated receive antennas), the bounds of diversity order D can be written as

$$M_r \leq D \leq M_r \cdot M_t, \tag{4.6}$$

where M_t is the number of transmit antennas. Replacing D with M_r in the equation (4.5), the upper bound of the average probability of SER in the high SNR regime is given by

$$\mathbb{E}\{P_e\} \leq \frac{1}{2} \bar{N}_e \left(\frac{\rho \cdot d_{\min}^2}{4 \cdot M_r}\right)^{-M_r}. \tag{4.7}$$

Using (4.7), the upper bound of the probability of error for cooperative MIMO with a particular number of receive antennas M_r can be estimated employing only the SISO pilot. Note that we have used the lowest value of D to arrive at a stricter upper bound in order to ensure that the QoS requirement on the SER is always

met. After this phase it is possible for each of the cluster-heads (CHs) to form a table of all the other clusters with which it can communicate by employing one or more of its cluster members. A list of the best nodes for these virtual MIMO connections can also be obtained in a decreasing order of the precedence. Thereby we introduce the concept of the cooperative MIMO neighboring clusters. This concept will be utilized in the next chapter to devise a new joint clustering and routing mechanism suitable for cooperative MIMO relaying networks.

4.3 Impact of Synchronization Errors

It has been shown in the last chapter that decreasing the number of hops can increase the capacity, particularly in the high SNR regime. Utilizing the advantages of the multiple input multiple output (MIMO) channels is a method to decrease the number of hops. In this chapter, the effect of synchronization errors on the performance of a cooperative multiple input multiple output scheme is studied which employs two and four transmit antennas. The point is to find a lower bound for the received Signal to Interference and Noise Ratio (SINR). The distributed nature of the scheme causes the synchronization error which is considered as inaccurate channel state information and is modeled as an additive deterministic norm-bounded inaccuracy matrix. A closed-form expression has been derived for the lower bound of the SINR. Considering it, a closed-form expression of the Bit Error Rate (BER) in the high SNR regime is derived in case of the worst error vector. System designers are interested in this worst case performance since it helps them to specify guarantees about the outage behavior of the system they design. From the results, it is interesting to observe that the interference limited high SNR region, in which there are no 'MIMO benefits', is reached faster, as the synchronization error becomes larger.

Employing space-time block coding (STBC) increases the diversity order of the transmission [Win98] which reduces the energy consumption. It is an important advantage in case of the wireless sensor networks with limited available power. STBCs are employed so that transmitter nodes do not need channel state information (CSI). This way, CSI is only needed at the receiver nodes which can be obtained via different methods, e.g., piloting and blind estimation meth-

ods. Considering that the receiver side is distributed, it is also favorable that for STBCs each receiver node needs only the CSI of the channel between itself and each node which sends the data to it, and not the CSI of the whole virtual MIMO channel. The diversity gain is achieved at the ultimate destination combining what each receiver node decodes separately.

In this section, we study the performance of the cooperative MIMO transmission which uses the Alamouti STBC, by considering the synchronization error and some inaccuracy in the CSI at the destination nodes. We translate these errors into an inaccuracy matrix, which is added to the perfect CSI. Note that the norm of the inaccuracy matrix is bounded and available at the destination. We analytically find a lower bound of the received Signal to Interference and Noise Ratio (SINR). Then the BER for the high SNR regime for the worst case error vector is also studied.

4.3.1 The model of inaccuracy

Cooperative MIMO communication comprises three phases of local data exchange. During the first phase the CH sends the data to the members of its cluster who are employed as the elements of the VAA. After that and during the second phase the users forward the data based on their schedule which is planned before. Then, during the third phase the receiver nodes decode the received data separately and forward this decoded data to CH at the receiver side. Figure 4.1 illustrates these three phases.

Here, it is considered that the destination nodes have imperfect channel state information which is modeled as an additive inaccuracy matrix. This model defines the inaccuracy in the magnitude of the channel besides the inaccuracy in the phase of the channel, which can be written as

$$\boldsymbol{H}' = \boldsymbol{H} + \boldsymbol{E}, \tag{4.8}$$

where

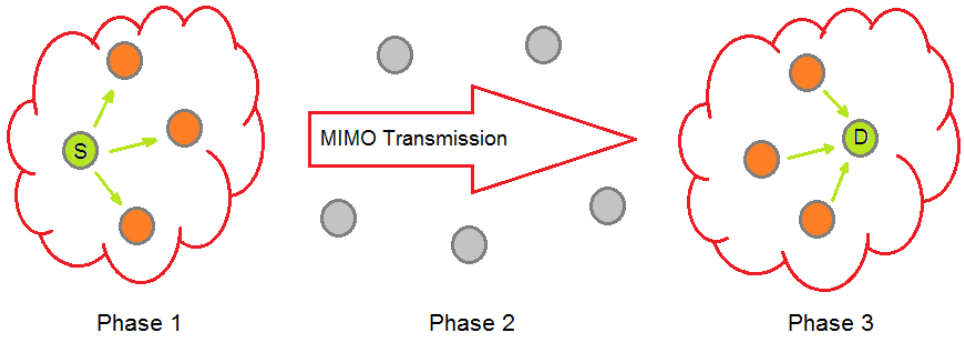

Figure 4.1: Different phases of Cooperative MIMO communication from [NBS08a]

$\boldsymbol{H}$	is the instantaneous channel matrix
$\boldsymbol{E}$	is the inaccuracy matrix
$\boldsymbol{H}'$	is the available channel matrix at the destination.

It is also assumed that the Frobenius norm of the inaccuracy matrix $\boldsymbol{E}$ is bounded by the deterministic of value β. Here, it is assumed that the effect of different processing delays at the users on the synchronization error is insignificant. There are some differences in the distances between the users and the CH at the transmitter side, which are comparable to the wavelength. As a result, during the second phase of the transmission, the signal is not received at the same time by the users in the VAA.

As a result of clustering, the transmitter and receiver nodes are distributed to different positions in a certain area which causes different delays and unsynchronized transmission. The channel remains frequency flat, considering that the delays are not comparable to the symbol duration; therefore the synchronization error can be modeled as an inaccuracy in the phase of the channel. It can be written as

$$h'_{k,l} = h_{k,l} \cdot \exp\left(\mathrm{j}2\pi f_c \tau_{k,l}\right), \tag{4.9}$$

where

$\tau_{k,l}$	is the delay of the channel $h_{k,l}$ in reference to the $\tau_{1,1}$
f_c	is the carrier frequency.

It is noteworthy to mention that $\tau_{1,1} = 0$, and the phase error is bounded as well, because the positions of the nodes are bounded in the cluster area. It is easily possible to show that this synchronization error can be rewritten using the additive inaccuracy model described in equation (4.8). Therefore, this synchronization error, which has only an effect on the phase of the channel, is converted into an imperfect knowledge of the channel state at the destination.

4.3.2 Alamouti Space time block codes

This section is based on Alamouti STBCs, described in section 3.2.1.3 in the last chapter, with linear processing at the receiver. It is shown in [TSC98] that the Alamouti code is the only rate 1 STBC which has the full diversity whereas all the other STBCs have to expend their diversity in order to achieve a higher rate or vice versa. It is considered that there are two (virtual) antennas ($M_t = 2$) at the transmitter side and M_r (virtual) antennas at the receiver side. Therefore, the channel matrix $\boldsymbol{H}$ can be written as

$$\boldsymbol{H} = \begin{bmatrix} \boldsymbol{h}_1 & \boldsymbol{h}_2 \end{bmatrix} \in \mathbb{C}^{M_r \times 2},$$

where

$\boldsymbol{h}_i$	is the Rayleigh fading channel between the ith transmitter and all of the receiver nodes.

It is imperative to mention that the elements of $\boldsymbol{h}_i$ are modeled as independent identically distributed zero-mean circulant symmetric complex Gaussian (ZMCSCG) random variables with a variance equal to 1. Considering an additive inaccuracy matrix $\boldsymbol{E}$ as

$$\boldsymbol{E} = \begin{bmatrix} \boldsymbol{\epsilon}_1 & \boldsymbol{\epsilon}_2 \end{bmatrix} \in \mathbb{C}^{M_r \times 2},$$

the available CSI at the destination can be written as

$$\boldsymbol{H}' = \boldsymbol{H} + \boldsymbol{E}. \tag{4.10}$$

Assuming a quasi-static block fading channel, i.e., a channel that remains constant during the transmission of the two symbol periods, the received signals in the first time interval $\boldsymbol{y}_1$ and the second time interval $\boldsymbol{y}_2$ are given as

$$\begin{bmatrix} \boldsymbol{y}_1 & \boldsymbol{y}_2 \end{bmatrix} = \sqrt{\frac{P_s}{2}} \cdot \boldsymbol{H} \cdot \begin{bmatrix} s_1 & -s_2^* \\ s_2 & s_1^* \end{bmatrix} + \begin{bmatrix} \boldsymbol{\nu}_1 & \boldsymbol{\nu}_2 \end{bmatrix},$$

where

$(.)^*$	is the complex conjugate of a complex number
P_s	is the transmit power per symbol period
s_i	is the ith transmitted symbol
$\boldsymbol{\nu}_i \in \mathbb{C}^{M_r \times 1}$:	uncorrelated ZMCSCG noise vectors ($i = 1, 2$).

It is noteworthy to mention that $\mathbb{E}\{|s_i|^2\} = 1$ and $\mathbb{E}\{\boldsymbol{\nu}_i \cdot \boldsymbol{\nu}_i^H\} = \sigma_\nu^2 \cdot \boldsymbol{I}_{M_r}$, in which $\boldsymbol{I}_n$ represents the identity matrix of size $n \times n$ and $(.)^H$ represents the conjugate transpose of a matrix. Defining the matrix $\boldsymbol{H}_{\text{eff}}$ as

$$\boldsymbol{H}_{\text{eff}} = \begin{bmatrix} \boldsymbol{h}_1 & \boldsymbol{h}_2 \\ \boldsymbol{h}_2^* & -\boldsymbol{h}_1^* \end{bmatrix} \in \mathbb{C}^{2 \cdot M_r \times 2},$$

a new received signal can be written as

$$\tilde{\boldsymbol{y}} = \sqrt{\frac{P_s}{2}} \cdot \boldsymbol{H}_{\text{eff}} \cdot \boldsymbol{s} + \tilde{\boldsymbol{\nu}}, \tag{4.11}$$

where

$\boldsymbol{H} \in \mathbb{C}^{M_r \times M_t}$	is the channel matrix
P_s	is the transmit power per symbol period
R	is the rate of the STBC

where $\boldsymbol{s} = \begin{bmatrix} s_1 & s_2 \end{bmatrix}^T$ and $(.)^T$ denotes the transpose of a matrix. A tilde over

a vector stands for the transformation of $\tilde{\boldsymbol{a}} = \begin{bmatrix} \boldsymbol{a}_1^T & \boldsymbol{a}_2^H \end{bmatrix}^T$. Employing (4.10), the processing at the receiver side can be written as

$$\begin{aligned} \boldsymbol{z} &= (\boldsymbol{H}'_{\text{eff}})^H \cdot \tilde{\boldsymbol{y}} \\ \boldsymbol{z} &= (\boldsymbol{H}_{\text{eff}} + \boldsymbol{E}_{\text{eff}})^H \cdot \tilde{\boldsymbol{y}}, \end{aligned}$$

where

$$\boldsymbol{E}_{\text{eff}} = \begin{bmatrix} \boldsymbol{\epsilon}_1 & \boldsymbol{\epsilon}_2 \\ \boldsymbol{\epsilon}_2^* & -\boldsymbol{\epsilon}_1^* \end{bmatrix}.$$

Employing (4.11), it is possible to write the signal, after the processing at the receiver, as

$$\boldsymbol{z} = \sqrt{\frac{P_s}{2}} \boldsymbol{H}_{\text{eff}}^H \cdot \boldsymbol{H}_{\text{eff}} \cdot \boldsymbol{s} + \sqrt{\frac{P_s}{2}} \boldsymbol{E}_{\text{eff}}^H \cdot \boldsymbol{H}_{\text{eff}} \cdot \boldsymbol{s} + (\boldsymbol{H}_{\text{eff}} + \boldsymbol{E}_{\text{eff}})^H \cdot \tilde{\boldsymbol{\nu}}. \tag{4.12}$$

If it is considered that $\boldsymbol{H}_{\text{eff}}^H \cdot \boldsymbol{H}_{\text{eff}} = \|\boldsymbol{H}\|_F^2 \cdot \boldsymbol{I}_2$, employing the following definitions

$$\begin{aligned} \alpha_1 &= \begin{bmatrix} \boldsymbol{\epsilon}_1^H & \boldsymbol{\epsilon}_2^T \end{bmatrix} \cdot \begin{bmatrix} \boldsymbol{h}_1 \\ \boldsymbol{h}_2^* \end{bmatrix} \\ \alpha_2 &= \begin{bmatrix} \boldsymbol{\epsilon}_1^H & \boldsymbol{\epsilon}_2^T \end{bmatrix} \cdot \begin{bmatrix} \boldsymbol{h}_2 \\ -\boldsymbol{h}_1^* \end{bmatrix}, \end{aligned}$$

it is possible to rewrite the equation (4.12) as

$$\begin{bmatrix} z_1 \\ z_2 \end{bmatrix} = \underbrace{\sqrt{\frac{P_s}{2}} \cdot \|\boldsymbol{H}\|_F^2 \cdot \begin{bmatrix} s_1 \\ s_2 \end{bmatrix}}_{\text{signal component}} + \underbrace{\sqrt{\frac{P_s}{2}} \cdot \begin{bmatrix} \alpha_1 \cdot s_1 + \alpha_2 \cdot s_2 \\ \alpha_1^* \cdot s_2 - \alpha_2^* \cdot s_1 \end{bmatrix}}_{\text{Interference component}} + \underbrace{(\boldsymbol{H}_{\text{eff}} + \boldsymbol{E}_{\text{eff}})^H \cdot \tilde{\boldsymbol{\nu}}}_{\text{noise component}}. \tag{4.13}$$

Having no perfect channel knowledge at the destination results in ISI, as it is also shown in (4.13). The ratio of the signal power P_r to the interference power P_i and the noise power P_n is called the SINR. The SINRs for the both received symbols (z_1 and z_2) are the same, therefore the SINR is calculated based on

z_1. Employing the equation (4.13), the power of the signal component can be obtained as

$$P_r = \frac{P_s}{2}\left(\|\boldsymbol{H}\|_F^2\right)^2 \underbrace{\mathbb{E}\{|s_i|^2\}}_{1}. \tag{4.14}$$

Employing the following change of variables

$$\boldsymbol{\delta}^H = \begin{bmatrix}\boldsymbol{\epsilon}_1^H & \boldsymbol{\epsilon}_2^T\end{bmatrix}, \qquad \boldsymbol{l}_1^H = \begin{bmatrix}\boldsymbol{h}_1^H & \boldsymbol{h}_2^T\end{bmatrix}, \qquad \boldsymbol{l}_2^H = \begin{bmatrix}\boldsymbol{h}_2^H & -\boldsymbol{h}_1^T\end{bmatrix},$$

we have

$$\alpha_1 = \boldsymbol{\delta}^H \cdot \boldsymbol{l}_1, \qquad \alpha_2 = \boldsymbol{\delta}^H \cdot \boldsymbol{l}_2. \tag{4.15}$$

Considering the fact that the symbols s_i and s_{i+1} are statistically independent, it is possible to write the interference power P_i as

$$\begin{aligned} P_i &= \frac{P_s}{2} \cdot \mathbb{E}\{|\alpha_1 \cdot s_1 + \alpha_2 \cdot s_2|^2\} \\ &= \frac{P_s}{2}\left(|\alpha_1|^2 \cdot \underbrace{\mathbb{E}\{|s_1|^2\}}_{1} + |\alpha_2|^2 \cdot \underbrace{\mathbb{E}\{|s_2|^2\}}_{1} + \alpha_1 \cdot \alpha_2^* \cdot \underbrace{\mathbb{E}\{s_1 \cdot s_2^*\}}_{0} + \alpha_2 \cdot \alpha_1^* \cdot \underbrace{\mathbb{E}\{s_2 \cdot s_1^*\}}_{0}\right) \\ &= \frac{P_s}{2} \cdot \boldsymbol{\delta}^H \cdot \left(\boldsymbol{l}_1 \cdot \boldsymbol{l}_1^H + \boldsymbol{l}_2 \cdot \boldsymbol{l}_2^H\right) \cdot \boldsymbol{\delta}. \end{aligned} \tag{4.16}$$

Considering that $\boldsymbol{E}_{\text{eff}}^H \cdot \boldsymbol{E}_{\text{eff}} = \|\boldsymbol{E}\|_F^2 \cdot \boldsymbol{I}_2$, the power of the noise component is given as

$$\begin{aligned} P_n &= \frac{1}{2}\text{tr}\left\{\left(\boldsymbol{H}_{\text{eff}} + \boldsymbol{E}_{\text{eff}}\right)^H \cdot \underbrace{\mathbb{E}\left\{\tilde{\boldsymbol{\nu}} \cdot \tilde{\boldsymbol{\nu}}^H\right\}}_{\sigma_\nu^2 \cdot \boldsymbol{I}_{2M_r}} \cdot \left(\boldsymbol{H}_{\text{eff}} + \boldsymbol{E}_{\text{eff}}\right)\right\} \\ &= \frac{\sigma_\nu^2}{2}\text{tr}\left\{\left(\|\boldsymbol{H}\|_F^2 + \|\boldsymbol{E}\|_F^2\right) \cdot \boldsymbol{I}_2 + \boldsymbol{E}_{\text{eff}}^H \cdot \boldsymbol{H}_{\text{eff}} + \boldsymbol{H}_{\text{eff}}^H \cdot \boldsymbol{E}_{\text{eff}}\right)\right\} \\ &= \sigma_\nu^2 \cdot \left(\|\boldsymbol{H}\|_F^2 + \|\boldsymbol{E}\|_F^2 + \alpha_1 + \alpha_1^*\right) \\ &= \sigma_\nu^2 \cdot \left(\|\boldsymbol{H}\|_F^2 + \|\boldsymbol{E}\|_F^2 + \boldsymbol{\delta}^H \cdot \boldsymbol{l}_1 + \boldsymbol{l}_1^H \cdot \boldsymbol{\delta}\right), \end{aligned} \tag{4.17}$$

where

$\mathrm{tr}(\boldsymbol{A})$ is the trace of the matrix $\boldsymbol{A}$

$\boldsymbol{E}_{\text{eff}}^{H} \cdot \boldsymbol{H}_{\text{eff}} = \begin{bmatrix} \alpha_1 & \alpha_2 \\ -\alpha_2^* & \alpha_1^* \end{bmatrix}$

Note that the factor of 1/2 is present here because the Alamouti scheme decouples the system into two parallel links, both having the same SINR. We need to compute the SINR for only one of these links. Therefore we also need the noise power for only one of these links. The trace operator here gives us the noise for both links, so we divide it by 2 to get the noise for one link.

Employing the equations (4.14) (4.16) and (4.17), also the change of variables $\boldsymbol{L} = \boldsymbol{l}_1 \cdot \boldsymbol{l}_1^H + \boldsymbol{l}_2 \cdot \boldsymbol{l}_2^H$, and considering that $\|\boldsymbol{E}\|_F^2 = \boldsymbol{\delta}^H \cdot \boldsymbol{\delta}$, it is possible to write the received SINR for the Alamouti scheme in the presence of the inaccuracy matrix as

$$\text{SINR} = \frac{P_s \cdot \left(\|\boldsymbol{H}\|_F^2\right)^2}{P_s \cdot \boldsymbol{\delta}^H \cdot \boldsymbol{L} \cdot \boldsymbol{\delta} + 2 \cdot \sigma_\nu^2 \cdot (\boldsymbol{\delta}^H \cdot \boldsymbol{l}_1 + \boldsymbol{l}_1^H \cdot \boldsymbol{\delta} + \boldsymbol{\delta}^H \cdot \boldsymbol{\delta} + \|\boldsymbol{H}\|_F^2)} \tag{4.18}$$

4.3.3 SINR lower bound for Alamouti STBCs

Now the goal is to study, how much the performance of the Alamouti STBCs degrades in the presence of the synchronization error. In other words, we find the lower bound of the SINR if the norm of the matrix $\boldsymbol{E}$ is bounded by β. This analysis studies the SINR of the STBCs in the worst case. This optimization problem is written as

$$\min_{\boldsymbol{E}} \quad \text{SINR} \quad \text{s.t.} \quad \mathrm{tr}\{\boldsymbol{E}^H \cdot \boldsymbol{E}\} \leq \beta^2. \tag{4.19}$$

Considering only the terms in (4.18), which are dependent on the inaccuracy vector $\boldsymbol{\delta}$, the problem (4.19) can be rewritten as the following maximization problem

$$\begin{aligned} \max_{\boldsymbol{\delta}} \quad & \boldsymbol{\delta}^H \cdot \boldsymbol{L} \cdot \boldsymbol{\delta} + 2 \cdot \frac{\sigma_\nu^2}{P_s} \cdot \left(\boldsymbol{\delta}^H \cdot \boldsymbol{l}_1 + \boldsymbol{l}_1^H \cdot \boldsymbol{\delta} + \boldsymbol{\delta}^H \cdot \boldsymbol{\delta}\right) \\ \text{s.t.} \quad & \boldsymbol{\delta}^H \cdot \boldsymbol{\delta} \leq \beta^2 \end{aligned} \tag{4.20}$$

It is easily possible to show that the objective function is maximized when the norm of the inaccuracy vector $\boldsymbol{\delta}$ is equal to its maximum value β, i.e., the inequality constraint in (4.20) is satisfied with equality at the optimum. Therefore the optimization problem can be given as

$$\begin{aligned} \max_{\boldsymbol{\delta}} \quad & \boldsymbol{\delta}^H \cdot \boldsymbol{L} \cdot \boldsymbol{\delta} + 2 \cdot \frac{\sigma_\nu^2}{P_s} \cdot \left(\boldsymbol{\delta}^H \cdot \boldsymbol{l}_1 + \boldsymbol{l}_1^H \cdot \boldsymbol{\delta} \right) \\ \text{s.t.} \quad & \boldsymbol{\delta}^H \cdot \boldsymbol{\delta} = \beta^2 \end{aligned} \tag{4.21}$$

The problem of (4.21) is not convex because the matrix $\boldsymbol{L}$ is positive semi-definite. Employing the method of Lagrange multipliers, the Lagrange function can be written as

$$\Lambda(\boldsymbol{\delta}, \lambda) = \boldsymbol{\delta}^H \cdot \boldsymbol{L} \cdot \boldsymbol{\delta} + 2 \cdot \frac{\sigma_\nu^2}{P_s} \cdot \left(\boldsymbol{\delta}^H \cdot \boldsymbol{l}_1 + \boldsymbol{l}_1^H \cdot \boldsymbol{\delta} \right) + \lambda \cdot \left(\boldsymbol{\delta}^H \cdot \boldsymbol{\delta} - \beta^2 \right), \tag{4.22}$$

where

λ is the Lagrange multiplier.

It is noteworthy to mention that the Lagrange multiplier can be either positive or negative. Setting the equation $\partial \Lambda(\boldsymbol{\delta}, \lambda) / \partial \boldsymbol{\delta}^*$ equal to zero, it is possible to write

$$\begin{aligned} \boldsymbol{L} \cdot \boldsymbol{\delta}_{\text{worst}} + 2 \cdot \frac{\sigma_\nu^2}{P_s} \cdot \boldsymbol{l}_1 + \lambda \cdot \boldsymbol{\delta}_{\text{worst}} &\stackrel{!}{=} \boldsymbol{0} \\ -2 \cdot \frac{\sigma_\nu^2}{P_s} \cdot \left(\boldsymbol{L} + \lambda \cdot \boldsymbol{I}_{2M_r} \right)^{-1} \cdot \boldsymbol{l}_1 &= \boldsymbol{\delta}_{\text{worst}}. \end{aligned} \tag{4.23}$$

Considering $\boldsymbol{l}_1^H \cdot \boldsymbol{l}_2 = \boldsymbol{h}_1^H \cdot \boldsymbol{h}_2 - \boldsymbol{h}_2^T \cdot \boldsymbol{h}_1^* = 0$ and the definition of the matrix $\boldsymbol{L}$, it is possible to rewrite it as $\boldsymbol{L} = \boldsymbol{U}_s \cdot \boldsymbol{\Sigma}_s \cdot \boldsymbol{U}_s^H$, in which

$$\begin{aligned} \boldsymbol{U}_s &= \left[\breve{\boldsymbol{l}}_1 \quad \breve{\boldsymbol{l}}_2 \right], \\ \boldsymbol{\Sigma}_s &= \operatorname{diag}\left(\left[\boldsymbol{l}_1^H \cdot \boldsymbol{l}_1 \quad \boldsymbol{l}_2^H \cdot \boldsymbol{l}_2 \right] \right), \end{aligned}$$

where

$\breve{\boldsymbol{l}}_i$	is the normalized vector of a vector $\boldsymbol{l}_i$
$\mathrm{diag}(\boldsymbol{a})$	is a diagonal matrix whose diagonal entries are the elements of the vector $\boldsymbol{a}$

Employing the change of variables $\breve{\boldsymbol{l}}_i = \boldsymbol{l}_i / \|\boldsymbol{l}_i\|_2$ it is possible to rewrite (4.23) as

$$\boldsymbol{\delta}_{\text{worst}} = -2 \cdot \frac{\sigma_\nu^2}{P_s} \cdot \boldsymbol{U}_s \cdot (\boldsymbol{\Sigma}_s + \lambda \cdot \boldsymbol{I}_2)^{-1} \cdot \boldsymbol{U}_s^H \cdot \boldsymbol{l}_1. \tag{4.24}$$

Now the objective is to find a λ which fulfills the equality constraint $\boldsymbol{\delta}_{\text{worst}}^H \cdot \boldsymbol{\delta}_{\text{worst}} = \beta^2$. Considering that $\boldsymbol{U}_s^H \cdot \boldsymbol{U}_s = \boldsymbol{I}_2$, it is possible to write this equality as

$$\begin{aligned} \beta^2 &= \left(2 \cdot \frac{\sigma_\nu^2}{P_s}\right)^2 \left(\boldsymbol{l}_1^H \cdot \boldsymbol{U}_s \cdot (\boldsymbol{\Sigma}_s + \lambda \cdot \boldsymbol{I}_2)^{-1} \cdot \boldsymbol{U}_s^H \cdot \boldsymbol{U}_s \cdot (\boldsymbol{\Sigma}_s + \lambda \cdot \boldsymbol{I}_2)^{-1} \cdot \boldsymbol{U}_s^H \cdot \boldsymbol{l}_1\right) \\ &= \left(2 \cdot \frac{\sigma_\nu^2}{P_s}\right)^2 \cdot \mathrm{tr}\left\{(\boldsymbol{\Sigma}_s + \lambda \cdot \boldsymbol{I}_2)^{-2} \cdot \boldsymbol{U}_s^H \cdot \boldsymbol{l}_1 \cdot \boldsymbol{l}_1^H \cdot \boldsymbol{U}_s\right\}, \end{aligned} \tag{4.25}$$

and we can write,

$$\begin{aligned} \boldsymbol{U}_s^H \cdot \boldsymbol{l}_1 \cdot \boldsymbol{l}_1^H \cdot \boldsymbol{U}_s &= \begin{bmatrix} \breve{\boldsymbol{l}}_1 & \breve{\boldsymbol{l}}_2 \end{bmatrix}^H \cdot \boldsymbol{l}_1 \cdot \boldsymbol{l}_1^H \cdot \begin{bmatrix} \breve{\boldsymbol{l}}_1 & \breve{\boldsymbol{l}}_2 \end{bmatrix} \\ &= \begin{bmatrix} \breve{\boldsymbol{l}}_1^H \\ \breve{\boldsymbol{l}}_2^H \end{bmatrix} \cdot \boldsymbol{l}_1 \cdot \boldsymbol{l}_1^H \cdot \begin{bmatrix} \breve{\boldsymbol{l}}_1 & \breve{\boldsymbol{l}}_2 \end{bmatrix} \\ &= \begin{bmatrix} \breve{\boldsymbol{l}}_1^H \cdot \boldsymbol{l}_1 \\ \breve{\boldsymbol{l}}_2^H \cdot \boldsymbol{l}_1 \end{bmatrix} \cdot \begin{bmatrix} \boldsymbol{l}_1^H \cdot \breve{\boldsymbol{l}}_1 & \boldsymbol{l}_1^H \cdot \breve{\boldsymbol{l}}_2 \end{bmatrix} \\ &= \begin{bmatrix} \breve{\boldsymbol{l}}_1^H \cdot \boldsymbol{l}_1 \\ 0 \end{bmatrix} \cdot \begin{bmatrix} \boldsymbol{l}_1^H \cdot \breve{\boldsymbol{l}}_1 & 0 \end{bmatrix} \\ &= \begin{bmatrix} \breve{\boldsymbol{l}}_1^H \cdot \boldsymbol{l}_1 \cdot \boldsymbol{l}_1^H \cdot \breve{\boldsymbol{l}}_1 & 0 \\ 0 & 0 \end{bmatrix} \\ &= \breve{\boldsymbol{l}}_1^H \cdot \boldsymbol{l}_1 \cdot \boldsymbol{l}_1^H \cdot \breve{\boldsymbol{l}}_1 \cdot \begin{bmatrix} 1 & 0 \\ 0 & 0 \end{bmatrix} \end{aligned} \tag{4.26}$$

It is known that $\breve{\boldsymbol{l}}_1^H$ is the normalized version of $\boldsymbol{l}_1$. Therefore, if

$$\boldsymbol{l}_1 = \begin{bmatrix} \boldsymbol{h}_1 \\ \boldsymbol{h}_2^* \end{bmatrix} \tag{4.27}$$

then it is possible to write

$$\breve{\boldsymbol{l}}_1 = \frac{\boldsymbol{l}_1}{\sqrt{\boldsymbol{h}_1{}^H \cdot \boldsymbol{h}_1 + \boldsymbol{h}_2{}^H \cdot \boldsymbol{h}_2}} = \frac{\boldsymbol{l}_1}{\parallel \boldsymbol{l}_1 \parallel} = \frac{\boldsymbol{l}_1}{\parallel \boldsymbol{H} \parallel_F}. \tag{4.28}$$

Thus, we can write

$$\breve{\boldsymbol{l}}_1^H \cdot \boldsymbol{l}_1 \cdot \boldsymbol{l}_1^H \cdot \breve{\boldsymbol{l}}_1 = \left(\breve{\boldsymbol{l}}_1^H \cdot \boldsymbol{l}_1\right)^2 = \frac{\left(\boldsymbol{l}_1^H \cdot \boldsymbol{l}_1\right)^2}{\parallel \boldsymbol{H} \parallel_F^2} = \frac{\left(\parallel \boldsymbol{H} \parallel_F^2\right)^2}{\parallel \boldsymbol{H} \parallel_F^2} = \parallel \boldsymbol{H} \parallel_F^2. \tag{4.29}$$

Finally, it can be be written that

$$\boldsymbol{U}_s^H \cdot \boldsymbol{l}_1 \cdot \boldsymbol{l}_1^H \cdot \boldsymbol{U}_s = \parallel \boldsymbol{H} \parallel_F^2 \cdot \begin{bmatrix} 1 & 0 \\ 0 & 0 \end{bmatrix}. \tag{4.30}$$

Using equation (4.30), we can write equation (4.25) as

$$\beta^2 = \left(2 \cdot \frac{\sigma_\nu^2}{P_s}\right)^2 \cdot \|\boldsymbol{H}\|_F^2 \cdot \mathrm{tr}\left\{(\boldsymbol{\Sigma}_s + \lambda \cdot \boldsymbol{I}_2)^{-2} \cdot \begin{bmatrix} 1 & 0 \\ 0 & 0 \end{bmatrix}\right\}. \tag{4.31}$$

It is obvious that $\boldsymbol{\Sigma}_s = \|\boldsymbol{H}\|_F^2 \cdot \boldsymbol{I}_2$, therefore (4.31) can be written as

$$\beta^2 = \left(2 \cdot \frac{\sigma_\nu^2}{P_s}\right)^2 \cdot \frac{\|\boldsymbol{H}\|_F^2}{\left(\|\boldsymbol{H}\|_F^2 + \lambda\right)^2} \tag{4.32}$$

Solving the equation (4.32) for λ results in

$$\lambda = -\|\boldsymbol{H}\|_F^2 \pm 2 \cdot \frac{\sigma_\nu^2}{P_s} \cdot \frac{\|\boldsymbol{H}\|_F}{\beta} \tag{4.33}$$

Substituting (4.33) into (4.24) and using $\boldsymbol{\Sigma}_s = \|\boldsymbol{H}\|_F^2 \cdot \boldsymbol{I}_2$, it is possible to write

$\boldsymbol{\delta}_{\text{worst}}$ as

$$\begin{aligned}\boldsymbol{\delta}_{\text{worst}} &= -2 \cdot \frac{\sigma_\nu^2}{P_s} \cdot \boldsymbol{U}_s \cdot \left(\|\boldsymbol{H}\|_F^2 \cdot \boldsymbol{I}_2 - \|\boldsymbol{H}\|_F^2 \cdot \boldsymbol{I}_2 \pm 2 \cdot \frac{\sigma_\nu^2}{P_s} \cdot \frac{\|\boldsymbol{H}\|_F}{\beta} \cdot \boldsymbol{I}_2 \right)^{-1} \cdot \boldsymbol{U}_s^H \cdot \boldsymbol{l}_1 \\ &= \pm \frac{\beta}{\|\boldsymbol{H}\|_F} \cdot \boldsymbol{U}_s \cdot \boldsymbol{U}_s^H \cdot \boldsymbol{l}_1 \end{aligned} \tag{4.34}$$

Substituting this worst inaccuracy vector into equation (4.16) the maximum Interference power can be obtained as

$$\begin{aligned} P_i^{\max} &= \frac{P_s \cdot \beta^2}{2 \cdot \|\boldsymbol{H}\|_F^2} \cdot \boldsymbol{l}_1^H \cdot \boldsymbol{U}_s \cdot \boldsymbol{U}_s^H \cdot \boldsymbol{L} \cdot \boldsymbol{U}_s \cdot \boldsymbol{U}_s^H \cdot \boldsymbol{l}_1 \\ &= \frac{P_s \cdot \beta^2}{2 \cdot \|\boldsymbol{H}\|_F^2} \cdot \boldsymbol{l}_1^H \cdot \left(\boldsymbol{l}_1 \cdot \boldsymbol{l}_1^H + \boldsymbol{l}_2 \cdot \boldsymbol{l}_2^H \right) \cdot \boldsymbol{l}_1 \\ &= \frac{P_s}{2} \cdot \beta^2 \cdot \|\boldsymbol{H}\|_F^2 \end{aligned} \tag{4.35}$$

Note that only the positive value of $\boldsymbol{\delta}_{\text{worst}}$ has been used because it corresponds to the worst case scenario. Employing equation (4.17), the maximum noise power can be written as

$$\begin{aligned} P_n^{\max} &= \sigma_\nu^2 \cdot \left(\|\boldsymbol{H}\|_F^2 + \beta^2 \pm 2 \cdot \frac{\beta}{\|\boldsymbol{H}\|_F} \cdot \underbrace{\boldsymbol{l}_1^H \cdot \boldsymbol{U}_s \cdot \boldsymbol{U}_s^H \cdot \boldsymbol{l}_1}_{\|\boldsymbol{H}\|_F^2} \right) \\ &= \sigma_\nu^2 \cdot \left(\|\boldsymbol{H}\|_F^2 + \beta^2 + 2 \cdot \beta \cdot \|\boldsymbol{H}\|_F \right) \end{aligned} \tag{4.36}$$

Employing the equations (4.14), (4.35) and (4.36), also considering that the norm of the inaccuracy matrix does not exceed β, the lower bound of the received SINR in the presence of the imperfect channel state information can be written as

$$\text{SINR}_{\text{LB}} = \frac{\left(\|\boldsymbol{H}\|_F^2 \right)^2}{\beta^2 \cdot \|\boldsymbol{H}\|_F^2 + 2 \cdot \frac{\sigma_\nu^2}{P_s} \cdot \left(\|\boldsymbol{H}\|_F + \beta \right)^2} \tag{4.37}$$

4.3.4 Analyzing the loss

In the following, the lower bound of the SINR is analyzed analytically and it is compared with the upper bound of the SINR which is realized when $\beta = 0$, i.e.,

no synchronization error. This way it is possible to know how much is the loss when the channel state information is not accurate.

4.3.4.1 Analyzing the loss in the high SNR regime

It is not difficult to show that in the high SNR regime, i.e., $P_s \gg \sigma_\nu^2$, the lower bound of the SINR converges to $\frac{\|\boldsymbol{H}\|_F^2}{\beta^2}$. Now the objective is to find a bound for the saturation region and its dependency on β^2. Assuming that a represents the desired threshold for the difference of the lower bound of the receiver SINR and $\frac{\|\boldsymbol{H}\|_F^2}{\beta^2}$, it is possible to write the bound of the high SNR regime as

$$\begin{aligned}
\left.\frac{P_s}{\sigma_\nu^2}\right|_{\text{bound}} &= \min\left\{\frac{P_s}{\sigma_\nu^2}\middle|\frac{\|\boldsymbol{H}\|_F^2}{\beta^2} - \text{SINR}_{\text{LB}} \leq a\right\} \\
&= \min\left\{\frac{P_s}{\sigma_\nu^2}\middle|\frac{\|\boldsymbol{H}\|_F^2}{\beta^2} - \frac{\left(\|\boldsymbol{H}\|_F^2\right)^2}{\beta^2\cdot\|\boldsymbol{H}\|_F^2 + 2\cdot\frac{\sigma_\nu^2}{P_s}\cdot\left(\|\boldsymbol{H}\|_F+\beta\right)^2} \leq a\right\} \\
&= \min\left\{\frac{P_s}{\sigma_\nu^2}\middle| g(\beta) \leq \frac{P_s}{\sigma_\nu^2}\right\} \\
g(\beta) &= \frac{2\cdot(\|\boldsymbol{H}\|_F+\beta)^2\cdot(\|\boldsymbol{H}\|_F^2 - a\cdot\beta^2)}{a\cdot\beta^4\cdot\|\boldsymbol{H}\|_F^2}
\end{aligned} \tag{4.38}$$

Obviously, $g(\beta)$ is a monotonically decreasing function with β, which means that the higher the synchronization error is, the faster is the transition to the saturation region. The received SINR versus the transmit power is shown in Figure 4.2 for different values of β^2.

4.3.4.2 Analyzing the loss in the low SNR regime

It has been shown that increasing the norm of the inaccuracy matrix decays the performance of the transmission. Therefore, in the high SNR regime, the lower bound of the SINR converges to a determined fixed value. In the low SNR regime, the lower bound has a relatively constant loss comparing with the upper bound ($\beta^2 = 0$). If there is no inaccuracy, i.e., $\beta = 0$, it is possible to rewrite Equation

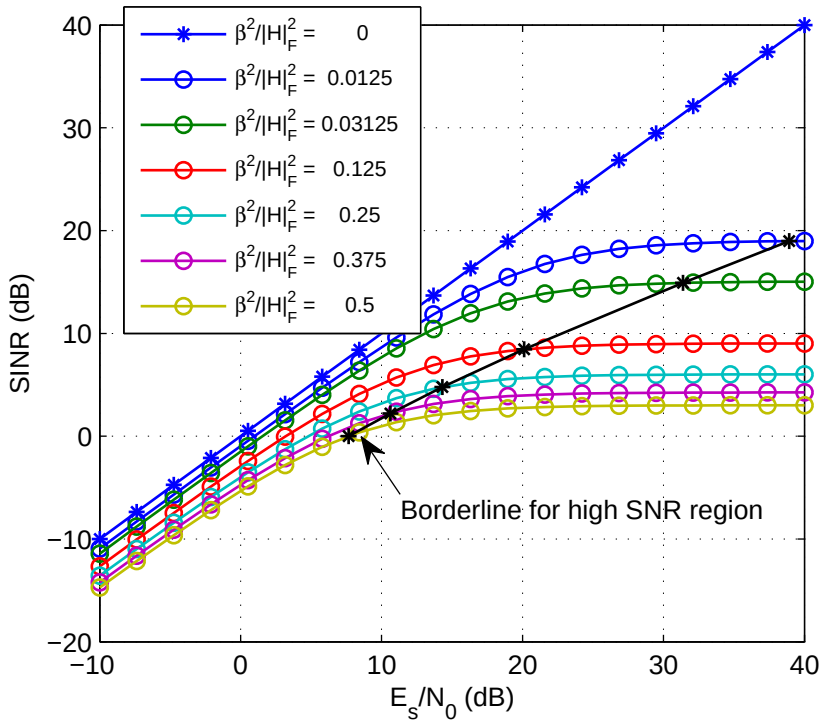

Figure 4.2: Effect of synchronization errors on the lower bound of the received SINR for the Alamouti scheme ($M_t = 2$ and $M_r = 2$). The borderline to the high SNR region is drawn using equation (4.38), and $a = 0.005$. $\rho = E_s/N_0 = P_s/\sigma_\nu^2$ is the SNR.

(4.37) as

$$\mathrm{SINR}_{\mathrm{UB}} = \frac{\left(\|\boldsymbol{H}\|_F^2\right)^2}{2 \cdot \frac{\sigma_\nu^2}{P_s} \cdot \left(\|\boldsymbol{H}\|_F\right)^2} = \frac{\|\boldsymbol{H}\|_F^2}{2 \cdot \frac{\sigma_\nu^2}{P_s}}, \tag{4.39}$$

therefore

$$\frac{\mathrm{SINR}_{\mathrm{UB}}}{\mathrm{SINR}_{\mathrm{LB}}} = \frac{\|\boldsymbol{H}\|_F^2 \cdot \beta^2 + 2 \cdot \frac{\sigma_\nu^2}{P_s} \cdot \left(\|\boldsymbol{H}\|_F + \beta\right)^2}{2 \cdot \frac{\sigma_\nu^2}{P_s} \cdot \|\boldsymbol{H}\|_F^2}, \tag{4.40}$$

and finally, we can write

$$\frac{\mathrm{SINR}_{\mathrm{UB}}}{\mathrm{SINR}_{\mathrm{LB}}} = \frac{P_s}{2 \cdot \sigma_\nu^2}\beta^2 + \left(1 + \frac{\beta}{\|\boldsymbol{H}\|_F}\right)^2. \tag{4.41}$$

Obviously, the amount of this loss depends on the Frobenius norm of the channel matrix. Therefore, considering the distribution of the Frobenius norm of the channel matrix, it is possible to calculate the average of the loss in order to make this analysis more clear.

As it has been discussed in the last chapter, the distribution of square of the Frobenius norm of Rayleigh MIMO channel matrix is a chi-squared distribution which has $2 \cdot M_t \cdot M_r$ degrees of freedom. Note that we focus only on the Alamouti STBC scheme in this chapter for which $M_t = 2$. Considering that the variance of the channel matrix's entries is 1, the distribution of the square of the Frobenius norm of the channel can be written as

$$f_Q(q) = \frac{q^{M_t \cdot M_r - 1} \cdot \exp\left(-q\right)}{(M_t \cdot M_r - 1)!},$$

where $q = \|\boldsymbol{H}\|_F^2$. Employing the PDF of the q, it is possible to write the CDF of $a = \frac{\beta}{\sqrt{q}}$ as

$$\begin{aligned} F_A(a) &= P\left(\frac{\beta}{\sqrt{q}} \leq a\right) \\ &= 1 - F_Q\left(\frac{\beta^2}{a^2}\right). \end{aligned}$$

PDF of a can be calculated, writing the derivative of the CDF of a as

$$\begin{aligned} f_A(a) &= \frac{\partial F_Q(q)}{\partial q} \cdot \frac{\partial q}{\partial a} \\ &= f_Q\left(\frac{\beta^2}{a^2}\right) \cdot \frac{2}{\beta} \cdot \left(\frac{\beta}{a}\right)^3 \\ &= \frac{2}{(M_t \cdot M_r - 1)!} \cdot \left(\frac{\beta}{a}\right)^{2 \cdot M_t \cdot M_r - 2} \cdot \exp\left(-\frac{\beta^2}{a^2}\right) \cdot \frac{\beta^2}{a^3} \end{aligned} \tag{4.42}$$

Employing equation (4.42), the average of a can be written as

$$\begin{aligned} \mathbb{E}\{a\} &= \int_0^\infty f_A(a) \cdot a \cdot da \\ &= \frac{\Gamma\left(M_t \cdot M_r - \frac{1}{2}\right) \cdot \beta}{(M_t \cdot M_r - 1)!}. \end{aligned} \tag{4.43}$$

Where $\Gamma(n)$ denotes the gamma function. It is defined as

$$\Gamma(n) = \int_0^\infty \exp(-t) \cdot t^{n-1} \cdot dt. \tag{4.44}$$

Note that $\Gamma(n) = (n-1)!$ if n is a positive integer. It is also possible to calculate the average of $\frac{\beta^2}{\|\boldsymbol{H}\|_F^2}$. Assuming that t denotes $\frac{\beta^2}{q}$, the CDF of T can be written as

$$\begin{aligned} F_T(t) &= P\left(\frac{\beta^2}{q} \leq t\right) \\ &= 1 - F_Q(\frac{\beta^2}{t}). \end{aligned}$$

Employing the CDF of t, the PDF can be easily obtained by differentiating as

$$\begin{aligned} f_T(t) &= \frac{\partial F_Q(q)}{\partial q} \cdot \frac{\partial q}{\partial t} \\ &= f_Q(\frac{\beta^2}{t}) \cdot \frac{\beta^2}{t^2} \\ &= \frac{1}{(M_t \cdot M_r - 1)!} \left(\frac{\beta^2}{t}\right)^{M_t \cdot M_r - 1} \cdot \exp\left(-\frac{\beta^2}{t}\right) \cdot \frac{\beta^2}{t^2}. \end{aligned}$$

Employing the PDF of t, the average of t can be written as

$$\begin{aligned} \mathbb{E}\{t\} &= \int_0^\infty f_T(t) \cdot t \cdot dt \\ &= \frac{\beta^2}{M_t \cdot M_r - 1}. \end{aligned} \tag{4.45}$$

Employing equation (4.43) and (4.45), the average of (4.41) with respect to $\|\boldsymbol{H}\|_F$ can be written as

$$\mathbb{E}\left\{\frac{\text{SINR}_{\text{UB}}}{\text{SINR}_{\text{LB}}}\right\} = \left(\frac{P_s}{M_t \cdot \sigma_\nu^2} + \frac{1}{M_t \cdot M_r - 1}\right)\beta^2 + 1 + 2 \cdot \beta \cdot \frac{\Gamma(M_t \cdot M_r - 1/2)}{(M_t \cdot M_r - 1)!}. \tag{4.46}$$

Assuming a constant number of transmit antennas, the objective is to decrease the loss, using an increased number of receive antennas. For simplicity, it is assumed that M_r belongs to the set of the real numbers. Considering that

$$\frac{\partial}{\partial a}\left(\frac{\Gamma(M_t \cdot a - 1/2)}{\Gamma(M_t \cdot a)}\right) \leq 0, \quad \text{and} \quad \frac{\partial}{\partial a}\left(\frac{1}{M_t \cdot a - 1}\right) \leq 0, \quad \forall a \in \mathbb{R},$$

it is possible to conclude that the equation (4.46) is a monotonically decreasing function with M_r which means that the impact of the synchronization errors can be reduced, increasing the number of receive antennas. Now the objective is to see that how far the synchronization error can be compensated by increasing the number of receive antennas. Assuming that a large number of users are available in the destination cluster, calculating the limit of the average of the loss, it can be written that

$$\lim_{M_r \to \infty} \mathbb{E}\left\{\frac{\mathrm{SINR_{UB}}}{\mathrm{SINR_{LB}}}\right\} = 1 + \frac{P_s}{M_t \cdot \sigma_N^2} \cdot \beta^2. \tag{4.47}$$

In other words, increasing the number of receive antennas can not decrease the average of loss lower than the given bound in equation (4.47). It can be concluded that the loss caused by the synchronization error can not be completely compensated by increasing number of receive antennas because equation (4.47) is always greater than 1.

Assuming that it is possible to increase the number of transmit antennas without changing the norm of the inaccuracy matrix β^2. Obviously, the average of the loss can be decreased, increasing the number of transmit antennas while

$$\lim_{M_t \to \infty} \mathbb{E}\left\{\frac{\mathrm{SINR_{UB}}}{\mathrm{SINR_{LB}}}\right\} = 1,$$

it can be concluded that increasing the number of transmit antennas can fully compensate the impact of the synchronization error, assuming a constant bound of the inaccuracy norm. But, this assumption is not realistic. Therefore, it is required to perform some analyses about the bound of the inaccuracy matrix norm as a function of the number of the transmit antennas.

4.3.5 Analyzing the BER

In the following, the BER of the worst possible inaccuracy vector is studied in order to help a failure resistant system design, assuming $\mathbb{E}\{|h_{i,j}|^2\} = 1$ for the ith transmitting node and jth receiving node. Studying the BER for all the SNRs is a difficult task. Therefore, only the high SNR regime is considered for simplicity. The BER for BPSK can be written as

$$P_b = \mathbb{E}_{\boldsymbol{H}}\{\frac{1}{2} \cdot \mathrm{erfc}\,(\sqrt{\eta})\}, \tag{4.48}$$

where

erfc is the complementary error function.

The complementary error function, erfc, can be written as

$$\mathrm{erfc}(x) = \frac{2}{\sqrt{\pi}} \cdot \int_x^{\infty} \exp(-a^2) da,$$

where

η is the received SINR.

The expected value is with respect to η. For the cooperative MIMO and in the presence of the synchronization error in the high SNR regime, the lower bound of the received SINR converges to a fixed value of $\eta = \frac{\|\boldsymbol{H}\|_F^2}{\beta^2}$, as pointed out in Section 4.3.4.1. The random variable η has a chi-squared distribution with $2 \cdot M_t \cdot M_r$ degrees of freedom because $\|\boldsymbol{H}\|_F^2$ is the sum of $M_t \cdot M_r$ complex random variables with the variance 1. Therefore, using the distributions derived in the last section, the BER is given by

$$P_b = \int_0^{\infty} \frac{1}{2}\mathrm{erfc}(\sqrt{\eta}) \cdot \frac{(\beta^2)^{M_t \cdot M_r}}{(M_t \cdot M_r - 1)!} \eta^{M_t \cdot M_r - 1} \cdot \exp\left(-\eta \cdot \beta^2\right) d\eta.$$

Employing the theoretical result of the BER in case of maximal ratio combining in [BLM03], the BER can be written as

$$P_b = [f(\beta)]^{M_t \cdot M_r} \sum_{n=0}^{M_t \cdot M_r - 1} \binom{M_t \cdot M_r + n - 1}{n} \cdot [1 - f(\beta)]^n \tag{4.49}$$

where

$$f(\beta) = \frac{1}{2} - \frac{1}{2}\left(1 + \beta^2\right)^{-\frac{1}{2}}. \tag{4.50}$$

The BER in case of the worst possible inaccuracy is shown in Figure 4.3 as a function of the transmit power assuming 2 receive antennas.

4.4 Conclusion

In this chapter, the focus is on the cooperative MIMO scheme in wireless communications. First, we have described a method devised by us to employ SISO piloting in order to gauge the quality of the prospective cooperative MIMO links.

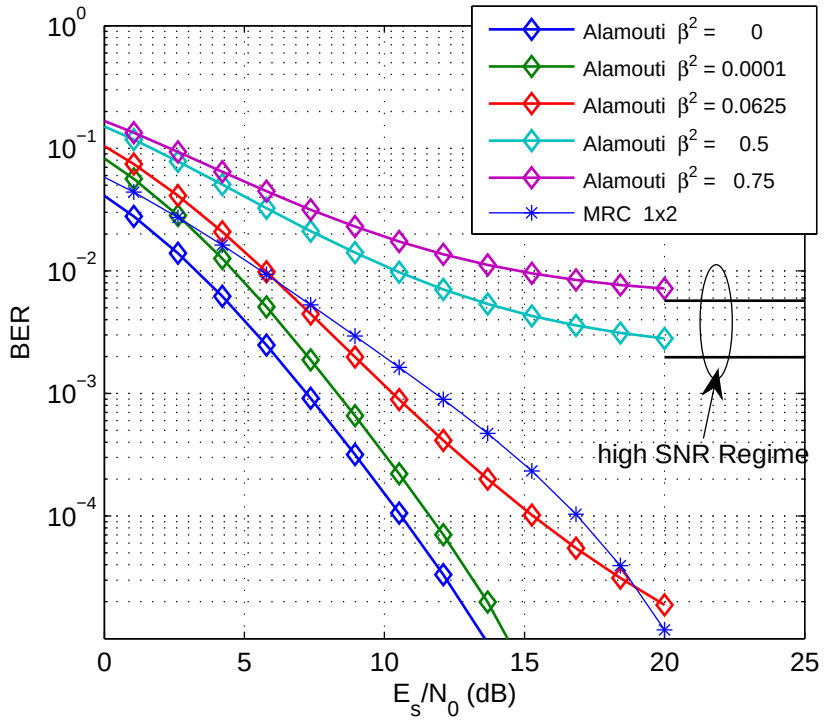

Figure 4.3: BER for the Alamouti scheme ($M_t = 2$) in case of the worst possible inaccuracy vector assuming $M_r = 2$, and BPSK modulation (4.49). $\rho = E_s/N_0 = P_s/\sigma_\nu^2$ is the SNR.

Then, the performance of the cooperative MIMO system in the presence of synchronization errors has been studied. The focus has been on the Alamouti STBC scheme. Also, closed-form expressions of the lower bound of the SINR, the BER for the high SNR regime, and the worst case inaccuracy vector (corresponding to the lowest SINR) have been derived. Furthermore, it has been shown that increasing the transmit power in the high SNR regime does not improve the quality of the transmission because of a saturation region which is caused by the synchronization error assuming a constant number of receive antennas. Additionally, it has been shown that higher synchronization errors result in a faster transition to the high SNR regime and the saturation region.

Part II

Ad-hoc Networking Solutions

Chapter 5

Clustering and Routing

In this chapter, proposed improvements for cluster-based ad-hoc networks on the data link layer and the network layer will be discussed. Specifically, we will be looking at clustering and routing for such a communication scheme involving cooperative relaying. The first part of the chapter describes a new clustering scheme that was proposed by us in [GZH12] to increase the network life-time. The second part of the chapter describes a joint clustering and routing scheme that was proposed by us in [ZGH11b] and [Ghe12], the need for which was discussed by us in [ZSGH11] which is suitable for clustered networks that want to employ cooperative MIMO relaying.

5.1 Introduction

Self-organized ad-hoc systems can play a major role in general mobile networks of the future. They will complement networks that rely on fixed infrastructure such as base stations. One option for operating such networks is to organize them into clusters and perform intelligent relaying for multi-hop transmission between transmitters and receivers. In such a system, mobile handsets present in a network are viewed as users as well as network resources. Many schemes have been proposed to improve the performance of such systems. Cooperative MIMO, where we employ nearby idle nodes to cooperate and form a virtual antenna array, is one such scheme. It is a good option for mobile nodes with a single antenna to be able to achieve the benefits of MIMO communication.

Ad-hoc networks [MC98] are decentralized wireless networks deployed where a pre-existing infrastructure is lacking. During the last years, the interest in employing wireless sensor networks (WSNs) [17006] in a lot of areas, e.g., military field surveillance and environmental monitoring with wireless sensor networks, has increased. In applications where small sensors are deployed to report some parameters, e.g., temperature, pressure, humidity, light, and chemical activity to observers, e.g., base stations, it is difficult to recharge the nodes' batteries because of the dense deployment and the intrinsic nature of the wireless sensor networks. Therefore, one of the most important goals in designing the wireless sensor networks is for it to be energy efficient.

In order to aggregate data in a large-scale deployment of wireless sensor net-

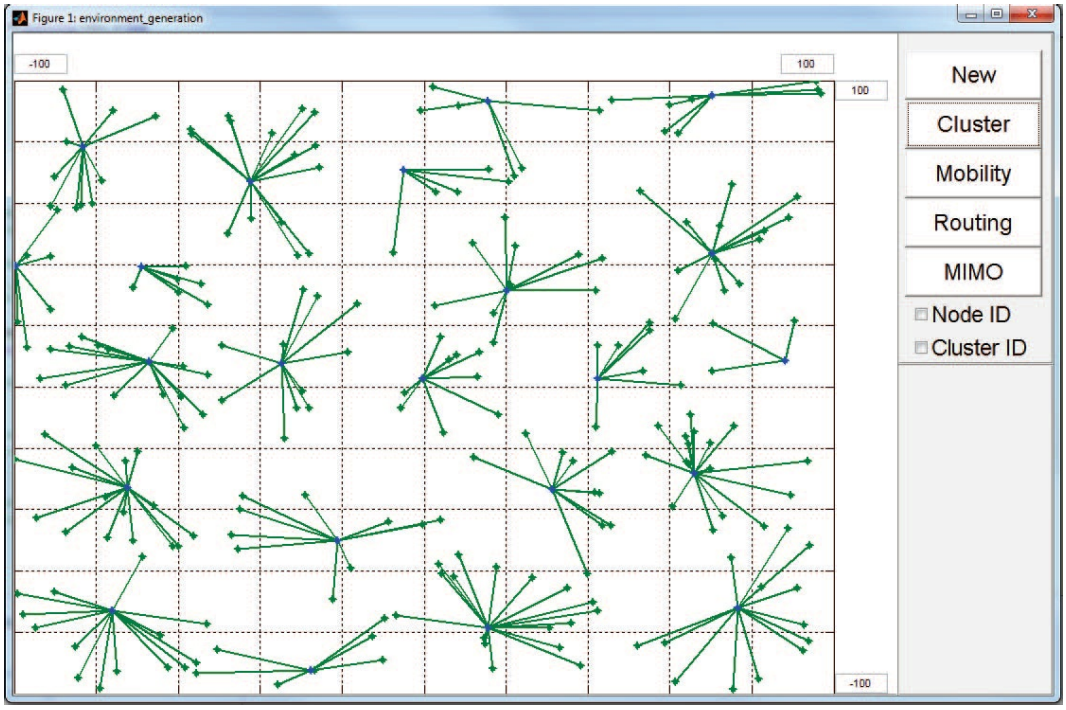

Figure 5.1: A clustered network

works, it is required to organize the network topology in an efficient way to balance the load and prolong the network's life-time. Therefore, nodes can be organized into smaller groups called clusters. Each of these clusters has a coordinator called cluster-head and some member nodes. A typical clustered network is shown in Figure 5.1.

Common clustering schemes include LEACH (Low-Energy Adaptive Clustering Hierarchy) [HCB00], a RSSI (Received Signal Strength Indicator) based method [FPL09], and a GPS based scheme to tackle mobility similar to [AP01]. Reference [FPL09] is one of the newest proposed clustering schemes and a good option to simplify the process of clustering through piloting and local information gathering but cannot deal well with the mobility of nodes. A very good scheme to maintain clustering in the face of the mobility of nodes in the system is presented in [AP01]. To privide an increased network life-time we have proposed a new clustering scheme, Enhanced Received Signal Strength Indicator based clustering (E-RSSI) [GZH12].

5.2 E-RSSI clustering scheme

Clustering results in a two-layered hierarchy in which the top layer comprises the cluster-heads and the bottom layer comprises the member nodes. In this structure, cluster-heads aggregate the data from their member nodes and communicate with other cluster-heads (and maybe even with a base station). This means that cluster-heads may have to transmit data over longer distances and therefore end up losing more energy in comparison with member nodes. This fact along with the existence of networks with limited energy nodes, makes the procedure of selecting the cluster-heads very critical.

We aim to select cluster-heads in an optimum manner to decrease the transmission cost and make the probability of becoming the cluster-head even for all the nodes, in order to increase the network′s life-time. There are different definitions of the network life-time depending on the application. Some define the network life-time as the time it takes until the first node runs out of enough energy to communicate. Others define the network life-time as the time it takes until the last node runs out of enough energy to communicate. In this chapter network life-time will refer to the first one, i.e., the time it takes until the first node runs out of enough energy to communicate, as we want to keep all nodes in the network operational, for as long as possible.

Clustering shows improvement in network life-time which is a primary parameter to evaluate the performance of an ad-hoc network. Also several clustering algorithms have been proposed until now using different approaches to maintain this goal.

In the rest of this section we have a look at the related work in the area. We will compare our proposed clustering scheme to two prominent clustering schemes from the literature: LEACH (Low-Energy Adaptive clustering Hierarchy) [HCB00], which is perhaps the most popular scheme, and RSSI (Received Signal Strength Indication) clustering [FPL09] which is a highly suitable scheme for sensor networks as the RSSI determination capability is a part of the 802.15.4 standard [17006] which is implemented in many commercial radios. The cluster-head selection procedures of both these schemes are described in detail first. Then we discuss our cluster-head selection algorithm (E-RSSI). Afterwards, the

experimental simulation results are represented.

The LEACH algorithm represents a probabilistic way of choosing cluster-heads which shows a large variation over the average link distances of clusters and leads to uneven energy consumption during transmission phase. But this way, the energy load of being cluster-head is distributed among all the nodes leading to a longer network life-time. On the other hand, the RSSI algorithm tries to reduce the variation over the average link distances between end nodes and cluster-heads by means of choosing cluster-heads in the areas of greater node density in order to have an even energy consumption during the transmission phase. Less average link distance between end nodes and cluster-heads means that there is a greater probability of data aggregation. But RSSI distributes the energy load of being cluster-head between some specific nodes which leads to a shorter network life-time.

Here, we propose a new clustering scheme based on the RSSI algorithm which combines the main advantages of RSSI and LEACH. The average link distance of E-RSSI (Enhanced RSSI) is similar to the average link distance of RSSI. Also E-RSSI, like RSSI, has a significantly smaller variation over the average link distances in comparison with LEACH and at the same time shows significant improvement in the network life-time. E-RSSI produces a low energy cost per node like RSSI and a more evenly distributed energy cost per node like LEACH, therefore a prolonged network life-time.

5.2.1 Related work

LEACH [HCB00], one of the most influential works in the cluster-head selection area, is a clustering protocol that applies randomized rotation of cluster-heads to distribute the energy load evenly among the nodes in the network. However, it shows a large variation over the average link distances of clusters and leads to an uneven energy consumption during transmission phase.

HEED [YF04] (Hybrid Energy-Efficient Distributed) clustering is an energy-efficient approach for clustering nodes in ad-hoc sensor networks which periodically selects cluster-heads according to a hybrid of their residual energy and a secondary parameter like distance of a node from its neighbors or node degree.

The randomness of LEACH and HEED causes the unfavorable fact that there is no guarantee to have enough cluster-heads in each round which leads to some problems like having a lot of orphaned nodes (nodes that do not belong to any cluster).

RSSI [FPL09] (Received Signal Strength Indication) clustering is an RF signal strength based algorithm using a competitive distributed scheme in which nodes attempt to reduce the overall required transmission energy and form favorable clusters based on the density and quality of the Received Signal Strength Indication (RSSI). RSSI algorithms try to reduce the variation over the average link distances of clusters by means of choosing cluster-heads in the areas of greater node density in order to have an even energy consumption during the transmission phase. But they distribute the energy load of being cluster-head between some specific nodes which leads to a shorter network life-time.

It is possible to utilize RSSI values in different ways. In [AR10], one proposed method is based on a multiple summation of RSSI values, while the other one is based on a multiple of the last sensed RSSI values.

5.2.2 Cluster-head selection in LEACH

As mentioned before, LEACH [HCB00] periodically assigns the task of being cluster-head between the nodes in a random manner in order to distribute the energy load evenly among the nodes in the network. The LEACH operation consists of several rounds. Each round starts with a set-up phase in which the clusters are organized and it continues with a steady-state phase in which data is transferred to the base station. The steady-state phase should be long in comparison to the set-up phase in order to minimize overhead.

5.2.2.1 Advertisement Phase

Initially, in order to create the clusters, each node decides by itself to become a cluster-head or not in the current round. Each node makes this decision based on the desired total number of cluster-heads in the network which is determined a priori and the number of previous rounds in which the node has been a cluster-head up to this point. Node n makes this decision by choosing a random number

between 0 and 1 and this node becomes a cluster-head for the current round if this number is less than a threshold $T(n)$. If P is the desired percentage of cluster-heads (e.g., $P = 0.05$), then based on P the whole network functions for some cycles, each consisting of $\frac{1}{P}$ rounds. Employing this threshold, each node becomes a cluster-head in some rounds within each cycle. Initially, round 0, there is a probability P that each node becomes a cluster-head. It is not possible anymore for the nodes which are cluster-head in round 0 to become cluster-head during the next $\frac{1}{P}$ rounds. Therefore the probability for the remaining nodes to become cluster-head is increased, as there are fewer eligible nodes left. After $\frac{1}{P} - 1$ rounds, i.e., the last round of the cycle, the threshold $T(n)$ becomes 1 for the nodes which have not been cluster-heads yet. After $\frac{1}{P}$ rounds, as in round 0, all the nodes are once again eligible to become cluster-head as in round 0. At the end of a round, any node that has elected itself as a cluster-head broadcasts an advertisement message to all the nodes employing a CSMA-MAC (carrier sense multiple access-media access control) protocol. Also, all the cluster-heads should transmit the advertisement with the same transmit energy. During this phase of advertisement, all the non-cluster-head nodes must keep their receivers on, in order to hear all the cluster-head nodes.

When this phase of advertisement is complete, each non-cluster-head node makes a decision regarding which cluster it will belong to for this round based on the received signal strength of the advertisement. The propagation channels are assumed symmetric. Therefore the received cluster-head advertisement with the largest signal strength is assumed to come from the most suitable cluster-head, because the minimum amount of transmit energy is needed to communicate with it. In the case of ties, a cluster-head is randomly chosen.

5.2.2.2 Cluster Set-Up Phase

After each node has decided which cluster it will join, it must tell the cluster-head node that it will be a member of its cluster. This transmission is again performed using a CSMA-MAC protocol. Obviously all the cluster-heads must keep their receivers on during this phase in order to be able to listen to the non-cluster-head nodes.

5.2.2.3 Schedule Creation

Based on the number of nodes that want to join the cluster, the cluster-head generates a TDMA schedule and informs each node when it is allowed to transmit. The cluster-head broadcasts this schedule back to the nodes in the cluster.

5.2.2.4 Data Transmission

Nodes can begin the data transmission as soon as the clusters are formed and the TDMA schedule is known. Assuming that all the nodes always have data to send, they can send it to the cluster-head during their assigned transmission time. The energy of this transmission is chosen based on the received signal strength of the cluster-head advertisement. The non-cluster-head nodes do not need to send or receive until the node's allocated transmission time is reached. Therefore in order to minimize the energy dissipation they can turn off their radio. On the other hand, the cluster-heads must keep their receiver on in order to receive all the data from the non-cluster-head nodes in their cluster. This leads to a greater depletion of the battery of the cluster-head compared to the normal nodes.

After receiving all the data, the cluster-heads perform some signal processing functions in order to compress the data into a single signal [SS06], [KS07], and [ZZS10]. For example, in case of a wireless sensor network which collects some data as audio or seismic signals, the cluster-head node can generate a composite signal after beamforming the individual signals. Afterwards, each cluster-head may send this composite signal to the base station which is far away. This would be a high-energy transmission. After a certain time, which is determined a priori, the data transmission phase is finished and the next round begins where each node determines if it should become a cluster-head for each round and so on.

5.2.2.5 Multiple Clusters

The previous sections describe how the individual cluster-heads communicate with their cluster nodes. However, transmission in one cluster affects the communication in an adjacent cluster. Therefore each cluster should communicate by employing different CDMA (code division multiple access) codes in order to reduce this interference. To do so, each node chooses a spreading code randomly

from a predefined list when it decides to become a cluster-head. The next step would be to inform the non-cluster-head nodes in the cluster to employ the same spreading code when they want to transmit.

5.2.2.6 Hierarchical Clustering

It is possible to extend LEACH in order to establish hierarchical clusters where the cluster-heads communicate with super-cluster-heads and so on until the point at which the data may be sent to the base station. This hierarchical clustering could save a remarkable amount of energy in case of large networks.

5.2.3 Cluster-head selection in RSSI

In the RSSI clustering algorithm each node considers two objectives. The node tries to join clusters that require the least transmission energy in order to optimize its own energy consumption. Moreover, if the link quality for a node falls below a specific threshold, then it will not associate with that cluster-head. Employing the RSSI clustering algorithm yields that the nodes located in an area with more node density become cluster-heads much more often than the other nodes, leaving them susceptible to rapid battery drainage. It works as follows:

5.2.3.1 Initial phase

In this phase, each node starts as a non-associated node. Therefore, each node actively scans its surroundings, through piloting, in order to find the active clusters. In case any cluster-heads are found, the node evaluates the RSSI of different cluster-heads responses and verifies if the signal strength is above a required threshold $\mathrm{RSSI}_{\mathrm{thres}}$. If multiple cluster-heads are found, the node associates itself with the cluster-head which shows the strongest RSSI.

5.2.3.2 Topology discovery phase

If no suitable cluster-head is available after scanning for the active clusters then the node goes to the topology discovery phase in which each non-associated node broadcasts a node discovery request having a time-out value. With this time-out

value the node specifies the maximum time duration allowed for a response to the node discovery message. The non-associated nodes which receive the node discovery message will respond by sending their configuration. All responses which are received after the time-out are ignored.

5.2.3.3 Promotion factor computation

After receiving the responses to the discovery request, each node sorts the received RSSI values in a decreasing order. After that, the node computes its promotion factor P_{fact} which determines the likelihood that a node promotes itself to a cluster-head. The promotion factor can be computed as:

$$P_{\text{fact}} = \begin{cases} e^n \cdot \frac{\sum_{i=1}^{n} \text{RSSI}_i}{n} & \text{if } n{>}0 \\ \infty & \text{if } n{=}0 \end{cases} \tag{5.1}$$

where

n	is the number of responses received
RSSI_i	is the strongest received signal strength from the ith responding node.

5.2.3.4 Cluster-head promotion phase

In this phase, each node waits x number of rounds before it attempts to promote itself to a cluster-head. The number of rounds can be calculated as $x = \frac{C}{P_{\text{fact}}}$ in which C is a network dependent constant. As it is obvious from the equation, a node with a larger value of the promotion factor promotes itself sooner. If $P_{\text{fact}} = \infty$, it means that no other non-associated nodes are detectable. Therefore the node promotes itself immediately to a cluster-head.

5.2.3.5 Periodic active scans

During the cluster-head promotion phase, each node runs periodic active scans in order to find new cluster-heads. If the node finds a cluster-head before promoting itself, it compares the RSSI of the cluster-head announcement message with

$RSSI_{thres}$. If it is above the threshold, the node terminates its cluster-head promotion algorithm and sends an association request to the corresponding cluster-head. If multiple cluster-heads are present, the node associates with the cluster-head which shows the strongest RSSI.

5.2.3.6 Optimization phase

Each node enters the optimization phase when it has been associated with a cluster-head or its cluster-head promotion algorithm has been completed. Each node continues to run periodic active scans in order to find cluster-heads. The objective is to minimize the transmission energy when communicating with its cluster-head in order to maximize life-time. If the node finds a more suitable cluster-head, it will end the association with its current cluster-head and send an association request to the new cluster-head.

At anytime, if a cluster-head dies or an association with a cluster-head is lost, the node scans for available cluster-heads and begin the cluster-head promotion phase in order to determine its new promotion factor. It is noteworthy to mention that the number of the cluster-heads is arbitrary and is determined by $RSSI_{thres}$, while in LEACH it is fixed, as was mentioned in the previous section. A larger value of $RSSI_{thres}$ results in a greater number of cluster-heads.

5.2.4 Cluster-head selection in E-RSSI

We propose a new clustering scheme, E-RSSI (Enhanced RSSI), based on the RSSI algorithm. The proposed scheme combines the main advantages of RSSI and LEACH. E-RSSI produces a low energy cost per node like RSSI and a more evenly distributed energy cost per node like LEACH. Thereby a prolonged network life-time is achieved.

In our proposed RSSI clustering algorithm each node goes through 5 different phases as follows:

5.2.4.1 Initial phase

At the starting point, each node is in a non-associated state in which it runs an active scan to search for active cluster-heads. For each cluster-head found, the

non-associated node verifies whether the strength of the received signal is above the predefined threshold $\text{RSSI}_{\text{thres}}$. If there are some cluster-heads available, the non-associated node compares the received signal strengths and associates with the best cluster-head.

5.2.4.2 Topology discovery phase

Each node that was not successful in finding a suitable cluster-head in the initial phase is a candidate node to be the cluster-head and broadcasts a node discovery message to the network. All the nodes that received this message will respond with their configurations. It is important to note that not only the non-associated nodes but even the associated nodes that received this message will respond with their configurations.

5.2.4.3 Promotion factor calculation phase

After receiving responses to the node discovery message, the candidate node starts to compute its promotion factor, P_{fact}. We can think of $1/P_{\text{fact}}$ as the likelihood that a candidate node promotes itself to a cluster-head. If $n \neq 0$, it is possible to say:

$$P_{\text{fact}} = \frac{e^n \sum_{i=1}^{n} \text{RSSI}_i}{n} \tag{5.2}$$

where

n	is the number of the received responses
RSSI_i	is the strength of the i^{th} received response which is more than $\text{RSSI}_{\text{thresh}}$.

Please note that in the above summation, only the received responses which are more than $\text{RSSI}_{\text{thresh}}$ are of interest.
It is obvious that for $n = 0$, P_{fact} is to be considered ∞ so that the likelihood of its promotion will be maximum.

Also it is important to note that each node compares its remaining battery with the average remaining battery of its neighbors B_{avg} and its minimum distance

to other cluster-heads with a reference distance D_{CH}. If its remaining battery is less than 90 % of B_{avg} or its distance to nearest cluster-head is less than D_{CH} then it puts its $P_{\text{fact}} = 0$ in order to not become a cluster-head as long as the result of at least one of these comparisons remains the same.

5.2.4.4 Promotion phase

Each candidate node with a $P_{\text{fact}} \neq \infty$ will wait for a number of cycles $x = C/P_{\text{fact}}$ in which C is network dependent constant number. On the other hand, each candidate node with a $P_{\text{fact}} = \infty$ instantly promotes itself to cluster-head because no other non-associated nodes are found.

Note that, during this phase each node also carries out a periodic active scan for new cluster-heads. For each cluster-head found, the candidate node verifies whether the strength of the received signal is above the predefined threshold $\text{RSSI}_{\text{thresh}}$ or not. If there are some cluster-heads available then the candidate node terminates its promotion algorithm, compares the received signal strengths, and associates with the best cluster-head.

5.2.4.5 Optimization phase

Once a node associates itself to a cluster-head, it enters the optimization phase in which each associated node continues to run an active scan to search for active cluster-heads with a better RSSI value than its current association. If a cluster-head with a better RSSI is found then the associated node breaks its association with current cluster-head and sends an association request to the new cluster-head.

At any time if an associated node loses its association, for example, because of a cluster-head running out of battery, it simply assume itself as a non-associated node and starts over from the initial phase.

Also each cluster-head compares its remaining battery with the average remaining battery of its neighbors B_{avg} and if it is less than 90 % of B_{avg} it decides for itself and its cluster members to become non-associated nodes in the next cycle to give a chance to other eligible nodes with higher amount of battery to become cluster-head.

5.2.5 Simulation results

A simulator has been built with MATLAB in order to test the proposed clustering algorithm and to compare it with RSSI [FPL09] and LEACH [HCB00]. Similar to [HCB02] (LEACH), we place 101 nodes randomly in a 100 m by 100 m grid. In order to have a fair comparison, there should be the same number of cluster-heads for all 3 algorithms and we aimed for 5 % of the nodes to be cluster-heads as it is suggested for these system parameters and topology in LEACH [HCB00]. Note that the number of cluster-heads is defined in LEACH explicitly but in RSSI it is defined implicitly based on parameters like $\text{RSSI}_{\text{thresh}}$ and C. Also, not all the nodes are able to communicate with each other. Therefore some nodes may remain orphaned.

We aggregate the simulation data over two cases for two different network topologies to compare the network life-time of E-RSSI, RSSI, and LEACH in a better way. In the first case, a central base-station/data-aggregation-unit is assumed to be outside of the 100 m by 100 m grid. We assume that each node has always a 2000-bit data packet to send (for example in sensor networks when nodes are sensing the environment at a fixed rate). In each transmission round (cycle) all the member nodes send their data packets to their cluster-head. Once a cluster-head gathers them all it tries to fine the best route with the minimum number of hops to the base-station and sends them. The simulation is repeated 100 times in the Monte Carlo fashion. The nodes are re-deployed randomly at teh start of each Monte Carlo simulation. In the second case, there is no base-station and nodes are communicating with each other. In this case, during each cycle 10 pairs of nodes are chosen randomly as the transmitter and receiver, then the best route with the minimum number of hops is found and finally a 2000-bit data packet will be sent to the receiver. The simulation data for both cases is then aggregated to find the mean and standard deviation of the various parameters of interest. For simplicity we assumed the symmetric AWGN channel model, for which we modeled RSSI as a function of distance:

$$\text{RSSI}(d) = P_{\text{tx}} L(d_{\text{ref}}) + 10 \cdot \alpha \cdot \log_{10} \frac{d}{d_{\text{ref}}} + X_g \tag{5.3}$$

where

P_{tx}	is the transmit power
$L(d_{\text{ref}})$	is the path loss for a reference distance d_{ref}
α	is the path loss exponent
X_g	is a Gaussian random variable with 0 dB mean (in case of no fading it is equal to 0 dB).

Note that for this simulation we have not considered fading to be present. We assume BPSK (Binary Phase-Shift Keying) modulation for simplicity. Uncoded transmissions with a transmit SNR of 37 dB and path loss exponent = 2 was used. In order to come up with an $RSSI_{thresh}$, we assume a required BER (Bit Error Rate). 100 Monte Carlo simulations were used for the figures shown in this section.

Using the proposed energy model in LEACH [HCB02] and the Friis free space model, the radio expends an amount of energy given by:

$$E_{\text{tx}} = N_b E_{\text{amp}} + N_b E_{\text{elec}} d^2 \tag{5.4}$$

to transmit an N_b-bit message and expends an amount of energy given by:

$$E_{\text{rx}} = N_b E_{\text{amp}} \tag{5.5}$$

to receive it. Here

E_{elec}	is the amount of energy that a radio dissipates to operate the circuitry of its transmitter or receiver
E_{amp}	is the amount of energy that a radio needs to use in order to achieve an acceptable E_b/N_0
$\rho = E_b/N_0$	is the ratio of energy per bit to noise power spectral density.

E-RSSI, RSSI and LEACH can be compared based on:

- The number of alive nodes as a function of the cycle
- The variance of remaining batteries of nodes as a function of the cycle
- The average number of orphaned nodes

- The number of cluster-heads
- The average distance between nodes and cluster-heads

As Figure 5.2 shows, in average, in the RSSI clustering the first node dies at the 15^{th} cycle, in LEACH the first node dies at the 30^{th} cycle and in E-RSSI clustering the first node dies at the 120^{th} cycle. Therefore, in E-RSSI it takes about 8 times longer than RSSI and 4 times longer than LEACH, for the first node to die.

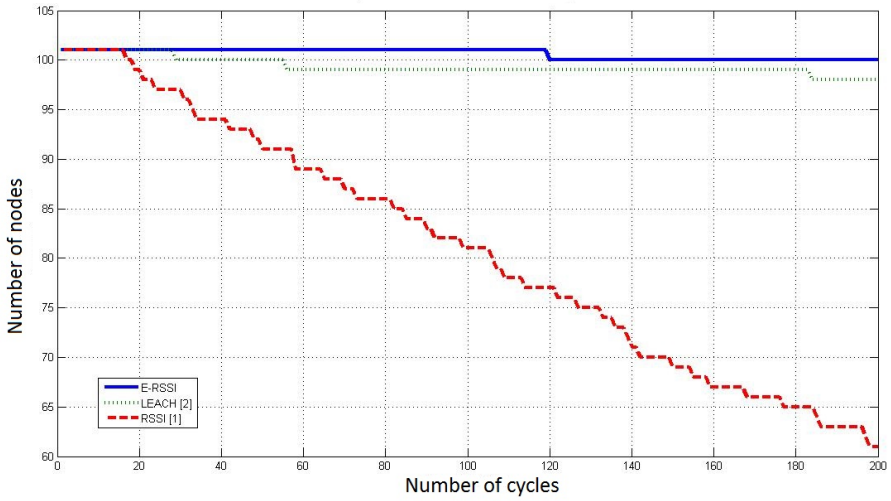

Figure 5.2: Number of alive nodes as a function of the cycle

From Figure 5.3, we see that the variance of the remaining batteries of nodes in E-RSSI and LEACH is significantly less than RSSI, which means that the energy load of being cluster-head is distributed among all the nodes in a better way leading to a longer network life-time.

Providing a longer network life-time is not the only advantage of E-RSSI over LEACH. Simulations show that after 100 cycles, having 5 cluster-heads out of 100 nodes, on average around 4 % of nodes in E-RSSI, 3 % of nodes in RSSI and 18 % of nodes in LEACH remain orphaned per cycle and it shows that E-RSSI and RSSI significantly outperform LEACH in terms of the average number of orphaned nodes. Figures 5.4, 5.5 and 5.6 show the histogram of the number of orphaned nodes in E-RSSI, LEACH and RSSI respectively. By looking at the

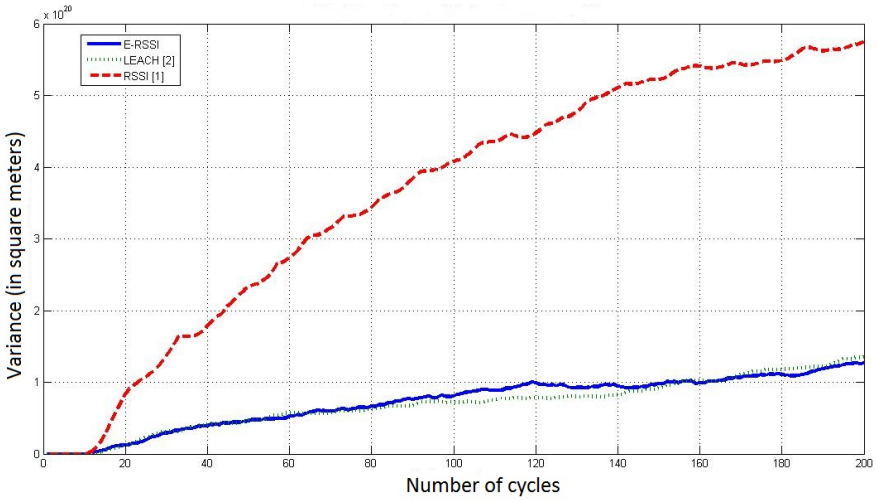

Figure 5.3: Variance of remaining batteries of nodes as a function of the cycle

spread of the histograms, we can see that higher number of orphaned nodes occur very seldom in E-RSSI compared to LEACH and RSSI.

We aimed at having 5 cluster-heads for all 3 algorithms during simulations to have a fair comparison and simulation results show that the average number of cluster-heads per cycle for E-RSSI, RSSI and LEACH are respectively around 5.4, 5.0 and 5.2. As Figures 5.7, 5.8 and 5.9 show, in case of E-RSSI and RSSI, the standard deviation is around 0.7 and 0.9 respectively which is significantly less than the standard deviation in LEACH which is 2.5.

As Figures 5.10, 5.11 and 5.12 show, the average link distances for E-RSSI, RSSI and LEACH are, respectively, about 19.2, 19.2 and 20.1 meters, which shows that both E-RSSI and RSSI have around 5 % improvement in the average link distance over LEACH. Also, in case of standard deviation of average link distance E-RSSI and RSSI show around 13 % and 8 % improvement, respectively, over LEACH.

According to equation (5.6), having a lower average link distance leads to a lower energy usage for transmission. Also having a lower standard deviation of average link distance leads to a more even distribution of the energy consumption over all the nodes. Moreover, distributing the load of being cluster-head between all the nodes leads to a better network life-time. Choosing the cluster-heads in

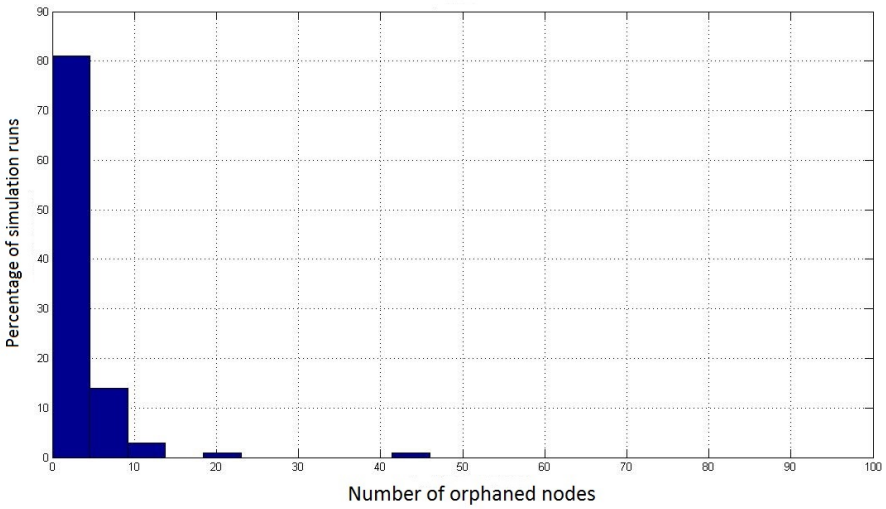

Figure 5.4: Number of orphaned nodes in E-RSSI

the right places also leads to less number of orphaned nodes and hence better connectivity in the network.

By looking at the Table 5.1 we can see that LEACH distributes the energy load of being cluster-head over all nodes in a random manner which is why it has a better network life-time than RSSI, but RSSI produces links with lower average distances and lower standard deviations in comparison with LEACH which leads to a lower transmission energy consumption. E-RSSI, on the other hand, has all the aforementioned benefits of both these schemes which leads to a significantly longer network life-time in comparison with both RSSI and LEACH.

clustering Algorithm	Link Distance - Mean (Std)	Percentage of Orphaned Nodes - Mean (Std)	Cycle Number for First Dead Node - Mean (Std)
RSSI	19.2 (8.7)	2.8 (0.8)	15 (3.4)
LEACH	20.1 (9.5)	17.7 (1.4)	30 (4.8)
E-RSSI	19.2 (8.3)	3.9 (1.4)	120 (23.8)

Table 5.1: Comparing LEACH, RSSI, and E-RSSI. (Std stands for the standard deviation.)

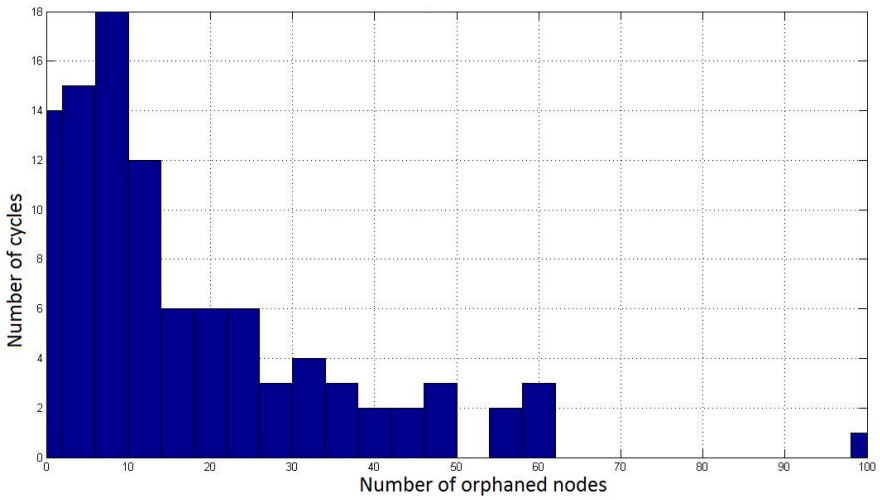

Figure 5.5: Number of orphaned nodes in LEACH

5.3 Joint clustering and routing mechanism for cooperative MIMO multi-hop networks

Ad-hoc networks that support multi-hopping can provide a range of solutions for range-limited sensor and machine-to-machine networks. However such networks have their own set of implementation and performance issues. Clustering helps in organizing the networks and providing a backbone for routing data packets over multi-hop links. However multi-hopping itself can cause a loss in performance compared to single-hop systems. This is because, as shown in the last chapters, the ergodic capacity of links in such networks is a decreasing function of the number of hops. Also error-propagation over multiple hops can result in a much reduced performance. Hence it is beneficial to reduce the number of hops in multi-hop networks. One way to do this is to employ cooperative MIMO (Multiple Input Multiple Output) techniques to increase the range of these devices. This will result in reducing the number of hops. However incorporating cooperative MIMO in an ad-hoc network without central control and with self-organised routing can be challenging. In this chapter, we present a novel joint clustering and routing mechanism to simplify and define the procedure for nodes to employ cooperative MIMO to gain an increase in performance. We introduce

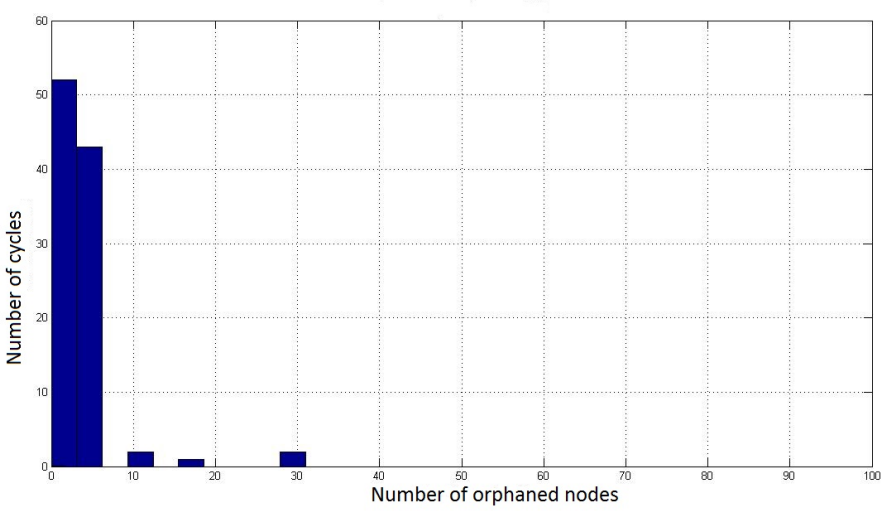

Figure 5.6: Number of orphaned nodes in RSSI

the concept of 'cooperative-MIMO-linked neighboring clusters' and describe how that can be used in conjunction with our specialized routing mechanism AOCMR (Ad-hoc On-Demand Cooperative MIMO Routing), to enable nodes to efficiently communicate in large scale networks in a decentralized manner.

We are rapidly approaching the era where the amount of communicating mobile devices will outnumber the human population by far [Haa]. This will bring into existence the so-called 'internet of things'. Thus machine to machine (M2M) networks are attracting a lot of attention from academia and industry alike. There are some specific attributes of these networks that sometimes makes them hard to set up. Indeed, there are some attributes that simplify the task of the network designer as well.

A major difficulty is that most of this communication should better be kept off the main backbone of communication being used by people. This is because the sheer number of these devices and their continuous communication with each other can seriously strain the bandwidth of a network in general use by the public. This can be accomplished by applying ad-hoc networking techniques to 'local' networks of machines. 'Clustering' (grouping together of nodes geographically located close to each other, with a pseudo base-station in each group known as the cluster-head) can help with self-organization and routing. Another diffi-

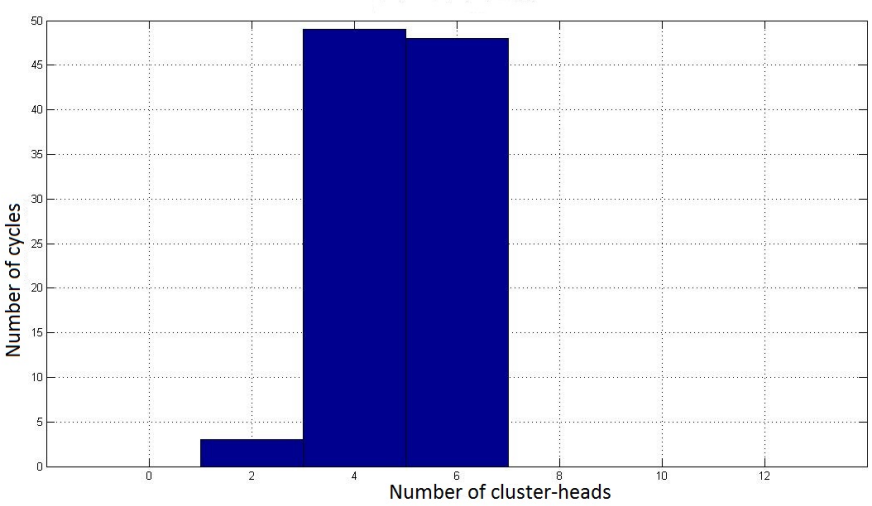

Figure 5.7: Number of cluster-heads in RSSI

culty with M2M networks is that most of the 'nodes' have limited range and are mostly equipped with a single antenna. Multi-hopping is a possible solution for communicating over large distances with such devices. This can solve the range issue as well as provide frequency re-use benefits.

In many cases, however, the multi-hopping can yield a reduced performance because of loss in capacity (explained in Chapter 2), and the effects of error propagation. Hence it is advisable to use cooperative MIMO to increase the range of these devices in order to reduce the number of hops. In this section we propose a joint clustering and routing method that makes it easier and simpler for nodes in ad-hoc and M2M networks to utilize the cooperative MIMO technique (of any diversity order) to increase the throughput capacity. This extends the range of each packet hop and increases the link performance by decreasing the delay as a result of having fewer hops from source to destination.

In the previous chapters it was mentioned that it is important to use more antennas to decrease the number of the hops. Co-operative or virtual MIMO is a good concept for mobile nodes with a single antenna to be able to achieve the benefits of MIMO communications. It is ideally suited for the distributed clustered system under investigation, where nearby nodes can be employed to cooperate and form a virtual antenna array. It is also imperative to modify the

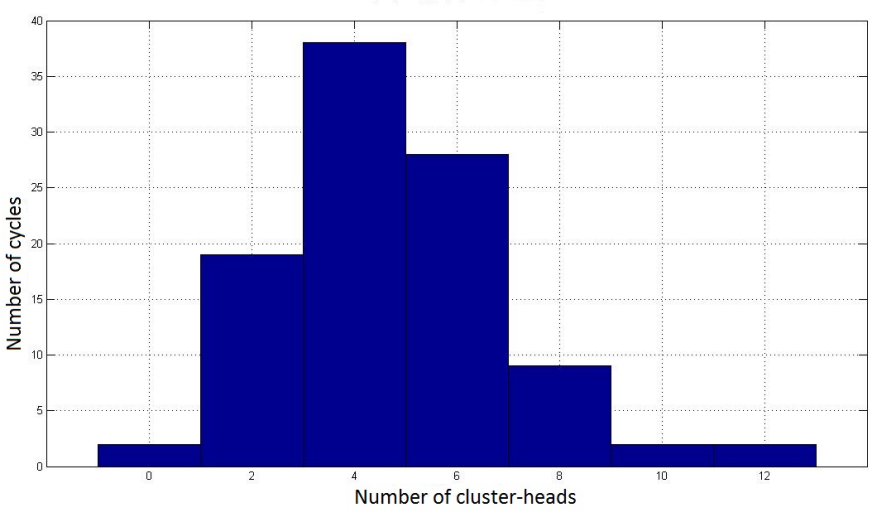

Figure 5.8: Number of cluster-heads in LEACH

routing scheme to incorporate the need for multiple paths between clusters. A routing example with 2×2 (virtual) MIMO channels between clusters is shown in the Figure 5.13. In Figure 5.14, the 2×2 virtual MIMO is compared to the SISO case, in terms of the Bit Error Rate (BER) for the example multi-hop communication scenario from Figure 5.13. The MIMO gain is clearly visible thus justifying the use of a virtual MIMO scheme wherever idle nodes are available. If, however, no extra nodes are available then SISO multi-hopping provides a good performance too, thus eradicating the need for fixed infrastructures such as base stations.

Cooperative MIMO can be employed to improve the performance of the links which results in an increase of the range of the hops while ensuring that the required QoS (bit error rate) is fulfilled. Though, employing this technique in an ad-hoc network is a difficult task where the lack of a centralized network controller, e.g., a base station makes it challenging to establish a link. Therefore a joint clustering and routing method is proposed to simplify this task. First we show the analysis of the ergodic capacity in multi-hop scenarios which highlights the need for the reduction in the number of hops per transmission in large scale multi-hop networks and then explain the proposed joint routing and clustering mechanism to employ cooperative MIMO.

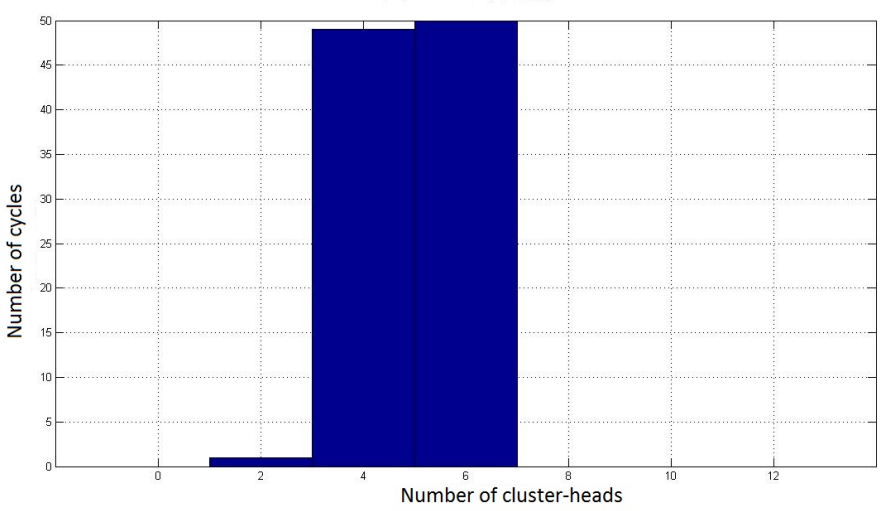

Figure 5.9: Number of cluster-heads in E-RSSI

5.3.1 Analysis of Ergodic Capacity for Multi-hop Scenarios

We will now briefly recap the analysis performed in Chapter 2 regarding the capacity of AF and DF relaying in order to highlight the need for a new routing mechanism that can keep the number of hops low.

The system model is the same as the one used in Chapter 2 and is shown in Figure 5.15.

We showed in Section 2.2 that the ergodic capacity for AF relaying systems, given by equation (2.20), is a decreasing function of the number of hops. This fact was illustrated in Figure 2.5. The same was true for the ergodic capacity of DF relaying systems, given by equation (2.26), and illustrated in Figure 2.7.

Our analysis points to a common misconception that shorter hops result in an increased performance. While it is true that the received SNR for each hop is better in that case, the amount of retransmissions due to the increased number of hops translates into a linear decrease in the throughput capacity of the multi-hop link which overtakes the logarithmic increase in capacity due to the increased SNR and in the end we are left with a reduced overall performance.

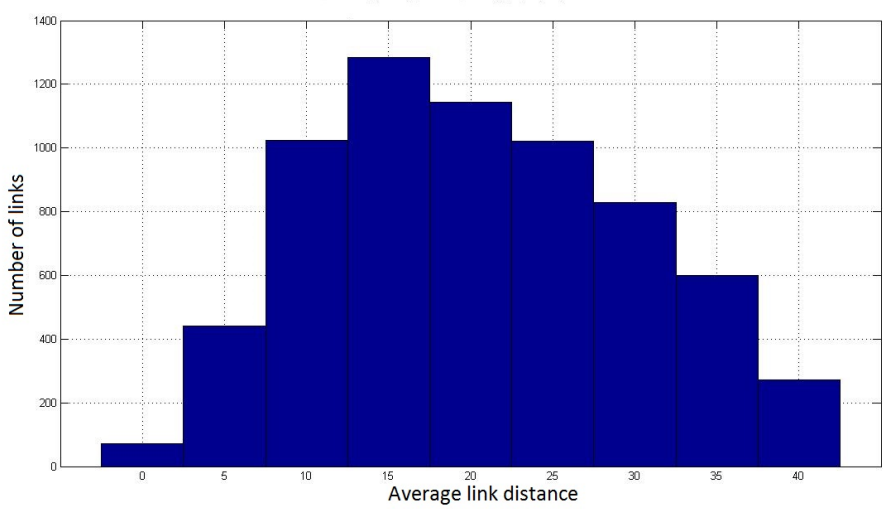

Figure 5.10: Average distance between nodes and cluster-heads in LEACH

5.3.2 Steps of the Joint clustering and routing mechanism

The analysis in the last section highlights the importance of trying to reduce the number of hops in a large scale multi-hop network. We can employ cooperative MIMO to improve the performance of the links and thereby increase the range of each 'hop' while ensuring that the QoS (quality of service) is met. However to use this technique in an ad-hoc networking scenario is challenging. The lack of a centralized controlling entity (e.g., a base station) makes the task of establishing a link, especially one which involves cooperative MIMO, challenging. Hence we propose a joint clustering and routing method to make this task simpler. Here are the three steps involved:

5.3.2.1 Clustering phase

Clustering is one of the widely used methods for ad-hoc networks. Nodes perform extensive piloting to gather information about their surroundings and then form groups with one of them designated as the cluster-head (CH). Additionally clusters form links with neighboring clusters in order to form 'gateways' used by routing algorithms such as AODV (Ad-hoc On-demand Distance Vector [PR99]) and LEACH (Low Energy Adaptive Clustering Hierarchy [HCB00]). The problem

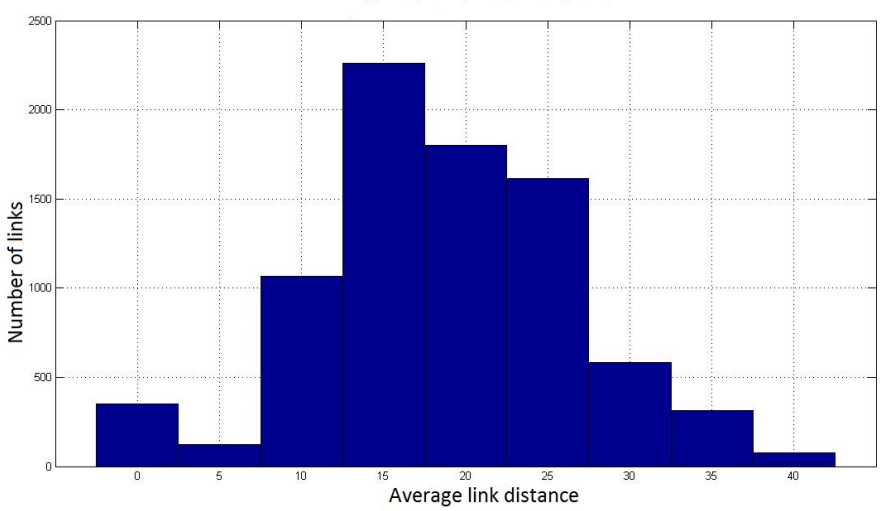

Figure 5.11: Average distance between nodes and cluster-heads in RSSI

with this is that these connections are all based on single links. When cooperative MIMO is employed in such scenarios [YCK06], [ZSGH11], the 'hops' are restricted to the immediate neighbors of the cluster only, even though with cooperative MIMO it is possible to 'hop' over much larger distances. This would be possible if the CH would know whether it can transmit to a cluster farther away using cooperative transmission with a particular MIMO diversity order. The restricting factor here is that the piloting is performed using single antenna nodes and only an estimate of the quality of the SISO links is formed at the CH. One possible way to accomplish this is to perform piloting in a cooperative way as well in order to estimate the quality of cooperative MIMO links between clusters. But this would cause a lot of overhead since we would have to try all possible combinations of nodes in order to grade the quality of the MIMO links to be able to choose the best ones when the time for transmission comes.

It is proposed to employ the link information from the SISO piloting in order to come up with an idea on how to perform a cooperative/collocated MIMO link in the same place. A high power pilot is used in order to reach distant clusters, even the ones for which the SISO link is not usable due to a high error rate. The following section shows how the performance of a virtual MIMO link can be derived based on the SISO links. The upper bound of the error probability

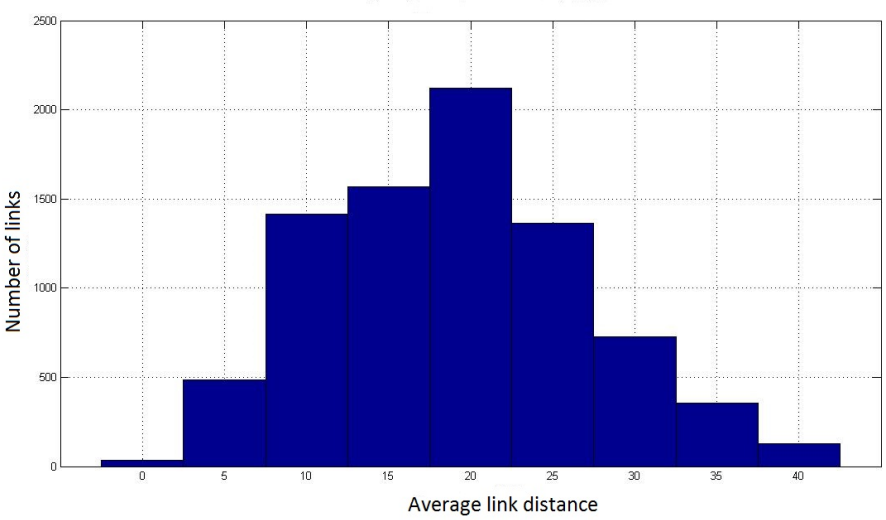

Figure 5.12: Average distance between nodes and cluster-heads in E-RSSI

estimates is considered to ensure that the Quality of Service (QoS) is met.

5.3.2.2 BER bound estimation

In this section we repeat the derivation from the last chapter that showed how the quality of transmission for higher order MIMO can be extracted from the available SISO link information. In this section we focus on the symbol error rate as a parameter of the link quality. Lets assume that the system has a diversity order D. The received signal at the receiver can be written as

$$y_i = \sqrt{\frac{P_s}{D}} h_i \cdot x + \nu_i, \quad i = 1, 2, \ldots, D, \tag{5.6}$$

where x denotes the transmitted signal, P_s denotes the transmit power, h_i, y_i, and w_i represent the channel transfer function, the received signal, and the additive noise which is modeled as a ZMCSCG random variable with variance σ_n^2 corresponding to the ith diversity branch, respectively. The symbol error rate can be approximated as

$$P_e(\eta) \approx \bar{N}_e \cdot Q\left(\sqrt{\frac{\eta \cdot d_{\min}^2}{2}}\right). \tag{5.7}$$

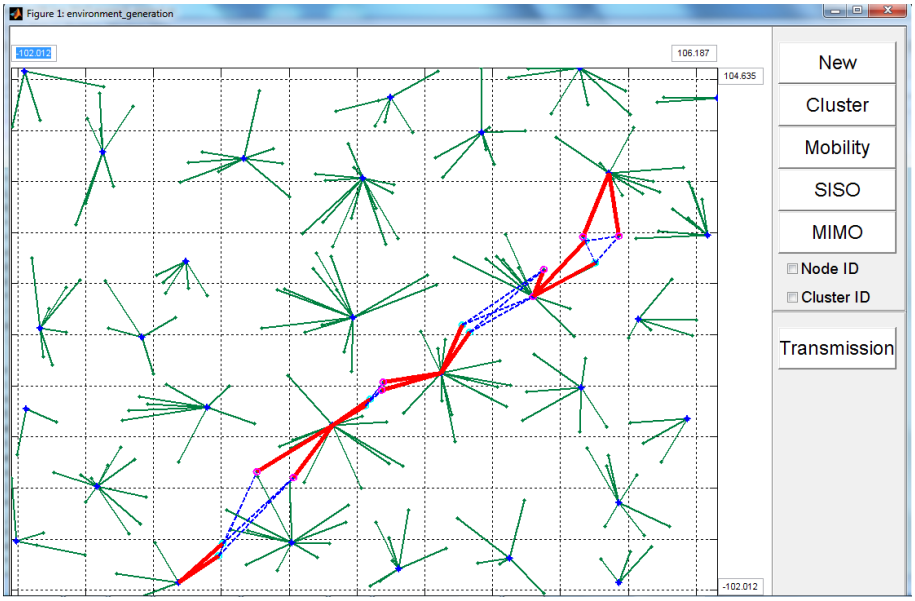

Figure 5.13: Routing in 2×2 Cooperative Multi-hop MIMO. The green lines denote the connections between the nodes and the cluster-heads, the blue lines show the communications between different clusters, and the red lines show the communications with the same cluster.

where Q represents the Q-function, defined in (3.3), which is the tail probability of the standard normal distribution. Moreover, $\bar{N}_e$ and $d_{\min}$ denote the number of nearest neighbors and the minimum Euclidean distance of the underlying scalar constellation. The variable η represents the received SNR over a fading channel h_i which, for maximum ratio combining, is given by

$$\eta = \frac{1}{D} \sum_{i=1}^{D} |h_i|^2 \cdot \rho, \tag{5.8}$$

where $\rho = P_s/\sigma_n^2$ is the received SNR of the equivalent SISO link. By using the Chernoff bound: $Q(x) \leq 1/2 \cdot \exp(-x^2/2)$, the equation (4.2) can be bounded, which yields

$$P_e(\eta) \leq \frac{1}{2} \bar{N}_e \cdot \exp\left(-\frac{\eta \cdot d_{\min}^2}{4}\right). \tag{5.9}$$

Assuming an uncorrelated Rayleigh fading channel with unit variance, it follows that the average probability of symbol error in the high SNR region is

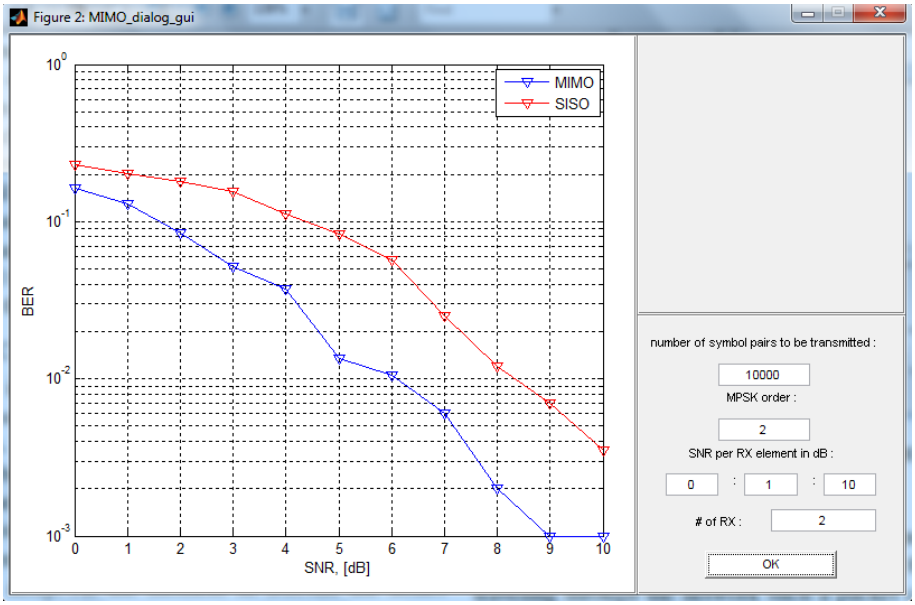

Figure 5.14: Comparison of 2×2 virtual MIMO multi-hop and SISO multihop from BER point of view after multi-hopping over five clusters. AODV-based routing for cooperative MIMO, RSSI-based clustering, path loss exponent of value 2, BPSK modulation, 250 randomly placed nodes, and Alamouti coding for the cooperative MIMO case were used for this simulation (whih was performed using SONIR).

upper-bounded by

$$P_e = \mathbb{E}\{P_e(\eta)\} \leq \frac{1}{2}\bar{N}_e \left(\frac{\rho \cdot d_{\min}^2}{4 \cdot D}\right)^{-D}. \tag{5.10}$$

The diversity order D should be minimized in order to find an upper bound which is independent of the MIMO scheme. We assume maximum ratio combining at the receiver. Then depending on the correlation between the transmit antennas (we assume uncorrelated receive antennas), the bounds of the diversity order D can be written as

$$M_r \leq D \leq M_r \cdot M_t, \tag{5.11}$$

where M_t is the number of transmit antennas. Replacing D with M_r in the equation (5.10), the upper bound of the average probability of SER in the high

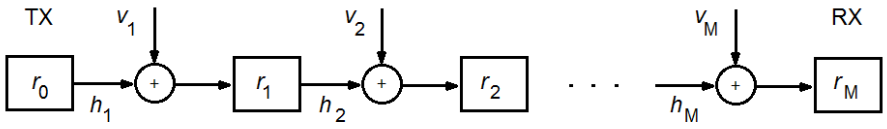

Figure 5.15: The relaying model in multi-hop scenarios.

SNR regime is given by

$$\mathbb{E}\{P_e\} \leq \frac{1}{2}\bar{N}_e \left(\frac{\rho \cdot d_{\min}^2}{4 \cdot M_r}\right)^{-M_r}. \tag{5.12}$$

Using (5.12), we can upper bound the probability of error for cooperative MIMO with a particular number of receive antennas by using only the normal (SISO) pilot. After this phase each CH can form a table of all the other clusters it can communicate with by using one or more of its cluster members. It can also list the best nodes for these virtual MIMO connections in decreasing order of precedence. This gives rise to the concept of 'cooperative MIMO neighboring clusters'. This concept is illustrated in Figures 5.16 and 5.17. Figure 5.16 shows an example of a clustered network. However, if the additional step of finding cooperative MIMO neighbors has been performed, the CHs also know the location of their MIMO neighbors. Figure 5.17 illustrates this for a particular cluster (marked in black) and its cooperative MIMO neighbors are depicted by different colors based on the diversity order of MIMO the CH wishes to, or is able to, use.

5.3.2.3 Ad-hoc On-demand Cooperative MIMO Routing (AOCMR)

Localization and routing for self-organized networks is a non-trivial task and has many implementational issues. Having GPS (Global Positioning System) equipped nodes helps with localization but it is still quite difficult for nodes to get accurate information about their surroundings and their neighboring nodes. In the proposed system, cluster-heads deal with most of the routing functions. They maintain tables of the IDs of nodes in their cluster and use the nodes to gather information about the presence of neighboring clusters. Moreover, they have tables indicating the most suitable node (or nodes, in case of cooperative MIMO) to use in order to communicate with a particular neighboring cluster. AODV

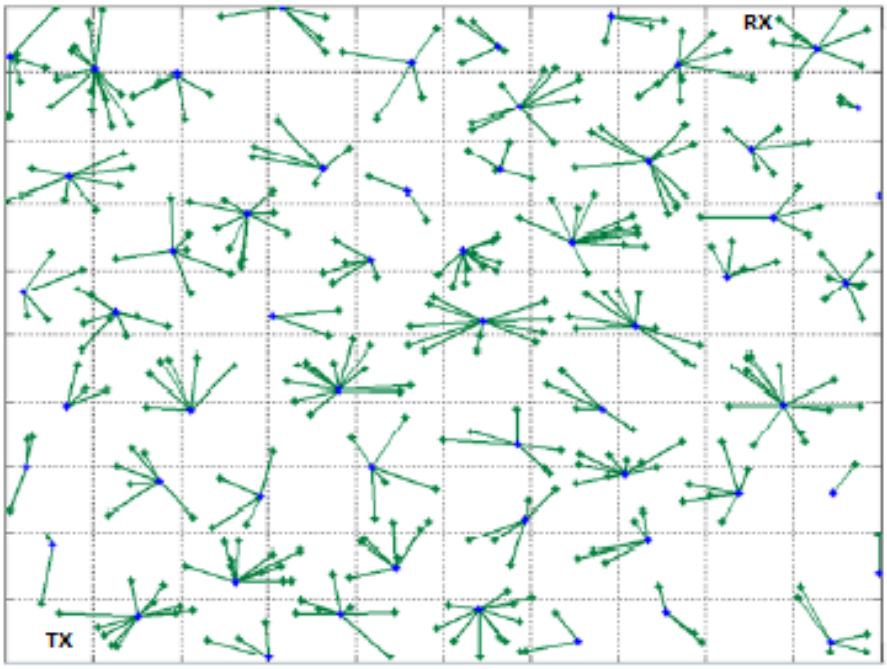

Figure 5.16: a Clustered Network

(Ad-hoc On-demand Distance Vector routing) [PR99] is a promising option to deal with the routing issue. In the proposed system, there is an improvement upon AODV in that the route is updated when re-clustering is performed even during the same session of communication between two nodes to cater for the movement of nodes in the network. AODV, on the other hand, maintains the same route during one session of communication. The cluster maintenance tables and the routing tables are also updated periodically, and the optimal update interval can be determined based on the quality-of-service (QoS) demand that is of immense interest to network planners. Thus, the optimal network reclustering time can be obtained as a function of the QoS [bit error rate (BER)] and the speed of the mobiles. Based on the simulation results, it is possible to eventually form a mathematical model to determine the reclustering time in relation to these quantities.

AOCMR (Ad-hoc On-demand Cooperative MIMO Routing [ZGS+11]) can be employed as soon as CHs obtain the tables with all the possible connections to the other clusters. It works similar to AODV except for the fact that it routes

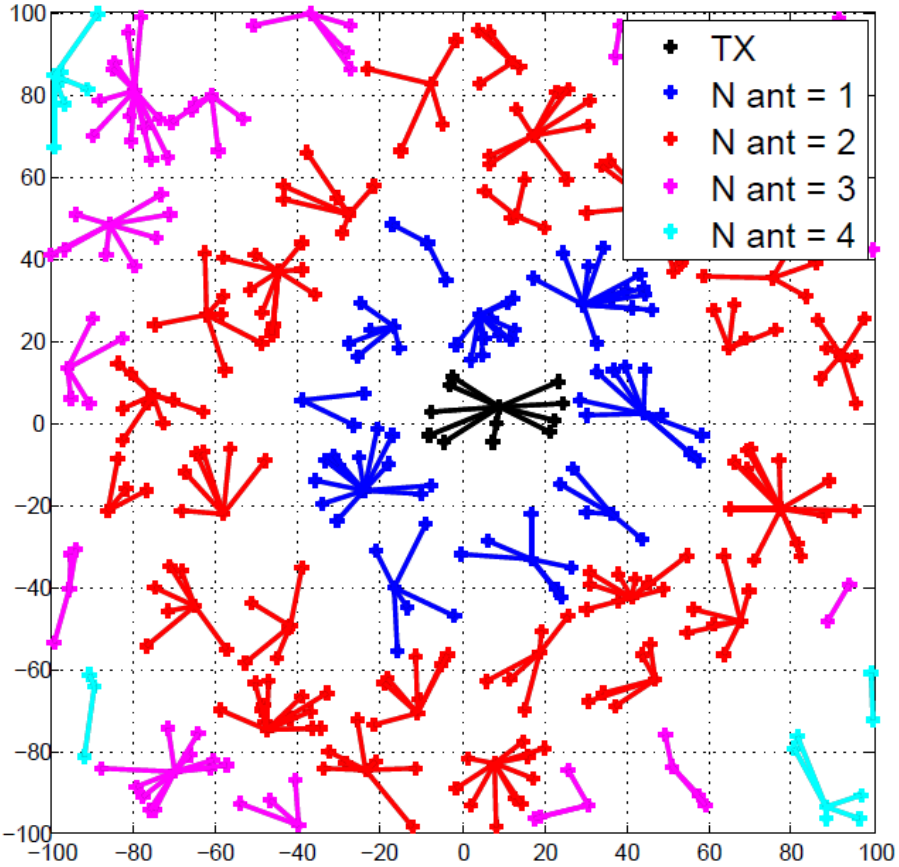

Figure 5.17: Cooperative MIMO neighbors

the packets through the cooperative MIMO links if it is possible. Depending on the number of the accessible nodes, each CH can decide about the transmissions diversity order with the aim of sending the packet as far as possible and as close as possible to the cluster with the final destination node for the packet.

Note that the overhead for AOCMR is greater than that for the existing schemes. To justify this overhead for practical networks, we should note that once the cooperating set of nodes are determined, then this knowledge can be stored at the cluster-head and used for future transmissions. Especially if we are dealing with networks that are relatively static, the one-time overhead for this determination is quite affordable and is further offset by the gain in throughput achieved by reducing the number of hops.

There is a possibility to have heterogeneous cooperative MIMO links in the

same multi-hop connection when each CH can decide about its diversity order. As in [YCK06] and [ZSGH11], for the clusters that are geographically next to each other, it is not enforced to perform the cooperative MIMO. Figure 5.18 gives an example of the case in which a multi-hop link is shown in three different configurations, with SISO hops in blue, with 3×3 cooperative MIMO hops between geographically neighbors as in [YCK06], [ZSGH11] in pink and with the proposed 3×3 joint clustering and routing scheme in red.

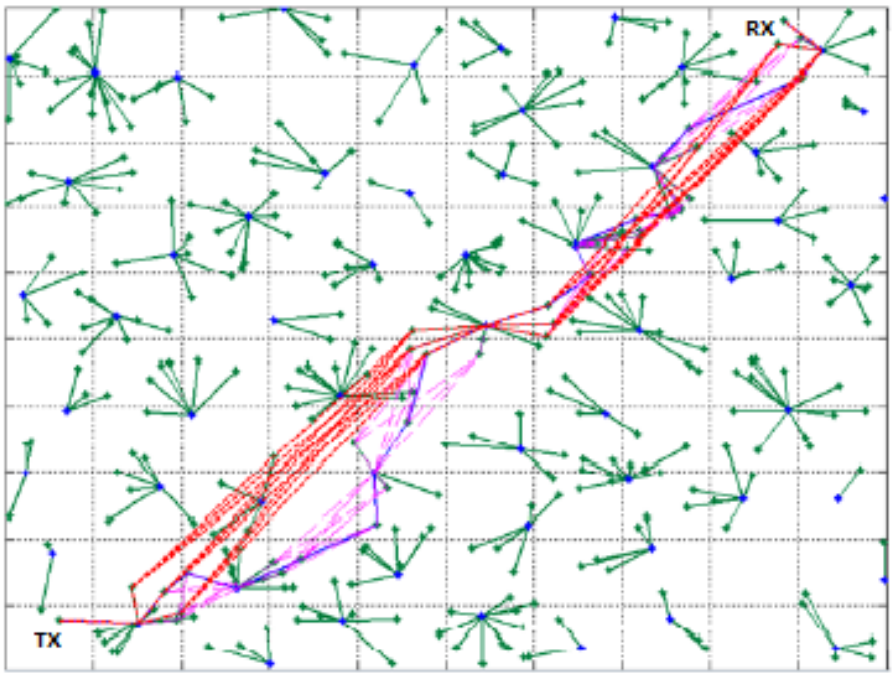

Figure 5.18: Multi-hoping with different methods (red lines represent AOCMR, blue lines represent AODV SISO routing and pink lines represent MIMO routing based on AODV).

Mobility management

If the nodes are mobile, the network can change quite rapidly. To counter this, the classical technique is to periodically re-cluster the network based on average mobility characteristics of the nodes in the network. In AOCMR, we re-draw the route every time the network is re-clustered in order to (periodically) determine the optimal link and avoid link breakage, which is a major drawback in AODV,

because the route is maintained for the entire duration of a transmission, regardless of the length of the transmission or the change in the network due to the mobility of the nodes.

5.3.3 Simulation Results

We have analysed our scheme for the case of 2×2 (cooperative) MIMO with Alamouti space time block codes (STBCs) for a large network with hundreds of nodes uniformly distributed in a certain area. Figure 5.19 shows that we can gain an immense reduction in the number of hops over large networks by employing AOCMR as compared to the older SISO route based schemes for cooperative MIMO. Figure 5.20 shows the gain in mutual information by employing our scheme with AOCMR as opposed to older AODV/SISO based schemes. The equations (2.26) and (3.32) are used for this figure.

A hidden benefit of employing AOCMR is that we end up using less nodes per transmission because we go over fewer hops and thus fewer cooperative nodes are employed. We should note that nodes are users as well as resources in cooperative relaying networks. So by using AOCMR, we end up freeing up more nodes, enabling them to potentially take part in other transmissions. Figure 5.21 illustrates this effect.

5.4 Conclusions and Future Work

The simulation results show that the E-RSSI clustering algorithm forms clusters in such a way that it enables low energy transmissions and distributes the transmission energy consumption over all the nodes in a more even way which leads to a significantly longer network life-time. As the E-RSSI algorithm makes no assumption about the type of network nodes (homogeneous or heterogeneous), it can adapt itself to different network configurations. Aforementioned advantages make E-RSSI a practical solution to the problem of cluster-head selection.

Future work could be to run a joint optimization (convex or non-convex) algorithm on all the parameters of the clustering algorithm in order to achieve an optimal performance in terms of life-time as well as the quality of service.

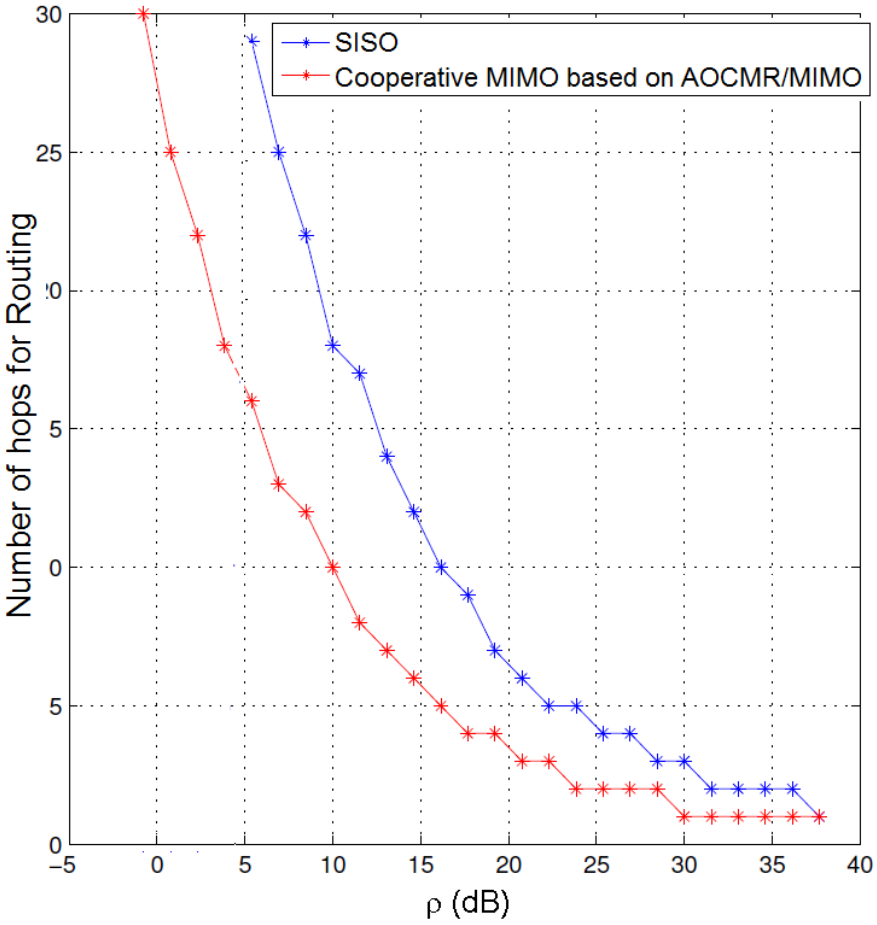

Figure 5.19: Required number of the hops for different SNRs

Comparison of E-RSSI with HEED is also an interesting option for future work.

Using cooperative MIMO for range extension of individual hops in a multi-hop network can give us a much improved link throughput capacity. Using our proposed routing scheme (AOCMR) can make it simpler for cluster-heads to employ cooperative MIMO techniques in an ad-hoc manner since we use simple piloting and employ that to form tables at the cluster-heads which will be used for routing between clusters using heterogeneous cooperative MIMO links.

For future work, it would be imperative to look at the overall network throughput as opposed to just a single link throughput. Also an evaluation in the presence of interference from other nodes and imperfect synchronization conditions should be performed.

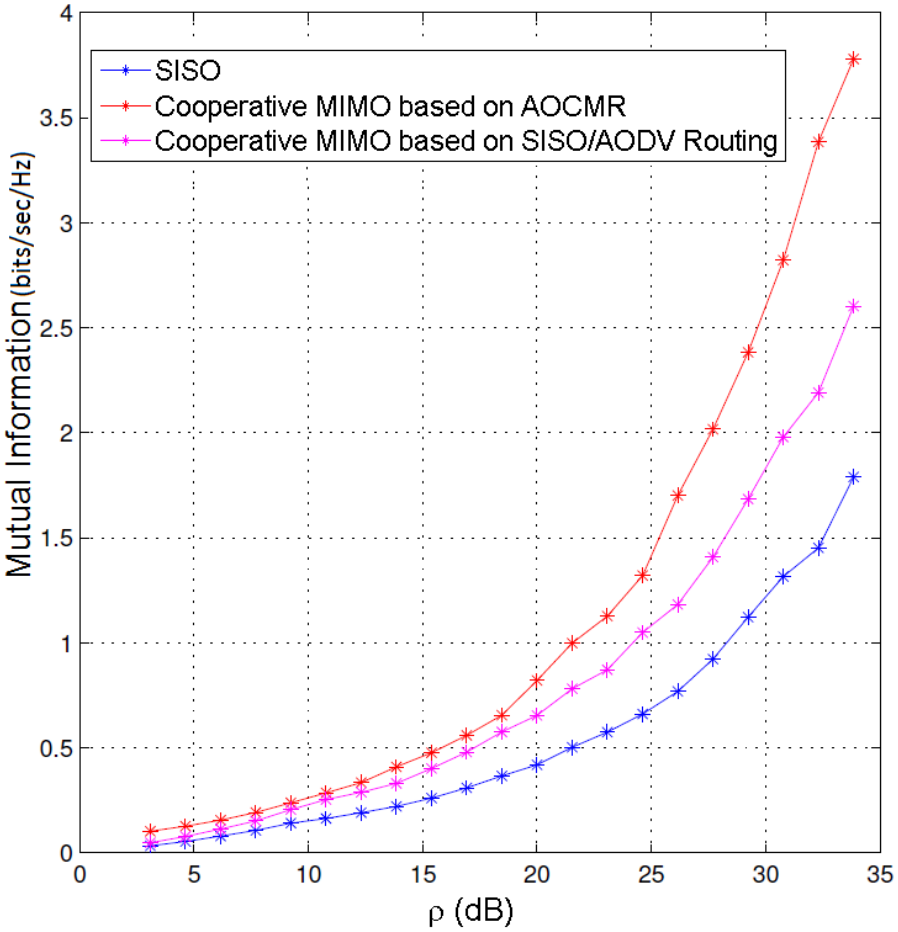

Figure 5.20: Comparing the mutual information

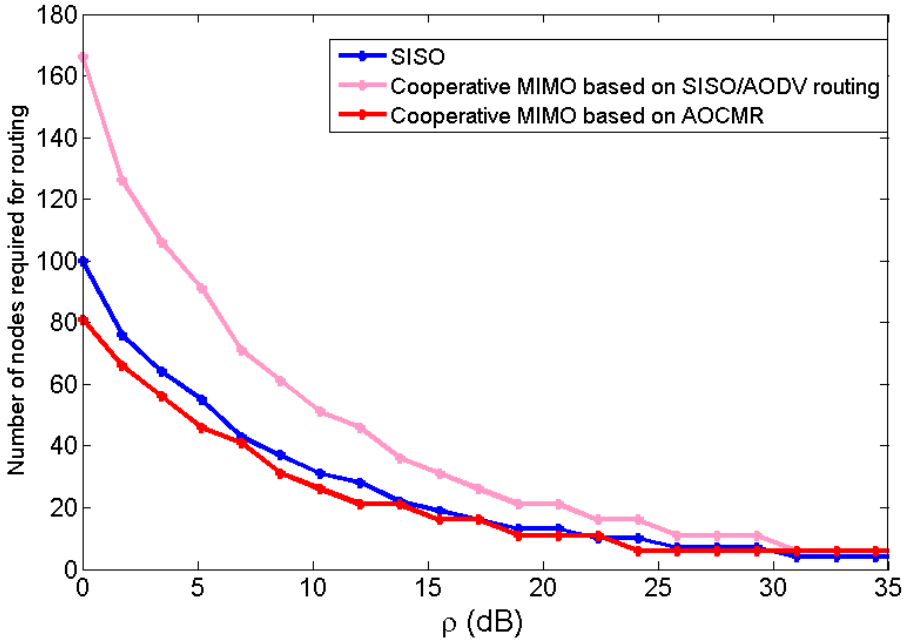

Figure 5.21: Comparison of the number of nodes required for routing

Chapter 6

Data management through DHTs

Distributed hash tables (DHTs) provide reliable distributed data management in a decentralized fashion that is well suited to self-organizing cluster-based ad-hoc networks. However, existing DHT approaches strive to optimize some combination of the total overlay message load, lookup delays, or load balance between the overlay nodes while ignoring the underlying physical characteristics of ad-hoc networks without infrastructure. In such networks, this inevitably leads to a high overhead in terms of the number of physical underlay transmissions. While location aware DHT approaches do reduce the number of underlay transmissions, they are not designed to exploit physical and link layer communication techniques such as cluster-based ad-hoc network structures or cooperative relaying. In this chapter, we introduce novel location and resource aware DHT protocols that incorporate underlay cluster information into their proximity link selection. These and existing DHT protocols are evaluated in simulations that use realistic wireless transmission protocols and parameters along with mobile nodes with limited lifetimes. Comparisons of the number of required overlay and underlay hops as well as the amount of consumed power suggest a tradeoff between the underlay and overlay overhead in existing schemes, while the proposed novel protocols demonstrate both overlay and underlay benefits. The results of this chapter have been publsihed in [ZARBH13].

6.1 Introduction

The decentralization of wireless networks in order to reduce the dependence on fixed infrastructure such as base stations has been the subject of vast interest in recent years [HDP03]. Decentralized communication schemes are inherently better suited to respond to unforeseen situations due to natural disasters or widespread network failures and, in the future, could possibly form the back-bone of general commercial mobile networks. There is thus a current interest in the creation of new methods to handle data in such decentralized wireless networks. Most of the techniques available in literature only look at the data management in such networks in terms on the overlay structure. The overlay structure refers to the logical connections between nodes that the higher OSI (Open Systems Interconnection) layers can see. The underlay structure refers to the physical structure of

the network with physical connections between nodes over actual wireless links.

There has been a rapid growth of distributed data management systems for large amounts of data that are either unstructured and therefore built directly on the existing underlay or structured such that participating nodes are abstracted from their underlay. While unstructured systems benefit from routing and searching using underlay logic, structured overlays have the decisive advantage of providing guarantees on data availability. In this chapter, we consider the compatibility of structured overlays, or distributed hash tables (DHTs), and decentralized wireless ad-hoc networks. In doing so, we must consider the complex and unpredictable nature of wireless ad-hoc networks - for example, the lack of Quality-of-Service (QoS) or high performance guarantees in mobile ad-hoc networks (MANETs) - and the restricted resources of wireless nodes - such as battery power, bandwidth, or computing power.

We assume a self-organizing and cognitive communications scenario where mobile handsets are used as ad-hoc network nodes, both for intelligent relaying in the absence of base stations as well as for data storage. To control stability, reconfigurability and scalability, self-organized ad-hoc networks often communicate via multi-hopping over relay nodes that have been clustered into various groups. The network is managed by local base-stations, or cluster heads (CHs). Meanwhile, overlay hops are based on virtual links to other nodes that may lie outside of the direct communication (i.e., transmission) range, so that a singe overlay hop often requires multiple underlay hops to reach its destination. Network interference and scheduling issues can also contribute to this increased stretch of overlay hops. Figures 6.1(a) and 6.1(b) visualize how a single DHT overlay hop is executed as multiple physical underlay transmissions for nodes using multi-hopping over relays to communicate. Reducing the number of necessary underlay hops per single overlay hop while maintaining a low number of overlay hops would decrease the overall network load and lookup delays while using nodes' resources more conservatively. However, the number of underlay hops per overlay hop depends on the specific implemented underlay network architecture, such as cluster head or hierarchically based network structures [Nee10]. This chapter offers a realistic evaluation of the effects of different underlay network configurations on the overlay link stretch and overall network performance.

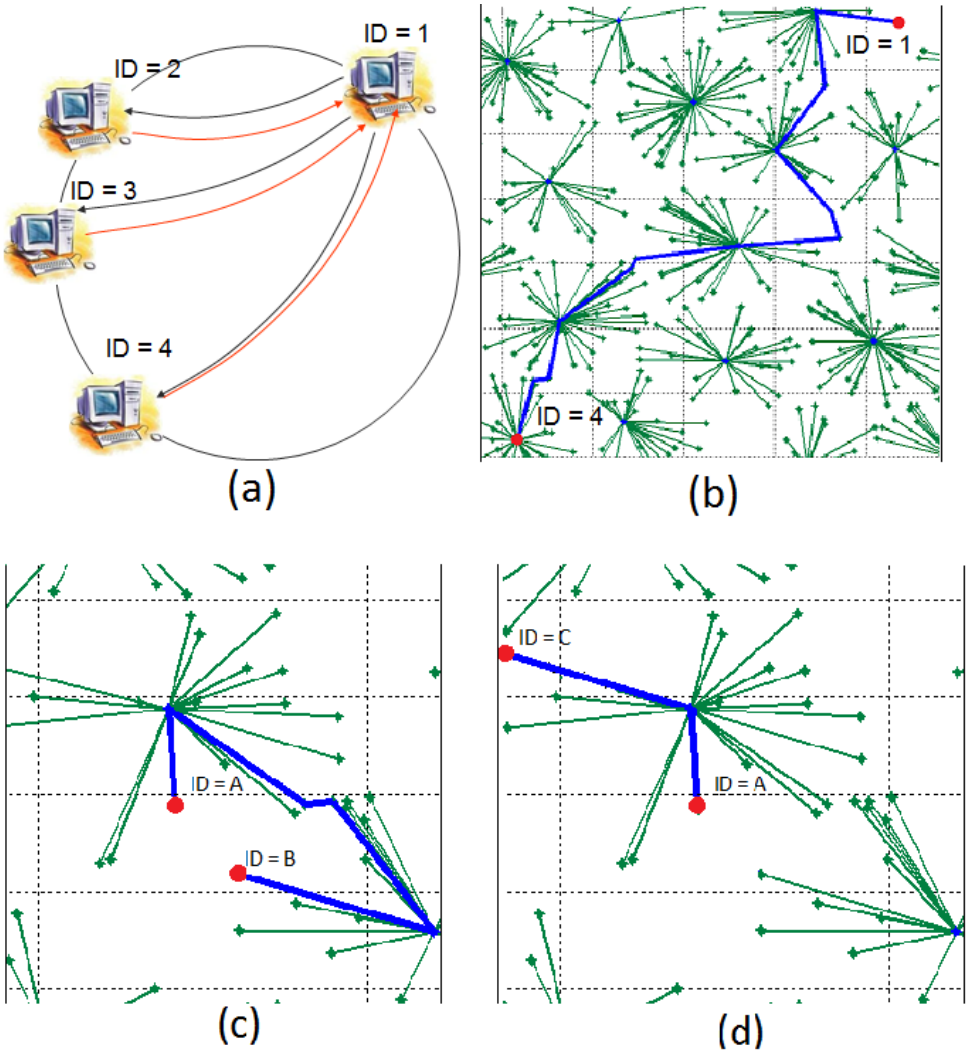

Figure 6.1: Data overlay via logical ID (a); corresponding node-to-node underlay communication (b); smallest underlay configuration involving two clusters: small physical distance does not always correspond to low number of underlay hops (c); smallest underlay configuration involving single cluster: small physical distance always corresponds to minimum number of underlay hops (d).

Some existing proximity aware DHT approaches, such as DHash++ [KAKH09] (which is an extension of Chord [SMLN+03]), and RBFM (resource based finger management, an extension of DHash++) [RB11], indirectly address the underlay overhead by reducing the total average physical distance that messages travel

by choosing nearby links. However, to the best of our knowledge, no current DHT scheme takes into account the inherent ad-hoc properties and utilizes them effectively to directly reduce the underlay load and lookup latency. Cluster-based multi-hop communication in particular has recently received much attention [ZSGH11] while cluster heads provide a concrete leverage point for DHT optimization [Nee10].

This chapter introduces a DHT approach that incorporates cluster head information for cluster-based multi-hop underlay communication into the choice of overlay links. This work was published by us in [ZARBH13]. This chapter's main contributions are:

- novel location, resource, and *cluster* aware DHT approaches C-DHash++ and C-RBFM that augment DHash++ and RBFM to incorporate cluster heads and cluster states,
- examples of network configurations for optimized underlay-overlay networks, and
- a comparison of the underlay overhead for the cluster-aware and other DHTs.

The rest of this chapter is organized as follows. Section 6.2 describes the related work in the area. Section 6.3 describes the proposed novel DHT protocols: C-DHash++ (cluster aware DHash++) and C-RBFM (cluster aware resource based finger management). Simulation results are presented in Section 6.4. Finally Section 6.5 summarizes the chapter and highlights important open research issues in this area.

6.2 Related Work

Originally developed as centralized protocols for fixed networks, today overlay networks work efficiently in a heterogeneous decentralized manner as well. Distributed hash tables (DHTs) are most common solution for data management in decentralized networks. Well established DHTs such as Chord [SMLN+03], CAN (Content Addressable Network) [RFH+01], and Kademlia [MM02] were designed

to route efficiently without taking into account the location information. Location awareness is added to DHTs using a combination of proximity-aware identifier selection (PIS, such as Mithos [WR03] and proximity-aware route selection (PRS, such as Tapestry [ZKJ01]), and SAT-Match [RGJZ04]), proximity-aware neighbor selection (PNS, such as DHash++ [KAKH09]), and has generally been used for reducing the overall traffic or average round trip times [GGG+03].

Applications of data overlay in Vehicular Ad Hoc Networks (VANETs) was the focus of [Nee10]. Both MANETs as well as overlay networks share the key characteristics of self-organization and decentralization. Such networks cannot rely on any fixed infrastructure and manage the data in a distributed manner. Even though VANETs have gained a lot of attention in recent years, there still remain a lot of open questions. For instance, proposed protocols for VANET consider relatively strict limitations of a network structure and do not leave much room for flexibility [Nee10], and consequently can not be fully utilized in other kinds of networks.

Developing overlay protocols which could efficiently route in heterogeneous environment (e.g., MANET) require a deep understanding of underlay network behavior and may significantly vary depending on network setups. Resource Based Finger Management (RBFM) [RB11], an extension to DHash++, which accounts not only location awareness but also resource awareness, even further improves overlay network performance in heterogeneous environment.

Nevertheless there has not been given enough attention to the specifics of the underlay technology in use. Such protocols may be well suited for some scenarios but could be completely useless for others. [RHKS02] extensively discusses and questions different DHT approaches, their applicability problems and limitations.

Currently many different mechanisms have been proposed to improve various parameters of ad hoc networks. From underlay prospective, in most of the cases data packets in ad hoc network are transmitted from the transmitter to the receiver node not directly but over other nodes in some specific manner. Most of the ad hoc routing protocols can be generalized by the following main groups: proactive (DSDV, HSR, etc.), reactive (AODV, DYMO), hybrid, and power aware protocols, etc. [BBB09]. The data transfer is possible after some sort of hierarchy is established in ad-hoc networks, usually through clustering, and transmissions

can follow different techniques such as multi-hopping through cooperative relaying and even virtual MIMO approaches [CDS07], [ZSGH11]. Since different transmission techniques influence network parameters in a different way, the most appropriate choice of the transmission technique to be applied depends on the current network task: boosting peak or mean data rate, providing maximum reliability of data transmission, etc. Taking into consideration that underlay network tasks are defined by upper layer protocols, a simultaneous co-influence of both underlay on overlay and overlay on underlay networks has to be further analyzed, and, to the best of our knowledge, was not yet investigated.

The question of how a given DHT overlay protocol effects the (MANET) underlay on which it is run remains largely unexplored. While DHTs are often evaluated using their average overlay hop count per message or overall overlay network message load, this has been ignored on the underlay level. Yet, in a network where nodes function simultaneously as overlay and underlay nodes, the underlay load is the more important performance factor, especially for nodes with restricted resource availability such as battery power. Hence, evaluating and designing DHTs over ad-hoc networks with highly varied underlay node parameters remains an open issue.

6.3 Cluster Aware Finger Management Concept

The impact of the overlay protocols and underlay network configurations on the underlay load is examined in this chapter for a small set of overlay approaches. We use Chord [SMLN$^+$03] as our basic reference DHT which displays neither location nor resource awareness, DHash++ as a Chord extension that displays location awareness, and RBFM as a Chord extension with both location and resource awareness. In order to incorporate cluster-based multi-hopping, which is widely used for communication in ad-hoc networks, both DHash++ and RBFM are augmented to take cluster states into consideration, thus directly incorporating underlay configuration information into the overlay design. The resulting C-DHash++ and C-RBFM are compared with the cluster-naive approaches. While this work is based on Chord, similar cluster-aware approaches could be analogously adapted for other DHTs as well.

Figure 6.1 shows how multi-hopping is performed in clustered networks and demonstrates how a single overlay hop most often translates into many underlay hops. The construction of clusters plays a significant role in how many hops are required. The cluster heads pose a bottleneck for this network, since all cluster communication goes through them, but are essential for routing and scheduling. Note that communication within one cluster requires no more than two hops (with the cluster head acting as the relay, see Figure 6.1(d)), while communication to a node in a neighboring cluster might involve as many as five hops (as shown in Figure 6.1(c)). Clearly, communicating within a single cluster has significant benefits. Thus, choosing overlay hops that are in the same cluster should reduce the number of underlay hops for a single overlay hop, thus reducing the underlay maintenance and lookup load and the resulting overall resource usage.

Finger Selection

DHash++ as well as RBFM are based on Chord and use consistent hashing to distribute keys to nodes. Each node x chooses a random (or hashed) nodeID x_{ID} from the binary key space $0 \ldots 2^m - 1$, which is viewed as a ring with key values increasing in a clockwise direction. Each node positions itself at its nodeID on the key ring and establishes links to its immediate predecessor and successor and maintains a successor list with its r nearest successors, making repairs possible after unexpected node failures. Each key κ is assigned to the first node whose nodeID is equal to or succeeds κ on the key ring. Each node x with nodeID x_{ID} chooses one link (finger) $x.f[i]$ from the finger interval $B_{x,i} := [x_{\mathrm{ID}} + 2^{i-1}, x_{\mathrm{ID}} + 2^i)$ for $i \in \{1, 2, \ldots, m\}$.

In DHash++, node information, including nodes' (virtual) coordinates, is piggybacked on network messages. Each node x maintains perspective finger lists of the information of the closest nodes it has thus seen for each finger interval $B_{x,i}$. Node x then chooses the node with the smallest physical distance from its perspective links list from its ith finger interval for its ith finger node. RBFM chooses its links base on, in addition to physical distance, information about the nodes' resource availabilities.

C-DHash++ and C-RBFM have been developed to work similarly but with a

link choice that incorporates even more knowledge about the underlay network.

6.3.1 Cluster Aware DHash++ (C-DHash++)

In DHash++ [KAKH09], fingers are established solely based on the proximity of the nodes as shown in Figure 6.2. Here we have an example of a key ring with six nodes in x's $m-1^{st}$ finger interval $B_{x,m-1}$, four of which x knows from its prospective links list. For DHash++ a finger is established to p_4, the node with the smallest physical distance to x, as shown by the dashed line on the key ring in Figure 6.2.

Prospective Links [m-1] DHash++

NodeID	Phy.Dist.
p_2	1.6
p_3	1.4
p_4	0.9
p_1	4.1

Prospective Links [m-1] C-DHash++

NodeID	Phy.Dist.	SameClust.
p_2	1.6	No
p_3	1.4	Yes
p_4	0.9	No
p_1	4.1	No

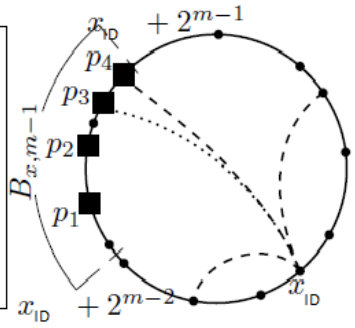

Figure 6.2: DHash++ (dashed line) finger selection procedure and C-DHash++ (dotted line) finger selection procedure

The proposed protocol C-DHash++ goes further and chooses a node which is available within the finger interval which is not only in close proximity but also belongs to the same cluster, hence a link to p_3 is established, shown by the dotted line in the key ring in Figure 6.2.

6.3.2 Cluster aware Resource Based Finger Management (C-RBFM)

The finger selection in RBFM is based on so-called resource distance, which uses a combination of resource level and physical distance to choose a strong and nearby

node from each finger interval. The resource distance of two nodes x and y is:

$$d_{\text{res}}(x, y) = d_{\text{phy}}(x, y) + c \cdot (l_{\max} - x_R). \tag{6.1}$$

where $l_{\max}$ is the maximum available resource distance, set to $l_{\max} = 3$ for our set up; $x_R \in \{0, 1, \ldots, l_{\max}\}$ is x's resource level; $d_{\text{phy}}(x, y)$ is the physical distance between x and y:

$$d_{\text{phy}}(x, y) = \sqrt{(x_1 - y_1)^2 + (x_2 - y_2)^2}. \tag{6.2}$$

and c >0, defined in [RB11], places higher priority on a desired parameter (i.e., either physical distance or resource distance) in the multi-parametric decision.

In RBFM [RB11], the nodes were assigned resource levels of 0, 1, 2, and 3 (3 being the highest), to illustrate the difference in the resources available to a particular node. These resources could be, for example, the battery power or the available bandwidth. Fingers were established based on the proximity and the resource level of nodes. The node with the smallest resource distance was chosen. Figure 6.3 illustrates how links are formed in RBFM. A finger is established to p_2, the known node with the best resource distance (dependent on distance and resource level) to x.

ProspectiveLinks[m-1]: RBFM

NodeID	Phy.Dist.	Res.Level	Res.Dist.
p_2	1.6	2	2.6
p_3	1.4	1	3.4
p_4	0.9	0	3.9
p_1	4.1	3	4.1

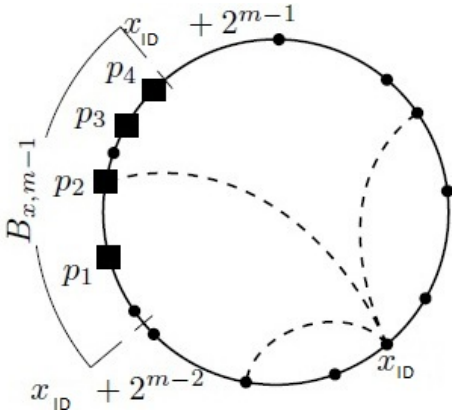

Figure 6.3: RBFM link selection procedure

Figure 6.4 illustrates how C-RBFM might form links given the same situation. In this case we also know about the cluster status of each node. So if a node can

select a link from its own cluster, it will do so for the reasons discussed above. Also, if there are multiple nodes that are possible links and are in the same cluster, then we choose the node with the smallest resource distance amongst them. After finding the most optimal node for communication, a finger is established to p_3.

Prospective Links [m-1]: C-RBFM

NodeID	Phy.Dist.	Res.Level	Res.Dist.	SameClust.
p_2	1.6	2	2.6	No
p_3	1.4	1	3.4	Yes
p_4	0.9	0	3.9	No
p_1	4.1	3	4.1	No

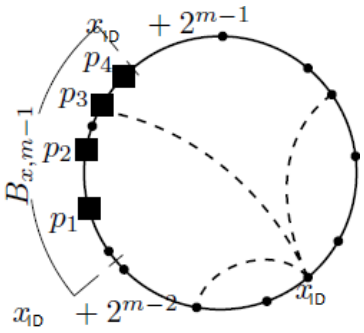

Figure 6.4: C-RBFM link selection procedure

6.4 Simulation and Evaluation

The network consists of 1000 stationary nodes grouped into 50 clusters. The transmissions are subject to Rayleigh fading as well as AWGN. Uncoded transmissions with BPSK modulation are used. The value of the path loss exponent was considered to be 2. We compare C-RBFM with RBFM, DHash++, C-DHash++, and Chord DHT protocols. Each protocol is used to perform 85000 random data lookups. This is done using OMNeT++. The corresponding number of overlay messages is different for each protocol, as is the number of physical (underlay) messages corresponding to those overlay messages.

The nodes have different resource levels, where the level 3 represented unlimited resource availability and levels 2, 1, 0 are assigned for nodes with limited resource levels where 0 corresponds to the minimum possible resource level. In our simulations, we randomly assign nodes with resource levels of 0, 1, 2, and 3 with equal probability. Nodes with low resource levels have a higher failure probability. This network setup is similar to the one in [RB11] and includes random node failures.

RBFM and C-RBFM protocols use either the same linear function (6.3) or the quadratic function (6.4), where nodes with higher resource levels are getting periodical maintenance messages less often since they are expected to fail with lesser probability:

$$g(x_R) = t_{\text{ref}} \cdot (x_R + 1) \tag{6.3}$$

$$\acute{g}(x_R) = t_{\text{ref}} \cdot (x_R + 1)^2 \tag{6.4}$$

where $g(x_R) \in N$ is the linear finger maintenance function; $\acute{g}(x_R) \in N$ is the quadratic finger maintenance function, $t_{\text{ref}} \in N$ is the reference time interval after which periodic finger maintenance of a certain overlay node starts, and $x_R \in 0, 1, 2, 3$ is the resource level of the corresponding node.

All scenarios were based on periodic finger maintenance to update the entries of the finger tables which are changed or do not exist anymore. Chord and DHash++ use periodic maintenance of all nodes in the network, sending update requests equally to all nodes in the network, i.e., the linear update function (6.3) is used.

We use two instances of c (see equation (6.1)), $c = 10$ represents the case where emphasis is placed on choosing nodes which are closer in terms of physical distance, while $c = 90$ represents the case when emphasis is placed on finding links to nodes with high resource levels.

The simulation is divided into two parts, the overlay part is simulated in OMNeT++ using the simulation framework OverSim. The obtained set of overlay messages is then passed onto the underlay simulation tool. The underlay simulation is done in MATLAB using SONIR (Self-Organizing Network with Intelligent Relaying) [ZGA+10] which is a purpose-built framework for simulating cluster-based ad-hoc networks with cooperative multi-hop relaying. A user's guide to SONIR is provided in Appendix A. The coordinates and resource levels of the nodes are identical to those used for the overlay simulation.

Note that using OMNeT++ and SONIR sequentially does not result in loss of generality of errors in the final result. We used OMNet++ as DHT mechanisms

are already defined there and we can get accurate information about the overhead and control information as well. Implementing these in Matlab is time-consuming and sub-optimal. However we only use OMNet++ to generate the list of all the communications that should take place and then use SONIR to simulate those exact transmissions over fading and path-loss affected wireless links, using the exact location of nodes as was used for the overlay simulation, which gives us a realistic underlay environment.

The simulation of underlay routing consists of the following steps: in the initial stage the network is divided into clusters, which can be done with or without knowledge about the resource levels of nodes, then the nodes collect all the information needed for routing via extensive piloting. Finally the route from the source to destination can be established by one of possible routing protocols.The AODV (Ad-hoc On-demand Distance Vector) routing protocol [BBB09] has been used by us, since it is a popular, scalable and loop free reactive routing protocol widely used in both simulation tasks as well as in real applications [BBB09].

Figure 6.5 shows the comparison of the different protocols in terms of the number of underlay messages required for each overlay message. Note that each overlay hop corresponds to one overlay message which might translate into several underlay hops as explained in Section 6.1 and illustrated in Figure 6.1. The addition of the clustering information to the finger selection procedure results in shorter overlay hops. The effect is even more pronounced when comparing C-RBFM to Chord which does not take into account distance information at all. When comparing to DHash++ and indeed the original RBFM, the advantage is still present, but the effect is less pronounced because they take into account physical proximity, which happens to be the main reason for nodes to belong to the same cluster and thus in many cases the links chosen belong to the same cluster anyways. Still we see a significant enough improvement and thus a reduction in the overhead. This is because, as shown in Figure 6.1(c), it might take several hops to reach a node that is in close proximity but belongs to another cluster. This benefit is even more visible if the ad-hoc network is sparse, which is quite often the case.

Figure 6.6 compares the total number of underlay messages required to perform the 85000 data lookups with different protocols. Here we again see an

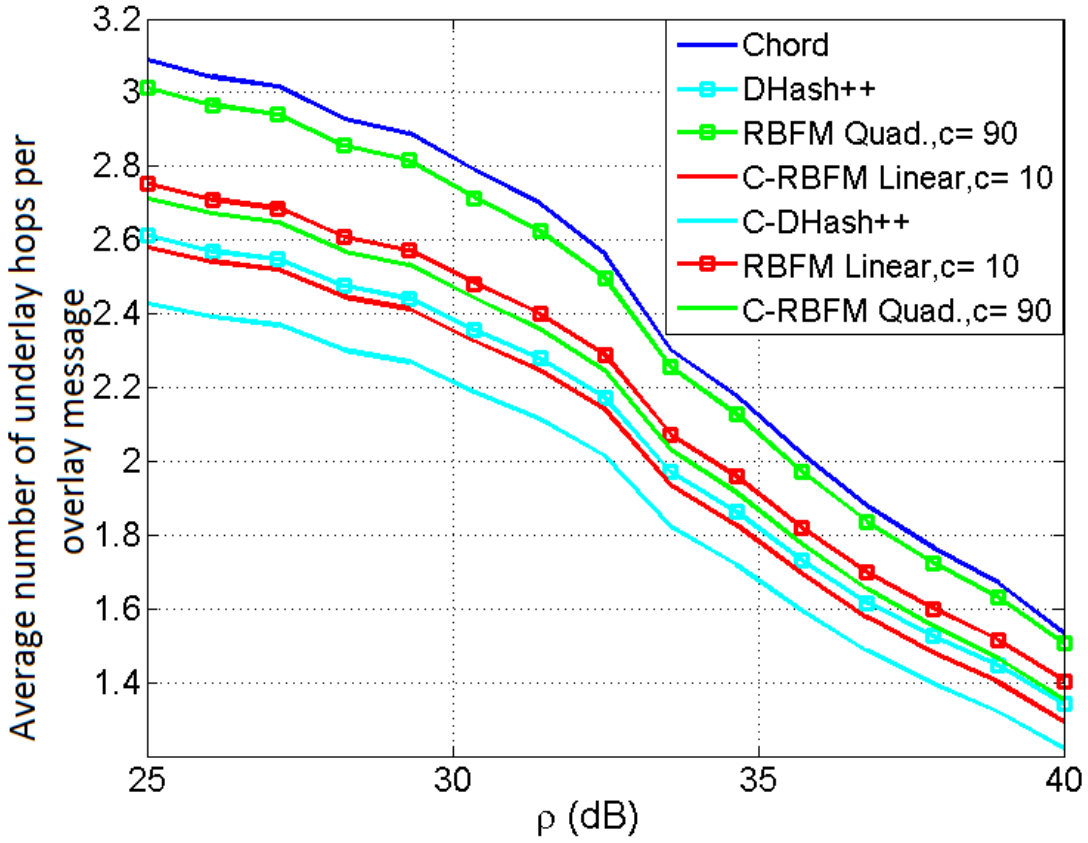

Figure 6.5: Average number of underlay hops per overlay message.

improvement for C-RBFM. Also we see that the overlay advantages claimed in [RB11] do in fact apply to underlay as well and RBFM has lower network overhead than DHash++ and much lower than that of Chord. C-RBFM even outperforms RBFM, as is to be expected. This figure also highlights the effect that protocol specific maintenance messages have on network load as the total number of underlay messages shown here also include those required to carry out maintenance as well.

Figure 6.7 shows the respective overlay and underlay messages for a fixed SNR (25 dB) required to carry out the 85000 data lookups. We see that adding clustering to the finger selection procedure (C-DHash++ and C-RBFM) reduces the network overhead by around 10 percent.

Figure 6.7 along with Figure 6.5 also shed light on another result claimed

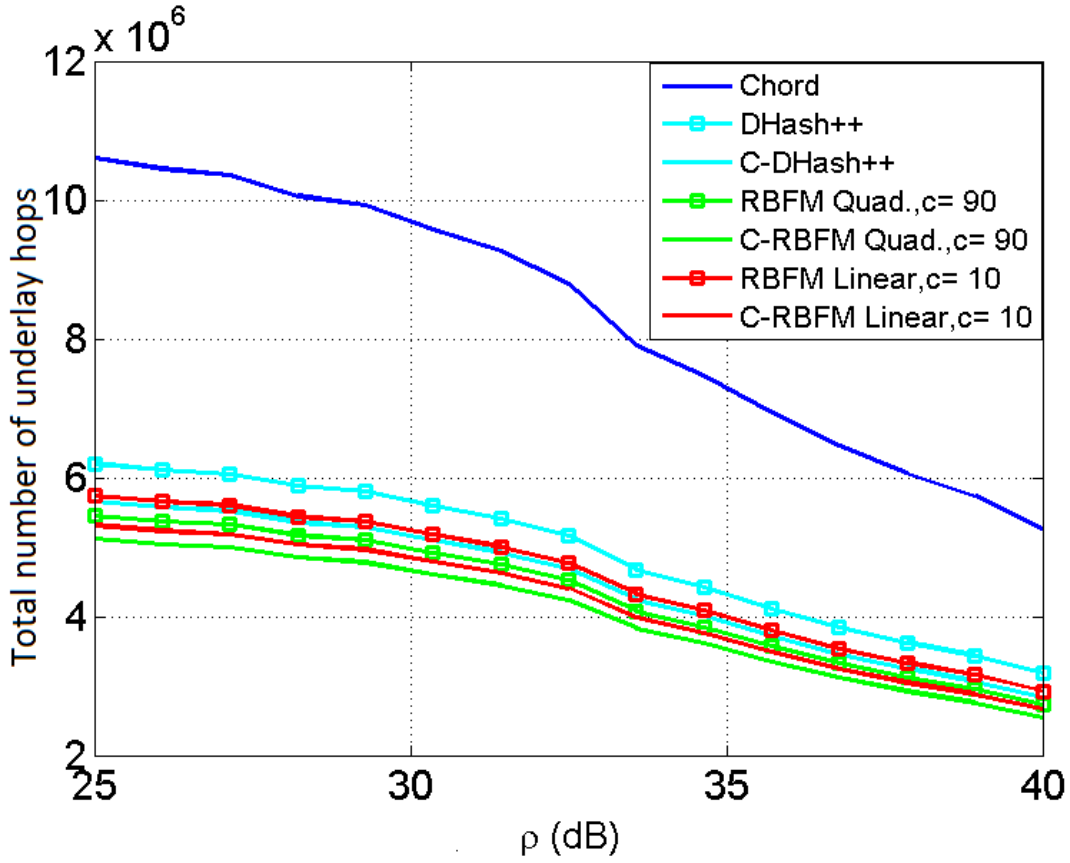

Figure 6.6: Total number of underlay hops.

in [RB11]. Overlay simulations show that RBFM (quadratic, $c = 90$) displays the least number of overlay overhead (around 25 % lower than DHash++), a fact our overlay simulation also verifies. However, as stated earlier, the real figures of overhead are the ones relating to the physical (underlay) transmissions. The Figure 6.5 shows that RBFM (quadratic, $c = 90$) has a higher value of underlay messages per overlay message, since it is a resource-centric method rather than proximity centric. This means that, as shown in Figure 6.6, the actual benefit of this scheme over DHash++ is of around 10 % reduction in the network overhead and not 25 %. This shows that the overlay benefits can be easily offset by the physical parameters of the network and it is important to look at both.

Another interesting result is given in Figure 6.8. Here we compare the effect

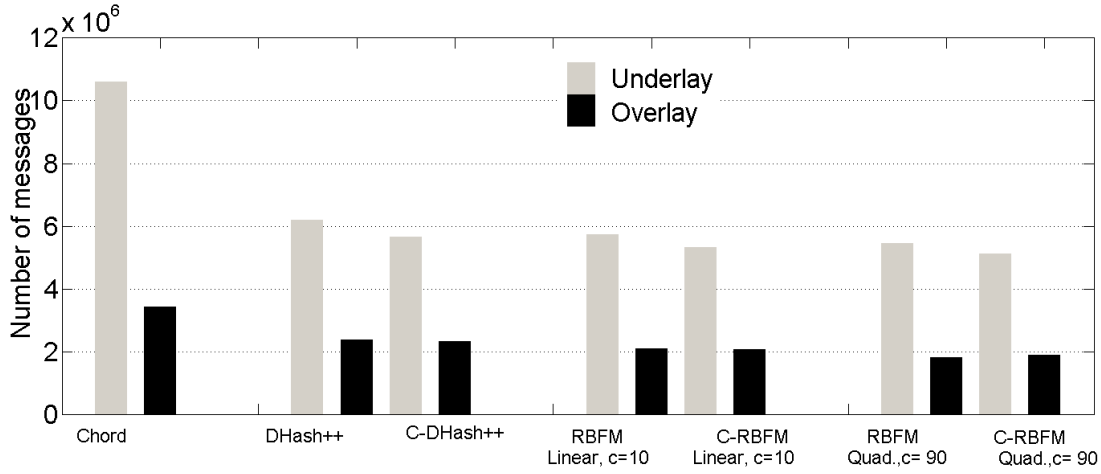

Figure 6.7: Comparison of overlay and underlay messages for different protocols for 85000 data lookups.

of different protocols on resource drainage in the network. The plot shows the average accumulated resource utilization per overlay hop. The resource utilization of a node is the difference of the current resource level to the maximum resource level (in this case 3). Thus a node with resource level 2 has a resource utilization of 1. And accumulated resource utilization is the sum of the resource utilization of individual nodes along the underlay route of an overlay message between two nodes. In our simulations, we assume that a node uses a unit of power every time it sends a message, which leads to a drainage of the resources. A counter is used to record how many units of power a node has used.

In [RB11] the RBFM (quadratic, c=90) protocol was designed specifically to show a low resource utilization in the network by placing emphasis on high resource availability in finger selection. Hence it should show the smallest resource utilization, which in reality it does not. In fact it is only marginally better than Chord which does not take into account any parameter of the nodes. This is due to the fact that even though we can choose fingers involving nodes with high resource levels, we have no control over the resource levels of the nodes that are being used along the multi-hop route as relays. In fact by placing emphasis on resource levels rather than proximity we end up with longer paths involving

greater number of hops and thus possibly greater resource utilization. C-RBFM (quadratic, c=90) serves to remedy this by choosing links that are closer as well (by virtue of being in the same cluster), and shows an improved performance as can be seen in Figure 6.7.

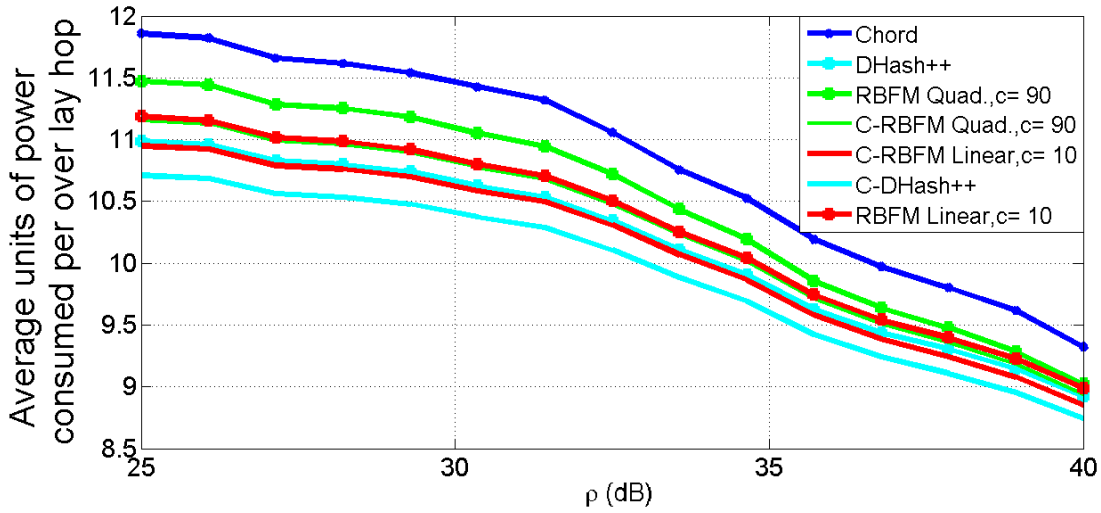

Figure 6.8: Resource utilization per overlay hop.

Simulation Results Incorporating Mobility and Heterogeneity of Nodes

In the remaining part of our work we evaluate protocols in the presence of nodes with mobility. We employ a dynamic network topology and tailor the DHT scheme to produce optimum performance in that scenario.

In order to incorporate realistic simulation results the proper choices of nodes' mobility pattern, nodes' resource drainage, failure and appearance of new nodes as well as reliable bootstraps nodes are very important [RB11]. Bootstrap nodes refer to the predecessor and successor of any node in the finger table. Initially we consider the simplest ad-hoc network set up consisting of N nodes, with nodes having 'random walk' mobility patterns with an average speed of 0.5 m/s. The nodes are uniformly and randomly distributed over the rectangular two dimensional space with side dimensions of 200m. The failure of nodes (zero battery) is

also random but related to the energy capacity level of each node as in previous simulation setups.

We perform a set of simulation setups incorporating the most underlay-aware protocols (C-RBFM and RBFM) from the first part of the chapter and DHash++ as a benchmark. All overlay protocols, analyzed in this chapter, require periodic and non-periodic direct predecessor's and successor's update. But the direct predecessor and successor cannot be chosen based on a proximity-aware selection procedure. The impact of such updates becomes significant in heterogeneous and dynamic networks, where each new node has to find its direct successor and predecessor via a bootstrapping procedure [RB11] in order to uniquely locate itself in the overlay network. The same applies when a node fails or disappears from the network. Such tasks cannot be optimized by a proximity aware selection algorithm.

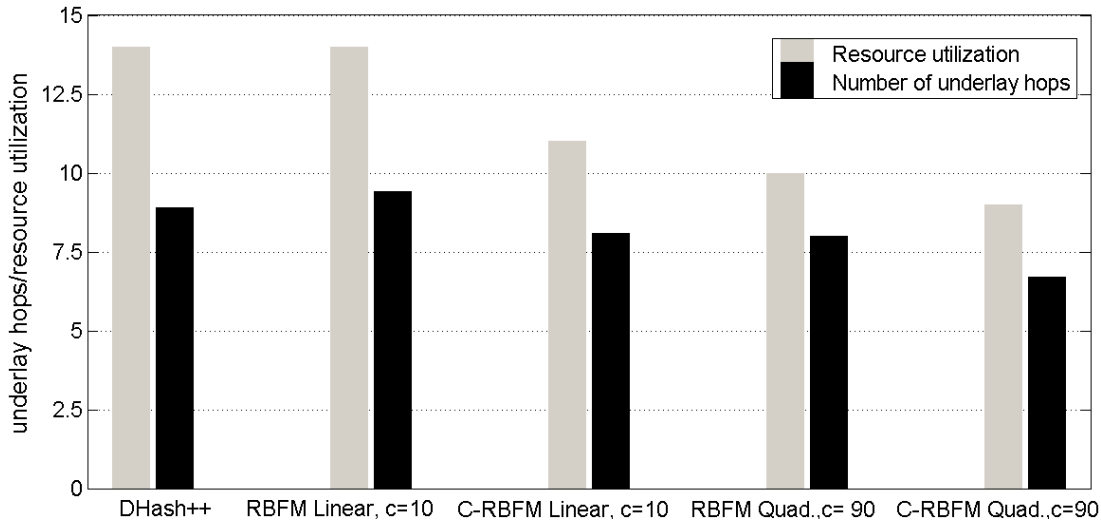

Figure 6.9: Dynamic network configuration. Resource utilization and number of underlay messages per overlay hop (with maintenance messages).

The proposed novel protocol (C-RBFM) again shows a very good performance with around 15 % decrease in the network overhead as well as a significant reduction in the resource utilization, as shown in Figure 6.9. This protocol was designed with the aim of providing the highest coupling with the physical parameters of the network (distances and resources). The obtained results also suggest that

underlay awareness in overlay protocols is an important part of overlay network functionality and can even be crucial in some specific network scenarios.

6.5 Conclusions and future work

Novel DHT protocols which incorporate knowledge about the underlay network clustering configuration are presented in this chapter and are designed to perform well on heterogeneous dynamic ad-hoc networks. We have shown a ten to fifteen percent decrease in the network load for our scenario compared to schemes which do not take clustering information into account. They also require a lower number of underlay hops and consume less energy resources to perform one overlay hop. Simulations have also shown that some claimed overlay benefits from earlier schemes are less pronounced when coupled with a real wireless underlay network. This highlights the importance of simulating both overlay and underlay networks together.

Future work should consider the evaluation of the presented protocols on an implemented testbed as well as comparisons with other DHT approaches for mobile ad-hoc networks. Furthermore, DHT adaptations for other network underlay configurations could be developed and compared in order to assess the suitability of varying underlay configurations for DHT applications.

Chapter 7

Physcial layer security

The focus of this chapter is on exploiting the benefits of cooperative communications to improve the information theoretic limit of reciprocal channel key generation (RCKG). The information theoretical limit of RCKG for co-located multiple input multiple output (MIMO) setup is compared with the cooperative MIMO setup using numerical simulations. Moreover, a novel scheme is developed for enhancing the performance of RCKG in multi-hop channels. This chapter highlights the benefits of cooperative communications over co-located communications in terms of physical layer security.

7.1 Introduction

One of the biggest challenges facing the wide-spread adoption of ad-hoc networks is the threat that the data is easily vulnerable to any eavesdroppers. The decentralized and ad-hoc nature of the connections render the usual data security mechanisms unsuitable for use in the networks under consideration. Physical layer security mechanisms [BBRM08] are an interesting and viable option for such networks. The ubiquitous and on-the-fly nature of such mechanisms are highly suited for providing security in self-organizing cooperative relaying networks.

The specific form of physical layer security that we will focus on is called reciprocal channel key generation (RCKG). It was proposed in [HHY95] and has recently been discussed extensively in [WS10]. RCKG can be used in conditions when the wireless channel between two communicating nodes is nearly reciprocal. Reciprocity is not an impractical assumption as it is practically achieved in a variety of wireless systems employing time-division duplex (TDD), such as IEEE 802.11 [IEE97], IEEE 802.16 (WiMAX) [IEE97], and 3rd Generation Partnership Project (3GPP) Long Term Evolution (LTE) [DPS11].

In this chapter, we will extend the analysis from [WS10] to the case of cooperative MIMO systems, and also propose a new incremental method for providing physical layer security to multi-hop networks.

7.2 Information theoretic limits of reciprocal channel key generation in cooperative MIMO scenario

In cooperative MIMO, the source and the destination can use some adjacent nodes as elements of the antenna array. By generating orthogonal channels, the benefits of MIMO transmission are exploited with single antenna devices. The cooperative MIMO transmission is accomplished in three steps. In the first step the source transmits the data to the selected group of relay nodes. Afterwards, these relays transmit the received data, at the same time, to some relays at the receiver side. Finally, the relays at the receiver transmit the data to the clusterhead which is actually the destination. Since the elements of this virtual antenna array are physically separated, the eavesdropper can be close to just one of the relay node at the same time. Figure 7.1 illustrates an eavesdropper in cooperative MIMO transmission which is located close to a relay node at the receiver side.

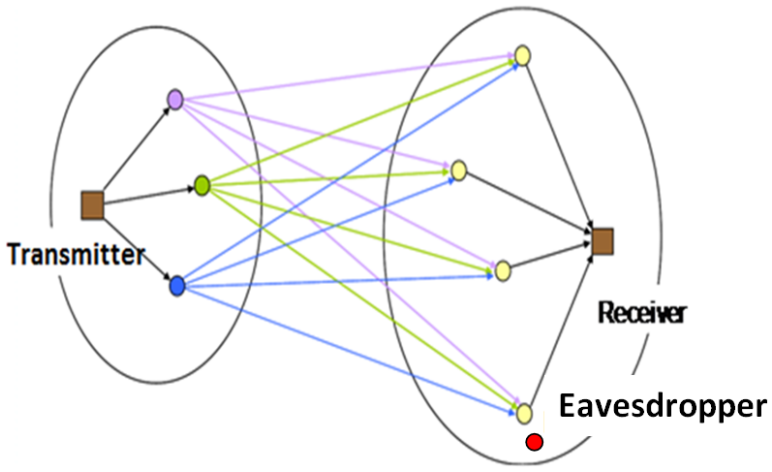

Figure 7.1: An eavesdropper near one of the relay nodes which is used as an element of the virtual antenna array at the receiver side in cooperative MIMO transmission.

Before investigating the numerical analysis for the cooperative MIMO scenario, let us review the theoretical limit of RCKG in [WS10] when all antennas are assembled at one device. Figure 7.2 shows corresponding wireless communi-

cation scenario for the co-located MIMO scheme.

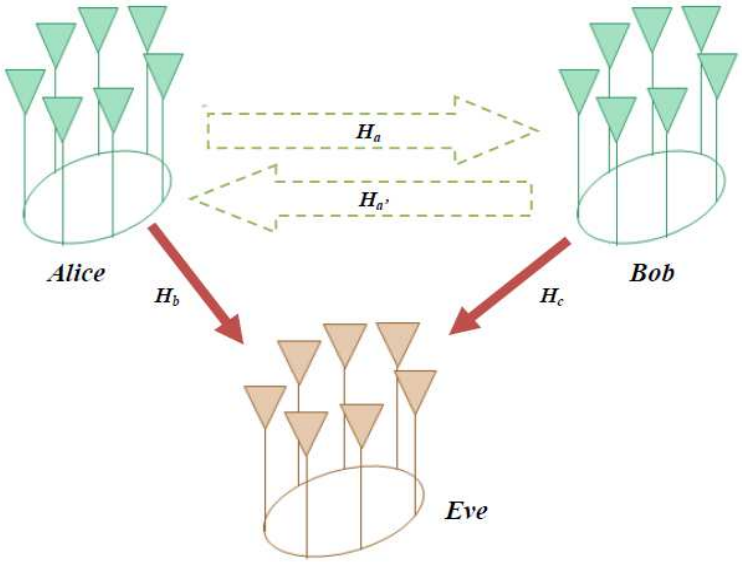

Figure 7.2: Wireless communications scenario

Alice and Bob (legitimate users) want to share information without providing any to Eve (eavesdropper). The channel between Alice and Bob is reciprocal. They use this channel as basis to generate a *key* which is used to code the data. If the eavesdropper can estimate this channel well, it can also generate the key and make the data, or some part of it, vulnerable.

It was shown, mathematically, in [WS10] that the amount of vulnerable information in this communication depends on how correlated the channel between one of the users and the eavesdropper is. In other words, the closer (physically) the antenna array of the eavesdropper is to that of one of the users, the greater is the probability for it to be able to extract some information from the legitimate communication. In [WS10], RCKG systems were analyzed for the case of co-located MIMO systems. It was shown that upon increasing the number of antennas in the array of the eavesdropper, the data becomes increasingly vulnerable when the physical separation between the eavesdropper and the user is small. Hence, the physical layer security is not so effective in this case.

Considering a reciprocal channel between the transmitter and the receiver, the forward and reverse channel matrices of the legitimate communication are

the transpose of each other. However, because of the noise and synchronisation errors the channel estimation is not perfect and we need to define an inaccuracy model. Hence, the available channel state information at the nodes is given by

$$\hat{\boldsymbol{h}}_a = \boldsymbol{h}_a + \epsilon_a, \quad \hat{\boldsymbol{h}}_{a'} = \boldsymbol{h}_{a'} + \epsilon_{a'}$$
$$\hat{\boldsymbol{h}}_b = \boldsymbol{h}_b + \epsilon_b, \quad \hat{\boldsymbol{h}}_c = \boldsymbol{h}_c + \epsilon_c,$$

where vector channels $\boldsymbol{h}_a$ and $\boldsymbol{h}_{a'}$ stand for the forward and reverse channel of the legitimate communication and $\boldsymbol{h}_b$ and $\boldsymbol{h}_c$ are the channel between the eavesdropper and the transmitter and the receiver respectively. Note that the channels here are vectorized versions of the channel matrices, e.g., $\boldsymbol{h}_a = \mathrm{vec}(\boldsymbol{H}_a)$. Moreover, the inaccuracy vector of the channel estimation at the node k is denoted as ϵ_k which is modeled as zero-mean circular symmetric Gaussian distribution with a variance σ_k^2.

In the reciprocal channel scenario, the available channel knowledge about the legitimate channel is almost the same at the transmitter and the receiver, and because of the physical separation of the eavesdropper and the transmitter and the receiver nodes, the eavesdropper is not able to estimate the legitimate channel accurately. In other words, a large part of the information about the legitimate channel state will be secure from the eavesdropper. Hence, the information about the legitimate channel is an appropriate random variable for generating the key. The maximum amount of information which can be extracted form the legitimate channel for key generation is called mutual information $I_k = I(\boldsymbol{h}_a, \boldsymbol{h}_{a'})$. By considering zero-mean circular Gaussian random vectors for the channels the mutual information is given by [WS10]

$$I_{\mathrm{K}} = h(\hat{\boldsymbol{h}}_a) + h(\hat{\boldsymbol{h}}_{a'}) - h(\hat{\boldsymbol{h}}_a, \hat{\boldsymbol{h}}_{a'}) = \log_2 \frac{|\hat{\boldsymbol{R}}_{a,a}| \cdot |\hat{\boldsymbol{R}}_{a',a'}|}{|\hat{\boldsymbol{R}}_{A,A'}|}, \tag{7.1}$$

where $h(x)$ denotes the differential entropy of a random variable x, $|\boldsymbol{A}|$ denotes the determinant of a matrix $\boldsymbol{A}$, and covariance matrices with lowercase subscripts

are defines as

$$\boldsymbol{R}_{p_1,p_2} = \mathbb{E}\left\{\boldsymbol{h}_{p_1} \cdot \boldsymbol{h}_{p_2}^H\right\} \quad \hat{\boldsymbol{R}}_{p_1,p_2} = \mathbb{E}\left\{\hat{\boldsymbol{h}}_{p_1} \cdot \hat{\boldsymbol{h}}_{p_2}^H\right\}$$

and the covariance matrices of the stacked channel vectors are given by uppercase subscripts as follow

$$\boldsymbol{R}_{P_1,P_2,\cdots,P_M} = \mathbb{E}\left\{\left[\boldsymbol{h}_{p_1}^H \boldsymbol{h}_{p_2}^H \cdots \boldsymbol{h}_{p_M}^H\right]^H \cdot \left[\boldsymbol{h}_{p_1}^H \boldsymbol{h}_{p_2}^H \cdots \boldsymbol{h}_{p_M}^H\right]\right\}.$$

Note that $(\boldsymbol{A})^H$ denotes the conjugate transpose (Hermitian) of a matrix $\boldsymbol{A}$. As it is mentioned before, because of the slight correlation between the eavesdropper channel and legitimate channel, a part of the information about the state of the legitimate channel is revealed to the eavesdropper. Therefore, the eavesdropper has access to a part of the generated key bits. The number of vulnerable key bits at the eavesdropper is given by $I_{\mathrm{VK}} = I_{\mathrm{K}} - I_{\mathrm{SK}}$, where I_{SK} denotes the number of key bits which remain secure and it can be written as

$$I_{\mathrm{SK}} = \log_2 \frac{|\hat{\boldsymbol{R}}_{\mathrm{A,B,C}}| \cdot |\hat{\boldsymbol{R}}_{\mathrm{A',B,C}}|}{|\hat{\boldsymbol{R}}_{\mathrm{B,C}}| \cdot |\hat{\boldsymbol{R}}_{\mathrm{A,A',B,C}}|}. \tag{7.2}$$

Considering the case that the eavesdropper is close to the transmitter or the receiver which are both the worst possible locations of the eavesdropper, either the channel $\hat{\boldsymbol{h}}_b$ or $\hat{\boldsymbol{h}}_c$ will be partly correlated to the legitimate channel, respectively, and the other channel is negligible. As in [WS10], we focus on the case when Eve is close to Alice. Moreover, Alice and Eve are stationary, which leads to correlated channels and thus a reduction in the number of secure key bits. When only the movement of Bob or the scatterers causes channel variation, $\boldsymbol{h}_b$ is not random and contains no information. Without loss of generality, the number of key bits which remain secure is rewritten as

$$I_{\mathrm{SK}} = \log_2 \frac{|\hat{\boldsymbol{R}}_{\mathrm{A,C}}| \cdot |\hat{\boldsymbol{R}}_{\mathrm{A',C}}|}{|\hat{\boldsymbol{R}}_{\mathrm{C}}| \cdot |\hat{\boldsymbol{R}}_{\mathrm{A,A',C}}|}. \tag{7.3}$$

It is very interesting to extend the analysis performed in [WS10] to the case of cooperative MIMO systems. As the amount of vulnerable information depends

upon the distance between the eavesdropper's array and the array of the user, the distributed nature of the cooperative MIMO set-up means that there is a good chance that the eavesdropper is only close to one of the cooperating nodes and hence can only access one of the data streams in a spatial multiplexing scenario. However, for cluster-based systems, the eavesdropper could be located next to the cluster-head and thus can, effectively, have access to all the data streams when they are transmitted to the cluster-head by the relays.

The information theoretical limits of reciprocal key generation for the cooperative MIMO scenario are exactly the same as for the co-located MIMO case. That means that the equations of this chapter can also be applied for the cooperative case. However, the locations of the antennas and the distances between the antennas of the eavesdropper and the antennas of the relay lead to the difference in the effectiveness of the generated keys in these two scenarios.

Numerical results

The numerical results of this chapter are based on the suggested model in [WS10]. Based on this model, we assume that the eavesdropper and the relay, which is located close to it, share the same multipath component. Therefore, their antennas are assumed as the elements of an effective array. The complex baseband channel between the transmitter and the relay/eavesdropper is given by [WS10]

$$h_{i,m} = \sqrt{\frac{K}{1+K}} + \sum_{l=1}^{N_{\text{path}}} \beta_l \cdot \exp\left[\mathrm{j}\left(\boldsymbol{k}_l \cdot \boldsymbol{r}_i + \boldsymbol{k}'_l \cdot \boldsymbol{r}'_m\right)\right] \tag{7.4}$$

where K is the Rician K-factor, N_{path} denotes the number of non-line-of-sight paths, $\boldsymbol{r}_i = \Big[x_i, y_i\Big]^T$ are the 2-D coordinates of the ith antenna at the transmitter, $\boldsymbol{k}_l = 2\pi \cdot \Big[\cos(\phi_l), \sin(\phi_l)\Big]$, ϕ_l and β_l are the 2-D wave vectors representing the angle and the complex baseband gain of the lth path, respectively, at the transmitter. Analogously, the parameters $\boldsymbol{r}'_i$ and $\boldsymbol{k}'_l$ are defined with respect to the relay/eavesdropper nodes. Note that the parameter β_l is zero-mean, circularly symmetric, complex Gaussian distributed with a variance $\sqrt{1/(N_{\text{path}} \cdot (1+K))}$ and the path angles (ϕ_l) are uniformly distributed on $\Big[0, 2\pi\Big]$. By using this

channel model and considering the aforementioned additive inaccuracy vectors the covariance matrices are generated and afterward the parameters I_{K}, I_{SK} and I_{VK} are computed.

In the simulations of this section, the covariance matrices are generated over 1000 channel realizations for 15 dB signal to noise ratio (SNR) and Rician K-factor of 0. Figure 7.3 shows the I_{K} versus different numbers of paths when the number of antennas at the transmitter/Alice is N_{TX} and the number of antennas at the receiver/Bob is N_{RX} and both are equal to N. As we can see I_{K} saturates with increased number of paths and converges to N^2 for rich multipath.

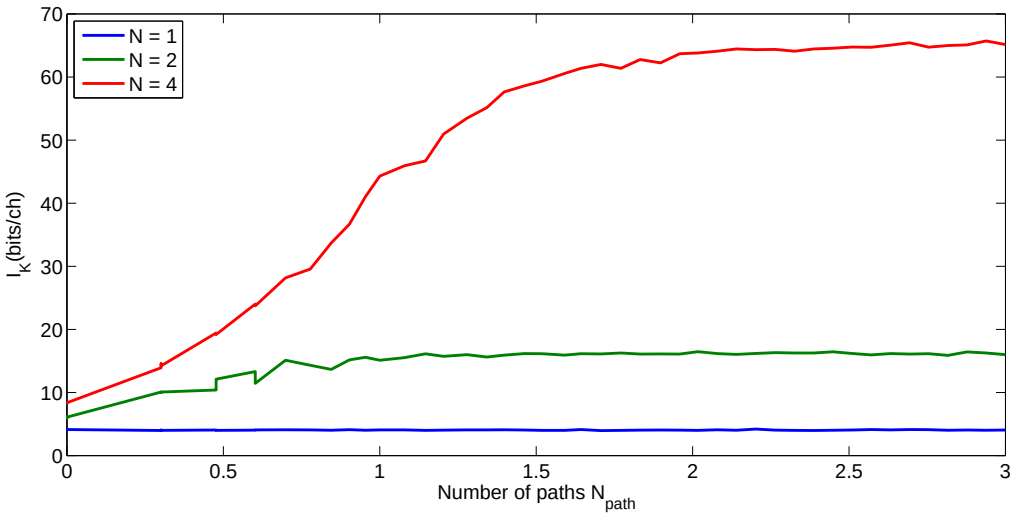

Figure 7.3: Theoretical key bits which can be generated at the terminals when they use N-element arrays

Figure 7.4 considers the scenarios when $N_{\mathrm{TX}} = N_{\mathrm{RX}} = 4$ antennas, and the number of antennas on Eve (N_{E}) is either 4 or 10. All nodes employ uniform linear arrays (ULAs) with $\lambda/2$ inter-element spacing where λ is the free-space wavelength. This simulation shows that RCKG is vulnerable when the eavesdropper has an array size advantage. We can also see that taking more multipaths into account increases the performance of the RCKG mechanism.

Figure 7.5 considers a similar scenario except that in this case the legitimate users will employ the cooperative MIMO scheme with 4 distributed antennas

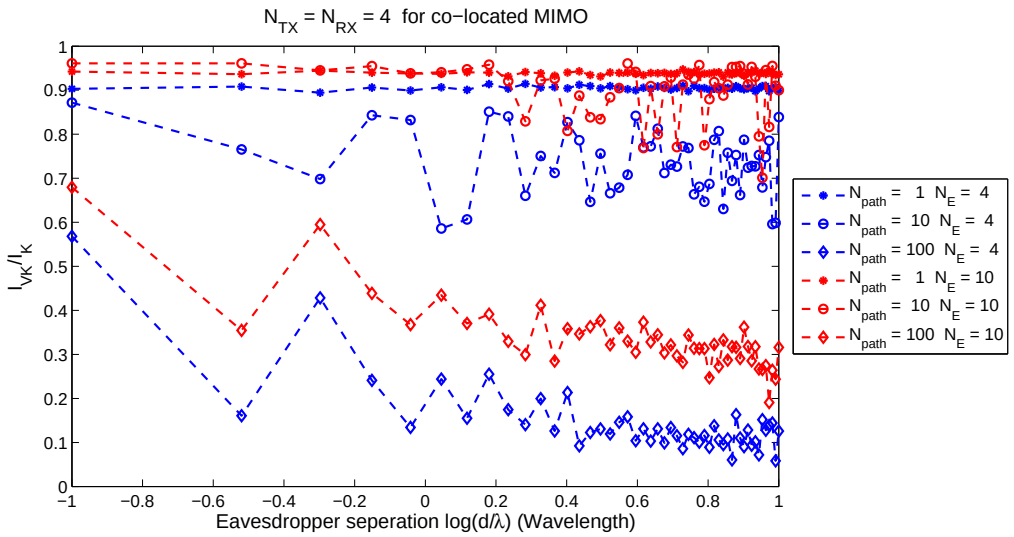

Figure 7.4: Relative number of vulnerable key bits when Eve has either 4 or 10 antennas and the users have co-located ULAs with 4 antenna elements

each. The eavesdropper can then be located close to only one of these distributed antennas. The simulation shows that the vulnerability of RCKG is reduced by half by employing cooperative MIMO instead of co-located ULAs.

Figure 7.6 considers a homogeneous network where all nodes (even eavesdropper nodes) are equipped with the same number of antennas, thus the eavesdropper has also only 1 antenna for the cooperative case. The number of vulnerable key bits are compared for the co-located and cooperative case in this figure.

As it is shown in Figure 7.6, the security of the transmission is increased by using cooperative MIMO, when the single antenna eavesdropper is located close to one of the relay nodes. Moreover, this result shows that increasing the number of paths leads to an increased number of secure key bits. The analysis of the security for the cooperative MIMO scenario is more critical for the phase of the transmission when the data is transmitted by a source to the cooperative relays or when the transmitted data from cooperative relays is received at the destination. In these steps the eavesdropper can be located close to the cluster-head (source or destination). This scenario is illustrated in Figure 7.7. Note that in this case, the legitimate channel is almost available at the eavesdropper. However, we show in

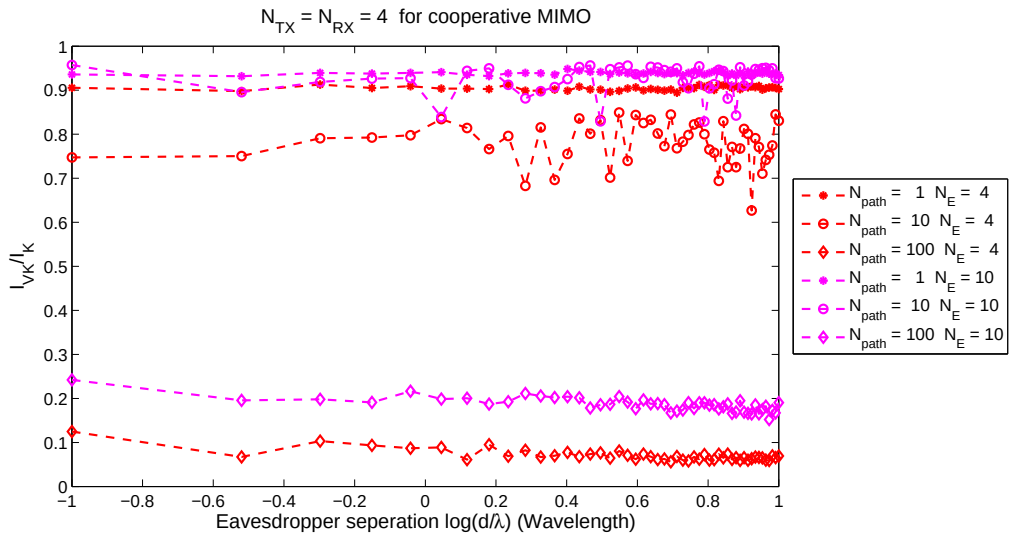

Figure 7.5: Relative number of vulnerable key bits when Eve has either 4 or 10 antennas and the users employ cooperative MIMO with 4 distributed antennas

the next simulations that choosing a good arrangement of the relays can improve the security performance in this scenario.

In this simulation, we try to change the ratio of the received power via the line of sight path by varying the Rician K-factor. It is obvious that the arrangement or selection of the cooperative relays determines the Rician K-factor. In this simulation, the number of relays is 4. As it is mentioned before, all devices such as the relays, the cluster-head, and the eavesdropper are single antenna nodes. The illustrated result of this simulation in Figure 7.8 shows that choosing the relays with large values of the Rician K-factor leads to the increase of the relative number of vulnerable key bits. In other words, if the relays are located in the position with relatively good line of sight connections, the eavesdropper is able to perform a good estimation of legitimate channel and consequently the key bits.

For the scenario when the eavesdropper is next to the cluster-head, the security performance is increased when faced with a smaller Rician K-factor, but this scenario is still the limiting case for physical layer security in cooperative MIMO communication. In the next section, we introduce a new encryption method by

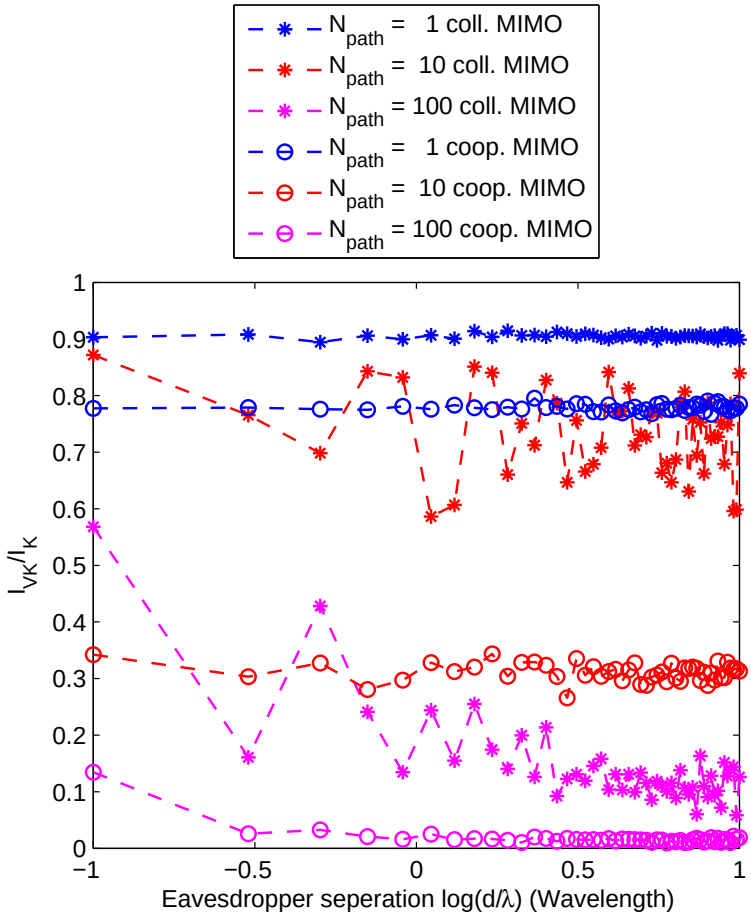

Figure 7.6: Comparing the relative number of vulnerable key bits for cooperative and co-located MIMO for the case that eavesdropper is located close to one of the relays for 15 dB SNR.

using multihop relaying to solve the presented problem.

7.3 Information theoretic limits of reciprocal channel key generation in two-hop relaying scenario

For the case when the eavesdropper is close to the cluster-head, the RCKG mechanism, described in the last section, might not be very effective if the separation

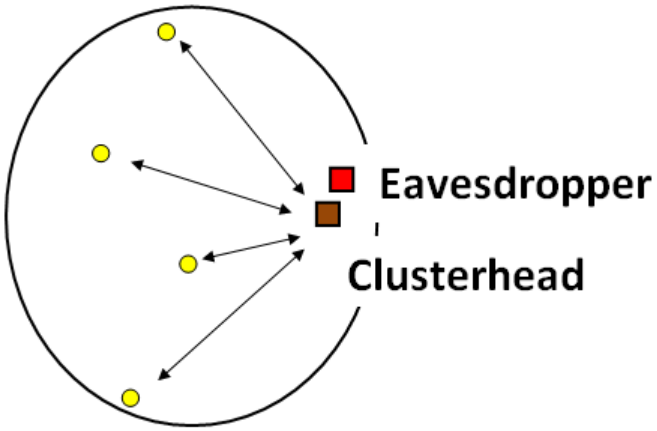

Figure 7.7: An eavesdropper near cluster-head.

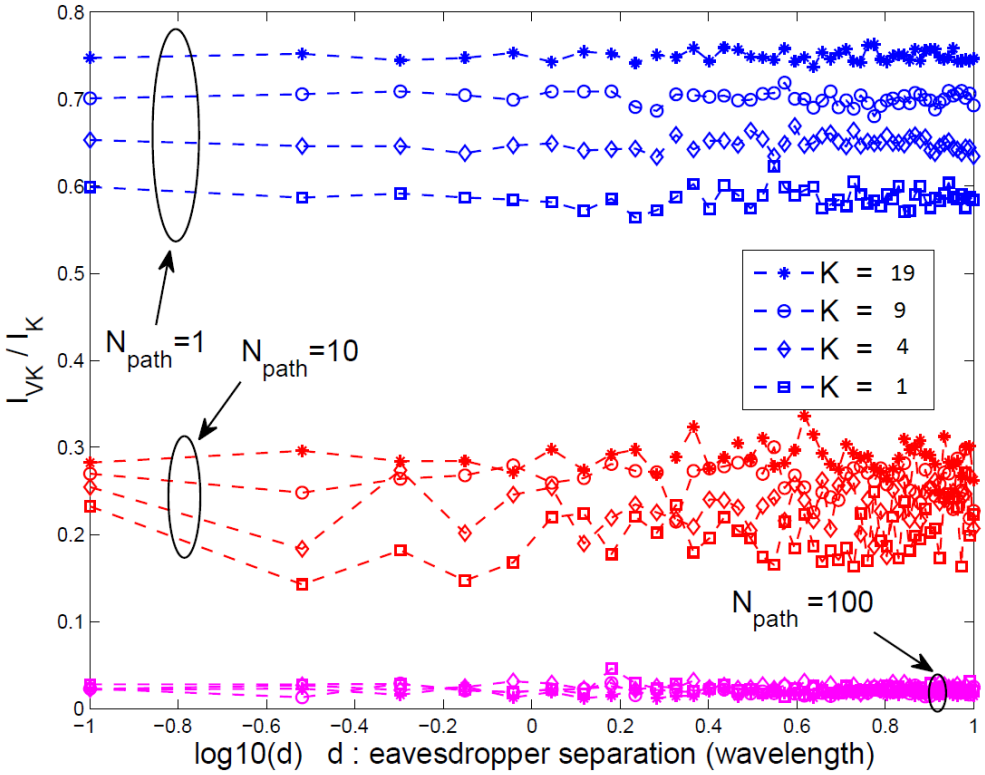

Figure 7.8: Relative number of vulnerable key bits for different values of Rician K-factor when the eavesdropper is located close to the cluster-head (source or destination).

between the eavesdropper and the legitimate node is small. This calls for some novel method to improve the security. One such method would be to use the inherent nature of multi-hopping in cooperative relaying to make the keys more sophisticated and thus encode the data more effectively. Consider the scenario depicted in Figure 7.9. In this model, TX which is one of the intermediate relay nodes wants to transmit the received data from $\text{TX}_{(-1)}$ which is the previous relay node to the RX (which can be the next relay node or the destination node).

The focus of this section is on developing a method for improving the theoretic limits of RCKG in multi-hop relaying. Multi-hop relaying (AF or DF relaying, as discussed in Chapter 2) is a promising technique for communication between a source and destination via some relay nodes, when the nodes have limited transmission ranges. In the multi-hop relaying technique, every relay retransmits the received signal after performing some processing of its own. The proposed method for generating keys in this section is based on using only one pre-TX relay. It can, however, be extended to more that one pre-TX relays and be used to provide even higher levels of security.

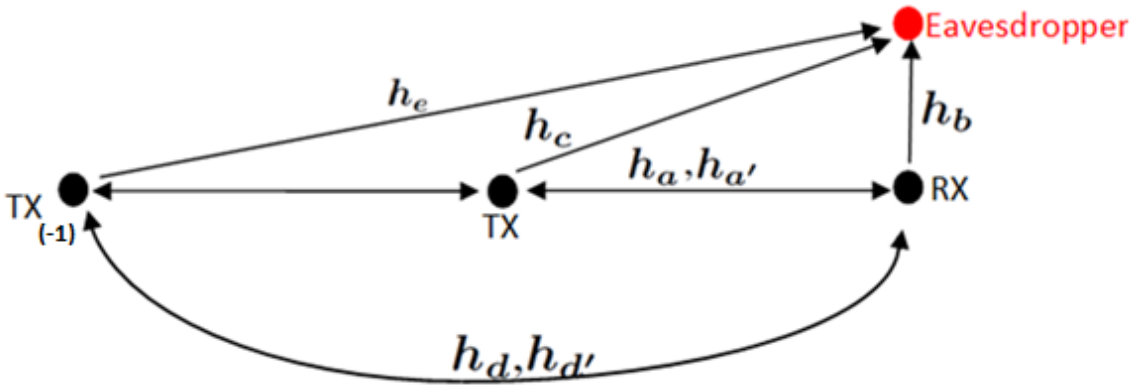

Figure 7.9: Considered model of multi-hop relaying.

In this method, the encryption is accomplished in two steps by the node TX. In the first step, TX uses the channel between TX and RX $(\hat{\boldsymbol{h}}_a, \hat{\boldsymbol{h}}_{a'})$ to generate the key bits and the data is encrypted based on the generated key. Then, in the second step, the TX encodes the encrypted data again but with a new key which is generated based on the channel between $\text{TX}_{(-1)}$ and RX $(\hat{\boldsymbol{h}}_d, \hat{\boldsymbol{h}}_{d'})$. Because the

information about the channel $\hat{\boldsymbol{h}}_d$ is not available at the TX, this information must be forwarded by the $\mathrm{TX}_{(-1)}$ to TX. In order to ensure that this information about the channel $\hat{\boldsymbol{h}}_d$ is not overheard by the eavesdropper, for example in the case that the eavesdropper is located next to the TX, the information about the channel $\hat{\boldsymbol{h}}_d$ is encrypted twice at $\mathrm{TX}_{(-1)}$, at first by using the key generated based on the channel between $\mathrm{TX}_{(-1)}$ and TX and then by using the other key generated based on the channel between $\mathrm{TX}_{(-2)}$ (the node preceding $\mathrm{TX}_{(-1)}$) and TX. After these two encryptions of the channel $\hat{\boldsymbol{h}}_d$, this information is forwarded to the TX by $\mathrm{TX}_{(-1)}$. Note that all notations in this section such as the accent hat ($\hat{}$) have the same meaning as in the last section. Moreover, all channels are assumed to be reciprocal.

Let R_i denote the relative secure information of the generated key in the level i. Since the presented encryption method has two levels, we can write

$$R_i = \frac{I_{\mathrm{SK},i}}{I_{\mathrm{K},i}}, \quad \text{for} \quad i \in \{1, 2\}. \tag{7.5}$$

Using the equations (7.1) and (7.3) in the last section, we can write

$$\begin{aligned}
I_{\mathrm{K1}} &= \log_2 \frac{|\hat{\boldsymbol{R}}_{\mathrm{a,a}}| \cdot |\hat{\boldsymbol{R}}_{\mathrm{a',a'}}|}{|\hat{\boldsymbol{R}}_{\mathrm{A,A'}}|} \\
I_{\mathrm{SK1}} &= \log_2 \frac{|\hat{\boldsymbol{R}}_{\mathrm{A,C}}| \cdot |\hat{\boldsymbol{R}}_{\mathrm{A',C}}|}{|\hat{\boldsymbol{R}}_{\mathrm{C}}| \cdot |\hat{\boldsymbol{R}}_{\mathrm{A,A',C}}|} \\
I_{\mathrm{K2}} &= \log_2 \frac{|\hat{\boldsymbol{R}}_{\mathrm{d,d}}| \cdot |\hat{\boldsymbol{R}}_{\mathrm{d',d'}}|}{|\hat{\boldsymbol{R}}_{\mathrm{D,D'}}|} \\
I_{\mathrm{SK2}} &= \log_2 \frac{|\hat{\boldsymbol{R}}_{\mathrm{D,E}}| \cdot |\hat{\boldsymbol{R}}_{\mathrm{D',E}}|}{|\hat{\boldsymbol{R}}_{\mathrm{E}}| \cdot |\hat{\boldsymbol{R}}_{\mathrm{D,D',E}}|}
\end{aligned}$$

By using this method of encryption, the eavesdropper should also perform the decryption in two steps. The number of vulnerable key bits after the first step of decryption at the eavesdropper is $I_{\mathrm{VK},1} = I_{\mathrm{K},1} \cdot (1 - R_1)$. The vulnerable key bits of the first step are actually all the information available at the eavesdropper at the second step of decryption and we can write $I_{\mathrm{K},2} = I_{\mathrm{VK},1}$. Therefore, the total

number of vulnerable key bits is given by

$$I_{\mathrm{VK,total}} = (1 - R_2) \cdot I_{\mathrm{K},2},$$
$$I_{\mathrm{VK,total}} = (1 - R_2) \cdot (1 - R_1) I_{\mathrm{K},1}.$$

Since the values of R_1 and R_2 are both smaller than 1, the number of vulnerable key bits is decreased by using this method of encryption compared to the usual method in the last section. For example in Figure 7.10 the relative number of vulnerable key bits is illustrated for the case that the eavesdropper is next to one of the cooperative MIMO relay nodes. The number of eavesdropper antennas is 1 and the numbers of antennas at the TX, RX, and $\mathrm{TX}_{(-1)}$are 4. Note that, as was the case in the last section, the antennas of the TX, RX, and $\mathrm{TX}_{(-1)}$ are not assembled on one device. Therefore, the cooperative MIMO issue of the last section is analysed in two cases, with and without using the $\mathrm{TX}_{(-1)}$ channel.

It is shown in Figure 7.10 that using the information about the $\mathrm{TX}_{(-1)}$ channel decreases the relative number of vulnerable key bits. Now the question is whether this method can also be beneficial for the case that the eavesdropper is located close to the cluster-head. For this purpose, we repeated the simulation of Figure 7.8 for the case that the encryption is based on the TX to RX channel and the $\mathrm{TX}_{(-1)}$ to RX channel. By comparing the results of the new simulation which is shown in Figure 7.11, with the results of the encryption based on only the TX to RX channel, shown in Figure 7.8, we can conclude that the proposed method improves the performance of the encryption. Hence, the main problem of physical layer security for cooperative MIMO communication is solved with the aid of the $\mathrm{TX}_{(-1)}$ channel state information.

7.4 Conclusions

We conclude that cooperative MIMO is more beneficial than co-located MIMO in terms of the information theoretic limits of RCKG when the eavesdropper is not close to the cluster-head. Generally, in order to increase the number of secure key bits, the cooperative relays must be selected such that a lower Rician K-factor is achievable. This fact is more important for the intra-cluster transmission when

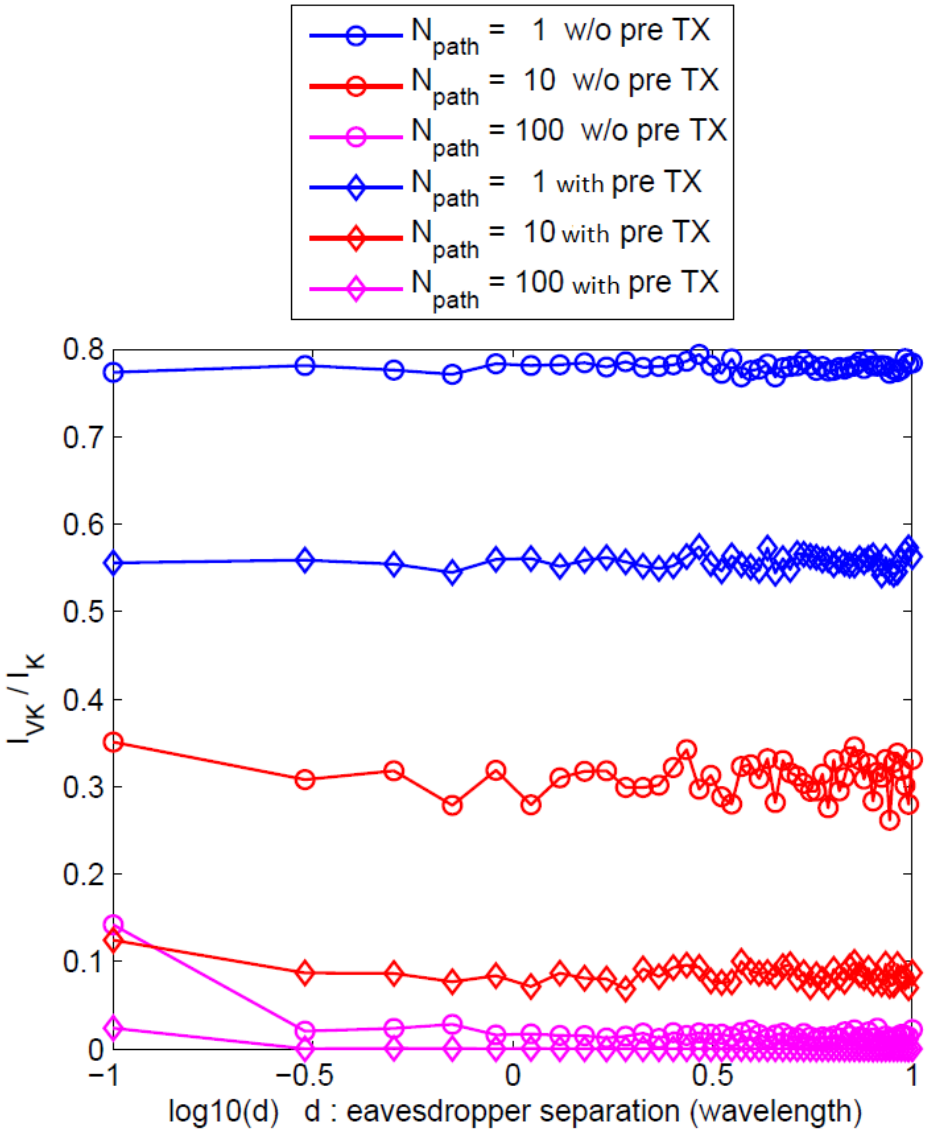

Figure 7.10: Relative number of vulnerable key bits for two different methods of encryption (with and without $TX_{(-1)}$) when the eavesdropper is next to one of the relays of cooperative MIMO.

the data is exchanged between the cluster-head and the cooperative relays. For the scenario that the eavesdropper is next to the cluster-head, the security performance can be increased when facing a smaller Rician K-factor, but this scenario is still the limiting case for the physical layer security for cooperative MIMO communications. We introduce a new encryption method, using multi-hop relaying,

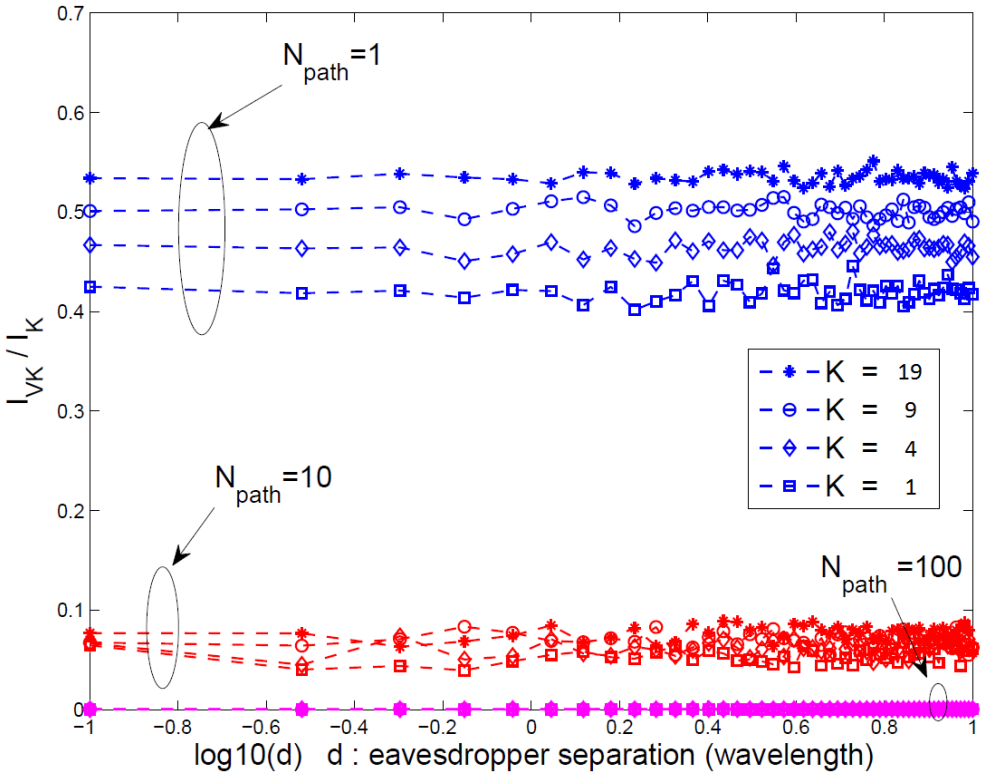

Figure 7.11: Relative number of vulnerable key bits for the case that the eavesdropper is located close to the cluster-head and the encryption is performed based on the TX/RX and $TX_{(-1)}$/RX channels.

to solve this problem. This two step encryption drastically reduced the vulnerability of RCKG and is very suitable when high levels of security are required. It is also especially suitable for providing security in cooperative MIMO communications as it performs well even for the specific scenario when the eavesdropper is close to the cluster-head.

For future work, we could look at practical methods for generating keys and optimize them for use in cooperative MIMO relaying scenarios.

Chapter 8

Conclusions and Outlook

8.1 Conclusions

The results presented in this thesis are of importance to network designers as we move towards the standardization of cooperative multi-hop networks. The analytical results can help to determine the thresholds at which nodes can switch between different modes of transmission, such as the relaying scheme, and the appropriate number of hops to ensure the QoS. Some algorithms for clustering, routing, security, and data management have also been presented in this thesis to assist the set-up and functioning of ad-hoc networks that employ cooperative relaying.

The ergodic capacity has been studied in case of the most popular relaying schemes of the multi-hop network (AF and DF relaying schemes). An optimum multi-hop network (equidistant relays) was assumed, in which the variances of the channels of all the hops is the same and the antennas at the relays are identical. The analysis of the ergodic capacity for both relaying schemes has identified that in the high SNR regime, decreasing the number of the hops yields an increase in the performance of the transmission. But in case of the low SNR regime, the environmental factors, e.g., the path loss exponent and the distance between the source and the destination have to be considered before increasing or decreasing the number of the hops in order to improve the performance of the network. In case of an environment which has a large path loss exponent, decreasing the number of the hops decays the performance in the low SNR regime. Using the

AF relaying scheme, as a result of transmitting the signal over more hops in the low SNR regime, the received SNR is decreased, because of the fact that by amplifying the received signal the noise component is also amplified. But using more hops in the high SNR regime increases the received SNR. Comparing AF and DF relaying schemes, it has been observed that the DF relaying scheme provides higher ergodic capacity than the AF relaying scheme using the same number of hops.

We have also studied the case of increasing the number of the antennas at the relay nodes (without considering antenna selection) in multi-hop networks. The analysis has revealed that even though the obtained gain by employing MIMO (Alamouti) multi-hop networks is more than that when employing SIMO multi-hop networks when assuming the same number of receive antennas, the gain obtained by employing SIMO multi-hop networks is more than that by MIMO (Alamouti) multi-hop networks when assuming the same total number of antennas. In other words, assuming a network with single antenna devices, increasing the transmit diversity should be given a lower priority over increasing the receive diversity.

We have also analyzed the cooperative MIMO scheme in wireless communications. We have described a method devised by us to employ SISO piloting in order to gauge the quality of the prospective cooperative MIMO links. Then, the performance of the cooperative MIMO system in the presence of synchronization errors has been studied. The focus has been on the Alamouti STBC scheme. Also, closed-form expressions of the lower bound of the SINR, the BER for the high SNR regime, and the worst case inaccuracy vector (corresponding to the lowest SINR) have been derived. Furthermore, it has been shown that increasing the transmit power in the high SNR regime does not improve the quality of the transmission because of a saturation region which is caused by the synchronization error assuming a constant number of receive antennas. Additionally, it has been shown that higher synchronization errors result in a faster transition to the high SNR regime and the saturation region.

We have presented a new clustering method (E-RSSI) for ad-hoc networks as well. The simulation results show that the E-RSSI clustering algorithm forms clusters in such a way that it enables low energy transmissions and distributes

the transmission energy consumption over all the nodes in a more even way which leads to a significantly longer network life-time. As the E-RSSI algorithm makes no assumption about the type of network nodes (homogeneous or heterogeneous), it can adapt itself to different network configurations. Aforementioned advantages make E-RSSI a practical solution to the problem of cluster-head selection.

Using cooperative MIMO for range extension of individual hops in a multi-hop network can give us a much improved link throughput capacity. We have proposed a new routing method (AOCMR) for ad-hoc networks in a cooperative MIMO communications scenario. Using our proposed scheme can make it simpler for cluster-heads to employ cooperative MIMO techniques in an ad-hoc manner since we use simple piloting and employ that to form tables at the cluster-heads which will be used for routing between clusters using heterogeneous cooperative MIMO links.

We have also presented methods for efficient data management in ad-hoc networks by employing distributed hash tables (DHTs). Novel DHT protocols which incorporate knowledge about the underlay network clustering configuration are presented in this thesis and are designed to perform well on heterogeneous dynamic ad-hoc networks. We have shown a ten to fifteen percent decrease in the network load for our scenario compared to schemes which do not take clustering information into account. They also require a lower number of underlay hops and consume less energy resources to perform one overlay hop. Simulations have also shown that some claimed overlay benefits from earlier schemes are less pronounced when coupled with a real wireless underlay network. This highlights the importance of simulating both overlay and underlay networks together.

We have also analyzed physical security mechanisms for ad-hoc networks. We conclude that cooperative MIMO is more beneficial than co-located MIMO in terms of the information theoretic limits of RCKG when the eavesdropper is not close to the cluster-head. Generally, in order to increase the number of secure key bits, the cooperative relays must be selected such that a lower Rician K-factor is achievable. This fact is more important for the intra-cluster transmission when the data is exchanged between the cluster-head and the cooperative relays. For the scenario that the eavesdropper is next to the cluster-head, the security performance can be increased when facing a smaller Rician K-factor, but this scenario

is still the limiting case for the physical layer security for cooperative MIMO communications. We introduce a new encryption method, using multi-hop relaying, to solve this problem. This two step encryption drastically reduced the vulnerability of RCKG and is very suitable when high levels of security are required. It is also especially suitable for providing security in cooperative MIMO communications as it performs well even for the specific scenario when the eavesdropper is close to the cluster-head.

8.2 Future Work

For future work, it would be interesting to evaluate these relaying schemes in the presence of interference from external users and from those within the network. In the analysis presented in this thesis we have only considered a single active multi-hop communication link at a time. Also, it would be essential to have a look at the overall network throughput instead of looking at only the link throughput and future work should take into account the effect of error propagation in the DF relaying scheme.

It is important to point out here that we are assuming that new resources such as frequency are considered to be used for each hop. A future analysis that takes into account frequency re-use will yield an even better spectral efficiency. .

We have also not considered the case where resources (frequency bands and time slots) are re-used in the network. This would be an interesting option for future work as well. The analytical expressions derived in the first part of this thesis consider the wireless communication to be affected by Raleigh fading. Another option for future work is to derive these expressions for the case of Rician fading.

Regarding the clustering mechanism presented, an option for the future work could be to run a joint optimization (convex or non-convex) algorithm on all the parameters of the clustering algorithm in order to achieve an optimal performance in terms of life-time as well as quality of service. For the routing mechanism, it would be imperative to look at the overall network throughput as opposed to just a single link throughput. Also an evaluation in the presence of interference from

other nodes and imperfect synchronization conditions should be performed.

For data management in ad-hoc networks, the future work should consider the evaluation of the presented protocols on an implemented testbed as well as comparisons with other DHT approaches, e.g., [ZKJ01] and [WR03], for mobile ad-hoc networks. Furthermore, DHT adaptations for other network underlay configurations could be developed and compared in order to assess the suitability of varying underlay configurations for DHT applications. For future work in the physical layer security domain, we could look at practical methods for generating keys and optimize them for use in cooperative MIMO relaying scenarios.

Appendix A

SONIR - A user's guide

SONIR (Self-Organized Network with Intelligent Relaying) simulator provides an ideal platform for the implementation and testing of various techniques for ad-hoc and cooperative MIMO-based multi-hop relaying networks, in order to see the benefits of these techniques on a system level. We have tested algorithms for a new clustering scheme, a new routing scheme, physical layer security, robust beamforming, as well as a DHT implementation in an ad-hoc scenario. Since it is MATLAB-based and designed for ad-hoc, mobile, and cooperative communication scenarios with a handy GUI and a visualization tool to boot, we have a greater flexibility to simulate new techniques as opposed to the other network simulators. Following is a user's guide for SONIR.

A.1 Initialization

Main folder: \SONIR\
Start program: **main_program.m**
It attaches all the required folders to the main path:
Grafic_folder**PLOT_Folder**,
Grafic_folder**GUI_Folder**,
programms

\programms\Clustering_Folder
\Mat_folder
\Tests
\Tests\Programs
\Demo
and starts the GUI to initialize and generate the environment via: **environmet_gui.m**.

Environment Generation

It generates the GUI to allow all the further steps in the simulator to operate.

Function **\environmet_gui.m** defines the global variables: **Nodes, Trans_Config, Cluster(.plot), Cluster_Connection, Route, stop_mobility, mobility_mode** and builds GUI for the initial data input, Figure A.1.

Initial setup: only **New** button is available which results to the further steps when pressed.

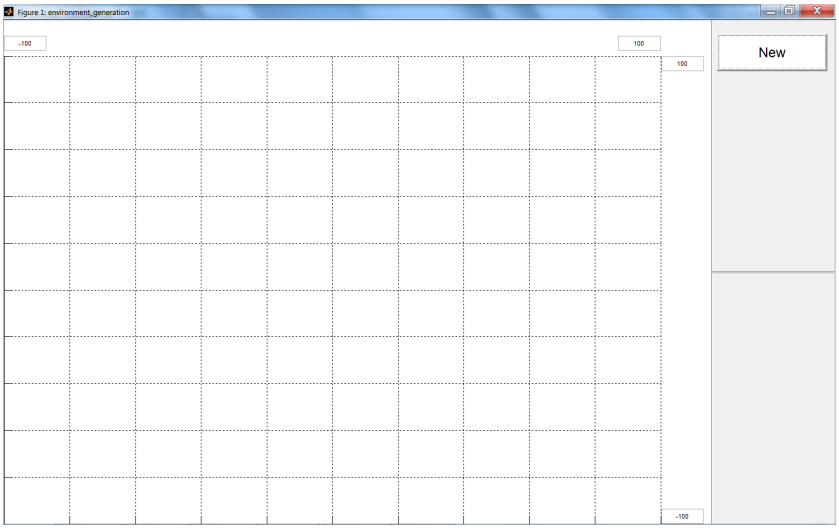

Figure A.1: GUI for initializing the environment.

Node Generation

newNode_Callback(source, eventdata), restarts the program if the global variable **Nodes.Node_plot** is not empty. Otherwise it starts the function **node_func(field, hTransmission, hmobile, hcheck)** and generates the GUI "**Node_dialog_gui**" in order to enable the new nodes to choose from the set of available parameters, Figure A.2. We can define the following points:

Goal:

- Generating the nodes in the environment (GUI), Figure A.2, and illustrating them in the figure. The position of the nodes can be selected based on different distributions, i.e. Uniform and Poisson.

Input:

- The struct 'field' indicates the length and width of the environment.

- 'hTransmission', 'hmobile' and 'hcheck' are used to make these two buttons visible.

Output:

- 'Nodes.N' = number of nodes.

- 'Nodes.Pos', gives the first, second and third rows of this matrix denote the x-, y- and z- coordinate of the nodes. Hence, the size of this matrix is 3 by the number of the nodes. Note that all of the nodes are on the same plane, and the z-coordinate is assumed 0.

- 'Nodes.Node_choose' is 1, if the nodes are selected, and 0, if they are not selected.

- 'Nodes.distribution' = distribution of nodes in the environment.

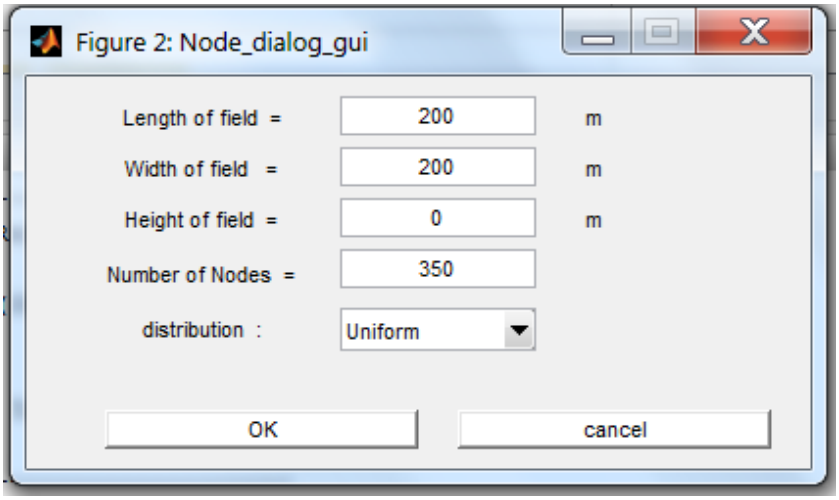

Figure A.2: GUI for nodes' initialization.

Setup of transmit parameters

PackageTransmission_Callback(source, eventdata): if transmission configuration is not assigned (corresp. global variable *Trans_Config.known*) then it starts transmission GUI, as shown in Figure A.3. The corresponding function is **Trans_Config_GUI(Nodes, hTransmission, hvalue, hFreqreuse)**. We can define the following points:

Goal:

- Determining the parameters of transmission SNR, the threshold of maximum distance between users and path loss exponent.

Input:

- 'Nodes', the configuration of nodes.

Output:

- 'Trans_Config.SNRdB', the transmit power / received noise variance at the receive antenna. This parameter is the same for all the nodes. Considering that the noise variance at the receive antennas is 1, then the transmit power is 'Trans_Config.SNRdB'.

- 'Trans_Config.Dist_ref', for computing the received signal power at the receiver, the ratio of the distance between transmitter and receiver and a reference distance is necessary.

- 'Trans_Config.Dist_ref', is a reference distance for evaluating the received power at the destination.

- 'Trans_Config.loss_EXP', Path loss exponent.

Note that the parameters such as sample rate and frequency band for each node can be added later to this program.

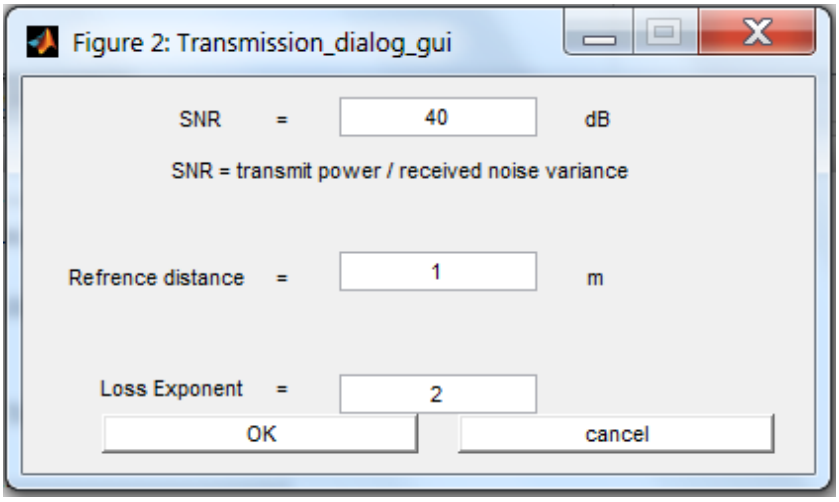

Figure A.3: GUI for initializing the transmission parameters.

When "OK" is pressed, it starts clustering the generated GUI, Fig. A.4. It

happens via the following function:

clustering_gui(hFreqreuse), where we can define the following points:

Goal:

- Determining the parameters of clustering e.g the algorithms of clustering and the threshold.

Input:

- 'Nodes', the configuration of nodes.

Output:

- 'Trans_Config.SNR_th', denotes the minimum value of received SNR. The received SNR for the transmission between cluster-head and one member in the cluster should be larger than or equal to 'Trans_Config.SNR_th'. Note that this threshold is selected based on BPSK modulation.

When "OK" is pressed, the buttons "Freq. Reuse" and "Cluster" are activated.

A.2 Clustering

Clustering_Callback(source, eventdata): if simulation setup is 'Demo' then it plots clusters based on the known configuration, otherwise it starts the function '**reclustering(Cluster,Nodes, figure_numer)**' where:

Goal:

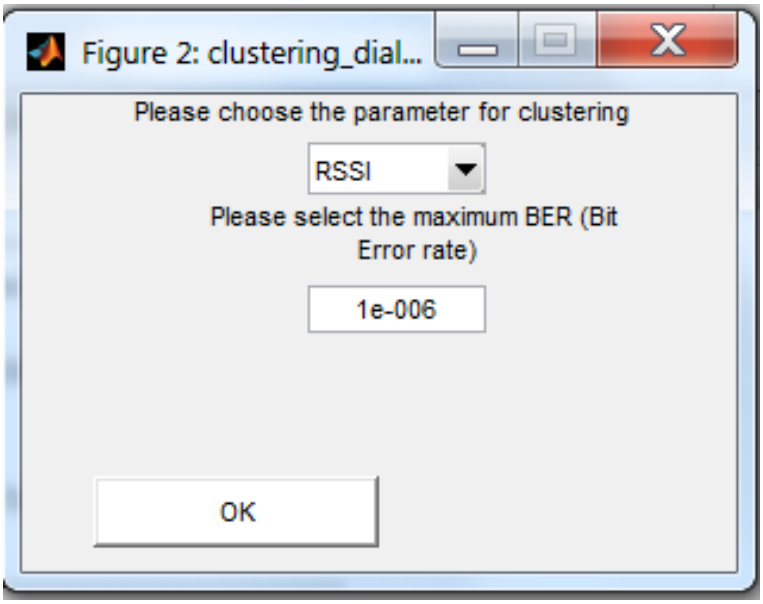

Figure A.4: GUI for initializing the clustering parameters: RSSI or Distance, max BER.

- Clustering the main function and illustrating in the main figure

Input:

- 'Cluster', contains the configuration of Clustering.

- 'Nodes', gives the configuration and positions of nodes.

Output: (Clustering is accomplished)

- 'Cluster.ID', contains the ID of clusters.

- 'Cluster.cl', denotes the members of the cluster. Note that the first element is always cluster-head.

- 'Cluster.cl_head', contains the IDs of cluster-heads.

- 'Cluster.cl_member_busy', indicates which members of the cluster are busy.

- 'Cluster.cl_member_not_busy', indicates which members of the cluster are not busy.

Then, the following functions are performed within the main clustering function (i.e. reclustering.m):

1. **Cluster = Clustering(Con_MTX, Cluster)**.

   Goal:

   - Clustering based on Connection matrix. In reality, each node has to send the candidate package to the adjacent node and they must respond to this package. The base of the clustering is the same, but in order to save much time for running the program, we will not send the package with the assumption that the channel has not changed in the last time slot and we will not achieve different results than before.

   Input:

   - 'Con_MTX' is the Connection matrix. This matrix contains '0's and '1's. The element of the ith row and jth column of this matrix is '1', if the ith node can have a connection with the jth node, otherwise it is '0'. This matrix can be generated based on the 'RSSI' algorithm or the distance between nodes.

   - 'Cluster', is the configuration of Clustering.

   Output: (Clustering is accomplished)

- 'Cluster.ID', contains the ID of the clusters.

- 'Cluster.cl', denotes the members of the cluster. Note that the first element always shows the cluster-heads.

- 'Cluster.cl_head', gives the IDs of the cluster-heads.

- 'Cluster.cl_member_busy', indicates which members of the cluster are busy or not busy.

2. **Cluster = Uniform_Clustering(Cluster,Nodes)**.

   Goal:

   - In the second part of the clustering, the generated clusters will be made more uniform. As the cluster-heads are known, the distance between nodes and cluster-heads is the parameter for this part of clustering.

   Input:

   - 'Cluster', gives the configuration of Clustering.

   - 'Nodes', contains the configuration of Nodes.

3. **Cluster = Cluster_Plot(Cluster,Nodes,figure_numer)**.

   Goal:

   - Illustration of the clusters, Fig. A.5.

Input:

- 'Cluster', gives the configuration of the Clustering and the cluster members.

After the end of clustering the "Busy" and "Routing" buttons are enabled.

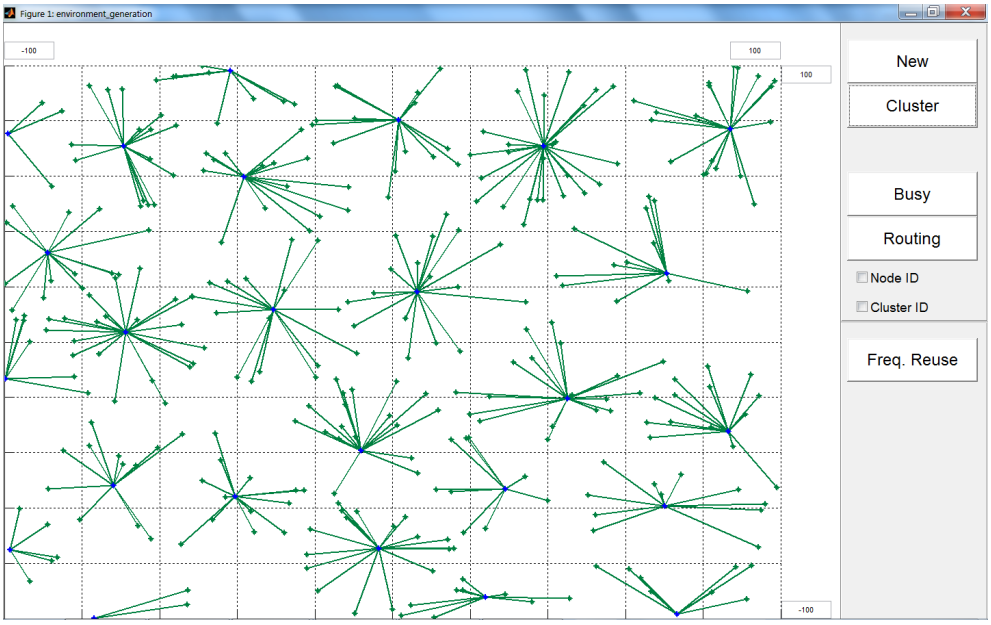

Figure A.5: GUI for initializing the transmission parameters (output).

A.3 Routing

Routing_Callback(source, eventdata), if the input is empty, then the routing is made invisible, otherwise it starts the GUI, Fig. A.6. the following functions are needed for routing:

routing_GUI(Nodes, Cluster, Trans_Config, figure_numer, hmobile, hTrans, hAMC)

Goal:

- Selecting a source (TX) and destination (RX), the number of transmit and receive nodes in each intermediate cluster (number of transmit and receive antennas in cooperative MIMO route.

- Finding an appropriate route between TX and RX.

- Drawing the route on the main figure.

Output1:

- Struct **Route**, in which:

'Route.sender_node', shows the source node

'Route.receiver_node', shows the destination node

'Route.dis_ref', shows the reference distance ('Trans_Config.Dist_ref')

'Route.BERth', shows the BER of every hop should be larger than this threshold

'Route.BERth_total', shows the BER at the destination should be larger than this threshold

'Route.N_sender', shows the number of transmit antennas for every hop

'Route.N_receiver', shows the number of receive antennas for every hop

'Route.SISO', shows the the route for SISO link between clusters

'Route.SISO.plot', shows the used to refer the plot of SISO route

'Route.SISO.route_cluster', shows the list of the clusters from source to destination based on the SISO route

'Route.SISO.route_node', shows the list of the nodes from source to destination based on the SISO route

'Route.MIMO', shows the the same struct as Route.SISO but for the MIMO route

'Route.MIMO_SISO', shows the the same struct as Route.SISO. The route is the same as SISO route. That means, the same intermediate clusters are used in this case, but the links between clusters are MIMO based

Output2 :

- struct **Cluster_Connection**, in which:

'Cluster_Connection.Node_ID_sender(ii,jj)' = [a1, a2, ..., aL] [a1, a2, ..., aL], is an N_sender by 1 row vector. The entities of this vector are the nodes belonging to the cluster ii, which can be used as the elements of the virtual antenna array at the transmit cluster ii to receive cluster jj.

'Cluster_Connection.Node_ID_sender_SISO(ii,jj)', shows the best possible node in the cluster ii which can be used for transmission to the cluster jj.

'Cluster_Connection.MIMO_distance_MTX(ii,jj)', is an N_sender by N_receiver matrix. The elements of this matrix give the distances between all the nodes in the cluster ii and cluster jj which are used in the transmission between these two clusters.

'Cluster_Connection.MIMO_distance_average(ii,jj)', shows the average of the elements of the matrix Cluster_Connection.MIMO_distance_MTX(ii,jj).

'Cluster_Connection.SISO_distance(ii,jj)', denotes the SISO distance between cluster ii and jj.

Note that cluster ii uses its nodes.

'Cluster_Connection.Node_ID_sender(ii,jj)', generates a transmission to the nodes 'Cluster_Connection.Node_ID_sender(jj,ii)' in cluster jj. And the distance between all the pairs of transmit and receive nodes are in the matrix 'Cluster_Connection.MIMO_distance_MTX(ii,jj)' and
'Cluster_Connection.MIMO_distance_MTX(jj,ii)'.

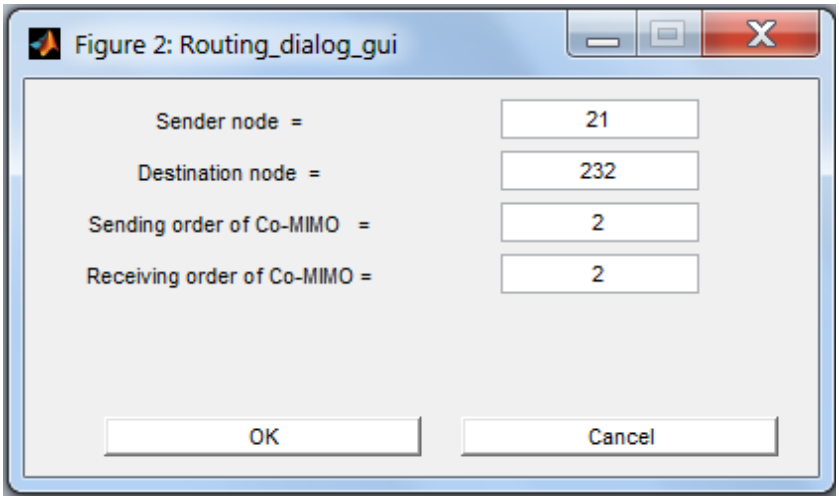

Figure A.6: GUI to setup the routing between two nodes over SISO, MIMO and MIMO based on SISO.

Then if routing is performed for the first time, (it is defined if variable *nn* = 1), then variable *nn* is changed from 1 to 2 and the procedure of finding the adjacent clusters and finding the intermediate nodes for intracluster transmission is executed over the function:

Cluster_Connection = Cluster_communication(Nodes, Cluster, Trans_Config, N_sender, N_receiver), for which:

Goal:

- Finding the adjacent clusters for MIMO and SISO case base on the number of transmit and receive antennas. Note: This struct is found for MIMO based on the selected number of transmit antennas and receive antennas (N_sender, N_receiver).

Input:

- Selfdescribing.

Output:

- 'Cluster_Connection'

- 'Cluster_Connection.Node_ID_sender(ii,jj)' = [a1, a2, ..., aL] [a1, a2, ..., aL], is an N_sender by 1 row vector. The entities of this vector are the nodes belonging to the cluster ii, which can be used as the elements of the virtual antenna array at the transmit cluster ii to receive cluster jj.

- 'Cluster_Connection.Node_ID_sender_SISO(ii,jj)', shows the best possible nodes in the cluster ii which can be used for transmission to cluster jj.

- 'Cluster_Connection.MIMO_distance_MTX(ii,jj)', is an N_sender by N_receiver matrix. The elements of this matrix are the distances between all the nodes in cluster ii and cluster jj which are used for transmission between these two clusters.

- 'Cluster_Connection.MIMO_distance_average(ii,jj)', gives the average of the elements of the matrix 'Cluster_Connection.MIMO_distance_MTXii,jj'.

- 'Cluster_Connection.SISO_distance(ii,jj)', shows the SISO distance between cluster ii and jj.

Note that cluster ii uses its nodes.

- 'Cluster_Connection.Node_ID_sender(ii,jj)', is employed for generating a transmission to the nodes 'Cluster_Connection.Node_ID_sender(jj,ii)' in cluster jj. And the distance between all the pairs of transmit and receive nodes are in the matrix 'Cluster_Connection.MIMO_distance_MTX(ii,jj)' and 'Cluster_Connection.MIMO_distance_MTX(jj,ii)'.

When variable $nn = 2$, then routing performed directly for BPSK or SISO, or MIMO, or MIMO based on SISO function:

Route = routing(Cluster_Connection, Nodes, Cluster, Route, figure_numer), where:

Goal:

- Finding the route between two nodes

Input:

- 'Cluster_Connection', is the matrix of connection between the clusters

It uses the following functions:

1. For BER estimation in SISO or MIMO, **BER_estimation(Eb_N0_dB, XIXO, N_tx, M_rx, Cluster_Connection)**, estimate the BER based on simulation. Simulation can be found in: 'Tests\SISO-MIMO-Comp\BPSK sim\BPSK_test.m'. The result of this simulation is compared with another result found in internet. The web page is saved in: 'references\Alamouti\Alamouti' STBC with 2 receive antenna.

   Input:

Eb_N0_dB, XIXO (can be SISO, MISO, MIMO)

Note that in the MISO and MIMO cases the result is based on Alamouti scheme.

2. **route = routing_cluster(Cluster_Connection, TX_CL, RX_CL, BER_RX)**.

Goal:

- Finding the route between two clusters.

Input:

- 'Cluster_Connection', is the matrix of the connection between the clusters.

- 'TX_CL', is the sender cluster.

- 'RX_CL', is the receiver cluster.

Then the routes for SISO, MIMO and MIMO based on SISO are plotted, Fig. A.7.

A.4 Frequency reuse

Frequency_Callback(source, eventdata) is activated, when "Freq" button is pressed. It starts the GUI for frequency configuration:

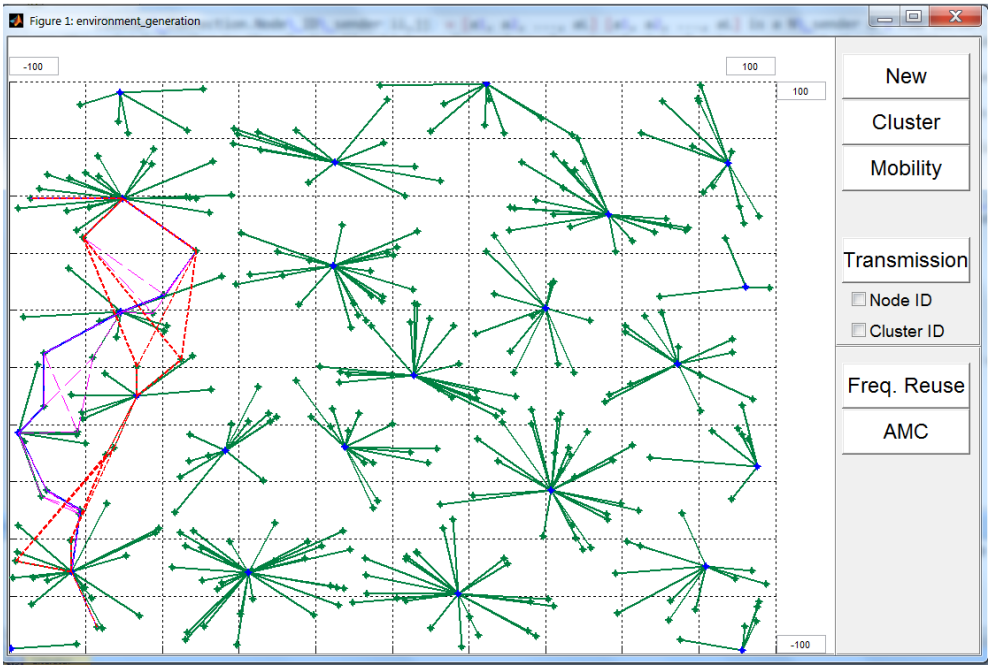

Figure A.7: The routing between two nodes over SISO, MIMO and MIMO based on SISO.

Freq_Config_GUI(Nodes, Route, Trans_Config, Cluster_Connection): the function allows to choose number of the subchannels, number of interfering nodes, and number of the Monte-Carlo runs. When 'OK' is pressed, the function of frequency reuse is being executed:

1. **Frequency_reuse(Nodes, Route, Trans_Config, number_sub_channels, N_busy, N_monte_carlo, Cluster_Connection)**.

   Goal:

   - Estimation of freq. reuse for SISO, MIMO and MIMO based on SISO over the total number of Monte-Calro runs. The nodes which are busy with other transmission are interferers and are not desired. Then, based on this, the desired frequency is estimated and the BER versus SNR, in Fig. A.8, and curves and throughput versus SNR, in Fig. A.9, for SISO, Co-MIMO and Co-MIMO based on SISO with and without interference are plotted.

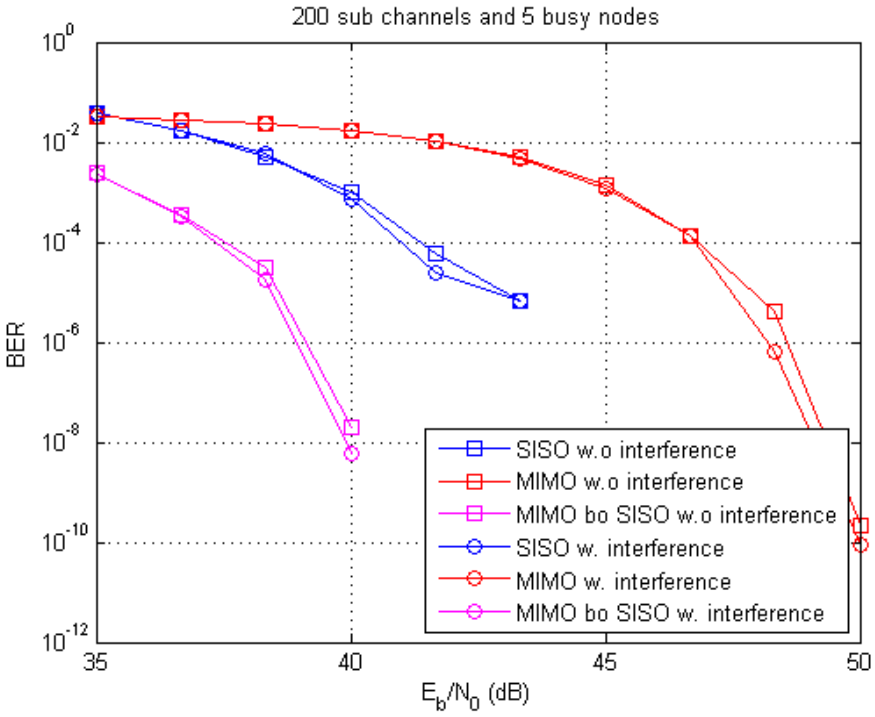

Figure A.8: BER vs. SNR with interfering nodes.

Busy Nodes

When button 'Busy' is available and pressed the function **Busy_Callback(source, eventdata)** activates the GUI, Fig. A.10, to make some nodes busy, due to interference or other reasons:

BUSY_NODE_GUI(figure_numer)

Goal:

- Selecting some nodes which are busy. These busy nodes cannot be used in other transmissions. Therefore, the routing algorithm does not consider these nodes.

- Illustrating the busy nodes as red circles in the main figure.

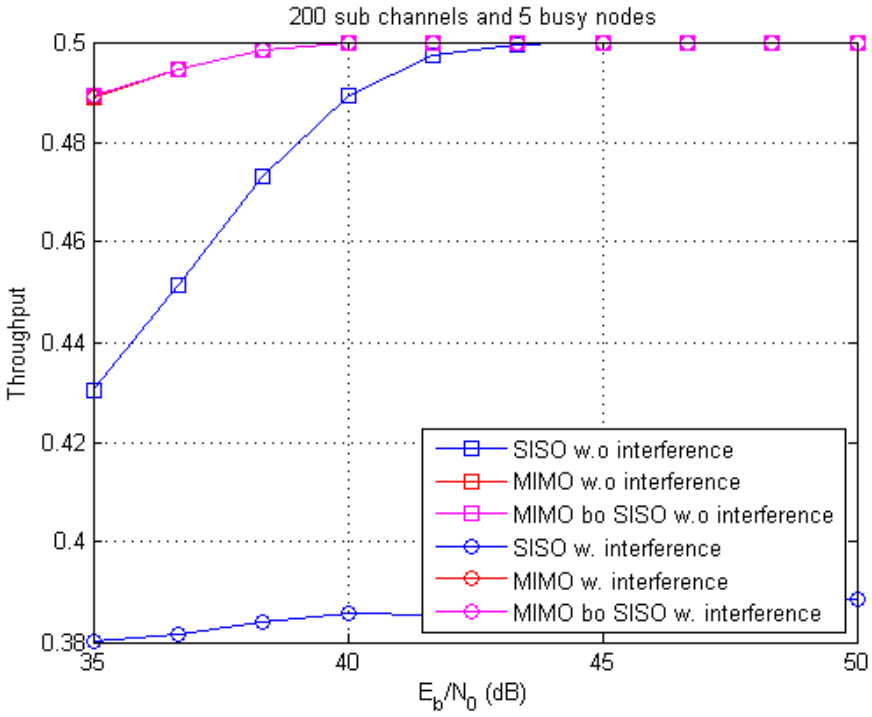

Figure A.9: Throughput vs. SNR with interfering nodes.

Output:

- 'Cluster.cl_member_busy', contains the IDs of the busy nodes. For example: Cluster.cl_member_busyi is the list of the node IDs belonging to the cluster I, which are busy.

- 'Cluster.cl_member_not_busyi', are the list of the node IDs belonging to the cluster i which are not busy.

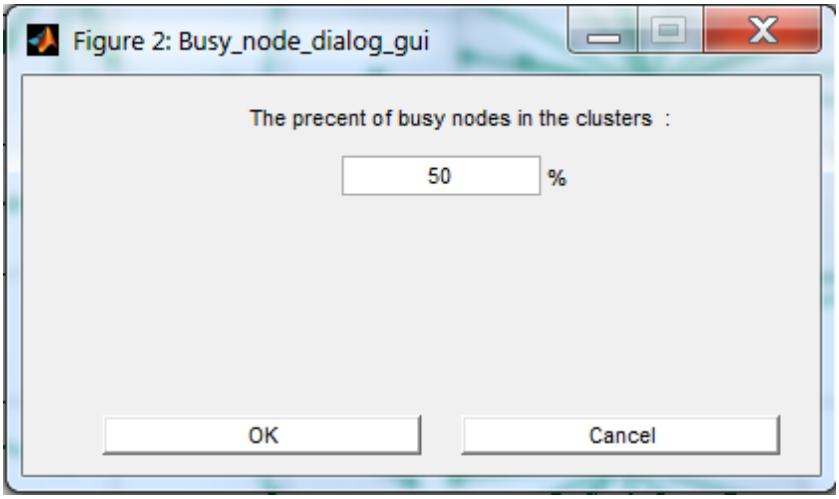

Figure A.10: GUI to set some nodes busy.

A.5 MIMO map

When the button 'MIMO map' is pressed, the function **Mimo_map_Callback(source, eventdata)** generates the MIMO map GUI function which asks about the transmitting cluster and Eb/No, to show the number of the parallel MIMO transmissions needed to reach each node, Fig. A.11. A MIMO map function is as follows:

MIMO_map_gui(Nodes, Cluster, Trans_Config, Route)

Goal:

- Generating a map of adjacent clusters based on the number of transmit and receive antennas.

After Ok is pressed, the following functions are performed:

1. The loop **'while'** starts calculating the required number of MIMO antennas starting from '1' till all clusters are connected. Each time it estimates cluster connections over the function:

   Cluster_Connection = Cluster_communication(Nodes, Cluster, Trans_Config, N_sender, N_receiver).

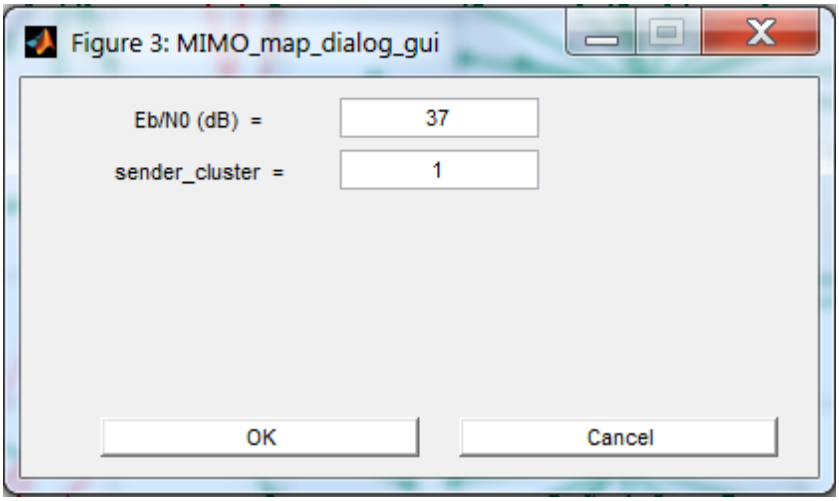

Figure A.11: GUI to set some nodes busy (part 2).

Goal:

- Finding the adjacent clusters for MIMO and SISO case, based on the number of transmit and receive antennas.

This function also includes a function which selects the 'best' combination of cluster connections, based on the defined parameter:

- [**Row_combination, Column_combination**] = **select_best_combination(A, M, N)** – selects optimal combination over the columns and rows for all the possible combinations.

2. Also, the function of BER estimation is performed for each iteration of the loop 'while':

   BER_est = BER_estimation(Eb_N0_dB, XIXO, N_tx, M_rx, Cluster_Connection)

Then it plots the resulting layout, Fig. A.12.

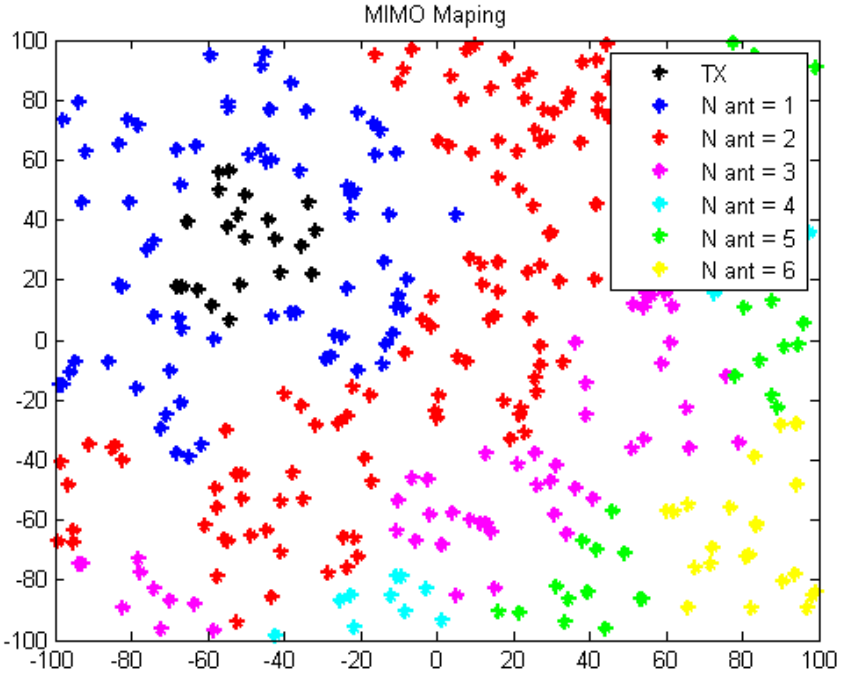

Figure A.12: Resulting MIMO map.

A.6 Adaptive Modulation and Coding

When 'AMC' button is activated and pressed, then, the function **AMC_Callback(source, eventdata)** activates a function which calculates the required modulation and coding schemes depending on SNR:

AMC(Route, Nodes, Trans_Config) starts from the assumption that the weakest link provides lowest BER ('weakest') and then calculates the modulation and channel coding for the worst link from the data found in function:

[Mode, a_n, b_n] = choose_AMC(SNR_dB_i).

One of the possible transmission modes i.e. 'BPSK', 'QPSK', '16QAM' or '64QAM' is selected depending on the received SNR level. Then, the same calculation is performed for all the possible links. After calculation of all the possible links, the Figure A.13 is plotted. This figure shows the BER curve, which is based on the link to the higher layer, and changes when the optimal AMC scheme is changed. The peaks denote the points when AMC scheme is changed.

At the same time, the change of AMC scheme leads to the change of the throughput of the link, which is shown in the Fig. A.14 – higher SNR leads to the higher throughput but the change happens stepwise depending on a selected AMC scheme.

A.7 Mobility of nodes

When 'Mobility' button is activated and pressed, and the mobility mode corresponds to '1', then the function **MobileNode_Callback(source, eventdata)** activates GUI, Fig. A.15, to define the mobility of the nodes over the following function:

Mobility_GUI(figure_numer, Nodes, hcheck3) allows to choose the 'speed', (relative change of nodes' position), while the direction is defined in a random way.

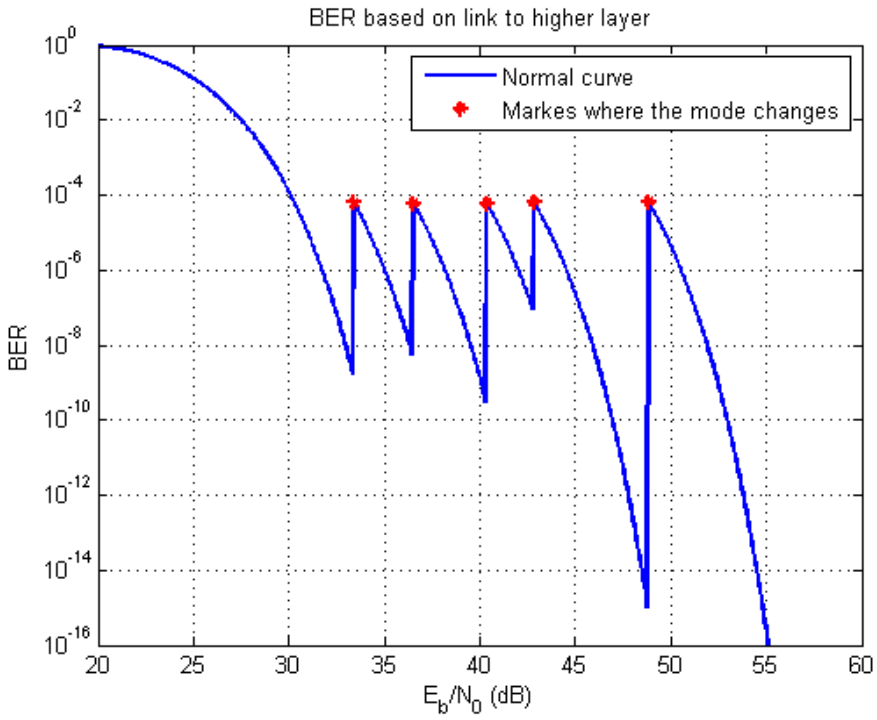

Figure A.13: Change of BER based on chosen AMC scheme versus SNR.

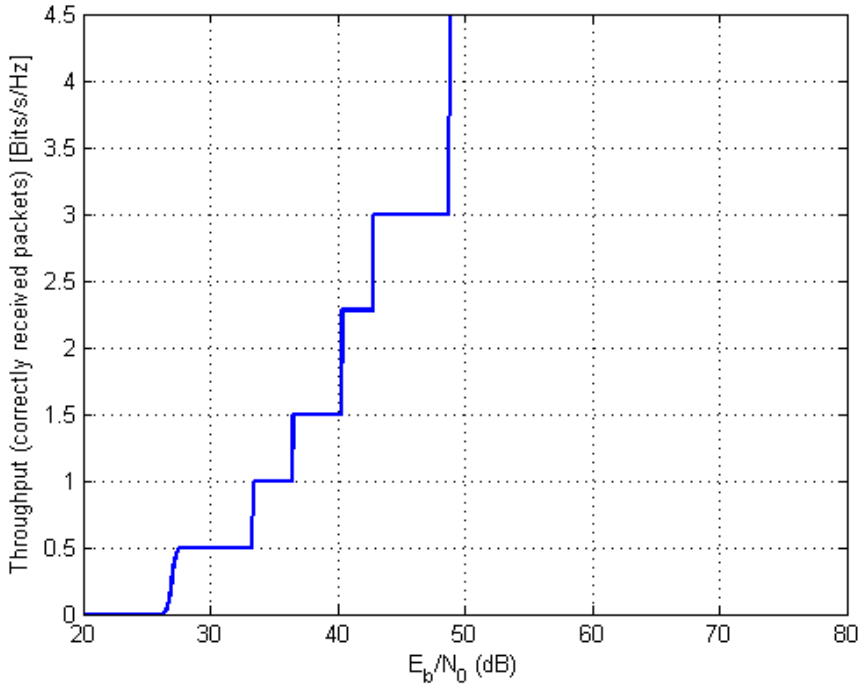

Figure A.14: Change of throughput (correctly received packets) based on chosen AMC scheme versus SNR.

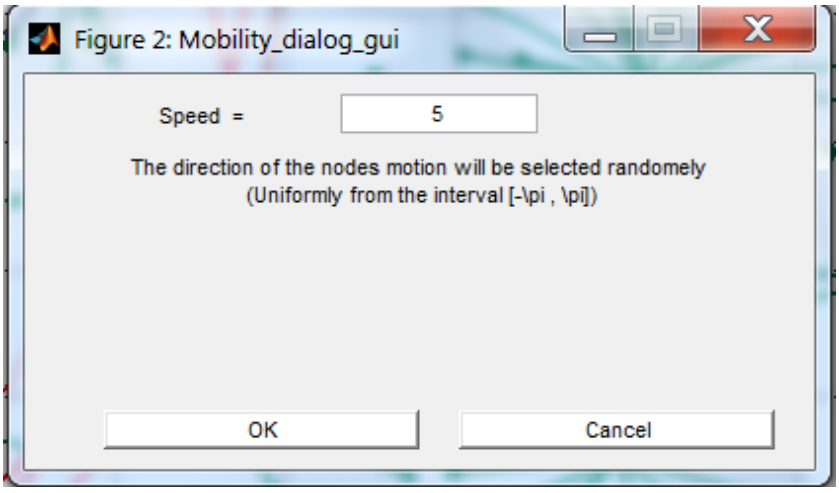

Figure A.15: GUI to setup the mobility of nodes.

When mobility is activated, then, after each change of the nodes' position, the retransmission of the data from the chosen transmitter to the chosen receiver is performed over SISO, MIMO and MIMO based on SISO and depicts on the main Figure, A.7, the corresponding function:

mobility(V, phase, figure_numer, hcheck3) starts a loop *'while'* as long as variable *stop_mobility* is '1' and inside of the loop starts all the functions needed for the data transmission:

1. **Cluster = Cluster_Plot(Cluster, Nodes, figure_numer)** to plot the changed clusters.

2. **Route = plot_route(Route, Nodes, figure_numer, mode)** to find a new route for SISO, MIMO and MIMO based on SISO.

3. Checks the maximum possible distance of the nodes to the corresponding cluster-heads, and if it is larger as maximum allowed distance, then the new clusters are being estimated over the function:

   Cluster = reclustering(Cluster, Nodes, figure_numer) and **Cluster_Connection = Cluster_communication(Nodes, Cluster, Trans_Config, N_sender, N_receiver)**

   After the new clusters are established, the function **Route = routing(Cluster_Connection, Nodes, Cluster, Route, figure_numer)** is executed to calculate the new routes between the transmitter and receiver nodes.

The process lasts as long as the checkbox 'Stop mobility', function: **mobility_stop_Callback(source, eventdata)**, is not checked and variable stop_mobility is not set to '0'.

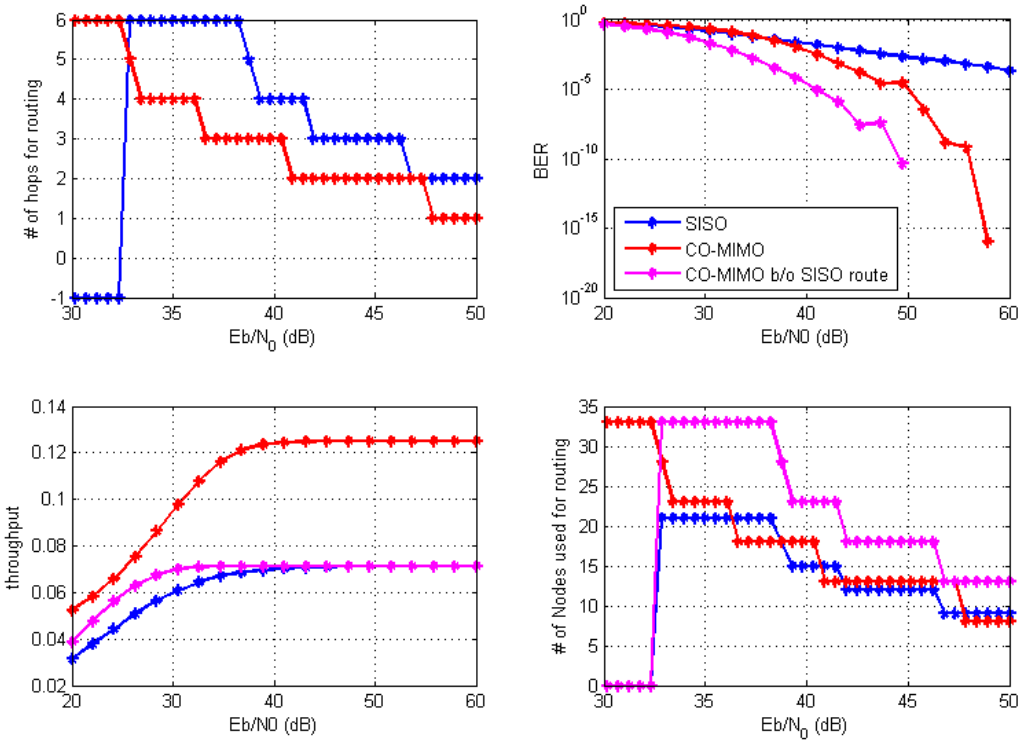

Figure A.16: Final plots of transmission simulation over different values of SNR.

A.8 Transmission

When 'Transmission' button is activated and pressed, then the function **Trans_Callback(source, evendata)** activates the process of estimating the transmission parameters for SISO, MIMO, and MIMO, based on SISO:

Transmission(Route, Cluster_Connection, Eb_N0dB) estimates the BER for all three types of transmission (SISO, MIMO, MIMO b/o SISO). Function **BER_est = BER_estimation(Eb_N0_dB, XIXO, N_tx, M_rx, Cluster_Connection)** estimates the number of hops, received bits (throughput), and number of nodes used for routing over different levels of SNR. Then it plots results of all the simulations, Fig. A.16.

Appendix B

List of Acronyms

Acronyms:

AF ..... Amplify and Forward relaying
AMC ..... Adaptive Modulation and Coding
AOCMR ..... Ad-hoc On-demand Cooperative MIMO Routing
AODV ..... Ad-hoc On-Demand Distance Vector
AWGN ..... Additive Wide Gaussian Noise
BER ..... Bit Error Rate
BPSK ..... Binary Phase-Shift Keying
CAN ..... Content Addressable Network
C-DHash ..... Cluster Aware Distributed Hash
CDMA ..... Code Division Multiple Access
CH ..... Cluster-Heads
C-RBFM ..... Cluster-aware Resource Based Finger Management
CSI ..... Channel State Information
CSMA-MAC ..... Carrier Sense Multiple Access-Media Access Control
DF ..... Decode and Forward relaying
DHT ..... Distributed Hash Table
DSDV ..... Destination-Sequenced Distance-Vector Routing
DYMO ..... Dynamic MANET On-demand
E-RSSI ..... Enhanced Received Signal Strength Indicator

FDMA ..... Frequency Division Multiple Access
GPS ..... Global Positioning System
GS-Mobicom ..... Graduate School on Mobile Communications
GUI ..... Graphical User Interface
HEED ..... Hybrid Energy-Efficient Distributed
HSR ..... Hierarchical State Routing
ISI ..... Inter Symbol Interference
LEACH ..... Low Energy Adaptive Clustering Hierarchy
LTE ..... Long Term Evolution
M2M ..... Machine to Machine
MANET ..... Mobile Ad-hoc Network
MIMO ..... Multiple Input Multiple Output
MRC ..... Maximal Ratio Combining
PDF ..... Probability Density Function
PRS ..... Proximity-aware Route Selection
QoS ..... Quality of Service
RBFM ..... Resource Based Finger Management
RCKG ..... Reciprocal Channel Key Generation
RSSI ..... Received Signal Strength Indicator
RX ..... Receiver
SER ..... Symbol Error Rate
SIMO ..... Single Input Multiple Output
SINR ..... Signal to Interference and Noise Ratio
SISO ..... Single Input Single Output
SNR ..... Signal to Noise Ratio
SONIR ..... Self-Organizing Network with Intelligent Relaying
STBC ..... Space-Time Block Coding
TDD ..... Time-Division Duplex
TDMA ..... Time Division Multiple Access
TX ..... Transmitter
ULA ..... Uniform Linear Array
VAA ..... Virtual Antenna Array
VANET ..... Vehicular Ad-Hoc Network

WiMAX ..... Worldwide Interoperability for Microwave Access
ZMCSCG ..... Zero Mean Circularly Symmetric Complex Gaussian

Appendix C

List of frequently used symbols and operators

Frequently used symbols:

M ..... Number of hops
$\hat{M}$ ..... Maximum number of hops possible
M_r ..... Number of the receive antennas
M_t ..... Number of the transmit antennas
β ..... Maximum norm of the accuracy vector or matrix
α ..... Path loss exponent
$\boldsymbol{I}_k$ ..... The $k \times k$ identitiy matrix
P_s ..... The transmit power of the nodes
x_{i-1} ..... The signal transmitted by the $(i-1)$th relay
ξ_1 ..... The path gain corresponding to the direct channel
$\boldsymbol{I}$ ..... The mutual information
ξ_M ..... The path gain of the channels, using M relay nodes
$\boldsymbol{H}$ ..... The channel matrix
$\boldsymbol{E}$ ..... The inaccuracy matrix
$\boldsymbol{N}$ ..... The noise matrix
h_i ..... The SISO quasi static frequency at block fading channel

ϵ_i ..... The corresponding inaccuracy vector of h_i
α ..... The path loss exponent
P_{noise} ..... The power of the received noise at the destination
P_{sig} ..... The signal component's power
R ..... Rate of the STBC
T ..... Number of the time slots
ν_i ..... The Additive white Gaussian noise (AWGN) for the i_th relay
A_i ..... The amplification gain of the ith relay node
$y_r x$ ..... Received signal at the destination
x ..... The transmitted signal by the source
C_{AF} ..... The capacity of the multi-hop AF transmission
C_{DF} ..... The capacity of the multi-hop DF transmission
$\overline{N}_e$ ..... The number of nearest neighbors
$d_{\min}$ ..... The minimum Euclidean distance of underlying constellation
$\frac{N_0}{2}$ ..... The noise power spectral density
$\breve{h}$ ..... The normalized SISO channel
λ_i ..... The i_th eigenvalue
$\boldsymbol{y}$ ..... The received signal vector
$\boldsymbol{Y}$ ..... The received signal
$\boldsymbol{\nu}$ ..... The ZMCSCG noise
η ..... The received SNR
τ ..... Delay of the channel
f_c ..... The carrier frequency
P_r ..... The received signal power
P_i ..... The interference power
P_n ..... The noise power
P ..... Desired percentage of cluster heads
r ..... Current round
G ..... Set of the nodes which have not been cluster-heads in this cycle
P_{fact} ..... Promotion factor
n ..... Number of responses received
RSSI_i ..... ith strongest received signal strength from a responding node
E ..... Energy

N_{path} ..... Number of non-line-of-sight paths
R_i ..... The relative secure information of the generated key in the ith level
$\boldsymbol{g}$ ..... The linear finger maintenance function
$\boldsymbol{t}_{\text{ref}}$ ..... The reference interval of the finger maintenance

Notations and operators:

a, b, c ..... Scalars
$\boldsymbol{a}$, $\boldsymbol{b}$, $\boldsymbol{c}$ ..... Column vectors
$\boldsymbol{A}$, $\boldsymbol{B}$, $\boldsymbol{C}$ ..... Matrices
a^* ..... Complex conjugate of the complex number a
$\boldsymbol{A^T}$ ..... Transpose of the matrix $\boldsymbol{A}$
$\boldsymbol{A^H}$ ..... Hermitian transpose of the matrix $\boldsymbol{A}$
Re{a} ..... Real part of the complex number a
Im{a} ..... Imaginary part of the complex number a
$\mathbb{E}\{\boldsymbol{a}\}$ ..... Expected value of the random vector $\boldsymbol{a}$
$\|\text{A}\|_F$ ..... The Frobenius norm of the matrix $\boldsymbol{A}$
tr$\{A\}$ ..... The trace of the matrix $\boldsymbol{A}$
$|a|$ ..... The magnitude of the complex number a

References

[17006] "IEEE Standard for Information technology– Local and metropolitan area networks– Specific requirements– Part 15.4: Wireless Medium Access Control (MAC) and Physical Layer (PHY) Specifications for Low Rate Wireless Personal Area Networks (WPANs)," *IEEE Std 802.15.4-2006 (Revision of IEEE Std 802.15.4-2003)*, pp. 1–320, 2006. 4, 87, 89

[AKK04] J. N. AL-Karaki and A. E. Kamal, "Routing techniques in wireless sensor networks: A survey," *IEEE Wireless Communications*, vol. 11, no. 6, pp. 6–28, Dec. 2004. 5

[Ala98] S. M. Alamouti, "A simple transmit diversity technique for wireless communications," *IEEE Journal on Selected Areas in Communications*, pp. 1451–1458, 1998. 50

[AP01] B. An and S. Papavassiliou, "A mobility- based clustering approach to support mobility management and multicast routing in mobile ad-hoc wireless networks," *CISS2001, Johns Hopkins, Baltimore*, 2001. 10, 88

[AR10] D. G. Aizat Ramli, "RF signal strength based clustering protocols for a self-organizing cognitive radio network," *7th International Symposium on Wireless Communication Systems (ISWCS)*, pp. 228–232, 2010. 91

[BBB09] M. Bouhorma, H. Bentaouit, and A. Boudhir, "Performance comparison of ad-hoc routing protocols AODV and DSR," *International*

Conference on Multimedia Computing and Systems, 2009. ICMCS '09., pp. 511 – 514, September 2009. 127, 134

[BBRM08] M. Bloch, J. Barros, M. R. D. Rodrigues, and S. McLaughlin, "Wireless information-theoretic security," *IEEE Transactions on Information Theory*, vol. 54, no. 6, pp. 2515–2534, 2008. 12, 142

[BLM03] J. R. Barry, E. A. Lee, and D. G. Messershcmitt, *Digital Communication*. Kluwer Academic Publishers, Third Edition, 2003. 82

[CDS07] P. Cornel, R. Doss, and W. Schott, "Geographic routing with cooperative relaying and leapfrogging in wireless sensor networks," in *IEEE GLOBECOM 2007*, IBM Research GmbH, Zurich Research Laboratory (ZRL), Zurich, Switzerland, November 2007, pp. 646 – 651. 128

[CE79] T. M. Cover and A. El Gamal, "Capacity theorems for relay channels," *IEEE Trans. Inform. Theory*, vol. 25, no. 5, pp. 572–584, Sept. 1979. 21, 33

[CGB04] S. Cui, A. J. Goldsmith, and A. Bahai, "Energy-efficiency of MIMO and cooperative MIMO techniques in sensor networks," *IEEE Journal on Selected Areas in Communications*, vol. 22, no. 6, pp. 1089–1098, August 2004. 8, 42, 61

[CH03] Y. Chang and Y. Hua, "Application of space time linear block codes to parallel wireless relays in mobile ad hoc networks," *in the 36th Asilomar Conf. on Signals, Systems and Computers*, Nov. 2003. 8, 42, 61

[Doh03] M. Dohler, "Virtual antenna arrays," Ph.D. dissertation, Kings College London, University of London, 2003.

[DPS11] E. Dahlman, S. Parkvall, and J. Skold, *4G: LTE/LTE-Advanced for Mobile Broadband*, 1st ed. Academic Press, 2011. 12, 142

[EDPK09] M. El Dick, E. Pacitti, and B. Kemme, "Flower-cdn: A hybrid p2p overlay for efficient query processing in cdn," in *EDBT '09*, 2009, pp. 427–438.

[EMZ06] A. El Gamal, M. Mohseni, and S. Zahedi, "Bounds on capacity and minimum energy-per-bit for AWGN relay channels," *IEEE Trans. Inform. Theory*, vol. 52, no. 4, pp. 1545–1561, Apr. 2006.

[ESWI02] C. Eklund, K. L. Stanwood, S. Wang, and E. C. Inc, "Ieee standard 802.16: A technical overview of the wirelessman air interface for broadband wireless access," *IEEE Communications Magazine*, vol. 40, pp. 98–107, 2002.

[EZ05] A. El Gamal and S. Zahedi, "Capacity of a class of relay channels with orthogonal components," *IEEE Trans. Inform. Theory*, vol. 51, no. 5, pp. 1815–1817, May 2005. 21

[FB08] G. Farhadi and N. C. Beaulieu, "On the performance of amplify-andforward cooperative links with fixed gain relays," *IEEE Trans. Wireless Commun.*, vol. 7, no. 5, pp. 1851–1856, May. 2008. 6, 21

[FPL09] S. Fazackerley, A. Paeth, and R. Lawrence, "Cluster head selection using RF signal strength," in *Proc. Canadian Conference on Electrical and Computer Engineering. CCECE*, 2009, pp. 334–338. 10, 88, 89, 91, 99

[GGG+03] K. Gummadi, R. Gummadi, S. Gribble, S. Ratnasamy, S. Shenker, and I. Stoica, "The impact of DHT routing geometry on resilience and proximity," in *SIGCOMM '03*, 2003, pp. 381–394. 127

[Ghe12] S. Gherekhloo, "Robust distributed communication techniques," Master's thesis, Ilmenau Univeristy of Technology, Germany, 2012. 22, 42, 60, 62, 87

[Gol05] A. Goldsmith, *Wireless Communications*. New York, NY, USA: Cambridge University Press, 2005. 45

[GZH12] M. T. Garrosi, B. Zafar, and M. Haardt, "Prolonged ad-hoc network life-time using a distributed clustering scheme based on RF signal strength," in *IEEE International Conference on Communications (ICC 2012), 4th Workshop on Cooperative and Cognitive Communications (CoCoNet 4)*, Ottawa, Canada, 06 2012. 87, 88

[HA03] M. O. Hasna and M. S. Alouini, "End-to-end performance of transmission systems with relays over rayleigh fading channels," *IEEE Trans. Wireless Commun.*, vol. 2, no. 6, pp. 1126–1131, Nov. 2003. 6, 21

[Haa] M. Haardt, "rapporteur, future mobile and wireless radio systems: challenges in european research," *Report on the FP 7 Consultation Meeting, European Commission, Information Society and Media, Brussels, Belgium, Feb. 2008*. 105

[HCB00] W. R. Heinzelman, A. Chandrakasan, and H. Balakrishnan, "Energy-efficient communication protocol for wireless microsensor networks," *Proceedings of the 33rd Annual Hawaii International Conference on System Sciences*, p. 10, 2000. 4, 10, 88, 89, 90, 91, 99, 109

[HCB02] W. Heinzelman, A. Chandrakasan, and H. Balakrishnan, "An application-specific protocol architecture for wireless microsensor networks," *IEEE Transactions on Wireless Communications*, pp. 660–670, 2002. 99, 100

[HDP03] Y. C. Hu, S. M. Das, and H. Pucha, "Exploiting the synergy between peer-to-peer and mobile ad hoc networks," in *In Proceedings of HotOS-IX: Ninth Workshop on Hot Topics in Operating Systems*, Lihue, Kauai, HI, May 2003, pp. 37–42. 123

[HHY95] J. Hershey, A. Hassan, and R. Yarlagadda, "Unconventional cryptographic keying variable management," *Communications, IEEE Transactions on*, vol. 43, no. 1, pp. 3–6, 1995. 12, 142

[HMZ05] A. Host-Madsen and J. Zhang, "Capacity bounds and power allocation for wireless relay channels," *IEEE Trans. Inform. Theory*, vol. 51, no. 6, pp. 2020–2040, June 2005. 7, 21

[HNSGL08] V. Havary-Nassab, S. Shahbazpanahi, A. Grami, and Z.-Q. Luo, "Distributed beamforming for relay networks based on second-order statistics of the channel state information," *IEEE Trans. Signal Processing*, vol. 56, no. 9, pp. 4306 –4316, Sept. 2008.

[HTR03] A. Hottinen, O. Trikkonen, and R.Wichman, "Multi-antenna transciever techniques for 3G and beyond," *John Wiley*, 2003. 8, 42

[IEE97] *Wireless LAN Medium Access Control (MAC) and Physical Layer (PHY) Specification*, IEEE Std. 802.11, 1997. 12, 142

[Jaf05] H. Jafarkhani, "Space time coding: Theory and practice," *Cambridge Academic Press*, 2005. 8, 42

[JH06] Y. Jing and B. Hassibi, "Distributed space-time coding in wireless relay networks," *IEEE Transactions on Wireless Communiction*, pp. 3524–3536, 2006. 9

[JHHN04] M. Janani, A. Hedayat, T. E. Hunter, and A. Nosratinia, "Coded cooperation in wireless communications: Space time transmission and iterative decoding," *IEEE Trans. Signal Process.*, vol. 52, pp. 362–371, Feb. 2004. 6, 21

[JJ09] Y. Jing and H. Jafarkhani, "Network beamforming using relays with perfect channel information," *IEEE Trans. Information Theory*, vol. 55, no. 6, pp. 2499 –2517, June 2009.

[KAKH09] T. Kojima, M. Asahara, K. Kono, and A. Hayakawa, "Embedding network coordinates into the heart of distributed hash tables," in *P2P '09 IEEE Ninth International Conference on Peer-to-Peer Computing*, Dept. of Inf. and Comput. Sci., Keio Univ., Yokohama, Japan, September 2009, pp. 155 – 158. 11, 125, 127, 130

[KGG05] G. Kramer, M. Gastpar, and P. Gupta, "Cooperative strategies and capacity theorem for relay networks," *IEEE Trans. Inf. Theory*, vol. 51, pp. 3037–3063, Sep. 2005. 6, 21

[KS07] N. Khajehnouri and A. H. Sayed, "Distributed mmse relay strategies for wireless sensor networks," *Signal Processing, IEEE Transactions on*, vol. 55, no. 7, pp. 3336–3348, 2007. 93

[KTM06] G. K. Karagiannidis, T. Tsiftsis, and R. K. Mallik, "Bounds for multihop relayed communications in Nakagami-m fading," *IEEE Trans. Commun.*, vol. 54, no. 1, Jan. 2006. 6, 21

[KV11] A. Khabbazibasmenj and S. A. Vorobyov, "A computationally efficient robust adaptive beamforming for general-rank signal models with positive semi-definitness constraint," in Proc. *4th IEEE Inter. Workshop on Computational Advances in Multi-Sensor Adaptive Processing, CAMSAP'11, San Juan, Puerto Rico*, pp. 185–188, Dec. 2011.

[LTW04] J. N. Laneman, D. N. C. Tse, and G. W. Wornell, "Cooperative diversity in wireless networks: Efficient protocols and outage behavior," *IEEE Trans. Information Theory*, vol. 50, no. 12, pp. 3062 – 3080, Dec. 2004. 6, 21

[LW03] J. N. Laneman and G. W. Wornell, "Distributed space time coded protocols for exploiting cooperative diversity in wireless betwork," *IEEE. Trans. Info. Theory*, vol. 49, pp. 2415–2425, Oct. 2003. 8, 42, 61

[MBK07] B. Maniymaran, M. Bertier, and A.-M. Kermarrec, "Build one, get one free: Leveraging the coexistence of multiple p2p overlay networks," in *ICDCS '07*, June 2007, pp. 33–33.

[MC98] J. P. Macker and M. S. Corson, "Mobile ad hoc networking and the IETF," *SIGMOBILE Mob. Comput. Commun. Rev.*, vol. 2, no. 1, pp. 9–14, Jan. 1998. [Online]. Available: http://doi.acm.org/10.1145/584007.584015 87

[MHMB05] R. Mudumbai, J. Hespanha, U. Madhow, and G. Barriac", "Scalable feedback control for distributed beamforming in sensor networks," in *Proc. IEEE International Symposium on Information Theory, September*, 2005, pp. 137–141. 9, 61

[MM02] P. Maymounkov and D. Mazieres, "Kademlia: A peer-to-peer information system based on the xor metric," in *Peer-to-Peer Systems*, ser. Lecture Notes in Computer Science, P. Druschel, F. Kaashoek, and A. Rowstron, Eds. Springer, 2002, vol. 2429, pp. 53–65. 126

[MS06] B. S. Merken and A. Scaglione, "Randomized space-time coding for distributed cooperative communication," in *Proc. IEEE International Conference on Communications 2006*, Istanbul, 2006, pp. 5003–5017.

[NBS08a] T. D. Nguyen, O. Berder, and O. Sentieys, "Impact of transmission synchronization error and cooperative reception techniques on the performance of cooperative MIMO systems," in *IEEE International Conference on Communication (ICC)*, 2008, pp. 4601–4605. xi, 8, 61, 66

[NBS08b] T.-D. Nguyen, O. Berder, and O. Sentieys, "Impact of transmission synchronization error and cooperative reception techniques on the performance of cooperative MIMO systems," in *Proc. IEEE International Conference on Communications 2008*, 2008, pp. 4601–4605. 9

[Nee10] D. Neelanjana, "A peer to peer based information sharing scheme in vehicular ad hoc networks," *Eleventh International Conference on Mobile Data Management (MDM)*, pp. 309 – 310, May 2010. 124, 126, 127

[PAR06] R. C. Palat, A. Annamalai, and J. H. Reed, "Upper bound on bit error rate for time synchronization errors in bandlimited distributed mimo networks," in *IEEE Wireless Communications and Networking Conference*, 2006, pp. 2058–2063. 9

[PNG08] A. Paulraj, R. Nabar, and D. Gore, *Introduction to Space-Time Wireless Communications*, 1st ed. New York, NY, USA: Cambridge University Press, 2008. 5, 6, 8, 46

[PR99] C. E. Perkins and E. M. Royer, "Ad-hoc on-demand distance vector routing," in *Mobile Computing Systems and Applications, 1999. Proceedings. WMCSA '99. Second IEEE Workshop on*, 1999, pp. 90–100. 10, 109, 115

[PWS+04] R. Pabst, B. H. Walke, D. Schultz, P. Herhold, H. Yanikomeroglu, S. Mukherjee, H. Viswanathan, M. Lott, W. Zirwas, M. Dohler, H. Aghvami, D. Falconer, and G. Fettweis, "Relay-based deployment concepts for wireless and mobile broadband radio," *Communications Magazine, IEEE*, vol. 42, no. 9, pp. 80–89, 2004. 21

[RB11] L. Ribe-Baumann, "Combining resource and location awareness in DHTs," *19th International Conference on Cooperative Information Systems (CoopIS 2011), Crete, Greece*, October 2011. 11, 125, 127, 131, 132, 135, 136, 137, 138, 139

[RFH+01] S. Ratnasamy, P. Francis, M. Handley, R. Karp, and S. Shenker, "A scalable content addressable network," in *SIGCOMM'01*, 2001. 126

[RGJZ04] S. Ren, L. Guo, S. Jiang, and X. Zhang, "Sat-match: A self-adaptive topology matching method to achieve low lookup latency in structured p2p overlay networks," in *IPDPS'04*, April 2004, pp. 83–91. 127

[RHKS02] S. Ratnasamy, M. Handley, R. Karp, and S. Shenker, "Topologically-aware overlay construction and server selection," in *INFPCOM 2002*, 2002. 127

[RKV04] A. Reznik, S. R. Kulkarni, and S. Verdu, "Degraded gaussian multirelay channel: capacity and optimal power allocation," *IEEE Trans. Inform. Theory*, vol. 50, no. 12, pp. 3037–3046, Dec. 2004.

[SEA03] A. Sendonaris, E. Erkip, and B. Aazhang, "User cooperation diversity. Part I. system description," *IEEE Trans. Communications*, vol. 51, no. 11, pp. 1927 – 1938, Nov. 2003. 2

[SMLN+03] I. Stoica, R. Morris, D. Liben-Nowell, D. Karger, M. Kaashoek, F. Dabek, and H. Balakrishnan, "Chord: a scalable peer-to-peer lookup protocol for internet applications," *Networking, IEEE/ACM Transactions on*, vol. 11, no. 1, pp. 17–32, 2003. 11, 125, 126, 128

[SMS07] B. Sirkeci-Mergen and A. Scaglione, "Randomized space-time coding for distributed cooperative communication," *IEEE Transactions on Signal Processing*, vol. 55, October 2007.

[SS+93] S. H. Strogatz, I. Stewart *et al.*, "Coupled oscillators and biological synchronization," *Scientific American*, vol. 269, no. 6, pp. 102–109, 1993. 61

[SS06] D. Smith and S. Singh, "Approaches to multisensor data fusion in target tracking: A survey," *Knowledge and Data Engineering, IEEE Transactions on*, vol. 18, no. 12, pp. 1696–1710, 2006. 93

[SV03] M. Sichitiu and C. Veerarittiphan, "Simple, accurate time synchronization for wireless sensor networks," in *IEEE Wireless Communications and Networking (WCNC)*, 2003, pp. 74–80. 8, 9, 61

[SW48] C. E. Shannon and W. Weaver, "A mathematical theory of communication," 1948. 6, 26

[TAB06] A. Tyrrell, G. Auer, and C. Bettstetter, "Firefly synchronization in Ad Hoc networks," in *Proc. MiNEMA*, 2006. 9, 61

[TJC99] V. Tarokh, H. Jafarkhani, and A. Calderbank, "Space Time Block Codes from Orthogonal Designs," *Information Theory, IEEE Trans.*, vol. 45, pp. 1456 – 1467, Jul. 1999. 8, 42

[TSC98] V. Tarokh, N. Seshadri, and A. Calderbank, "Space time codes for high data rate wireless communication: Performance analysis

and code construction," *IEEE Transactions on Information Theory*, vol. 44, pp. 744 – 765, Mar. 1998. 8, 42, 67

[TT08] T.-R. Tsai and D.-F. Tseng, "Subspace algorithm for blind channel identification and synchronization in single-carrier block transmission systems," *Signal Processing*, vol. 88, no. 2, pp. 296–306, 2008. 9, 61

[Tur61] G. L. Turin, "On optimal diversity reception," *IRE Trans. Information Theory*, vol. IT 7, no. 3, pp. 154–166, July 1961.

[vdM68] E. C. van der Meulen, "Transmission of information in a t-terminal discrete memoryless channel," Dept. Statistics, Univ. California, Berkeley, CA, USA, 1968.

[vdM71] ——, "Three-terminal communication channels," *Adv. Appl. Prob.*, no. 3, pp. 120–154, 1971.

[VGL03] S. A. Vorobyov, A. B. Gershman, and Z.-Q. Luo, "Robust adaptive beamforming using worst-case performance optimization: a solution to the signal mismatch problem," *IEEE Trans. Signal Processing*, vol. 51, no. 2, pp. 313 –324, Feb. 2003.

[Win98] J. Winters, "The diversity gain of transmit diversity in wireless systems with Rayleigh fading," *IEEE Transactions on Vehicular Technology*, vol. 47, no. 1, pp. 119–123, 1998. 64

[WR03] M. Waldvogel and R. Rinaldi, "Efficient topology-aware overlay network," *SIGCOMM Comput. Commun. Rev.*, vol. 33, pp. 101–106, January 2003. 127, 162

[WS10] J. W. Wallace and R. K. Sharma, "Automatic secret keys from reciprocal MIMO wireless channels: measurement and analysis," *Trans. Info. For. Sec.*, vol. 5, no. 3, pp. 381–392, Sep. 2010. [Online]. Available: http://dx.doi.org/10.1109/TIFS.2010.2052253 5, 12, 142, 143, 144, 145, 146, 147

[WZHM05] B. Wang, J. Zhang, and A. Host-Madsen, "On the capacity of MIMO relay channels," *IEEE Trans. Inform. Theory*, vol. 51, no. 1, pp. 29–43, Jan. 2005. 42

[XK04] L. L. Xie and P. R. Kumar, "An achievable rate for the multiple level relay channel," in Proc. *IEEE Symp. Inform. Theory*, June/July 2004.

[YC05] J. Y. Yu and P. H. J. Chong, "A survey of clustering schemes for mobile ad hoc networks," *IEEE Communications Surveys Tutorials,*, vol. 7, no. 1, pp. 32–48, 2005. 5

[YCK06] Y. Yuan, M. Chen, and T. Kwon, "A novel cluster-based cooperative MIMO scheme for multi-hop wireless sensor networks," *EURASIP Journal on Wireless Communications and Networking*, 2006. 110, 117

[YF04] O. Younis and S. Fahmy, "Distributed clustering in ad hoc sensor networks: A hybrid, energy-efficient approach," *IEEE Transactions on Mobile Computing*, pp. 366–379, 2004. 90

[YKR06] O. Younis, M. Krunz, and S. Ramasubramanian, "Node clustering in wireless sensor networks: Recent developments and deployment challenges," *7th International Symposium on Wireless Communication Systems (ISWCS)*, pp. 20–25, 2006.

[ZARBH13] B. Zafar, R. Alieiev, L. Ribe-Baumann, and M. Haardt, "Dhts for cluster-based ad-hoc networks employing multi-hop relaying," in *17th International Workshop on Wireless Mesh and Ad Hoc Networks (WiMAN 2013), in conjunction with the 22nd International Conference on Computer Communications and Networks (ICCCN)*, Nassau, Bahamas, 07 2013. 123, 126

[ZGA+10] B. Zafar, S. Gherekhloo, A. Asgharzadeh, M. T. Garrosi, and M. Haardt, "Self-organizing network with intelligent relaying

(SONIR)," in *Proc. IEEE International Conference on Mobile Ad-hoc and Sensor Systems (IEEE MASS), San Francisco, CA*, Nov. 2010. 5, 10, 12, 133

[ZGH11a] B. Zafar, S. Gherekhloo, and M. Haardt, "A joint clustering and routing algorithm to maximize link performance in cooperative MIMO ad-hoc networks," in *22nd IEEE Symposium on Personal, Indoor, Mobile and Radio Communications (PIMRC 2011), Toronto, Canada*, 2011, pp. 90–100.

[ZGH11b] ——, "A joint clustering and routing scheme to maximize link performance in cooperative mimo ad-hoc networks," in *Invited paper, IEEE PIMRC*, Toronto, Canada, 09 2011. 22, 60, 87

[ZGH12a] ——, "Analysis of cooperative multi-hop relaying networks," in *WWRF 28*, Athen, Greece, 04 2012. 22, 42

[ZGH12b] ——, "Analysis of multihop relaying networks: Communication between range-limited and cooperative nodes," *Vehicular Technology Magazine, IEEE*, vol. 7, no. 3, pp. 40–47, 2012. 22, 42

[ZGRH12] B. Zafar, S. Gherekhloo, F. Roemer, and M. Haardt, "Impact of synchronization errors on Alamouti-STBC-based cooperative MIMO schemes," in *7th IEEE Sensor Array and Multi-channel Signal Processing (SAM 2012)*, New Jersey, USA, 06 2012. 62

[ZGS+11] B. Zafar, S. Gherekhloo, D. Schulz, M. Haardt, and J. Seitz, "A novel multi-hop routing scheme for ad-hoc cooperative MIMO systems," *in Proceedings of the 26th Wireless World Research Forum (WWRF), Doha*, April 2011. 22, 115

[ZKJ01] B. Y. Zhao, J. D. Kubiatowicz, and A. D. Joseph, "Tapestry: An infrastructure for fault-tolerant wide-are location and routing," UC Berkeley, Tech. Rep. UCB/CSD-01-1141, 2001. 127, 162

[ZSGH11] B. Zafar, D. Schulz, S. Gherekhloo, and M. Haardt, "Ad-hoc networking solutions for cooperative MIMO multi-hop networks," *IEEE*

Vehicular Technology Magazine, pp. 31 – 36, 2011. 2, 87, 110, 117, 126, 128

[ZWPO09] G. Zheng, K.-K. Wong, A. Paulraj, and B. Ottersten, "Collaborative-relay beamforming with perfect CSI: Optimum and distributed implementation," *IEEE Signal Processing Letters*, vol. 16, no. 4, pp. 257 –260, April 2009.

[ZZS10] Q. Zou, S. Zheng, and A. H. Sayed, "Cooperative sensing via sequential detection," *Signal Processing, IEEE Transactions on*, vol. 58, no. 12, pp. 6266–6283, 2010. 93